# CONTENTS

# Research on the design of smart mountaineering gear based on solar power technology

Xiying Zhang[1], Lei Shen[1], Xiangfang Ren[1], Han Chen[1], Ying Tang[1.2]

[1]Department of Design, Jiangnan University, Lihu Avenue, Wuxi, China
[2] Department of Design, Politecnico di Milano, Milan, Italy

**Corresponding Author:** Lei Shen, sl999@sina.com

## ABSTRACT

Wearable devices were eagerly anticipated in science and technology circles and have led to large changes in the field of clothing. In addition to medical, military, industrial and other special fields, wearable devices are used in sports, fitness, entertainment and other tasks. The outdoor fitness field should promote new technology products; therefore, a new type of solar-charging mountaineering wear was designed using flexible solar cells sewn into a detachable double cap that is easy to use and has a high conversion efficiency. This paper introduces the overall system design, circuit design, and process design of the mountaineering gear and describes the experimental effects and prospects in detail.

## 1. INTRODUCTION

Wearable devices are the most remarkable development in the world of technology in the modern era. Devices were used in sneakers by Puma and Adidas when the companies experimented with wearable technology in the mid-1980s[1]. With the development of complex new technology, the miniaturization and simplification of scientific and technological products, and the impetus of high-tech giants such as Google and Apple, wearable devices are now known to everyone and are increasingly being pursued. It is not a whim for these high-tech companies to make wearable devices the object of intense research and promotion, and some research institutes predict that by 2021, the market size for smart wearable devices will reach $46.2 billion, with a compound growth rate of 22% in the next four years[2]. This shows that the wearable market has a huge margin of profitability. In addition, high-tech products have a subtle impact on people's lives, changing their way of life. Smart phones have become popular electronic devices that have become

inseparable from users in just a few years, and wearable devices will be the next tech fad, especially in the field of smart wearable clothing. Many famous brands have been developing smart wearable clothing. For instance, Ralph Lauren, a well-known fashion brand, launched Polo Tech, a smart compact sports T-shirt[3], becoming another new player in the wearable field. Adidas also introduced an intelligent basketball vest[4], and the Hexoskin brand has been leading the world in the field of motion sensing clothing and introduced a variety of men's and women's models of motion-sensing clothing[5] that can transmit real-time motion data to Bluetooth data points, including heart rate, number of steps, calorie consumption, respiration rate and other indexes, in a very advanced manner.

At present, smart wearable clothing involves medical, military, industrial and other special fields[6] and has immensely influenced people's daily life such as in sports, fitness, entertainment and other fields, especially in exercise fitness as heart rate bands, sensor clothing, and colour-changing clothes. Moreover, it increased the popularity of

and created an upsurge in sports enthusiasts. However, the outdoor fitness field also needs the impetus of new technology products. Mountaineering is one of the most popular outdoor sports. However, according to the 'relevant data analysis in the China mountaineering and outdoor sports accident analysis report' released by the Chinese mountaineering association, wayfinding accidents account for 45%, and are one of the main types of outdoor mountain sports accident[7]. The three commonly used rescue methods are all based on positioning assistance, which needs unblocked positioning tools, like smartphones, navigation devices or GPS-enabled mountain watches. However, it is difficult to ensure that the electronic devices are always on during long climbing activities, and the power bank is not able to provide a continuous supply of energy.

A supply of energy is required in every field of electronic technology in the modern era. In this energy-scarce society, the development and utilization of renewable resources are predominantly important, and solar power generation is an emerging renewable resource. Approximately 40 minutes of solar energy on the earth are sufficient for the global human consumption in one year, it has no environmental pollution, is "green" and clean, inexhaustible, has no regional restrictions, and has broad application prospects. In recent years, researchers have made great progress in the study of solar textiles. In 2014, researchers at the MIT developed a new printing technology and successfully used it to make paper solar cells[8]. Traditional manufacturing methods require destructive conditions - printing substrates must be immersed in liquid or require high temperatures, whereas this new printing technology requires only steam and ambient temperatures below 120°C. In this way, raw paper, clothing and plastic can all be used to make batteries that greatly reduce the cost of solar cells. In 2015, professors Trisha Andrew and Marianne Fairbanks of the University of Wisconsin-Madison and Noon Solar, co-founder of a solar-powered rechargeable handbag, developed solar textiles using polymers to coat different fabric types and structures, which increased the electrical conductivity of the fabric tenfold[9]. The same year, AdvancedMaterials described a solid-state photovoltaic textile in which the electro-linear photoanode wire (the negative electrode of the photovoltaic cell) and the counter electrode (the auxiliary electrode) are woven into a fabric layer. The two electrodes are placed on flexible, lightweight and inexpensive polymer fibres using a low-temperature wet treatment process. The new structure differentiates it from previous solar clothing made up of small solar cell elements. The new fabric receives energy from the natural solar radiation from the outside, charges the 2 mF capacitor and reaches 3 V within 60 s, generating enough electricity to power a digital calculator[10]. In 2018, researchers at the University of Tokyo developed a bendable ultra-thin organic solar cell with an energy conversion efficiency of 10.5 percent, setting a new record for the conversion efficiency of a bendable solar cell. The researchers, whose work is published in the journal Nature, combined the ultra-thin organic solar cells with sensors to create an ultra-thin ECG monitor that can be attached to the skin[11]. In 2019, Nottingham Trent University researchers developed a technique using "miniature solar cells"; the technique allows the wearer to generate electricity in action and charge items such as watches and mobile phones, employing a battery the size of a flea that can be embedded in the yarn and woven into textiles like any other form of clothes with wash-and-wear resistance[12].

This paper is based on the use of solar energy resources and the latest industrialized solar textile technology to solve the needs and problems of mountaineering enthusiasts through the design and development of a new solar charging mountaineering clothing using the optical principle of converting light energy into electricity. A brief review of current research in the field of solar-charging clothing is presented below. In 2013, Pauline van Dongen, a fashion designer from Nijmegen University of Applied Science in Holland, and Christiaan Holland of Gelderland Valoriseert launched a solar rechargeable suit[13]. The rechargeable suit used rigid solar cells as its core device, and was paired with wool and leather as the main materials for the clothing. Although one hour could fill half the battery of an ordinary mobile phone, with 48 solar cells installed in the clothes, the overall weight of the clothing was heavy so it could only be worn in winter. American clothing brand Tommy Hilfiger is selling a unique winter coat that can recharge mobile phones[14] using flexible solar cells integrated in a removable part on the back; though the wearability is enhanced a lot, installing large charging cells on the back affects the activity and comfort of the wearer. Although those designs achieved energy conversion and realized the function of using clothing as a carrier to charge electronic equipment, they did not focus on the key points of wearer comfort for practical clothing and were not suitable for daily life activities. The solar charging mountaineering gear proposed in this paper is novel based on the above research. The flexible solar cell greatly reduces the weight of the item, and only 12 solar cells are installed to achieve the function of charging a mobile phone. In addition, the clothing combines the solar cells in a double hat structure that does not affect the wearer's activities and improves comfort. In the mountaineering clothing field, there is no mountaineering clothing that can charge electronic equipment, revealing an outdoor mountaineering power shortage problem or gap. Considering the above problems, this paper describes the design of a new type of solar charging mountaineering gear that uses renewable solar energy as the charging energy, perfectly integrating the charging device and clothing to achieve a union of functionality and aesthetics. The gear was designed on the premise that it should not add to the burden of climbing, it should be convenient for the wearer to use, and be exposed

to the most light to maximize the conversion of solar energy into electricity.

## 2. MATERIAL AND METHOD

### 2.1 Material

Solar cells based on the principle of the semiconductor photovoltaic effect are an effective way to utilize solar energy. Thin-film solar cells are a new generation of solar cells, which can be divided into two categories of hard substrates and flexible substrates according to the type of substrates[15]. Considering the comfort level of clothing, this paper adopts the flexible ultra-thin solar cell as the

carrier, and it will be the future direction of solar energy development that greatly surpasses the traditional silicon crystal laminates or the performance of film. The size and weight is 1/5th that of traditional solar cells, and the thickness is only 1/3rd that of the original cells, which will significantly promote the application of solar energy and enable solar energy technology in any shape or attached to any surface. As shown in Figure 1, the flexible solar cells are made by Wuxi Warmspace Tech C O., LTD, are bendable to nearly 180 degrees and have the advantage of being waterproof and sewn. The price is $3.50 apiece. Data on the flexible ultra-thin solar cell are shown in Table 1, and the gauge is 0.5 W/2 V/250 mA.



**Figure 1.** Flexible solar cell

**Table 1.** Data on monolithic flexible solar cells

(Note: The following electrical performance parameters were measured under standard test conditions: Light intensity 1000 W/L, spectrum AM1.5, cell temperature 25 ℃)

| Brand | Capacity | Enviroment temperature | Capability | Data | Specification | Others |
|---|---|---|---|---|---|---|
| WARMSPACE | 0.5W | -40℃~80℃ | Antiseptic and moisture-proof | Working voltage: 1.5V | Length: 165mm (Effective length), 195mm (Overall length) | Packaging materials: Durable, High transmittance ETFE film |
| | | | | Working current: 250mA | Width: 38mm (Effectivewidth), 58mm (Overall width) | Adhesive: Weatherproof, high transmittance fast setting EVA film |
| | | | | Open-circuit voltage: 2.0V | Thickness: 0.5mm | Battery type: Three junctions of flexible amorphous silicon thin film solar cells |
| | | | | Short-circuit current: 420mA | Weight: 18g±2g | |

The clothing fabric was selected from the latest high-quality DINTEX technical fabric. As shown in Figure 2, it uses the principle of nano-porous air permeability of top nanotechnology, integrates wind protection, air permeability and thermal technology, and has a double waterproof effect. The surface of the fabric is coated with a waterproof and breathable coating, and the inside is made of high-end 100% polyester fibre. DINTEX waterproof and breathable glue is used to adhere the inner waterproof and breathable film; the breathable coefficient reaches 5000, and rain and snow can be blocked from outside while the air inside can pass through the fabric. It has super-strong anti-rainstorm ability and has relaxed comfort.

## 2.2 Method

The circuit design mainly comprised study of the assembly structure of flexible ultra-thin solar cells and whether the attained energy/current can supply normal charging to electronic equipment. Considering the beauty of the clothing from an aesthetics point of view, the total area of the battery cell should be kept to a minimum. Using the flexible solar cell described above, theoretically, to meet the 3.7 V/2000 mAh capacity of an ordinary mobile phone lithium battery, 3 cells in series would take 8 hours to fill, 3 cells in series and 2 cells in parallel would take 4 hours to fill, 3 cells in series and 3 cells in parallel would take 2.7 hours to fill.

Considering the size of a normal hat and the process of combining a double hat (see details below), in this paper, 12 flexible ultra-thin solar cells were used to optimize the design; for the circuit design, three schemes were compared and tested.

Figure 3(a) shows the first scheme in which we adopted a LY9890 chip. The input end with 2 cells in series and 6 cells in parallel, the voltage after parallel is 4 V and the output is 5 V after the booster module. The LY9890 chip is a compact, efficient and low start voltage booster DC/DC converter chip that includes an error amplifier, slant wave signal generator, comparator, switch and drive component. When the load current varies in a large range, it can work stably and efficiently without any external compensation circuit. The input start voltage of the chip is below 1.6 V. The higher switching frequency prominently reduces the size of the external components. In addition, the low static current of 5 uA and high working efficiency ensure the battery has a long life. The output voltage is set by two external resistors. The output interface adopts a USB interface.

Figure 3(b) shows a second scheme using a TD1410 chip with an input of 6 cells in series and 2 cells in parallel; the voltage after parallel is 12 V and the output is 5 V after the depressurization module. TD1410 is a monolithic integrated buck switching power converter with internal power MOSFET. It has a wide voltage input range and can output 2 A current continuously. Using current mode, it has extremely high transient stability. Integrated heat turns off the function. In the turn-off mode, the current is less than 20 μA, and only a few peripheral devices are needed. The device includes a reference voltage source, oscillating circuit, error amplifier, and internal PMOS. The PWM control circuit can adjust the duty cycle from 0 to 100% linearly. It has a built-in overcurrent protection function and short-circuit protection function. Compensation modules are integrated to reduce the number of external components. TD1410 is the ideal power unit for portable devices.

Figure 3(c) shows the third scheme using a 3 cells in series and 4 cells in parallel connection mode, adding an anti-recharge Schottky diode and parallel in each series to improve the efficiency of the solar charger as much as possible.
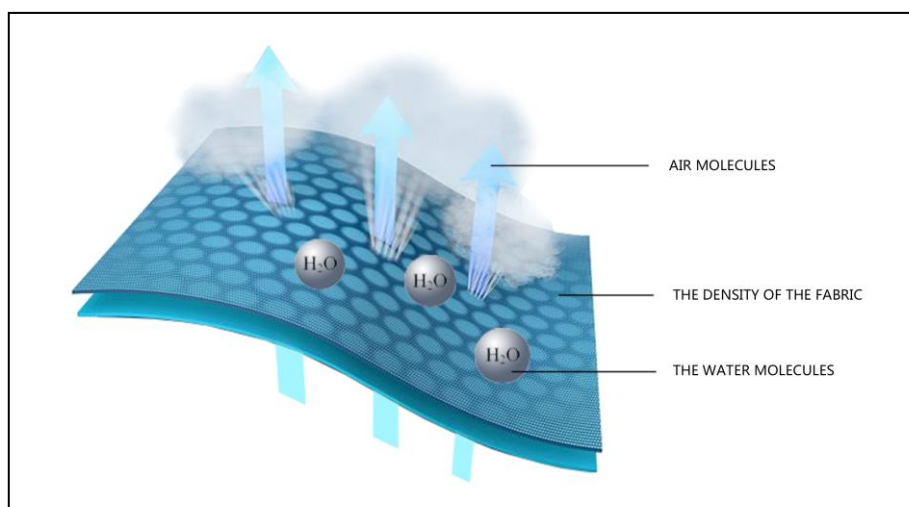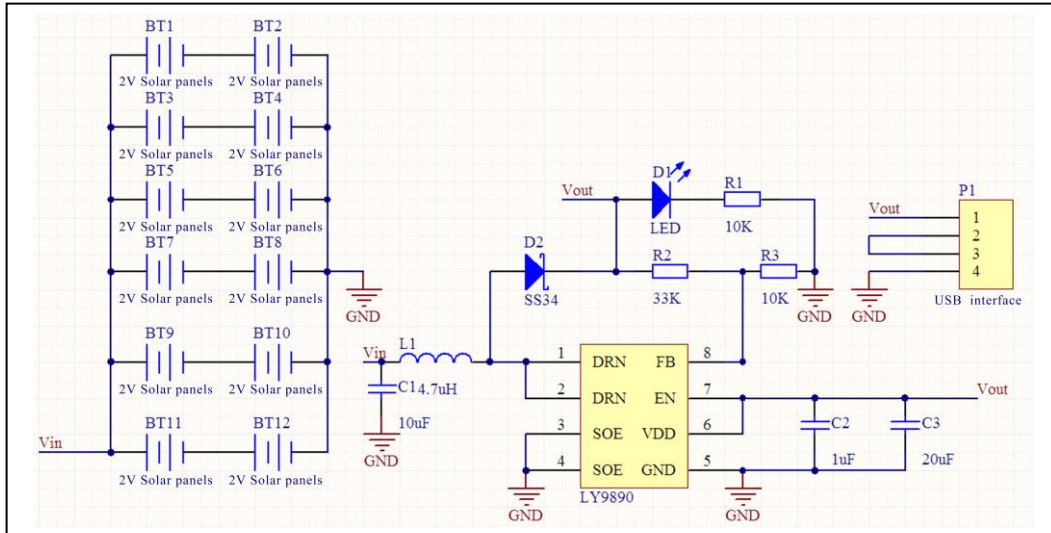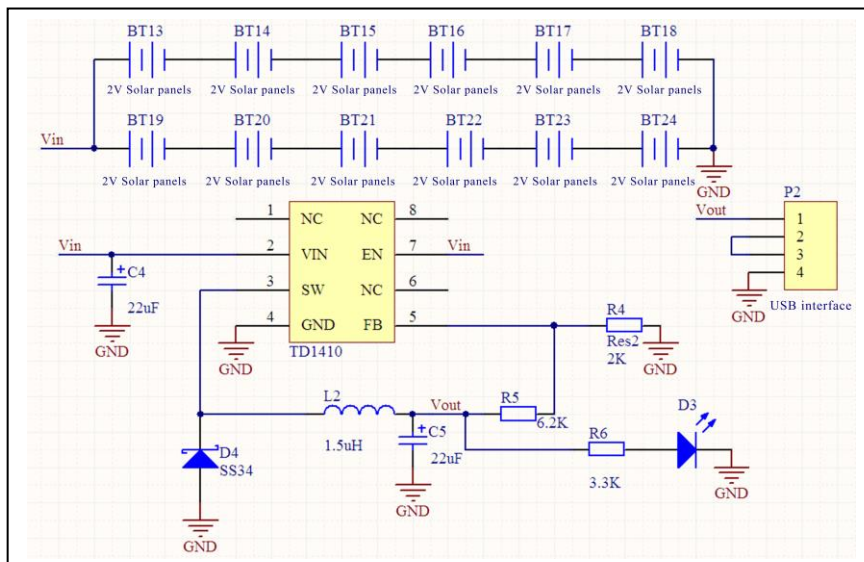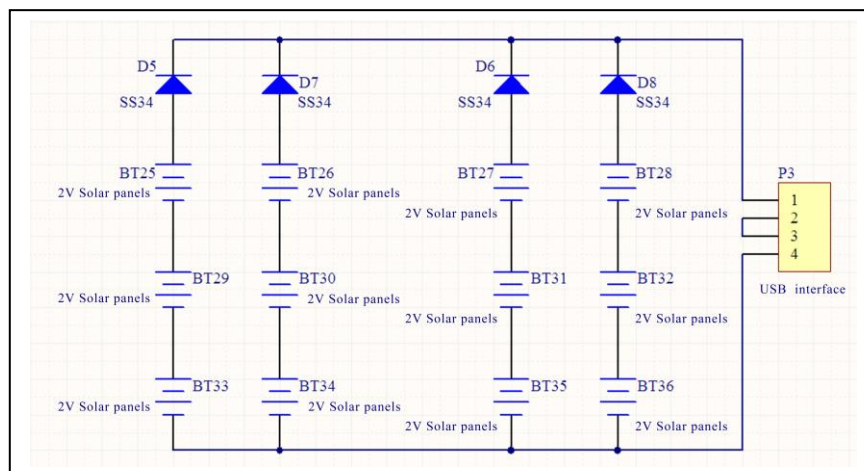


**Figure 2.** The principle of nano-porous air permeability

(a) 5V boost circuit diagram



(b) 5V buck circuit diagram



(c) Scenario 3 circuit diagram

**Figure 3.** Three circuit designs

Although the output power of the flexible solar cell was stable, the light intensity was good and the conversion rate was only approximately 10%, therefore, we must improve the efficiency of the circuit as much as possible to obtain the highest output current possible. Table 2 shows the results of above three schemes under normal sunlight.

The comprehensive comparison of the above three experimental schemes and did not consider the conversion cell rate; the conversion scheme efficiency of programme 1 was an average of 85%, conversion efficiency of programme 2 was an average of 90%, and programme 3 only had line and diode loss with an efficiency of up to 95%. Therefore, the third scenario was used in the design case.

## 3. RESULTS AND DISCUSSION

As a design for the special group of climbers, we took the circumstances and habits of their activities into account. Climbers usually need to carry a hiking bag during hiking, so solar cells cannot be covered by backpacks and still receive the maximum amount of light. Considering the above special requirements, the author combined the flexible solar cell with the fabric, stitched it skilfully and made a removable mountaineering hat. The overall effect is shown in Figure 4. To achieve better power, and allow for more solar cells to receive light, it was designed as a double-decked hat. The whole hat is detachable; the outer layer of the hat is stitched together in six flexible ultra-thin solar cells and the outer hat is stitched into the interior. The outer hat is fitted with zippers in the middle that allow for it be expanded into a plane, as shown in Figure 5. This allows for more linear illumination and energy conversion for significant efficiency. In the cap fastener part, the design has a USB interface with an external hardware output module and an indicator light in the middle. When the solar cell is in the working state, the red indicator light will be on. The USB interface and design details are shown in Figure 6. Hikers can use this solar charging mountaineering gear at any time during the climb; all they need to do is put the inner hat on their head, open the outer cap zipper and put it on the their back or backpack, and connect an electronic device to charge via USB interface. Then, the hiker waits until the charging is complete.

**Table 2.** Results of three programs under normal sunlight irradiation

| Programme | Total panel power(W) | Open circuit output voltage(V) | Output current(mA) |
|---|---|---|---|
| 1 | 6 | 5.15 | 120 |
| 2 | 6 | 5.20 | 260 |
| 3 | 6 | 5.75 | 320 |



**Figure 4.** The front and back of the new solar-charging mountaineering gear
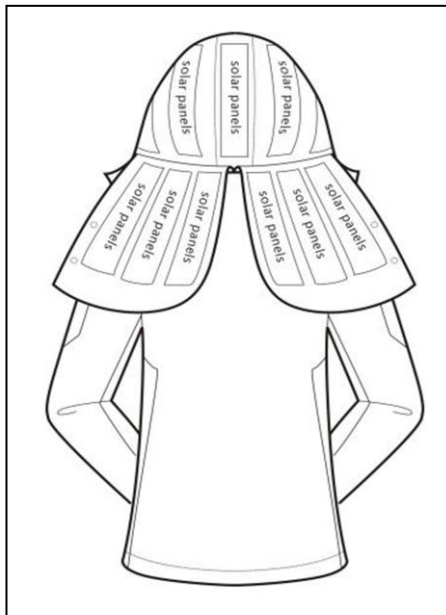
**Figure 5.** Expanding effect of the new solar-charging mountaineering gear
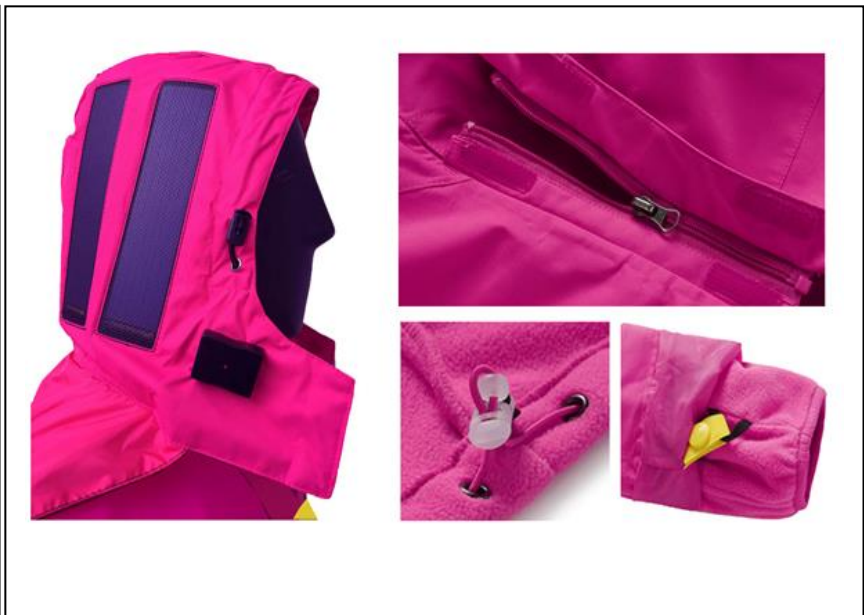


**Figure 6.** Details of the new solar-charging mountaineering gear

To ensure the normal use of the assembly structure of flexible solar cells combined with fabric, the author tested the clothing. The test method comprised connecting the flexible solar cell cell with a wire to a root number of two terminal units connected to a multimeter. The multimeter resistance reading was observed to determine whether the current and voltage met the charging requirements of general mobile phone lithium batteries, and conductive testing of all copper wires was performed to ensure the normal use of the charging system for solar-powered climbing gear.

Table 3 shows the experimental charging results for an ordinary mobile phone measured by sunlight exposure at different periods within 20 consecutive days in April. The table shows that, from 8 AM to 6 PM, the solar-charging mountaineering work efficiency with parabola distribution increased from 8 AM to 12 PM, reached the peak at 12 with the best charging effect and maximum output current of 291 mA ± 23mA. After 2 hours, the battery can be filled to 522mAh ± 60mAh. After 12 PM, the working efficiency began to decrease, as the illumination intensity gets weaker, so does the charging effect. The data for this experiment were the average of 20 days, and the statistical analysis of the data used Microsoft Excel 2013.

The climber's hiking activity time is generally on days of pleasant weather and there is little demand for cell phones in the mountaineering process, so this solar charging mountaineering gear can meet the requirements of climbers in the normal state of emergency charging.

## 4. CONCLUSION

Compared with previous solar clothing designs, this new solar mountaineering gear is lighter, softer, and more comfortable to wear. In addition to comfort, more solar cells are integrated so it has a higher conversion rate. Moreover, it is clean and environmentally friendly, makes full use of solar renewable resources, is easy to use, and can make up for the shortage in outdoor mountaineering power supply, promote the intelligent process of climbing clothes design. However, one inadequacy of the study lies in that the final test session only collected data for 20 days in April, which is not comprehensive enough for the use of the product. Subsequent laboratory tests should be more comprehensive and take measurements on days in each month of the year to generate average values for each month to provide a more instructive set of recommendations for future research.

**Table 3.** Average experimental sunlight exposure in different periods for 20 consecutive days in April

|  | 8:00 | 10:00 | 12:00 | 14:00 | 16:00 | 18:00 |
|---|---|---|---|---|---|---|
| Illumination intensity (×100 Lux)* | 706 ± 161 | 829 ± 177 | 936 ± 227 | 871 ± 198 | 740 ± 177 | 547 ± 140 |
| Output current (mA)* | 239 ± 25 | 267 ± 23 | 291± 23 | 279 ± 25 | 256 ± 23 | 227 ± 22 |
| Open circuit output voltage (V)* | 5.3 ± 0.1 | 5.5 ± 0.2 | 5.7 ± 0.2 | 5.6 ± 0.2 | 5.4 ± 0.2 | 5.2 ± 0.1 |
| Charging time (H) | 2 | 2 | 2 | 2 | 2 | 2 |
| Charge quantity (mAh) | 290 ± 28 | 406 ± 58 | 522 ± 60 | 435 ± 59 | 348 ± 56 | 261 ± 26 |

* Represents the result of the data within 20 days (average number±Standard deviation)

The 21st century is the green age, also known as the ecological age, in which new forms of energy are being explored to make rational use of them with the common goal of eradicating this struggle. The emergence of new technology and materials as well as their processing, compounding and finishing will increase the growing trend of high-performance clothing and add to the trend of multifunctional progress for improvement of clothing efficiency. New materials of flexible solar cells have better wearability and durability than rigid solar cells, and can encourage designers' creativity in clothing design and promote the process of using solar energy resources in clothing. However, at present, there is still a contradiction between the combination of the electronic components and the clothing fabric, and the contradiction between energy consumption and performance makes the battery a bottleneck. For higher performance, the energy consumption is bound to increase and more solar cells can provide higher efficiency but the area for components and clothing is limited and design has become a difficult aspect. Safety, environmental protection and health are requirements of intelligent clothing in the new era. The harmonization and assimilation of electronic mechanisms and clothing design and development of smaller, thinner and more suitable methods for clothing electronic components will be a common goal.

## Acknowledgement

## REFERENCES

1. Wen ZW. 2014. Clothing wearable technology. *Textile machinery* 14(5), 96-99.

2. Austen K. 2015. What could derail the wearables revolution? *Nature* 525(7567), 22-24.

3. Phau I, Sequeira M, Dix S. 2009. To buy or not to buy a "counterfeit" Ralph Lauren polo shirt: the role of lawfulness and legality toward purchasing counterfeits. *Asia-Pacific Journal of Business Administration* 1(1), 68-80.

4. Sun XF, Liu L. 2013. Wearable fashion design and innovation practice based on luminescent materials. *Design Art Research* 5 (2), 35-39.

5. Li L. 2014. A wearable device design-clothing computer. *Electronics World* 0 (11), 178-178.

6. Shen L, Hong W J, Tang Y. 2013. Design of new type of safety clothing based on the green era. *Shanghai textile science & technology* 41(6), 48-50.

7. Chen GS. 2018. Research on development status and countermeasures of the mountain outdoor rescue (Master's thesis). Retrieved from Wuhan Institute of Physical Education.

8. LARGE. 2020, April 21st. Scientists develop technology to make paper solar cells. Retrieved from http://www.juda.cn/news/132376.html.

9. CIECC. 2015, September 9th. American researchers have developed new solar textile technology. Retrieved from http://gpj.mofcom.gov.cn/article/zuixindt/201509/20150901108291.shtml.

10. Huang YT. 2017. Self-charging textiles that do not require batteries. *Dyeing & Finishing* 43(06), 55-56.

11. Science and Technology Daily, 2018, January 8th. Rubber made of very strong and tough materials could make washable solar battery. Retrieved from http://digitalpaper.stdaily.com/http_www.kjrb.com/kjrb/html/2020-04/30/node_2.htm

12. Jinqiao textile net. 2019, January 17th. Mobile phones can be charged by clothing made from tiny solar cells. Retrieved from https://www.sinotex.cn/newsHtml/190117/141256/.

13. Zhongguancun online, 2013, June 26th. Dutch designer pushes solar charging suit. Retrieved from http://news.zol.com.cn/382/3820472.html.

14. Guangzhou vocational training school of fashion art, 2014, Tommy Hilfiger entering the high-tech market, and pushing the solar charging jacket. December 16th. Retrieved from http://gzfatr.com/ninfo.asp?id=2406.

15. Nie ZY. 2010. New flexible solar cells. *Functional Materials Information* 7(Z1), 127.

# Computational modelling of hospital mattresses made from spacer fabrics

Dimitroula Matsouka[1], Savvas Vassiliadis[1], Clio Vossou[1], Arzu Marmarali[2]

[1]University of West Attica, Department of Electrical and Electronics Engineering, Thivon 250, Egaleo, 122 44 Athens, Greece
[2]Ege University, Department of Textile Engineering, 35100 Bornova/İzmir, Turkey

Corresponding Author: Dimitroula Matsouka, dmats@uniwa.gr

## ABSTRACT

The appearance of pressure ulcers is a very common occurrence, especially for people with limited mobility who are obliged to spend a long time prone on a support surface. Pressure ulcers in severe cases can cause damage to underlying muscle and bone. Damage to deeper tissues, tendons and joints may also occur. Serious complications, such as infection of the bone (osteomyelitis) or blood (sepsis), can occur if pressure sores progress. While the main strategy for dealing with pressure ulcers is centred around the interaction of patient and care-giver (manually changing the position of the patient every two hours in order to relieve pressure on critical body areas, examination of patient for signs of pressure ulcer formation) there are auxiliary approaches, such as the choice of a pressure relieving support surface. Currently, a variety of support surfaces exists. The criteria of choice are dependent on factors such as the medical history of the patient and economic. The emergence of 3D spacer fabrics as textile materials with good compression behaviour makes them suitable candidates to produce support surfaces that contribute to the prevention of pressure ulcers. In order to decide on their suitability, extended clinical trials involving actual patients must be performed. In the present paper, a computational methodology utilizing a tool widely used in the area of engineering, namely Finite Element (FE) Method, is proposed as a supporting tool for the preliminary evaluation of the suitability in terms of mechanical behaviour of certain 3D spacer fabrics, providing an insight of the deformation, stress and strain developed on the bodies (human body – mattress) as well as on their interface.

## 1. INTRODUCTION

Decubitus ulcers are associated with tissue necrosis, which is itself connected to several factors that include, but are not limited to, pressure, friction, shear, moisture and ischemia. Decubitus ulcers are not necessarily connected with the application of high pressure on a specific body area but can also be caused by the application of medium pressure which affects a body area continually for a long time. The appearance of decubitus ulcers is quite common. Epidemiological studies report frequencies of decubitus ulcer appearance ranging from 8.3% to 23% in European hospitals, 10.2% in UK based care units and 12.3% in care units located in the U.S.A. Estimations regarding the appearance and frequency of pressure ulcers, which are based on hospital surveys, differ a lot depending on the definition and stage of ulcers, the population of patients under investigation and care procedures. For home care situations the frequency of decubitus ulcers reaches 16.5%

in the USA and Canada [1, 2, 3].

Populations under greater risk of developing decubitus ulcers include people of limited mobility and/ or limited sensory perception and people undergoing operations with durations counted in hours. In summary, high risk groups include the elderly, patients in intensive care units, patients with neurological problems, trauma patients (including spinal cord injury) and patients subjected to operations lasting several hours. [2, 4] Body areas with the greatest frequency of decubitus ulcer appearance are areas where body weight is concentrated over bony projections such as the hips, sacrum, heels and elbows [4, 5].

In order to decrease the possibility of decubitus ulcer appearance different support surfaces are being used. The support surfaces have particular specifications and aim to support the sensitive parts of the body and to redistribute the pressure as evenly as possible [2, 4, 6, 7].

**To cite this article:** *Matsouka D, Vassiliadis S, Vossou C, Marmarali A. 2020. Computational modelling of hospital mattresses made from spacer fabrics. Tekstil ve Konfeksiyon, 30(4), 239-250.*

Support surfaces that are used for the prevention of decubitus ulcers belong to one of the following two categories [2, 4, 7].

1. Low-tech devices – They offer a support surface which adapts to the body curvature and distributes body weight across a large surface (pressure management). Low-tech devices include standard foam mattresses, alternative foam mattresses/overlays e.g. high specification foam, convoluted foam, cubed foam, viscoelastic foam. This category also includes mattresses/overlays which contain gel, liquids, fibrous materials and air.

2. High-tech devices – Dynamic systems that include:

   a. Mattresses/overlays of alternating pressure: patients lie on air-filled sacs that inflate and deflate sequentially to relieve pressure at different anatomical sites for short periods; these may incorporate a pressure sensor.

   b. Beds/mattresses/overlays air fluidised: warmed air circulates through fine ceramic beads covered by a permeable sheet; allowing support over a larger contact area.

   c. Beds/mattresses/overlays of low-air-loss: patients are supported on a series of air sacs through which warmed air passes

   d. Turning beds/frames: those function either by aiding manual repositioning of the patient, or by motor driven turning and tilting.

Strategies for decubitus ulcer prevention include systematic inspection of the dermal condition of the patient, moisturizing of the patient skin using appropriate creams, review of patient's diet and change of patient's positioning / posture by the health care providers according to a set schedule (usually every two hours) [2, 6].

Investigation of the ability of support surfaces to reduce the possibility of decubitus ulcer appearance is carried out either through measurement of the pressure applied to the patient body during the use of the support surface (interface pressure) or by controlled clinical trials that monitor the clinical course of patients when using the support surfaces under test. The non-invasive measurement of the interface pressure by placing a pressure sensor mat between the patient body area containing a bony prominence and the support surface provides an approximation of the pressure applied to a specific bony prominence. It is generally accepted that lower interface pressure means lower pressure applied on the surrounding tissues and capillaries [11]. A useful value that can be used as a guideline for a critical value of interface pressure is 32 mm Hg. This value has been used in the literature as an interface pressure limit. Exceeding this limit is possible to facilitate the appearance of decubitus ulcers [5, 8].

Clinical trials, while forming an inevitable stage of the development and production process of a medical device, also possess certain characteristics that can only be described as risks or burdens (to borrow some words used in the Declaration of Helsinki). First and foremost are the risks and burdens that are related to the test subjects, i.e. human beings either healthy or ailing. Further to the ethical considerations when working with human subjects there exist the monetary and time requirements for conducting clinical trials. According to DiMasi et al., [13] the estimated average out-of-pocket cost per new drug is US$ 403 million (2000 dollars). While the cost mentioned pertains to the development of new drugs and not medical devices as is the case in this paper, it can logically be argued that costs for the development of medical devices should be proportionally comparable to the costs for drug development [8 – 10, 12, 13].

Lately, the finite element (FE) method, which is a computational method popular in engineering, is used in order to computationally evaluate the developed pressure on the interface between the patient's body and the support surface. The basic idea of the FE method is to segment a continuous 2D or 3D - space into smaller surfaces or volumes [14]. Its main advantage comes from the fact that one can simulate different anthropometric data and different base materials for the support surface in one FE model just by changing the geometry or the material properties. Yoshida et al. developed three different 2D FE models of human body, simulating male and female subjects, lying on a mattress. They monitored the interface stress distribution resulting from FE analysis and compared it to sensory results concluding that computational stress values are in accordance with sensory tests [15]. A FE simulation of human tissue and support device interaction has also been performed by Silber et al., Makhsous et al. and Levy et al., using the FE method focus on the pressure distribution on the anatomical area of the buttock. The first research group creates a 3D FE model at the area along with the support surface, while the second research group creates a 2D FE model [16, 17, 18]. Finally, Vassiliadis et al. [19] presented a preliminary study on the modelling of spacer fabrics used in the development of support surfaces.

Spacer fabrics, in the present study, are proposed as a technologically interesting textile alternative for the development of support surfaces that can help to the prevention of the medical condition of pressure ulcers. Their construction principle namely, fabric layers interconnected by a layer of monofilament yarns, provides them with characteristics such as good compression behaviour. This characteristic is affected by the overall composition of the fabric, the composition of the connecting fibres, the angle of the fibres and the number of connecting monofilaments per unit length. Furthermore, spacer warp knitted fabrics are characterised by high breathability (low water vapour resistance) allowing moisture to be guided away from the body which reduces the chances of skin maceration. Skin maceration causes greater friction between skin and sheeting material and between skin and skin (e.g. at skin fold areas). Greater friction in turn causes greater shearing forces that could

lead to pressure ulceration [20]. The mechanical properties of spacer fabrics and their ability to manage the microclimate near the patient skin make spacer fabrics suitable for medical applications such as compression bandages and support surfaces for hospital beds and operating room tables concerning decubitus ulcers [21]. In 2009 Vassiliadis et al. [22] used the FE method in order to predict the micro and macro compression performance of typical spacer fabrics.

In the present paper, a methodology for the preliminary qualitative assessment of materials used for the construction of medical support surfaces (e.g. hospital mattresses), is presented. The methodology is based in the evaluation of the compression properties of the base material for the support surface with the combined use of experimental and computational procedures and the computational evaluation of the interface pressure developed on the human body while it is lying on such a support surface. The proposed methodology is implemented for the assessment of different spacer fabrics. For these purposes a generic setup for compression testing of spacer fabrics has been built, along with computational FE models in ANSYS® Workbench software which simulate the compressive behaviour of support surfaces made of these materials.

## 2.  MATERIAL AND METHOD

In the present section, the proposed methodology is outlined followed by its implementation for the assessment of seventeen spacer fabrics with different technical characteristics.

The proposed methodology comprises of three distinct steps, one experimental and two computational ones. In the first step, a compression test is performed on specimens of each of the materials under examination. Then, computational modelling of each experiment is performed in order to inversely evaluate an equivalent isotropic elastic modulus for each material. Finally, one computational model for each material under investigation is built, consisting of a human body lying down on a support surface with the corresponding material properties of the base material is built. The outcome of the proposed methodology is a sorted listing of the tested materials with respect to various mechanical quantities, such as the maximum vertical displacement of the upper area of the support surface, the maximum developed pressure on the interface between the human body and the support surface etc.

### 2.1 Material

The materials under assessment for the use in the development of support surfaces are seventeen different warp knitted spacer fabrics. All spacer fabric samples were a mix of open and closed constructions, i.e. front and back side, either both open or both closed, or front side open back side, closed (open and closed refers to the presence or absence of significant openings in the structure  of the outside layers of the samples). The thickness of the connecting monofilament in all cases was 0.2 mm. The yarns used for knitting the front and back sides had yarn counts of 1080 dTex or 600 dTex. The fabrics were all constructed with 100% polyester yarns, with variations on their construction parameters such as thickness and weight. The specimens had been produced on a Karl Mayer 3D warp knitting machine.

Figure 1 illustrates the appearance of two typical spacer fabrics as seen from the top and the side while, Table 1 presents the technical characteristics of all the spacer fabrics that were examined, as well as the specimen dimension that were used.
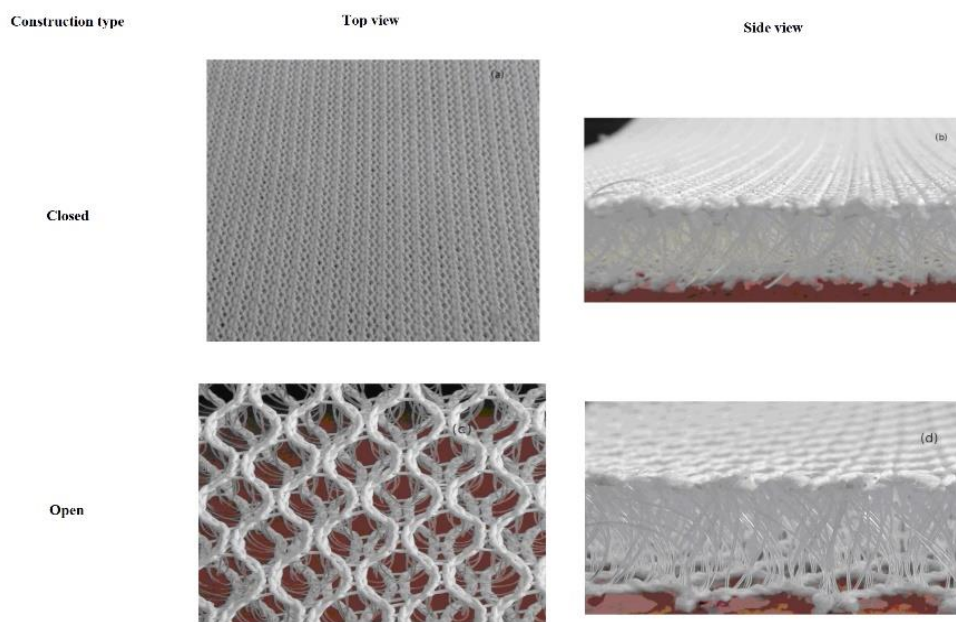


**Figure 1.** Typical constructions of warp knitted spacer fabrics

**Table 1.** Technical characteristics of the spacer fabrics

| Sample | Thickness (mm) | Width (mm) | Length (mm) | Mass per unit area (g/m²) |
|--------|----------------|------------|-------------|----------------------------|
| A1 | 10 | 202 | 300 | 510 |
| A2 | 10 | 210 | 302 | 625 |
| A3 | 10 | 215 | 304 | 1035 |
| A4 | 11 | 205 | 310 | 430 |
| A5 | 12 | 305 | 210 | 825 |
| A6 | 12 | 300 | 212 | 980 |
| A7 | 12 | 304 | 211 | 1100 |
| A8 | 13 | 200 | 292 | 600 |
| A9 | 8 | 204 | 293 | 490 |
| A10 | 12 | 205 | 293 | 880 |
| A11 | 12 | 205 | 295 | 1120 |
| A12 | 10 | 207 | 293 | 850 |
| A13 | 10 | 200 | 297 | 460 |
| A14 | 10 | 209 | 290 | 500 |
| A15 | 10 | 202 | 285 | 900 |
| A16 | 10 | 150 | 200 | 1030 |
| A17 | 10 | 150 | 200 | 535 |

## 2.2 Method

The spacer fabrics were experimentally tested in compression and their indentation under a known load was monitored.
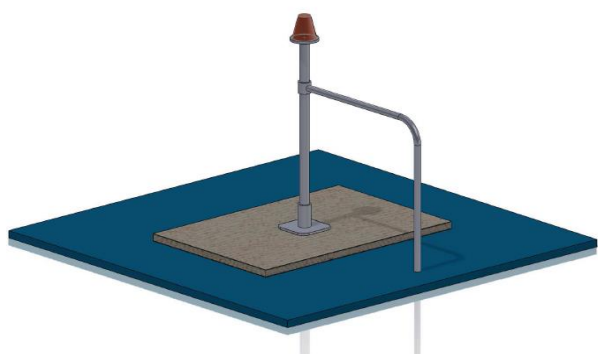


**Figure 2.** 3D representation of the experimental setup

Using the experimental setup presented in Figure 2, a weight (red volume) of 1300 g (12.753 N) was placed on the upper circular area of the setup acting on each spacer fabric sample through the square surface of area equal to 0.0025 m². This square surface was acting as an indenter, causing the vertical deformation of the fabric sample (brown volume) which was placed on a rigid surface (blue volume). The magnitude of the weight was chosen in order to prevent indentations higher than 80% of fabric thickness in any sample. For every spacer sample the resulting indentation was measured. Since the following computational modelling of the spacer fabrics was supposed to consider the materials as linear elastic, only one point on the force - displacement curve was considered. The applied force could not be directly converted to stress value since the axial force was not acting on the centroid of the cross section of the sample. This resulted from the fact that the cross – sectional area of the sample is larger than this of the experimental setup.

In order to retrieve the equivalent linear elastic modulus of each spacer fabric, the abovementioned experiment was computationally simulated using the FE method and an optimization procedure, with the objective of the minimization of the difference between the experimentally measured and the computationally evaluated vertical deformation, was implemented. For this procedure, all spacer fabrics were considered as isotropic and homogenous materials. Seventeen different FE models were built incorporating the exact geometrical dimensions of the samples as they are presented in Table 1.

The FE model simulating the experiment performed for sample 1 is, indicatively, presented in Figure 3. A square plate (green volume), simulating the square, load bearing, end of the experimental setup (25 x 25 mm²), was loaded with a force of 1300 g (12.753 N). The square plate was placed on the top of the upper surface of the spacer fabric (grey volume). The vertical displacement of the lower surface of the spacer fabric has been constrained simulating the rigid surface below the 3D spacer fabric. Both volumes are segmented with 4632 hexahedral, 20-nodded FE.
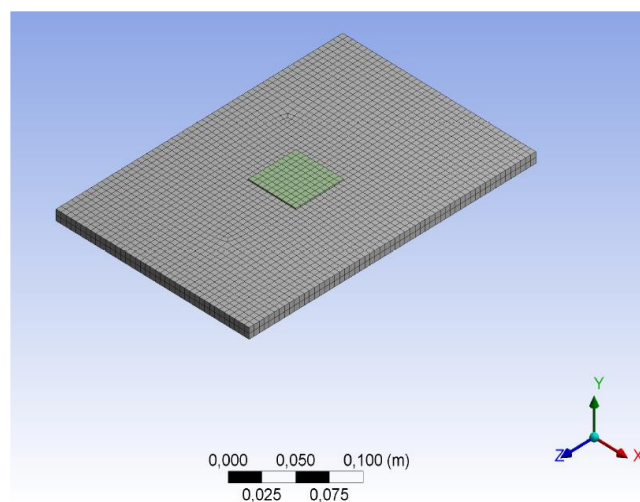


**Figure 3.** FE model of the simulation of the compression test of the spacer fabric

Next, the computed equivalent elastic modulus of each spacer fabric was used in seventeen FE models simulating a human body, [23] of exact geometrical representation, lying down on a mattress consisting in each model of one spacer fabric. This FE model consists of two solid bodies, one simulating the human body and one simulating a mattress of typical dimensions. The geometrical model of the human body corresponds to a male subject of height 180 cm and weight of 90 kg. As far as the elastic modulus of the FE belonging to the human body is concerned, a weighted average of the elastic modulus of soft tissue and bone has been considered. In more details, according to Mukherjee et al. [24] if flesh and bone are considered linear isotropic materials, they have elastic moduli equal to $6 \times 10^4$ and $2 \times 10^{10}$ Pa respectively. The human body consists of 15% of bone while the rest is a type of soft tissue (dermis, muscles, fat, etc.). [25] Given that, the elastic modulus of the human body was considered $3 \times 10^9$ Pa and its Poisson ratio equal to 0.4. [26]

The model simulating the interaction of human body and the support surface consists of a total of 6966 FE, from which 3974 belong to the human body and are tetrahedral, 10-nodded FE, in order to represent the exact geometry of the body, and the rest are hexahedral 20-nodded elements and belong to the mattress. In Figure 4 the final FE model of human body and mattress is presented in an isometric view. For purposes of meshing simplicity, the face and the hands of the geometrical model of the human body have been removed not altering the final FE method results.

Between the human body and the support surface a rough contact was considered, and its status is presented in Figure 5. For the modelling of the contact 138 contact and 138 target quadrilateral FE have been used.

The performed analysis is static structural and as far as the loading is considered, in order to simulate the supine body posture on the mattress, gravity is applied while the displacement of the lower surface of the mattress is constrained in the vertical direction simulating the existence

of a base for the support surface as it is presented in Figure 6.

In the FE method various results are available in order to monitor the performance of each setup. For the implementation of the proposed methodology, the results that are monitored in order to provide the listed sorting are (a) the vertical displacement of the upper surface of the mattress, (b) the equivalent stress, (c) the normal stress on Z-axis, (d) the shear stress on the XY plane developed on the human body, and (e) the status, (f) the pressure and (g) the frictional stress on the interface between the human body and the mattress.

## 3. RESULTS AND DISCUSSION

The presented results are divided in two sections: (a) the results of the first two steps of the methodology which lead to the computational evaluation of the equivalent elastic modulus of the seventeen samples of spacer fabrics and (b) the results of the third step which lead to the sorted listing according the suitability of the spacer fabrics for their use in the development of support surfaces.
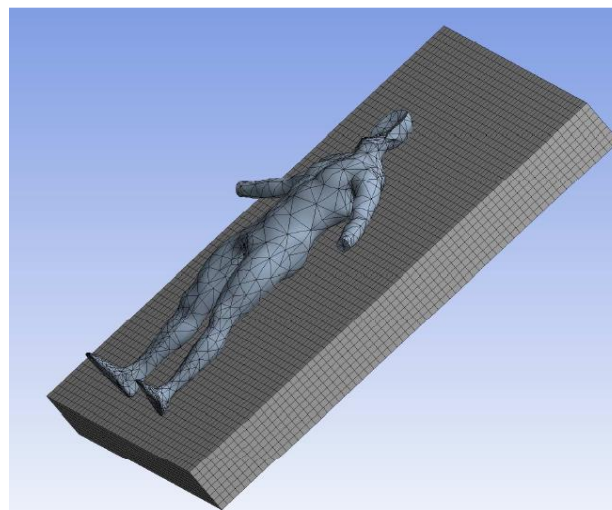


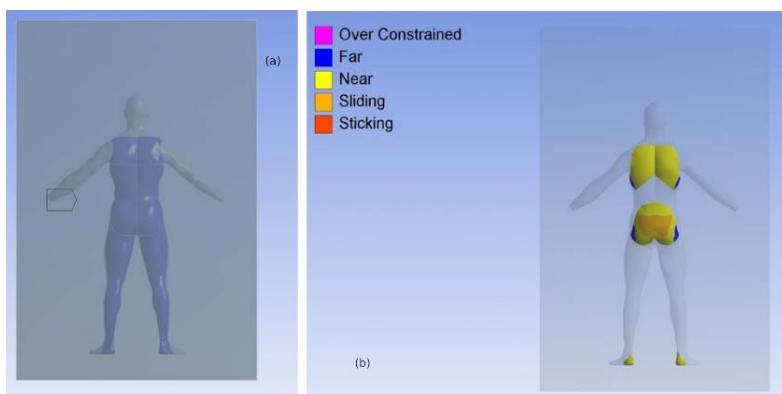**Figure 4.** FE model of human body and mattress



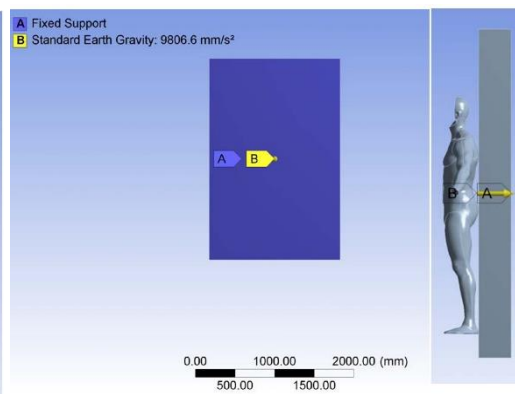**Figure 5.** Contact areas and contact status between the human body and the support surface



**Figure 6.** FE model boundary conditions

### 3.1 Computational evaluation of the equivalent elastic modulus of the spacer fabrics

The experimental results of the compression test performed in the first step are presented in Table 2 in terms of indentation and calculated elastic modulus under the constant load.

In Table 3 the measured density along with the evaluated equivalent elastic modulus of all the spacer fabrics is presented along with the error between the experimental and computationally calculated indentation on the vertical axis.

In Figure 7 the computationally evaluated vertical displacement is presented for samples A4 and A9 which have the maximum and minimum indentation and minimum and maximum computationally evaluated equivalent elastic modulus, respectively.

**Table 2.** Maximum indentation and calculated elastic modulus of each spacer fabric

| Sample | Indentation (mm) | Calculated E (Pa) |
|--------|------------------|-------------------|
| A1 | 1.00 | 51012 |
| A2 | 1.68 | 30364 |
| A3 | 0.99 | 51527 |
| A4 | 8.19 | 6851 |
| A5 | 1.68 | 36437 |
| A6 | 1.21 | 50590 |
| A7 | 1.01 | 60608 |
| A8 | 2.48 | 26740 |
| A9 | 0.04 | 1020240 |
| A10 | 0.35 | 174898 |
| A11 | 1.04 | 58860 |
| A12 | 0.94 | 54268 |
| A13 | 1.43 | 35673 |
| A14 | 0.12 | 425100 |
| A15 | 1.15 | 56057 |
| A16 | 1.21 | 44358 |
| A17 | 0.91 | 42159 |

**Table 3.** Calculated density and computed elastic modulus for all spacer fabrics

| Sample | Sample Density (kg/m³) | Computed Elastic Modulus (Pa) | Error (%) |
|--------|------------------------|-------------------------------|-----------|
| A1 | 51.00 | 32500 | -0.19 |
| A2 | 62.50 | 19250 | 0.09 |
| A3 | 103.50 | 32500 | -0.20 |
| A4 | 39.09 | 4220 | 0.02 |
| A5 | 68.75 | 22500 | 0.86 |
| A6 | 81.67 | 32000 | -0.34 |
| A7 | 91.67 | 37750 | 0.29 |
| A8 | 46.15 | 17000 | 0.30 |
| A9 | 61.25 | 670000 | 2.19 |
| A10 | 73.33 | 112500 | 0.37 |
| A11 | 93.33 | 37500 | 0.45 |
| A12 | 85.00 | 35500 | -0.49 |
| A13 | 46.00 | 23000 | -0.92 |
| A14 | 50.00 | 280000 | 0.71 |
| A15 | 90.00 | 29000 | -0.09 |
| A16 | 103.00 | 20900 | -0.08 |
| A17 | 53.50 | 37500 | -0.85 |
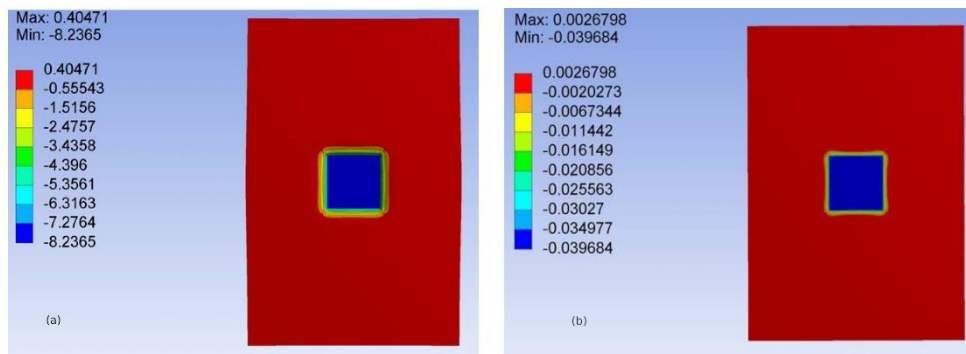


**Figure 7.** Vertical displacement of samples A4 (a) and A9 (b)

### 3.2 Computational evaluation of the base materials used as support surfaces

As mentioned above, in order to monitor the performance of all the spacer fabrics three different types of results are selected and presented below. The first group of results concerns the vertical deformation of the top surface of the mattress. In Table 4 the minimum and maximum values of vertical displacement are presented for all the samples.

**Table 4.** Vertical displacement of the upper surface of the mattress

| Sample | Minimum Uz [mm] | Maximum Uz [mm] |
|--------|-----------------|-----------------|
| A1 | -41.07 | -0.10 |
| A2 | -58.53 | -0.36 |
| A3 | -41.47 | -0.50 |
| A4 | -163.99 | -0.25 |
| A5 | -51.03 | -0.35 |
| A6 | -41.30 | -0.34 |
| A7 | -36.46 | -0.34 |
| A8 | -62.08 | -0.17 |
| A9 | -4.45 | -0.01 |
| A10 | -17.01 | -0.07 |
| A11 | -37.25 | -0.36 |
| A12 | -39.55 | -0.34 |
| A13 | -52.02 | -0.12 |
| A14 | -9.74 | -0.01 |
| A15 | -38.51 | -0.11 |
| A16 | -45.23 | -0.47 |
| A17 | -47.04 | -0.62 |

The maximum absolute value of the vertical displacement on the top surface of the mattress appears for sample A4 while the minimum one appears for sample A9. In Figure 8 the results of the vertical displacement in terms of contour are presented for these two samples. It is obvious that the body sinks further in the model consisting of the sample A4. The more the human body is sunk into the mattress the higher the interface area between the human body and the mattress is.

The second group of results concerns the stress distributions on the human body. In Table 5 these results are presented in terms of maximum/minimum absolute values.

Although the computational evaluation indicated that all spacer fabrics cause development of stresses in a similar way, the exact values of the mechanical magnitudes on the human body vary according to the spacer fabric used for the mattress. Sample A4 has the minimum value for the Von Mises Equivalent stress and the minimum values of Shear stress on XY plane, while sample A8 has the minimum value of Normal stress on Z axis. Figure 9 presents the contours of Von Mises Equivalent stress, Normal stress on Z axis and Shear stress on the XY plane for samples A4 and A8.

The maximum value of equivalent von Mises stress appears in the middle of the calves of the human body, while maximum Normal and Shear stress appear on the heels. This group of results is highly depended on the elastic modulus of the human body, so it can be only used if a full model of the human body is built with bones and soft tissue.
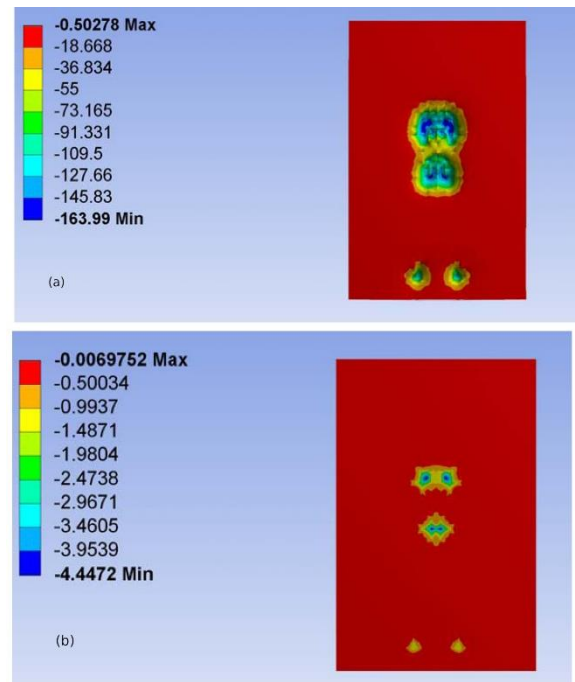


**Figure 8.** Vertical displacement of the upper area of the mattress for samples A4(a) and A9 (b)

**Table 5.** Stress results on human body

| Sample | Maximum Von Mises Equivalent Stress [MPa] | Minimum Normal Stress on Z Axis [MPa] | Minimum Shear Stress on XY plane [MPa] | Maximum Shear Stress on XY plane [MPa] |
|--------|---------|---------|---------|---------|
| A1 | 0.194 | -0.057 | -0.024 | 0.0194 |
| A2 | 0.182 | -0.049 | -0.023 | 0.0195 |
| A3 | 0.195 | -0.057 | -0.024 | 0.0193 |
| A4 | 0.158 | -0.085 | -0.019 | 0.0169 |
| A5 | 0.186 | -0.051 | -0.023 | 0.0194 |
| A6 | 0.195 | -0.057 | -0.024 | 0.0194 |
| A7 | 0.197 | -0.060 | -0.024 | 0.0195 |
| A8 | 0.180 | -0.047 | -0.023 | 0.0199 |
| A9 | 0.177 | -0.051 | -0.022 | 0.0181 |
| A10 | 0.190 | -0.054 | -0.023 | 0.0184 |
| A11 | 0.197 | -0.058 | -0.024 | 0.0194 |
| A12 | 0.196 | -0.057 | -0.024 | 0.0195 |
| A13 | 0.185 | -0.050 | -0.023 | 0.0193 |
| A14 | 0.199 | -0.054 | -0.024 | 0.0190 |
| A15 | 0.196 | -0.058 | -0.024 | 0.0194 |
| A16 | 0.191 | -0.054 | -0.023 | 0.0192 |
| A17 | 0.190 | -0.053 | -0.023 | 0.0190 |
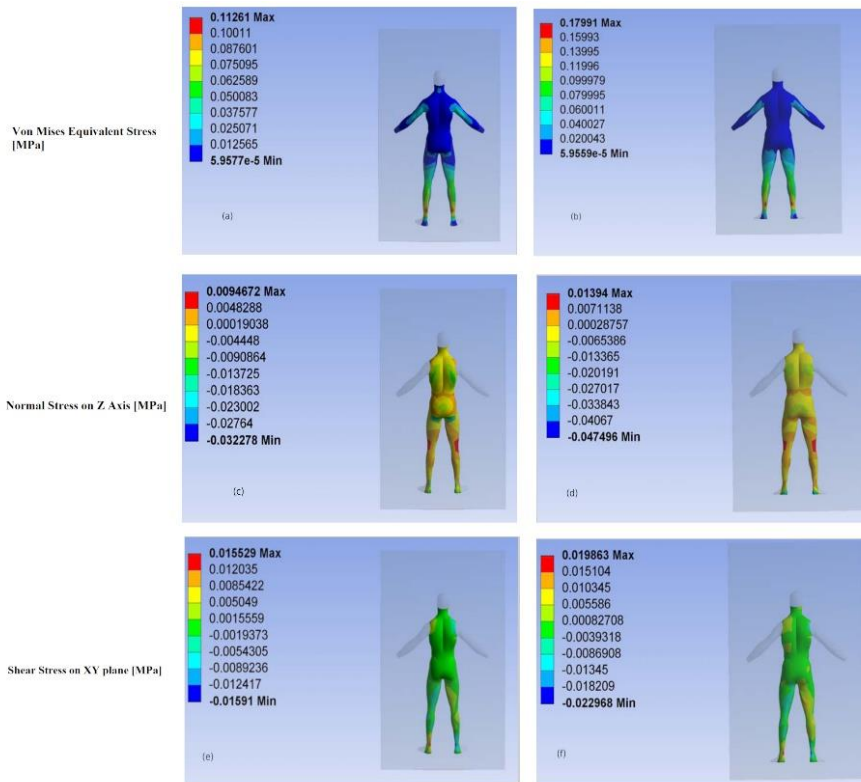
**Figure 9.** Stress contour of status, pressure and frictional stress on human body for samples A4 (a, c, e) and A8 (b, d, f)

In Table 6 the maximum values of pressure and frictional force on the interface between the human body and the mattress are presented.

**Table 6.** Maximum Pressure and frictional force on the interface

| Sample | Maximum Interface Pressure [MPa] | Maximum Frictional Stress [MPa] |
|--------|----------------------------------|----------------------------------|
| A1 | 0.0708 | 0.0163 |
| A2 | 0.0539 | 0.0241 |
| A3 | 0.0707 | 0.0162 |
| A4 | 0.0865 | 0.0305 |
| A5 | 0.0588 | 0.0150 |
| A6 | 0.0707 | 0.0162 |
| A7 | 0.0799 | 0.0156 |
| A8 | 0.0514 | 0.0229 |
| A9 | 0.0661 | 0.0138 |
| A10 | 0.0749 | 0.0080 |
| A11 | 0.0765 | 0.0156 |
| A12 | 0.0732 | 0.0151 |
| A13 | 0.0587 | 0.0182 |
| A14 | 0.0750 | 0.0076 |
| A15 | 0.0746 | 0.0163 |
| A16 | 0.0650 | 0.0150 |
| A17 | 0.0629 | 0.0154 |

The third group of results is presented in Figure 10, which concerns the area of the interface between the human body and the mattress. The contours of the interface pressure and the frictional stress for samples A8 and A14 that have the lower values of interface pressure and frictional stress respectively are presented. It is obvious that the areas of higher stresses are the areas of the calcaneus, the gluteus and the dorsum. As mentioned above the pressure threshold for non-developing pressure ulcers is considered the value of 32 mmHg i.e. 4266 Pa.

The maximum value of the pressure presented in Figure 10 is higher than the pressure threshold existing in the literature. On the other hand, the area of high pressure is very small, so it is interesting to see the percentage of contact area above this threshold.

### 3.3 Discussion

In this section the results of the preliminary qualitative evaluation of the seventeen spacer fabrics are going to be analysed proving the ability of the implemented methodology to produce useful sorted listings. Also, the proper interpretation and use of these listings is going to be discussed.

As far as the experimental results are concerned, the spacer fabric with maximum indentation under the load of 12.753 N is A4 with 8.19 mm while the spacer fabric with minimum indentation is A9 with 0.04 mm. In Figure 11 the experimentally measured indentation of each spacer fabric is presented as a percentage of its total thickness.

It is obvious that the most deformed sample is A4 while the less deformed are A9 and A14 with 0.5% and 1.2% of deformation. This means that A4 will have the lower elastic modulus, while A9 and A14 the larger. Observing Table 3 that correlation becomes clear. The rest of the samples show deformation ranging from 9 to 17%. In Figure 12 the values of the elastic modulus for every spacer fabric is presented. The samples are sorted according to the percentage of vertical deformation in the experiment from maximum to minimum.
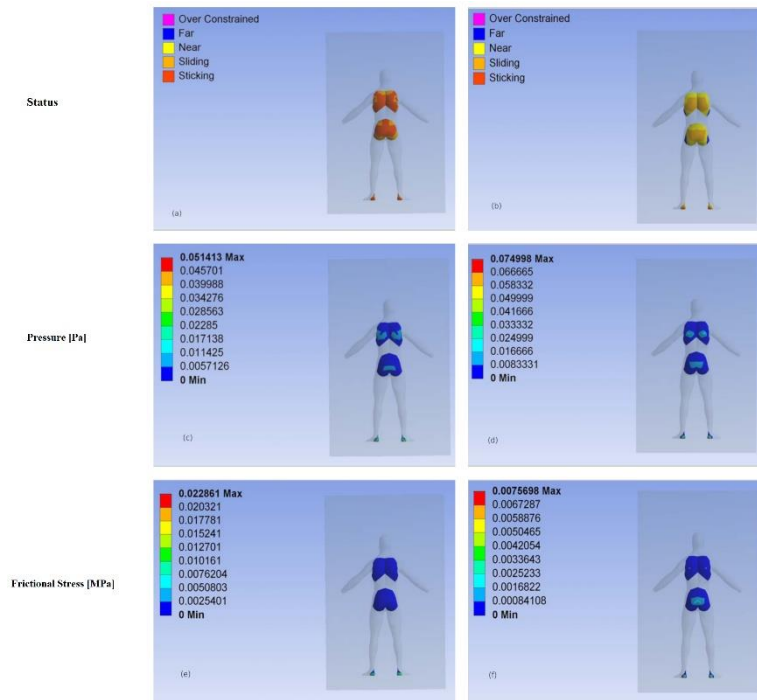


**Figure 10.** Stress contour of status, pressure and frictional stress on human body for samples A8 (a, c, e) and A14 (b, d, f)
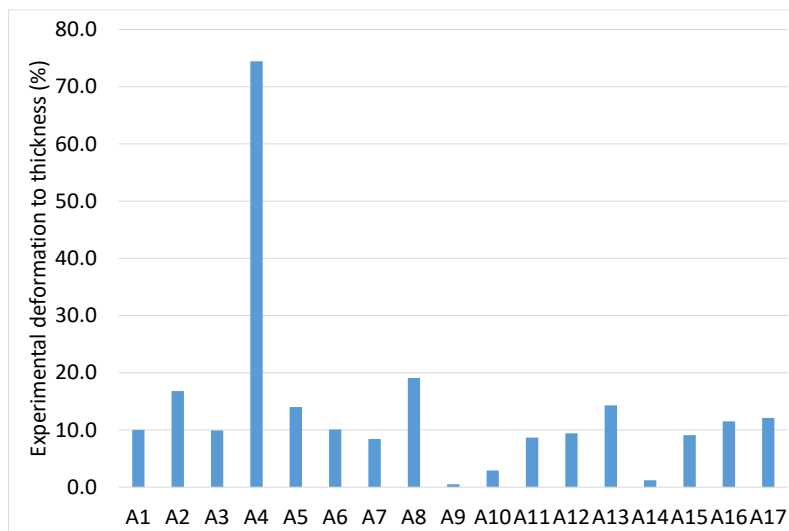


**Figure 11.** Experimental Indentation as a percentage of the total thickness of its sample

Most of the samples in Figure 12 (A13 – A7) have an elastic modulus in the range of (0.022 to 0.038 MPa). In Figure 13 the sorted listing of the samples used in the mattress according to their vertical deformation is presented.

In Figure 14 a sorted listing is presented. The spacer fabrics with the lowest percentage of area above the pressure threshold are A9, A14, A10, A7 and A11. For these samples the percentage under investigation is below the threshold under discussion. These samples represent also the samples with the lowest values of vertical deformation.

From the above results it appears that there is a strong correlation between the elastic modulus of the fabrics and the resultant stress on the human body. The specimens with lower vertical displacement had the greater elastic modulus and the smallest areas with pressure above the threshold. While this paper is indented to present a selection method for support surfaces, this finding illuminates an interesting aspect of the behaviour of the support surfaces on the human body providing a quantitative criterion.

The fabrics with best behaviour based on the lower pressure area are A9, A14, A10, A7 and A11. Thus, it is of interest to obtain more information about these samples. Figures 15 and 16 present the outside layer of the 3D fabrics and the connecting filament layer respectively, and at Table 7 the structural characteristics of the samples are presented as well.
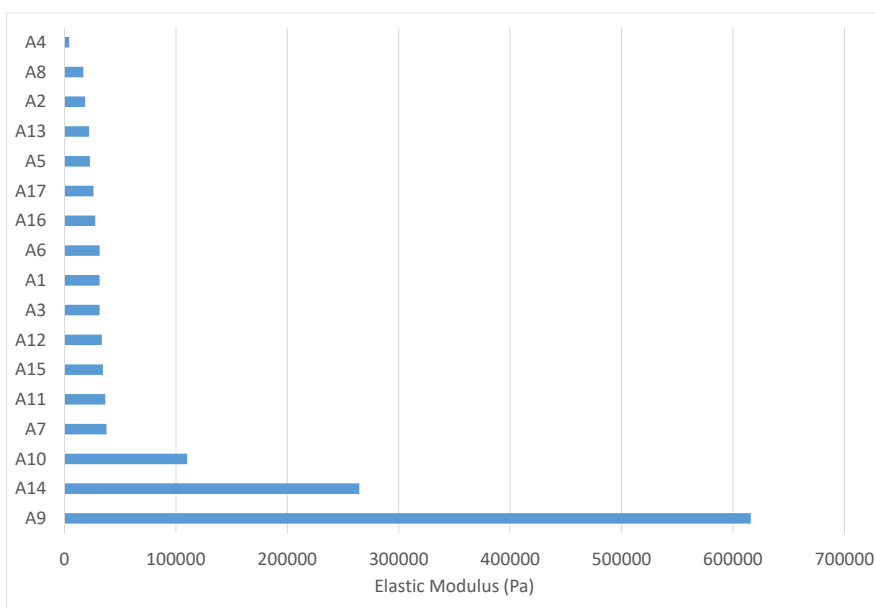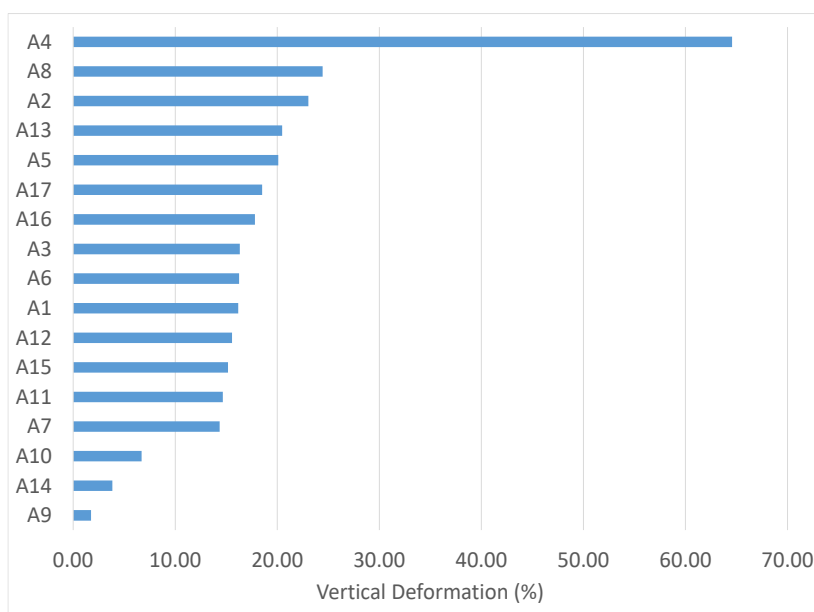


**Figure 12.** Computed elastic modulus per sample



**Figure 13.** Percentage of the maximum vertical displacement of the top area of the mattress
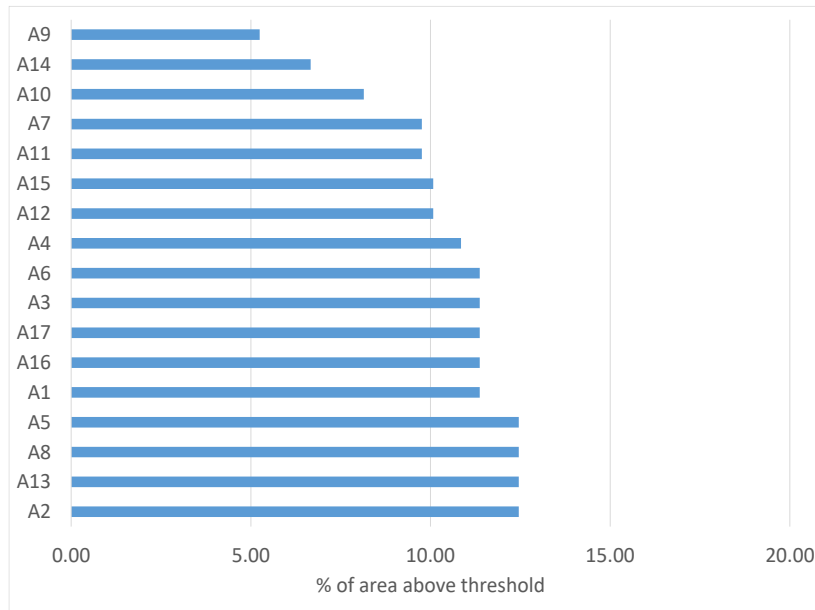
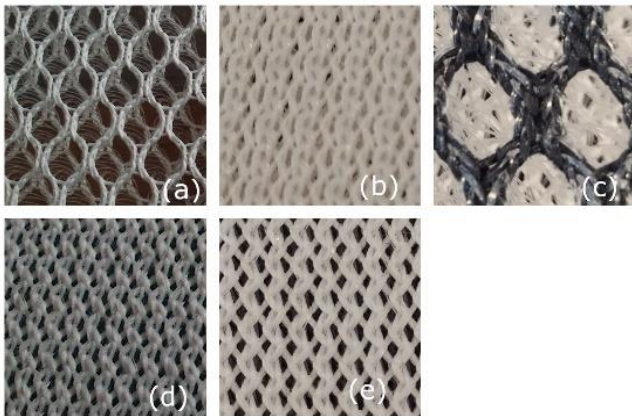**Figure 14.** Area with pressure above threshold



**Figure 15.** Outside layer of samples (a) A9, (b) A14, (c) A10, (d) A7, (e) A11.
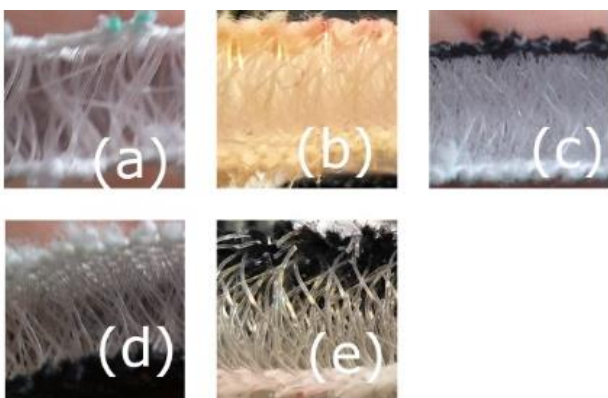


**Figure 16.** Interconnecting filament layer of samples (a) A9, (b) A14, (c) A10, (d) A7, (e) A11.

As can be seen, the specimens show an evident variability to their structural characteristics – i.e. a mixture of open and closed structures as well as a variety of the number of yarn loops on the outer surfaces of the samples. The relationship between this variety of structures and the elastic modulus of each specimen can be subject to future research.

**Table 7.** Structural characteristics of specimens with the lowest percentage of area above the pressure threshold

| Sample | Yarn count (dTex) | | Number of loops per 10 cm$^2$ | |
|--------|-------|------|-------|------|
| | **Front** | **Back** | **Front** | **Back** |
| A9 | 600 | 600 | 20x74 | 21x74 |
| A14 | 600 | 600 | 66x54 | 66x52 |
| A10 | 1080 | 600 | 28x32 | 60x50 |
| A7 | 1080 | 600 | 36x27 | 70x34 |
| A11 | 600 | 600 | 64x60 | 62x62 |

## 4. CONCLUSION

In the present paper a methodology for the preliminary assessment of medical support surfaces, based on simulation driven design is presented. This methodology can be used, before the clinical trial, and it involves FE modelling of the interaction between the support surface and the human body while lying down. The main advantage of the proposed methodology is that it can eliminate materials unsuitable for the use as primary material for medical support surface from the time consuming and costly stage of clinical trial. More specifically, in the present paper, this methodology has been used for the evaluation of different spacer fabrics suitable for support surfaces. The outcome of the proposed methodology is sorted listings of the candidate materials based on their properties and suitability for the specific use. This methodology can be a precious selection tool based on the mechanical performance of different materials, before

creating the actual prototype support surface which must undergo through clinical trials.

A significant advantage of the proposed methodology is that it can be easily expanded to other materials and different body types or body positions because of the versatility of the FE method. Thus, it can be used, also, for the evaluation of materials like foams, since FE method can incorporate non-linear material properties, such as creep, present in materials like foam. Additionally, the weight of the simulated human body, as well as its material properties and body posture, can be altered leading to the evaluation of different anthropometry data.

Although, within this paper, sorted listings, concerning, mainly, the deformation and the interface pressure of different fabric spacers have been provided implementing the proposed methodology, these listings can become more detailed enhancing the experimental investigation of the materials and subsequently the computational models. The FE models, used for the final evaluation of the spacer fabrics, could contain information for time – depended material properties, such as stress relaxation and fatigue. Additionally, also the computational model of the human body can become more accurate embedding also material nonlinearities. The FE model of human body used in this methodology can be created using CTs, including the changes in the pressure contours because of bony areas, muscle and ligament topology inside the body. The creation of patient specific models of the human body could allow the development of patient specific support surfaces.

## REFERENCES

1. Stannard, D. 2012. Support Surfaces for Pressure Ulcer Prevention. *Journal of PeriAnesthesia Nursing*, *27*(5), 341–342. DOI 10.1016/j.jopan.2012.07.007

2. McInnes, E., Jammali-Blasi, A., Bell-Syer, S. E., Dumville, J. C., & Cullum, N. 2011. Support surfaces for pressure ulcer prevention. In The Cochrane Collaboration (Ed.), *Cochrane Database of Systematic Reviews*. Chichester, UK: John Wiley & Sons, Ltd. DOI 10.1002/14651858.CD001735.pub4

3. Zeller, J. L., Lynm, C., & Glass, R. M. 2006. Pressure Ulcers. *JAMA*, 296(8), 1020. DOI 10.1001/jama.296.8.1020

4. Thomas, D. R. 2006. Prevention and Treatment of Pressure Ulcers. *Journal of the American Medical Directors Association*, 7(1), 46–59. DOI 10.1016/j.jamda.2005.10.004

5. Landis, E. M. (1930). Micro-injection studies of capillary blood pressure in human skin. *Heart*, *15*, 209–228.

6. Campbell, C., & Parish, L. C. 2010. The decubitus ulcer: Facts and controversies. *Clinics in Dermatology*, *28*(5), 527–532. DOI 10.1016/j.clindermatol.2010.03.010

7. Support Surface Standards Initiative (S3I), Terms and Definitions, National Pressure Ulcer Advisory Panel (NPUAP) accessed 12.03.14

8. Phillips, L. 2007. Interface pressure measurement: Appropriate interpretation of this simple laboratory technique used in the design and assessment of pressure ulcer management devices. *Primary Intention: The Australian Journal of Wound Management*, *15*(3), 106–113.

9. Phillips, L., Goossens, R., Takahashi, M., & Clark, M. (2012). Defining 'active' pressure redistribution. *Wounds International*, *3*(3), 52–56.

10. Tissue Viability Society. 2010. Laboratory measurement of the interface pressures applied by active therapy support surfaces: A consensus document. *Journal of Tissue Viability*, *19*(1), 2–6. DOI 10.1016/j.jtv.2009.11.010

11. Whittemore, R. 1998. Pressure-reduction support surfaces: A review of the literature. *Journal of WOCN*, *25*(1), 6–25. DOI 10.1016/S1071-5754(98)90009-2

12. World Medical Association Declaration of Helsinki. 2001. Ethical principles for medical research involving human subjects. *Bull World Health Organ*, (79), 373–374.

13. DiMasi, J. A., Hansen, R. W., & Grabowski, H. G. 2003. The price of innovation: new estimates of drug development costs. *Journal of Health Economics*, *22*(2), 151–185. DOI 10.1016/S0167-6296(02)00126-1

14. Taktak, A. F. G., Ganney, P., Long, D., & White, P. (Eds.). 2014. *Clinical engineering: a handbook for clinical and biomedical engineers* (First edition). Amsterdam Waltham, MA: Elsevier : Academic Press.

15. Yoshida, H., Kamijo, M., & Shimizu, Y. 2012. A Study to Investigate the Sleeping Comfort of Mattress using Finite Element Method. *Kansei Engineering International Journal*, *11*, 155–162. DOI 10.5057/kei.11.155

16. Silber G, & Then C. 2009. Numerical analysis of the interactions between human body soft tissue and body supports.Simulia Customer Conference. 2009.

17. Makhsous, M., Dohyung Lim, Hendrix, R., Bankard, J., Rymer, W. Z., & Fang Lin. 2007. Finite Element Analysis for Evaluation of Pressure Ulcer on the Buttock: Development and Validation. *IEEE Transactions on Neural Systems and Rehabilitation Engineering*, *15*(4), 517–525. DOI 10.1109/TNSRE.2007.906967

18. Levy, A., Kopplin, K., & Gefen, A. 2014. An air-cell-based cushion for pressure ulcer protection remarkably reduces tissue stresses in the seated buttocks with respect to foams: Finite element studies. *Journal of Tissue Viability*, *23*(1), 13–23. DOI 10.1016/j.jtv.2013.12.005

19. Vassiliadis, S., Matsouka, D., Vossou, C. G., & Prekas, K. 2014. Computational evaluation of hospital mattresses. "Computational evaluation of hospital mattresses." 2nd International Congress On Healthcare And Medical Textiles, September 25-26, 2014, Izmir, Turkey.

20. Defloor, Tom. 1999. The Risk of Pressure Sores: a Conceptual Scheme. *Journal of Clinical Nursing*, *8*(2), 206–216.

21. Wollina, U., Heide, M., Muller-Litz, W., Obenauf, D., & Ash, J. 2003. Functional Textiles in Prevention of Chronic Wounds, Wound Healing and Tissue Engineering. In P. Elsner, K. Hatch, & W. Wigger-Alberti (Eds.), *Current Problems in Dermatology* (Vol. 31, pp. 82–97). Basel: KARGER. DOI 10.1159/000072239

22. Vassiliadis S., Kallivretaki A., Psilla N., Provatidis C., Mecit D. and Roye A., 2009 Numerical modelling of the compressional behaviour of warp-knitted spacer fabrics. Fibres & Textiles in Eastern Europe 17.5: 76

23. Grabcad. (n.d.). [CAD Library]. Retrieved 15 March 2014, from www.grabcad.com

24. Mukherjee, S., Chawla, A., Mohan, D., & Metri, M. 2003. Modelling of body parts consisting of bones as well as soft tissues: an experimental and finite element study. In *Proceedings of IRCOBI conference* (pp. 567–568).

25. Gropper, S. S., & Smith, J. L. (2012). *Advanced nutrition and human metabolism* (6th Ed). Belmont, OH: Cengage Learning.

26. Yoshida, H., Kamijo, M., & Shimizu, Y. 2012. A Study to Investigate the Sleeping Comfort of Mattress using Finite Element Method. *Kansei Engineering International Journal*, *11*, 155–162. DOI 10.5057/kei.11.155

# Investigation of Electromagnetic Shielding and Solar Properties of Woven Fabrics made by Barium titanate/Polyester Bicomponent Yarns

Rumeysa Celen, Yusuf Ulcay

Bursa Uludag University/ Faculty of Engineering/ Department of Textile Engineering

**Corresponding Author:** Rumeysa Celen, rumeysa@uludag.edu.tr

## ABSTRACT

In this study, electromagnetic shielding and solar properties of woven fabrics which were produced barium titanate/polyester bicomponent yarns were investigated. 1, 2 and 3% additive ratios of barium titanate and three different fabric structures (1/1 plain, sateen and special weave) were used in the experiments. The effect of additive ratio and the fabric structure on sheet resistance and electromagnetic shielding properties were evaluated. Electromagnetic Shielding Effectiveness (EMSE) of the woven fabrics was determined according to the ASTM D4935-10 standard by using coaxial transmission line measurement technique in the frequency range of 15–3000 MHz. The fabric with the highest content of the barium titanate (3%) and special weave showed the highest shielding effectiveness, reaching 13.96 dB at 15 MHz. The solar properties were measured according to EN14500 using a UV/VIS/NIR spectrophotometer and results were calculated according to EN 410 standard. The reflectance values of barium titanate added polyester fabrics increased and the transmittance values decreased.

## 1. INTRODUCTION

With the advancement of wireless technology, electronic devices become indispensable parts of our daily lives. These devices raise different radiations in different frequency bands [1]. The electronic devices are capable of emitting electromagnetic waves that will result in some electromagnetic interference (EMI) troubles [2, 3, 4]. Electromagnetic interference (EMI) shielding is a process of limiting the penetration of electromagnetic rays into a space by blocking them by a barrier made of conductive material. It is a very popular method of protecting electronic and electrical equipment and even people against electromagnetic radiation. The material or protector which protects a body, environment or circuit from harmful electromagnetic radiation is called a shield. Shields are used either to isolate a space from outside sources of electromagnetic radiation or to prevent the unwanted emission of electromagnetic energy radiated by internal sources [5].

The EMI phenomena can be viewed as a kind of environmental pollution of the electromagnetic spectrum [6, 7]. It is one of the major problems to be resolved. Various researchers and industrial companies have shown keen interest in providing solutions to overcome this problem. Among the various solutions offered, textile products and textile-based composite materials have caught the attention of researchers [8, 9]. In recent years, conductive fabrics have been considered for electromagnetic shielding and anti-electrostatic purposes in various applications for the defense, electrical, and electronic industries. This is mainly due to their desirable properties in terms of flexibility, electrostatic discharge, EMI protection, radio frequency interference protection, thermal expansion matching, and weight [10]. In the literature, there are many studies about

**To cite this article:** *Celen R, Ulcay Y. 2020. Investigation of Electromagnetic Shielding and Solar Properties of Woven Fabrics made by Barium titanate/Polyester Bicomponent Yarns. Tekstil ve Konfeksiyon, 30(4), 251-261.*

conductive textiles and their electromagnetic shielding applications [11-17 etc.]

In the advancement of EM wave absorber technology, wide variety of materials have received much attention, such as dielectric/magnetic materials [18-25] and conducting polymers [26-29]. Barium titanate (BaTiO3) is a member of the perovskite compounds family has ferroelectric properties with high dielectric constants [30]. Due to its unique properties (mechanical and chemically stable, high dielectric constant, etc.), barium titanate is one of the most important ferroelectric materials studied in a wide range [31]. Among other ferroelectrics, BaTiO3 is a well-referenced, relatively cheap to produce, and lead-free material [32, 33]. In the literature, there are some studies about electromagnetic shielding properties of barium titanate additive textile structures and the results of these studies are promising. Most of these studies have focused on the composite structures [26, 34, 35] and also in the literature, there is a gap in the use of barium titanate in conductive fiber/yarn production. However, there are limited studies about the solar properties of barium titanate and these studies focused on barium titanate added composites and film structures [36-38].

In our previous study [39], mechanical properties and electrical conductivity properties of barium titanate/ polyester bicomponent yarns were investigated. Knitted fabrics were produced from bicomponent yarns with two different fabric densities using a circular knitting machine. The effects of additive ratio and the fabric density on electromagnetic shielding efficiency (EMSE) were investigated. In the present study, woven fabrics were produced from the same bicomponent yarns with three different fabric constructions (plain, sateen and special weave). EMSE performance of the fabrics was determined according to the ASTM D4935-10 standards by using a coaxial transmission line measurement technique in the frequency range of 15–3000 MHz. The effect of additive ratio and the fabric weave type on EMSE were investigated. Besides EMSE properties, solar properties of woven fabrics were also evaluated in the 280-2500 nm range of the electromagnetic spectrum. For the first time, electromagnetic shielding and solar properties of barium titanate added textiles were evaluated together.

## 2. MATERIAL AND METHOD

### 2.1 Bicomponent Yarns

Barium titanate/polyester (core/sheath) bicomponent yarns were used in the study. Bicomponent yarns were spun using the Spinboy melt spinning machine. Three different adding ratios of the barium titanate masterbatch (1%, 2% and 3%) were tested. The core/sheath ratio was 30/70. Bicomponent yarns consist of 72 filaments.

Optical microscope images of bicomponent yarns were taken with Projectina optical microscope with an objective of 40 X. Scanning electron microscope (SEM) images of bicomponent yarns were taken with Carl Zeiss / Gemini 300. The magnification rate was chosen as 2000X and 3000 X. Differential scanning calorimeter (DSC) thermal analysis of reference (%100 polyester) and bicomponent yarns were carried out on a Mettler Toledo DSC 823 according to ISO 11357-7 standard. To determine the inorganic (barium titanate) content of bicomponent yarns, % ash content test was applied according to the ASTM D5630-01 standard. Three measurements were taken for each bicomponent yarn, and the average % ash content was calculated.

### 2.2 Woven Fabrics

The woven fabrics used in this study were successfully produced on a dobby weaving machine (DORNIER®). The woven fabrics with 1/1 plain, sateen and special weave were made using the three different additive ratios of the bicomponent yarns. Fabric weave types were shown in Figure 1 schematically.

The properties of the reference and woven fabrics were given in Table 1. Mass per unit area measurements were carried out by the TS 251 standard. Each sample was weighed three times on a precision scale, and the average value was calculated. Thickness measurements were made according to TS 7128 EN ISO 5084 standard with James Heal's R & B Cloth thickness tester. Three measurements were taken for each fabric, and the average thickness values were calculated.

Optical microscope images were taken with Mshot MS 60 digital microscope instrument. Figure 2 showed the optical images of 1B, 1S and 1O coded fabrics.
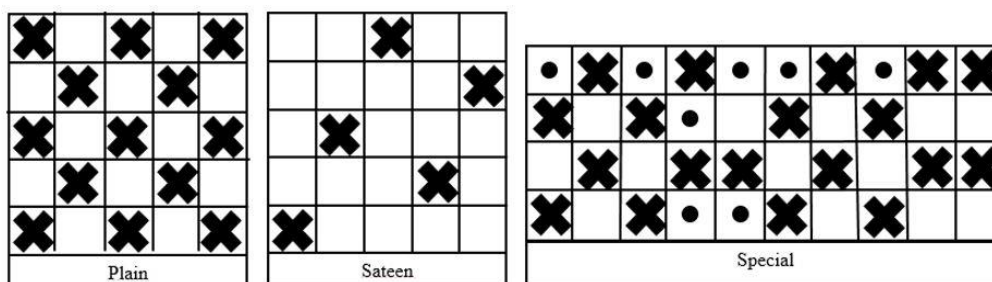


**Figure 1.** Schematic view of woven fabrics

**Table 1.** Specifications of the woven fabrics

| Fabric Code | Yarn Count (dtex) | Warp Density (1/cm) | Weft density (1/cm) | Mass per unit area (g/m²) | Fabric Thickness (mm) | Constructions |
|---|---|---|---|---|---|---|
| REF-B | 260 | | | 157 | 0.31 | 1/1 Plain |
| 1B | 261 | | | 192 | 0.37 | 1/1 Plain |
| 2B | 261 | | | 192 | 0.41 | 1/1 Plain |
| 3B | 263 | | | 195 | 0.40 | 1/1 Plain |
| REF-S | 260 | | | 157 | 0.35 | Sateen |
| 1S | 261 | | | 184 | 0.47 | Sateen |
| 2S | 261 | 45 | 18 | 180 | 0.47 | Sateen |
| 3S | 263 | | | 183 | 0.48 | Sateen |
| REF-O | 260 | | | 156 | 0.39 | Special |
| 1O | 261 | | | 189 | 0.52 | Special |
| 2O | 261 | | | 187 | 0.55 | Special |
| 3O | 263 | | | 189 | 0.52 | Special |
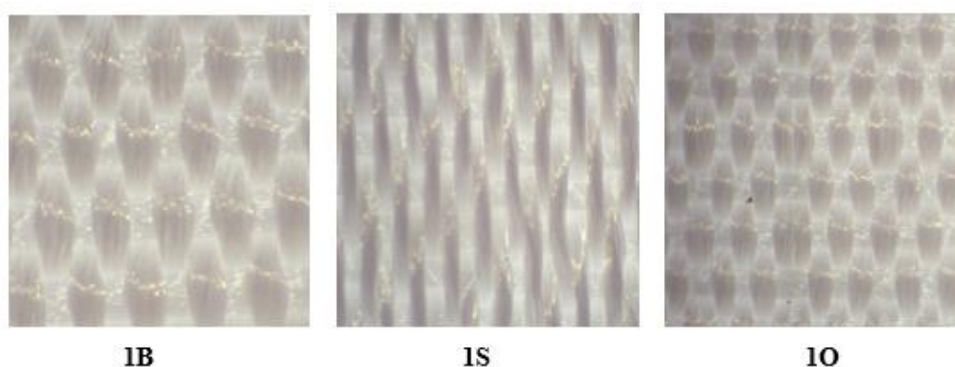


**Figure 2.** Optical images of woven fabrics

### 2.3 Sheet Resistance and Electromagnetic Shielding Effectiveness Measurement

The sheet resistance of the fabrics was measured ENTEK Electronics Four Point Probe instrument. Ten measurements were taken for each fabric, and the average sheet resistance values were calculated.

EMSE of woven fabrics was determined according to the ASTM D4935-10 standards by using coaxial transmission line measurement technique in the frequency range of 15–3000 MHz. The compact testing equipment (Electro-Metrics Inc., model EM-2107 A) (Figure 3) was utilized to measure the EMSE of the materials. Woven fabrics were conditioned at 20ºC± 2°C temperature and 65% ± 2% relative humidity. Measurements were repeated three times on different areas of the fabrics and the average values of the measurements were calculated according to Equation (1)

$$SE\ [dB] = 20 \log \frac{E_0}{E_1} \qquad (1)$$

where $E_0$ is measured without the fabric sample and $E_1$ is measured with the fabric sample on the test area.

Requirements for electromagnetic shielding textiles are specified and classified (Table 2) by the Functional Technical Textiles Standard [40]. To test the EMSE of the textiles, the coaxial transmission line method specified in ASTM D 4935 was referred to in this classification. According to this standard, professional uses include medical equipment, quarantine material, professional security uniform for an electronic manufacturer, electronic kit, or other new applications; general uses include casual wear, office uniform, maternity dress, apron, consumptive electronic products, and communication-related products.

### 2.3 Spectroscopic Analysis

The solar properties of the fabrics were examined with measurements that performed with Shimadzu UV-3600 Plus spectrophotometer with an integrating sphere at the range of 280-2500 nm. Transmission and reflection were measured and the results were calculated with an excel program according to EN 410 standard. The visible transmittance ($T_V$: 380-780 nm), visible reflectance ($R_V$: 380-780 nm), solar transmittance ($T_S$: 300-2500), solar reflectance ($R_S$: 300-2500) and UV transmittance ($T_{UV}$: 280-380 nm) were calculated by using Equations (2-6) according to the EN 410 standard.
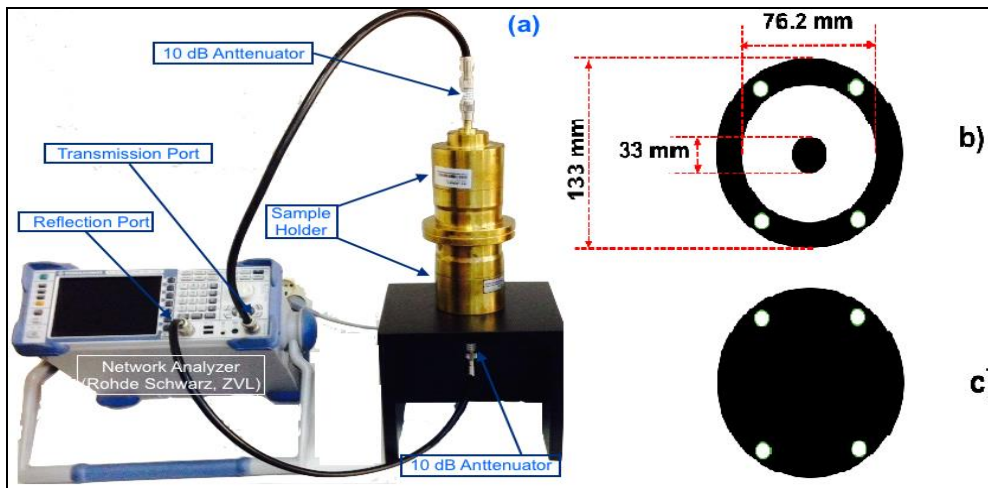
**Figure 3.** EMSE test instrument, (a) Set up of the EMSE testing apparatus; (b) and (c) Specimen for reference and load, respectively.

**Table 2.** Functional technical textile standard [40]

| Type | Grade | Shielding Effectiveness [dB] | Classification |
|---|---|---|---|
| | AAAAA | SE> 60 dB | Excellent |
| | AAAA | 60 dB ≥SE> 50 dB | Very Good |
| Class I | AAA | 50 dB ≥SE> 40 dB | Good |
| [Professional Use] | AA | 40 dB ≥SE> 30 dB | Moderate |
| | A | 30 dB ≥SE> 20 dB | Fair |
| | AAAAA | SE> 30 dB | Excellent |
| | AAAA | 30 dB ≥SE> 20 dB | Very Good |
| Class II | AAA | 20 dB ≥SE> 10 dB | Good |
| [General Use] | AA | 10 dB ≥SE>7 dB | Moderate |
| | A | 7 dB ≥SE> 5 dB | Fair |

$$T_V(\%) = \frac{\sum_{\lambda=380}^{780} D_\lambda \tau(\lambda) V(\lambda) \Delta\lambda}{\sum_{\lambda=380}^{780} D_\lambda V(\lambda) \Delta\lambda} \qquad (2)$$

$$Rv(\%) = \frac{\sum_{\lambda=380}^{780} D_\lambda \rho(\lambda) V(\lambda) \Delta\lambda}{\sum_{\lambda=380}^{780} D_\lambda V(\lambda) \Delta\lambda} \qquad (3)$$

$$Ts(\%) = \frac{\sum_{\lambda=300}^{2500} S_\lambda \tau(\lambda) \Delta\lambda}{\sum_{\lambda=300}^{2500} S_\lambda \Delta\lambda} \qquad (4)$$

$$Rs(\%) = \frac{\sum_{\lambda=300}^{2500} S_\lambda \rho(\lambda) \Delta\lambda}{\sum_{\lambda=300}^{2500} S_\lambda \Delta\lambda} \qquad (5)$$

$$T_{UV}(\%) = \frac{\sum_{\lambda=280}^{380} U_\lambda \tau(\lambda) \Delta\lambda}{\sum_{\lambda=280}^{380} U_\lambda \Delta\lambda} \qquad (6)$$

where $D\lambda$ is relative spectral distribution of illuminant D65, $\tau(\lambda)$ is the spectral transmittance of the material, $V(\lambda)$ is the spectral luminous efficiency for photonic vision, $\Delta\lambda$ is the wavelength interval, $\rho(\lambda)$ is the spectral reflectance of the material, $S\lambda$ is the relative spectral distribution of the solar radiation and $U\lambda$, is the relative distribution of the UV part of the global solar radiation [41].

## 3. RESULTS AND DISCUSSION

### 3.1 Characterization Results of Bicomponent Yarns

Table 3 showed the % ash content of bicomponent samples. With this analysis, an inorganic additive ratio (%) was

observed. Ash values of bicomponent samples were almost consistent with applied additive ratios.

**Table 3.** Ash content of samples

| Description | Ash Content [%] |
|---|---|
| 1% BaTiO$_3$ additive bicomponent yarn | 1.02 |
| 2% BaTiO$_3$ additive bicomponent yarn | 1.91 |
| 3% BaTiO$_3$ additive bicomponent yarn | 2.88 |

Optical cross-section images and SEM images of bicomponent yarns were given in Figures 4 and 5, respectively. The core-sheath structure of bicomponent yarns was seen obviously. It was seen that bicomponent yarns had homogenous structures.

DSC analysis of the barium titanate additive bicomponent yarns and reference polyester yarn was given in Figure 6. In the DSC graphic, an endothermic melting peak belonging to the polyester was observed at approximately 250 ºC. The melting began at 246 ºC and finished at 259 ºC in the DSC graph of the reference polyester yarn. The increase of 8 ºC for the melting point of the melting curve of the 3% additive bicomponent yarn was evaluated to reflect the effect of the barium titanate on the melting temperature. No

peak related to the barium titanate, which does not degrade below 1650 ºC, was observed.

## 3.2 Sheet Resistance and Electromagnetic Shielding Effectiveness Test Results

It is well known that electrical conductivity depends on the amount of the conductive component. The electrical conductivity is inversely proportional to the sheet resistance. The effect of the additive ratio and fabric type on the sheet resistance of woven fabrics was investigated, and it was shown graphically in Figure 7. Sheet resistance values decreased slightly, with an increasing additive ratio. Consistent with previous studies [26, 34, 49], barium titanate additive decreased electrical resistance. Fabric weave type did not affect sheet resistance significantly. The lowest sheet resistance was 125 M$\Omega$/sq for the 3S coded sample.
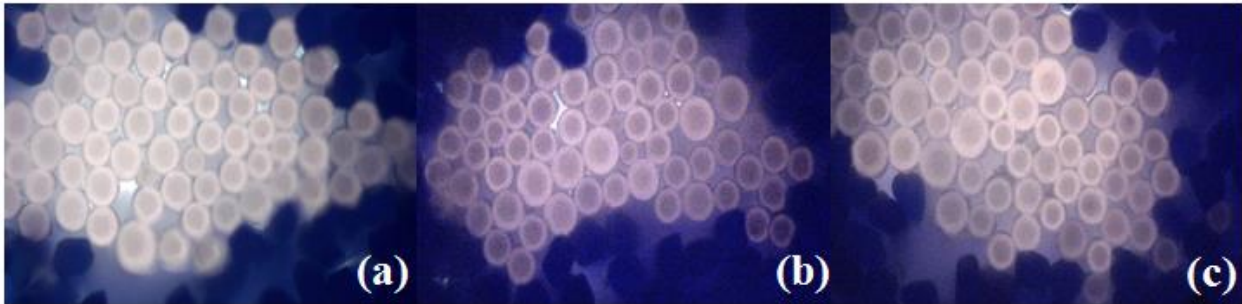


**Figure 4.** Optical cross-section images of bicomponent yarns; (a) 1% BaTiO$_3$ additive, (b) 2% BaTiO$_3$ additive, (c) 3% BaTiO$_3$ additive (Mag= 40X)
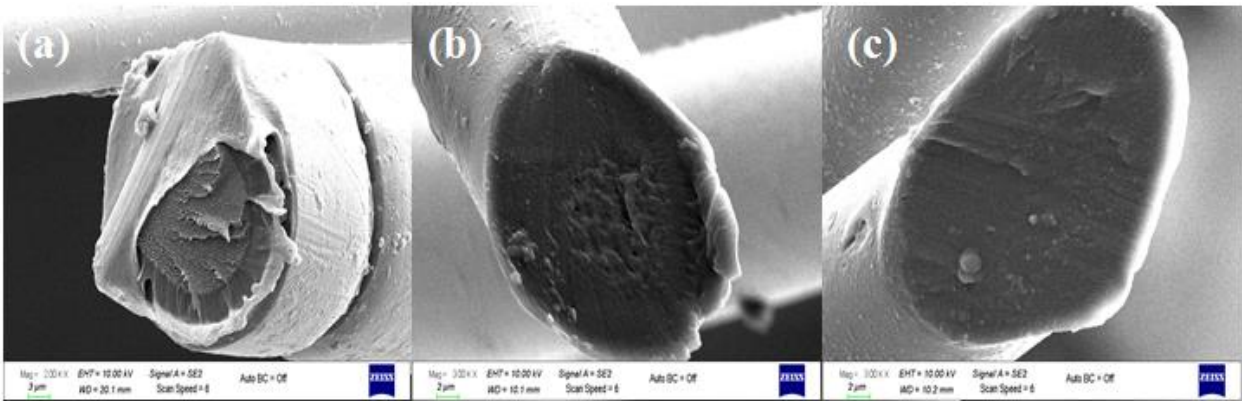


**Figure 5.** SEM images of bicomponent yarns; (a) 1% BaTiO$_3$ additive (Mag= 2000X), (b) 2% BaTiO$_3$ additive (Mag= 3000X), (c) 3% BaTiO$_3$ additive (Mag= 3000X)
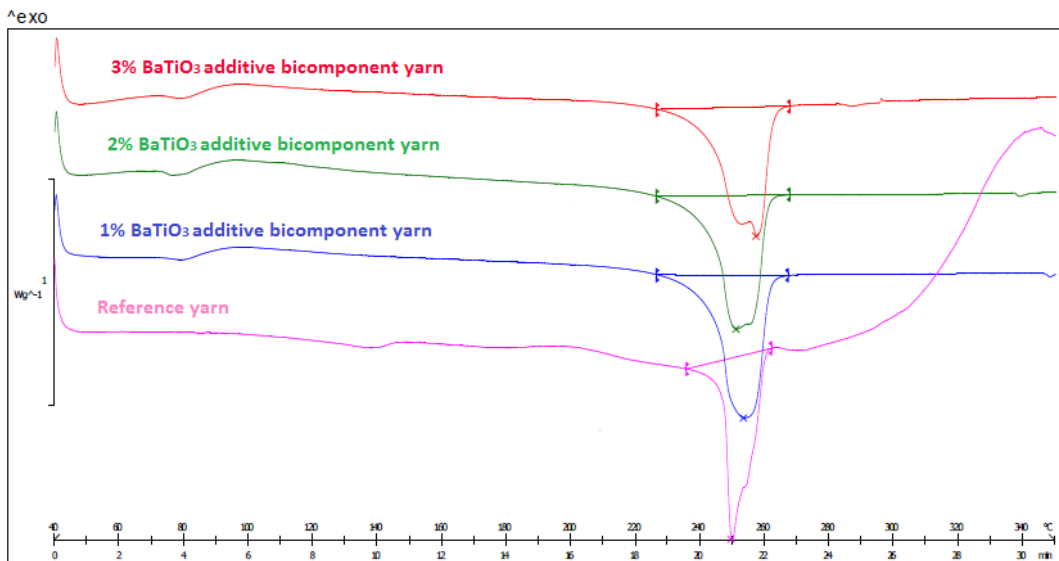
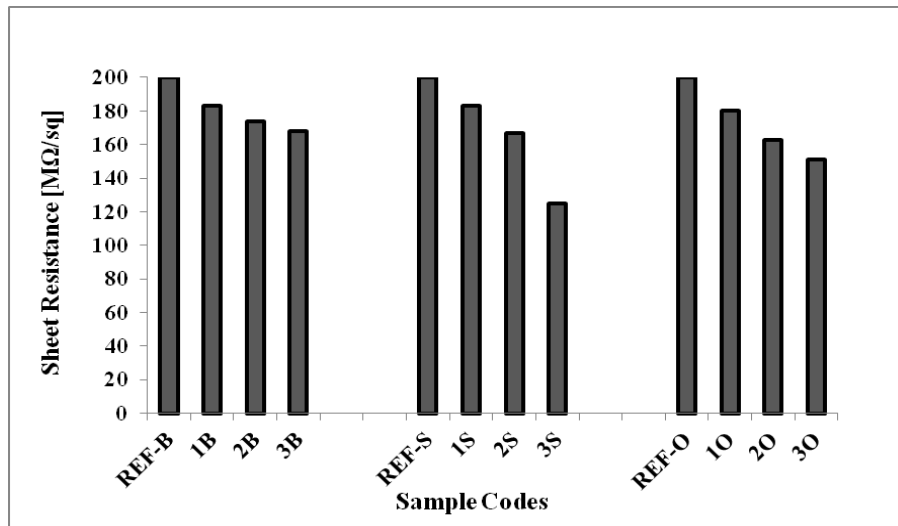

**Figure 6.** DSC analysis of yarns

**Figure 7.** Sheet resistance test results

EMSE results of fabrics at 15 MHz were summarized in Table 4. Figure 8 displayed the EMSE values of REF-B, 1B, 2B and 3B coded plain fabrics with the frequency in the range from 15 MHz to 315 MHz. Although the measurements were performed in 15-3000 MHz frequency range, shielding efficiency values were 0 dB after 315 MHz. Therefore, the graphics only covered the frequency range at 15-315 MHz. The shielding effectiveness values of the reference fabrics (REF-B, REF-S and REF-O) produced with 100% polyester yarns were found to be 0-2 dB, as could be seen in Figures 8, 9 and 10. It is well known that polymers are generally insulating materials and can not shield the electromagnetic waves. The SE values of 1B, 2B and 3B were in the range of 4-7 dB until 45 MHz. The highest SE values were recorded 11.93, 11.98 and 12.32 dB at 15 MHz for 1B, 2B and 3B coded fabrics.

**Table 4.** EMSE results

| Fabric codes | EMSE [dB], f= 15 MHz |
|---|---|
| REF-B | 0.94 |
| 1B | 11.93 |
| 2B | 11.98 |
| 3B | 12.32 |
| REF-S | 0.95 |
| 1S | 13.23 |
| 2S | 13.03 |
| 3S | 13.44 |
| REF-O | 0.93 |
| 1O | 13.93 |
| 2O | 13.90 |
| 3O | 13.96 |

Figure 9 displayed the EMSE values of REF-S, 1S, 2S and 3S coded sateen fabrics with the frequency range from 15 MHz to 315 MHz. The SE values of 1S, 2S and 3S were in the range of 4-8 dB until 45 MHz. The highest SE values were recorded 13.23, 13.03 and 13.44 dB at 15 MHz for 1S, 2S and 3S coded fabrics.

Figure 10 displayed the EMSE values of REF-O, 1O, 2O and 3O coded special weave fabrics with the frequency range from 15 MHz to 315 MHz. The SE values of 1O, 2O and 3O were in the range of 4-9 dB until 60 MHz. The highest SE values were recorded 13.93, 13.90 and 13.96 dB at 15 MHz for 1O, 2O and 3O coded fabrics.
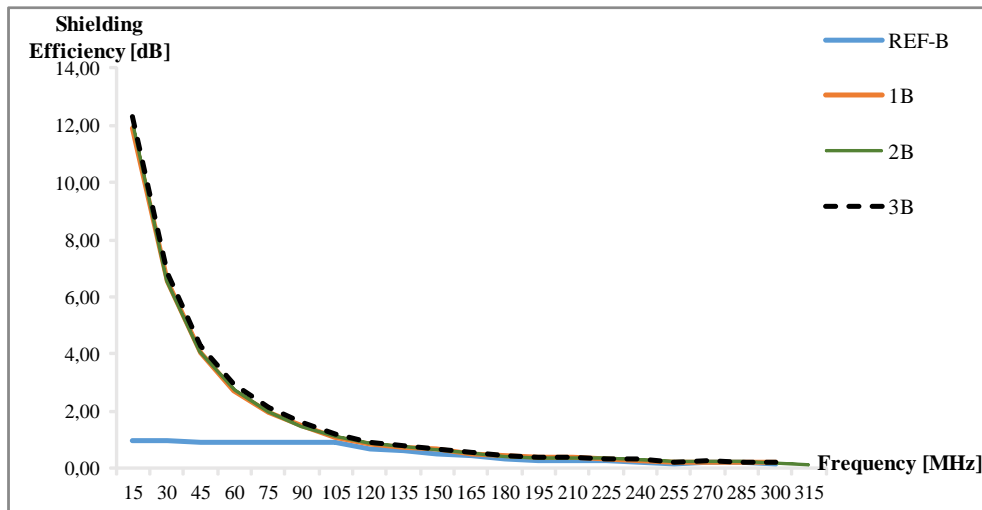
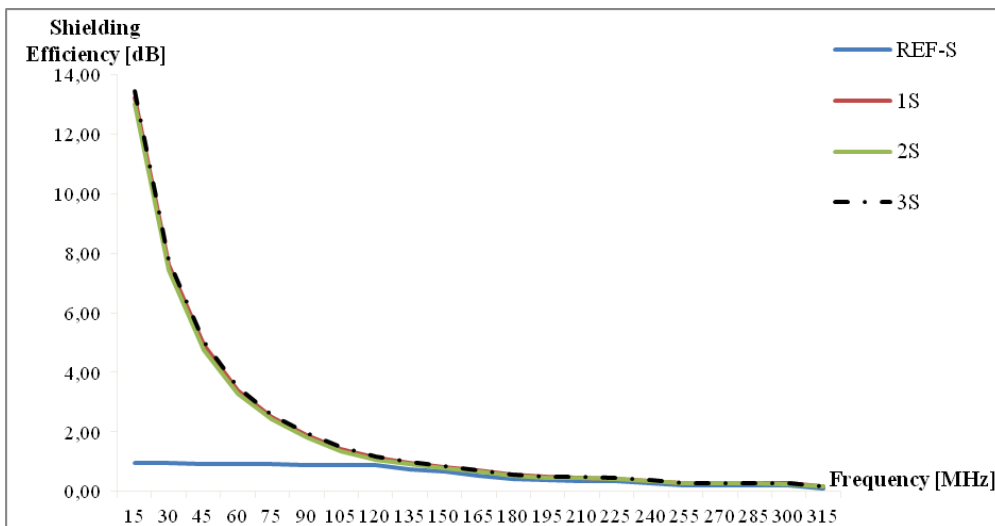**Figure 8.** EMSE results of plain weave fabrics



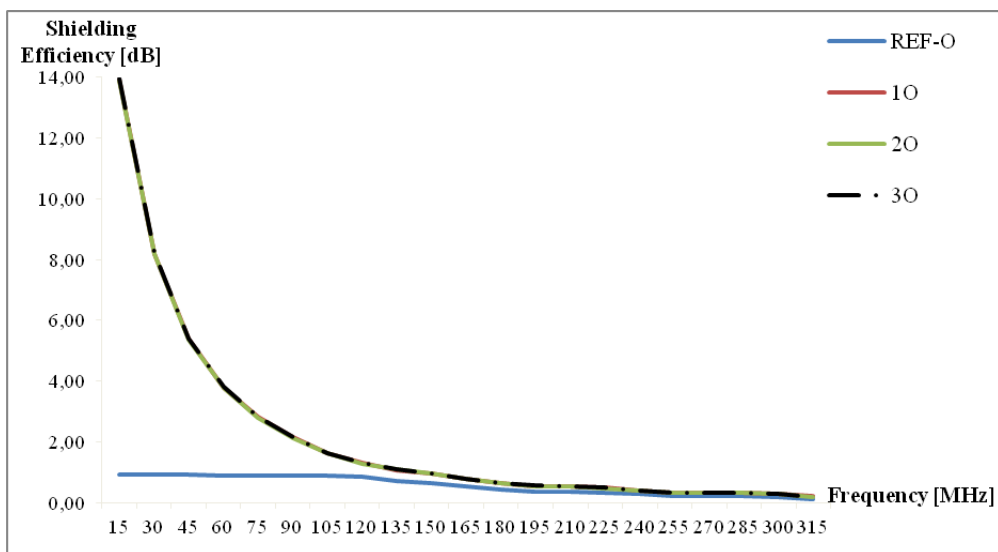**Figure 9.** EMSE results of sateen weave fabrics



**Figure 10.** EMSE results of special weave fabrics

Additive concentration is a parameter that affects the SE values of fabrics. In the literature, the effect of additive concentration on EMSE results was investigated [42, 43, etc.]. However, when different barium titanate concentrations were compared at the same fabric structure, all samples had close EMSE values. This situation was the same in different fabric weave types. There was no significant change between the concentrations tested. SE results of fabrics showed that SE values generally have a decreasing tendency depending on the increasing frequency. Previous studies stated that fabric structures have higher EMSE in low frequencies [44-46].

Fabric weave type is a parameter that affects the SE values of fabrics. In the literature, the effect of fabric weave type on EMSE results was investigated [15, 47, 48, etc.]. To evaluate the effect of fabric weave type on shielding efficiency of woven fabrics with the same additive ratio but different woven structures, the shielding efficiency values of coded fabrics were given in Figures 11, 12 and 13, respectively. When Figures 11, 12 and 13 were examined, while special weave fabrics had the highest shielding efficiency, plain weave fabrics had the lowest shielding efficiency for each additive ratio. Shielding efficiency values of sateen fabrics were close to special weave but slightly lower. The highest SE values were recorded 13.93, 13.90 and 13.96 dB at 15 MHz for 1O, 2O and 3O coded fabrics, respectively. The SE values of all samples were above 5 dB until 45 MHz. It was found that barium titanate affected the electromagnetic shielding properties of fabric samples. Consistent with our previous study [39], EMSE values of fabrics increased compared to the reference fabrics.
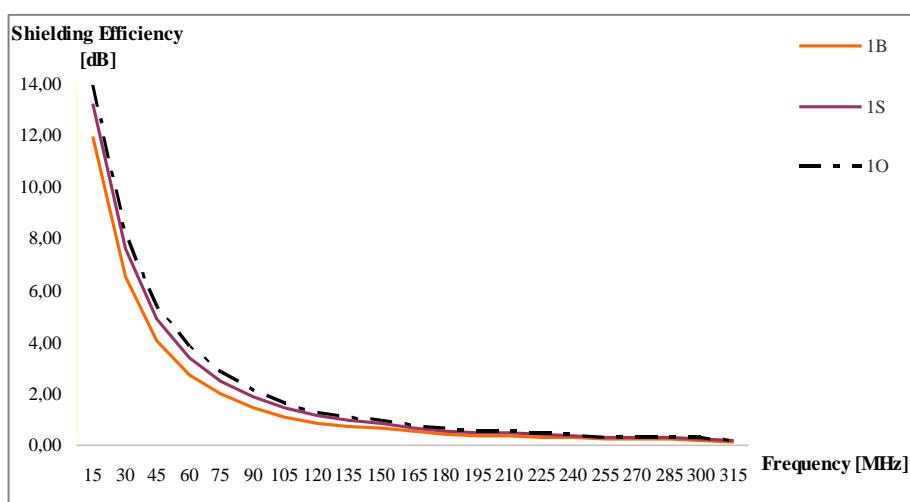


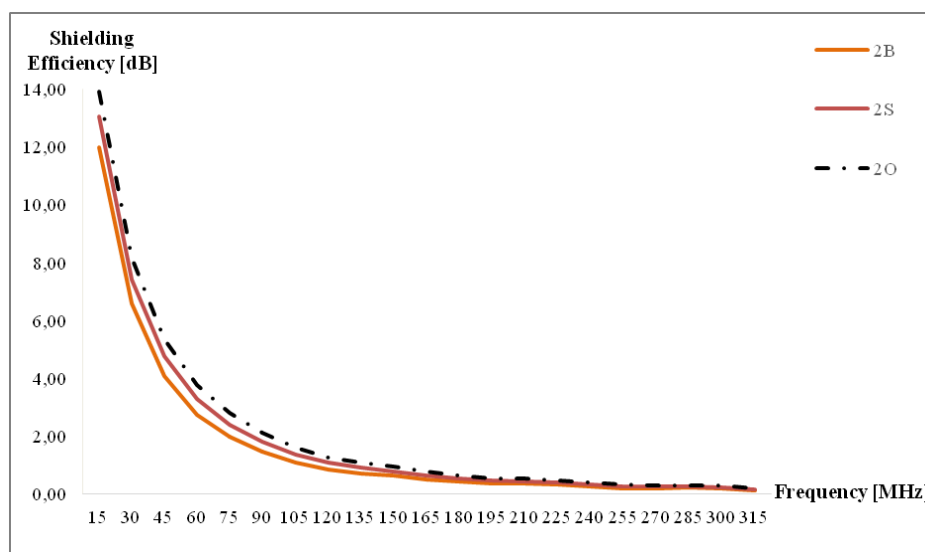**Figure 11.** Effect of fabric weave type on EMSE results for 1% additive ratio



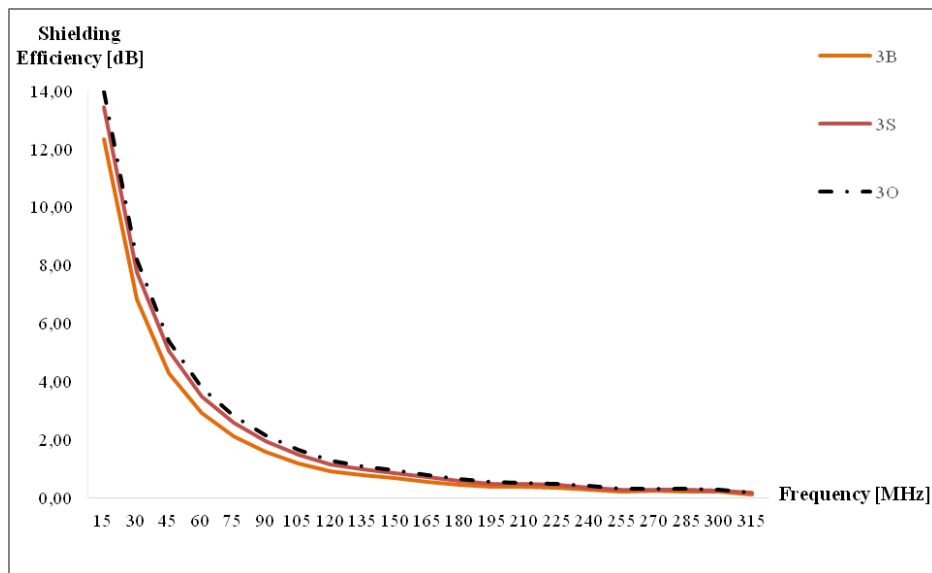**Figure 12.** Effect of fabric weave type on EMSE results for 2% additive ratio

**Figure 13.** Effect of fabric weave type on EMSE results for 3% additive ratio

The range of 20 dB ≥SE> 10 dB EMSE is classified as "good" and 10 dB ≥ SE > 7 dB EMSE is classified as "moderate" in "General Use" by The Functional Technical Textiles Standard. SE values of the woven fabrics were "good" at 15 MHz and they were "moderate" up to 45 MHz. When it was considered in conjunction with the previous studies [26, 49-51], barium titanate could be a promising electromagnetic shielding material. However, using barium titanate alone in the woven fabric structure did not provide sufficient SE for general use.

## 3.3 Spectrophotometry Results

The spectrophotometry results of fabrics were given in Table 5. It was observed that when wavelength was between 280 and 2500 nm, ultraviolet, visible and solar transmittance values of woven fabrics decreased with barium titanate additive. Similarly, in the study of Cai et. al. [38], the transmittance values reduced, even for the lowest barium titanate concentration (1%) compared to the reference fabrics for each fabric weave type.

When the transmittance results of plain weave fabrics were investigated, it was shown that UV transmittance ($T_{UV}$) values decreased by 78%, the visible transmittance ($T_V$) values decreased by 19%, the solar transmittance ($T_S$) values decreased by 16% for 3% barium titanate additive ratio compared to REF-B coded fabric, respectively. The lowest ultraviolet, visible and solar transmittance values 2.14 %, 30.39% and 31.94 % were obtained at maximum barium titanate additive ratio. When the results of sateen weave fabrics were investigated, it was shown that UV transmittance ($T_{UV}$) values decreased by 77%, the visible transmittance ($T_V$) values decreased by 16%, the solar transmittance ($T_S$) values decreased by 11% for 3% barium titanate additive ratio compared to REF-S coded fabric, respectively. The lowest ultraviolet, visible and solar transmittance values 2.21%, 29.35% and 30.93% were obtained at maximum barium titanate additive ratio. When

the results of special weave fabrics were investigated, it was shown that UV transmittance ($T_{UV}$) values decreased by 80%, the visible transmittance ($T_V$) values decreased by 23%, the solar transmittance ($T_S$) values decreased by 19% for 3% barium titanate additive ratio compared to REF-O coded fabric, respectively. The lowest ultraviolet, visible and solar transmittance values 2.10%, 29.34% and 31.03% were obtained at maximum barium titanate additive ratio. However, the transmittance values slightly reduced with increasing barium titanate concentration for each fabric weave type.

In contrast with transmittance values, it was observed that visible and solar reflectance values of fabrics increased with barium titanate additive. Similarly, in the the study of Xiang and Zhang [37], the reflectance values increased even for the lowest barium titanate concentration (1%) compared to the reference fabrics for each fabric weave type. When the reflectance results of plain weave fabrics were investigated, it was shown that visible reflectance ($R_V$) values increased by 15% and the solar reflectance ($R_S$) values increased by 12% for 3% barium titanate additive ratio compared to REF-B coded fabric. When the reflectance results of sateen weave fabrics were investigated, it was shown that visible reflectance ($R_V$) values increased by 9% and the solar reflectance ($R_S$) values increased by 5% for 3% barium titanate additive ratio compared to REF-S coded fabric. When the reflectance results of special weave fabrics were investigated, it was shown that visible reflectance ($R_V$) values increased by 10% and the solar reflectance ($R_S$) values increased by 5% for 3% barium titanate additive ratio compared to REF-O coded fabric. In all regions, the highest reflectance values 68.18% ($R_V$) and 62.80% ($R_S$) were obtained with maximum barium titanate additive ratio at plain weave fabric structure. The results showed that the changes in the fabric structure did not cause a significant effect on the solar properties of woven fabrics.

**Table 5.** Spectrophotometry results

| Fabric Code | $T_{UV}$ % (280-380 nm) | $T_V$ % (380-780 nm) | $R_V$ % (380-780 nm) | $T_S$ % (300-2500nm) | $R_S$ % (300-2500 nm) |
|---|---|---|---|---|---|
| **REF-B** | 9.90 | 37.62 | 59.23 | 37.98 | 56.29 |
| 1B | 3.00 | 32.21 | 63.56 | 33.55 | 58.73 |
| 2B | 2.15 | 31.62 | 65.86 | 33.30 | 60.07 |
| 3B | 2.14 | 30.39 | 68.18 | 31.94 | 62.80 |
| **REF-S** | 9.58 | 34.87 | 61.50 | 34.94 | 58.06 |
| 1S | 3.06 | 30.62 | 66.22 | 31.28 | 61.11 |
| 2S | 2.43 | 30.63 | 67.34 | 31.97 | 61.59 |
| 3S | 2.21 | 29.35 | 66.78 | 30.93 | 61.17 |
| **REF-O** | 10.51 | 38.15 | 60.10 | 38.35 | 57.51 |
| 1O | 3.09 | 32.24 | 64.57 | 33.47 | 59.82 |
| 2O | 2.17 | 30.63 | 66.27 | 32.49 | 60.69 |
| 3O | 2.10 | 29.34 | 66.01 | 31.03 | 60.55 |

## 4. CONCLUSION

In this study, sheet resistance, electromagnetic shielding and solar properties of woven fabrics, which were produced barium titanate/polyester core/sheath bicomponent yarns were investigated. The effect of barium titanate additive ratio and the fabric structure on sheet resistance, electromagnetic shielding and solar properties were evaluated.

The addition of barium titanate caused a small increase in the melting temperature of bicomponent yarns. With the increasing additive ratio, the sheet resistance values slightly decreased. The lowest sheet resistance value was obtained for the 3% barium titanate added sateen fabric.

Barium titanate had a positive effect on the shielding efficiency of woven fabrics. Compared to the reference fabrics, EMSE values increased by 92%, 93% and 94% at 15 MHz for plain, sateen and special weave fabric, respectively. In future works, different woven fabrics will be produced using barium titanate and carbon-based additive bicomponent yarns to provide higher SE values for general use according to the FTTS standard. On the other hand, the barium titanate additive improved visible and solar reflectance properties. In the highest barium titanate additive ratio, the highest decrease rate in solar transmittance was 19% for special weave fabric. In contrast, the highest increase rate of solar reflectance was 5% for plain weave fabric.

This study showed that woven fabrics produced from barium titanate added bicomponent yarns could provide improvements electromagnetic shielding and solar reflectance, which were one of the most important issues in the technical textile industry. Barium titanate can be preferable due to its unique properties such as low cost, environmentally friendly, etc. and as it provides multifunctional properties to textile products.

### Acknowledgement

## REFERENCES

1. Malik P, Sharma A, Gianender, Sharma JP. 2018. Textiles for protection against electromagnetic radiations: A review. *Pratibha Malik Journal of Engineering Research and Application*, 8(6), 32-37.

2. Bonaldi RR, Siores E, Shah T. 2014. Characterization of electromagnetic shielding fabrics obtained from carbon nanotube composite coatings. *Synthetic Metals*, 187, 1-8.

3. Chen AP, Lin CM, Lin CW, Hsieh CT, Lou CW, Young YH, Lin JH. 2010. Electromagnetic shielding effectiveness and manufacture technique of functional bamboo charcoal/metal composite woven. *Advanced Materials Research,* 123, 967-970.

4. Das A, Kothari VK, Kothari A, Kumar A. 2009. Effect of various parameters on electromagnetic shielding effectiveness of textile fabrics. *Indian Journal of Fibre &Textile Research,* 34, 144-148.

5. Maity S, Chatterjee A. 2018. Conductive polymer-based electro-conductive textile composites for electromagnetic interference shielding: A review. *Journal of Industrial Textiles*, 2018; 47. 8: 2228-2252.

6. Neruda M, Vojtech L. 2014. Modelling of conductive textile materials for shielding purposes and RFID textile antennas. *Elektronika IR Elektrotechnika,* 20(8), 63-67.

7. Ott HW, Ott HW. 1988. *Noise reduction techniques in electronic systems*. New York: Wiley.

8. Chen KB, Lee KC, Ueng TH, Mou KJ. 2002. Electrical and impact properties of the hybrid knitted inlaid fabric reinforced polypropylene composites, *Composites Part A*, 33(9), 1219–1226.

9. Cheng KB, Cheng TW, Lee KC, Ueng TH, Hsing WH. 2003. Effect of yarn constituent and fabric specifications on electrical properties of hybrid woven fabrics, *Composites Part A*, 34(10), 971–978.

10. Dordevic Z. 1992. Textile fabric shielding electro-magnetic radiation and clothing made thereof. 5,103,504. U.S.

11. Lin ZI, Lou CW, Pan Y J, Hsieh CT, Huang CH, Huang CL, ..., Lin JH. 2017. Conductive fabrics made of polypropylene/multi-walled carbon nanotube coated polyester yarns: Mechanical properties and electromagnetic interference shielding effectiveness. *Composites Science and Technology*, 141, 74-82.

12. Gültekin BC. 2018. Evaluation of the electromagnetic shielding effectiveness of carbon-based screen printed polyester fabrics. *Fibers and Polymers*, 19(2), 313-320.

13. Duran D, Kadoğlu H. 2015. Electromagnetic shielding characterization of conductive woven fabrics produced with silver-containing yarns. *Textile Research Journal*, 85(10), 1009-1021.

14. Örtlek HG. Güneşoğlu C, Okyay G, Türkoğlu Y. 2012. Investigation of electromagnetic shielding and comfort properties of single jersey fabrics knitted from hybrid yarns containing metal wire. *Journal Of Textile & Apparel,* 22(2), 90-101.

15. Özdemir H, Özkurt A. 2013. The effects of weave and conductive yarn density on the electromagnetic shielding effectiveness of cellular woven fabrics. *Journal Of Textile & Apparel,* 23(2).

16. Eren S, Ulcay Y. 2015. Production of bi-component polyester fibres for EMR (electromagnetic radiation) protection and examining EMR shielding characteristics. *Journal Of Textile & Apparel,* 25(2).

17. Özen MS, Sancak E, Soin N, Shah TH, Siores E. 2016. Investigation of electromagnetic shielding effectiveness of needle punched nonwoven fabric produced from conductive silver coated staple polyamide fibre. *The Journal of The Textile Institute,*107(7), 912-922.

18. Ni QQ, Melvin GJH, Natsuki T. 2015. Double-layer electromagnetic wave absorber based on barium titanate/carbon nanotube nanocomposites. *Ceramics International*, 41(8), 9885-9892.

19. Qiu J, Qiu T. 2015. Fabrication and microwave absorption properties of magnetite nanoparticle–carbon nanotube–hollow carbon fiber composites. *Carbon*, 81, 20-28.

20. Wang Z, Wu L, Zhou J, Cai W, Shen B, Jiang Z. 2013. Magnetite nanocrystals on multiwalled carbon nanotubes as a synergistic microwave absorber. *The Journal of Physical Chemistry C*, 117(10), 5446-5452.

21. Zhu Y-F, Ni Q-Q, Fu Y-Q. 2015. One-dimensional barium titanate coated multi-walled carbon nanotube heterostructures: synthesis and electromagnetic absorption properties *RSC Advances*, 5, 3748–3756.

22. Yusoff AN, Abdullah MH, Ahmad SH, Jusoh SF, Mansor AA, Hamid, SAA. 2002. Electromagnetic and absorption properties of some microwave absorbers *Journal of Applied Physics*, 92, 876–882.

23. Melvin GJH, Ni QQ, Natsuki T. 2014. Electromagnetic wave absorption properties of barium titanate/carbon nanotube hybrid nanocomposites. *Journal of Alloys and Compounds*, 615, 84-90.

24. Melvin GJH. Ni QQ, Natsuki T, Wang Z, Morimoto S, Fujishige M,…, Endo M. 2015. Ag/CNT nanocomposites and their single-and double-layer electromagnetic wave absorption properties. *Synthetic Metals*, 209, 383-388.

25. Melvin GJH, Ni QQ, Suzuki Y, Natsuki T. 2014. Microwave-absorbing properties of silver nanoparticle/carbon nanotube hybrid nanocomposites. *Journal of Materials Science*, 49(14), 5199-5207.

26. Saini P, Arora M, Gupta G, Gupta BK, Singh VN, Choudhary V. 2013. High permittivity polyaniline–barium titanate nanocomposites with excellent electromagnetic interference shielding response. *Nanoscale*, 5(10), 4330-4336.

27. Saini P, Arora M. 2013. Formation mechanism, electronic properties & microwave shielding by nano-structured polyanilines prepared by template free route using surfactant dopants. *Journal of Materials Chemistry A*, 1(31), 8926-8934.

28. Ting TH, Jau YN, Yu RP. 2012. Microwave absorbing properties of polyaniline/multi-walled carbon nanotube composites with various polyaniline contents. *Applied Surface Science*, 58(7), 3184-3190.

29. Makeiff DA, Huber T. 2006. Microwave absorption by polyaniline–carbon nanotube composites. *Synthetic Metals*, 156(7-8), 497-505.

30. Vijatović MM, Bobić JD, Stojanović BD. 2008. History and challenges of barium titanate: part II. *Science of Sintering,* 403, 235–244.

31. Celen R, & Ulcay Y. 2018. The use of barium titanate in electromagnetic shielding applications at textiles. *Uludağ University Journal of The Faculty of Engineering*, 23(2), 29-44.

32. Infante IC, Volkova H, Gemeiner P, Geneste G, Guillot J et al. 2018. Third Seminar on the Mechanics of Multifunctional Materials, Bad-Honnef, Germany.

33. Sharma S, Tomar M, Puri NK, Gupta V. 2015. Ultraviolet radiation detection by barium titanate thin films grown by sol–gel hydrothermal method. *Sensors and Actuators A: Physical*, 230, 175-181.

34. Kilic A, Shim E, Yeom BY, Pourdeyhimi B. 2013. Improving electret properties of PP filaments with barium titanate. *Journal of Electrostatics,*711, 41–47.

35. Yu CR, Wu DM, Liu Y, Qiao H, Yu ZZ, Dasari A,…, Mai YW. 2011. Electrical and dielectric properties of polypropylene nanocomposites based on carbon nanotubes and barium titanate nanoparticles. *Composites Science and Technology,* 7115, 1706–1712.

36. Cai MQ, Yin Z, Zhang MS. 2003. First-principles study of optical properties of barium titanate. *Applied Physics Letter*, 83(14), 2805-2807.

37. Xiang B, Zhang J. 2018. A new member of solar heat-reflective pigments: BaTiO₃ and its effect on the cooling properties of ASA (acrylonitrile-styrene-acrylate copolymer). *Solar Energy Materials and Solar Cells,*180,67-75.

38. Cai W, Fu C, Gao J, Guo Q, Deng X, Zhang C. 2011. Preparation and optical properties of barium titanate thin films. *Physica B: Condensed Matter*, 406(19), 3583-3587.

39. Celen R, Ulcay Y. 2019. Investigating electromagnetic shielding effectiveness of knitted fabrics made by barium titanate/polyester bicomponent yarn. *Journal of Engineered Fibers and Fabrics*, 14, 1558925019837806.

40. Committee for Conformity Assessment of Accreditation and Certification on Functional and Technical Textiles. 2005. Specified requirements of electromagnetic shielding textiles.(Standard No. FTTS-FA-003). Taipei/Taiwan.

41. Yildirim K, Kanber A, Karahan M, Karahan N. 2018. The solar properties of fabrics produced using different weft yarns. *Textile Research Journal*, 88(13), 1543-1558.

42. Kim B, Koncar V, Devaux E, Dufour C, Viallier P. 2004. Electrical and morphological properties of PP and PET conductive polymer fibers. *Synthetic Metals*, 146(2), 167-174.

43. Yu B, Qi L, Ye JZ, Sun H. 2007. Preparation and radar wave absorbing characterization of bicomponent fibers with infrared camouflage. *Journal of Applied Polymer Science*, 104(4), 2180-2186.

44. Tezel S, Kavuşturan Y, Vandenbosch GA, Volski V. 2014. Comparison of electromagnetic shielding effectiveness of conductive single jersey fabrics with coaxial transmission line and free space measurement techniques. *Textile Research Journal,* 845, 461–476.

45. Ortlek HG. Kilic G, Okyay G, Bilgin S. 2011. Electromagnetic shielding characteristics of different fabrics knitted from yarns containing stainless steel wire. *Industria Textila*, 62(6), 304–308.

46. Lin JH, Lou CW, Liu HH. 2007. Process and anti-electrostatic properties of knitted fabric made from hybrid staple/metallic-core spun yarn. *Journal of Advanced Materials*, 39(1), 11-16.

47. Liu Z, Wang XC. 2012. Influence of fabric weave type on the effectiveness of electromagnetic shielding woven fabric. *Journal of Electromagnetic Waves and Applications*, 26(14-15), 1848-1856.

48. Okyay G, Bilgin S, Akgul E, Ortlek HG. 2011. Farklı yapılardaki dokuma kumaşların elektromanyetik ekranlama özelliklerinin incelenmesi. *Tekstil Teknolojileri Elektronik Dergisi*, 5(1), 1-10.

49. Su J, Zhang J. 2016. Preparation and properties of barium titanate (BaTiO3) reinforced high density polyethylene (HDPE) composites for electronic application. *Journal of Material Science,* 27(5), 4344–4350.

50. Qing Y, Mu Y, Zhou Y, Luo ., Zhu D, Zhou W. 2014. Multiwalled carbon nanotubes– BaTiO3/silica composites with high complex permittivity and improved electromagnetic interference shielding at elevated temperature. *Journal of the European Ceramic Society,* 34, 2229– 2237.

51. Melvin GJH, Ni QQ, Wang Z. 2017. Performance of barium titanate@carbon nanotube nanocomposite as an electromagnetic wave absorber. *Physica Status Solidi A,* 214(2), 160054.

# Dyeing of wool yarn with natural dyes of *Lactarius deliciosus* and *L. sanguifluus* from Turkey

Halil Özdemir[1], Fuat Bozok[2]

[1]Osmaniye Korkut Ata University/ Osmaniye Vocational School, Textiles, Clothing, Footwear and Leather Department, 80000/ Osmaniye, Turkey
[2]Osmaniye Korkut Ata University/ Faculty of Arts and Science, Department of Biology, 80000/ Osmaniye, Turkey

**Corresponding Author:** Halil ÖZDEMİR, halilozdemir@osmaniye.edu.tr

## ABSTRACT

In recent years, the use of synthetic dyes and pigments in textile finishing companies has been discussed for their harmful effects on human health and environment. For this reason, the use of plant–based dyestuffs from the nature has begun to increase because of the biodegradability, non–toxicity, human health and waste water contamination. Natural dyes are substances synthesized by some plants, animals, lichens and fungi in nature. Fungal species, including lichenized fungi have been used as natural colorants in different parts of the world throughout the history. In this study, natural dyes were extracted from *Lactarius deliciosus* and *Lactarius sanguifluus* collected from Osmaniye province (East Mediterranean region) of Turkey. The adsorption UV–Vis spectra of the mushrooms were measured to examine major colorants, and FTIR analysis of natural dyes obtained from the mushrooms extracts was performed. According to the analyses, major colorants in the edible Lactarius species could be azulene and its derivatives. Wool yarn (for carpet) was dyed with these natural dyes by using different mordants. CIELab (L*, a*, b*, c* and h), color differences (ΔE) and color strength (K/S) values of dyed wool yarns were determined. According to the dyeing results, cream and brown colors were obtained from *L. deliciosus* and *L. sanguifluus* respectively; the use of mordant (ferrous sulfate) increased the color strength of dye goods. Besides, properties of rubbing and washing fastness were investigated, and the results of the dyed yarns were low/moderate. This is the first study on dyeing of wool yarns with natural dyes obtained from *L. deliciosus* and *L. sanguifluus* collected from East Mediterranean (Osmaniye province) of Turkey.

## 1. INTRODUCTION

Natural pigments and dyes, isolated from different natural sources, have attracted people's attention since ancient times [1–3]. Fungal species containing special natural dyes are widely used as colorants in Europe, America and North Africa [4,5]. Fungal dyestuffs and pigments can be isolated from a wide variety of fungal species and divided into two sections (carotenoids, bensole derivative (I) and quinones, anthraquinones, azulenes, heterocyclic nitrogen–bearing pigments (II)) [6–8]. These products are among the natural chemicals for use in pharmaceutical, food, cosmetic and textile industries [9].

Many dyes found in fungi, are benzoquinone derivatives, especially terpenylquinone compounds [10]. In earlier studies, red colour from *Echinodontinum tinctorum* were obtained by

Indians living in America and some species of the genus *Boletus* were also used for painting of furs [11,12]. In Europe, fungi were used as textile colorants [13]. It was known that some species which belong to the genera *Telephora* sp., *Hydnellum* sp., *Sarcodon* sp. and *Phelledon* sp. containing benzoquinone derivatives were expressed to give blue hues to wool yarns [4,10,13,14]. Further on, some colorant components such as atromentin, polyphoric acid, telephoric acid, grevillin, physcion, emodin, hispidin, anthraquinones, iminoquinone, dermoquinone, dermocybin, pulvinic acid, norbadione A, laetiporic acids were found in *Boletus* sp., *Xerocomus* sp., *Polyporus* sp., *Trametes* sp., *Hydnum* sp., *Suillus* sp., *Dermocybe* sp., *Paxillus atrotomentosus*, *Sarcodon squamosus*, *Hapalopilus nidulans*, *Cortinarius sanguineus*, *Pisolithus arhizus*, *Laetiporus sulphureus* [15–21].

The genus *Lactarius* belonging to the family Russulaceae (Basidiomycota) has more than one thousand species [44]. *L. deliciosus* and *L. sanguifluus* (kanlıca, çıntar or çam mantarı in Turkish) are often used as food among local people in Turkey.

Previous studies found different pigments such as red colour 7–acetyl–4–methylazulene–1–carbaldehyde, 7–(1,2–dihydroxy–1–methylethyl)–4–methylazulene–1–carbaldehyde, 7–acetyl–4–methylazulene–1–carboxylic acid in *L. deliciosus* [22] and as beige colour (azulene) in *L. deliciosus* [23], 1,3,5,7(11),9–pentaenyl–14–guaianal) in *L. sanguifluus* [24], brilliant blue colour (1–hydroxymethyl–4–methyl–7–(1–methylethenyl) azulene) in *L. indigo* [25–28], pale green colour aminobenzoquinone blennione [29]. Considering related publications, major colorants in the edible Lactarius mushrooms may be azulene and their structural formula are given in Figure 1.
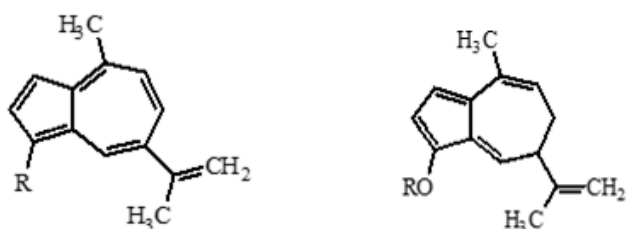


**Figure 1.** Chemical structure of azulene (lactarazulene (R =CH3), dihydroazulen–1–ol (R =H))

Mycologists have so far identified about 120.000 fungal species [30], but this number increases day by day with the detection of new species [31-36]. However, the number of fungal species in the world is estimated to be 2.2-3.8 million [37]. When examined ecologically, mushrooms serve as an interesting source of raw materials and have faster growth potential and high yields in a short time than higher plants [38]. Thus, mushrooms are more suitable and economical for new technologies such as biotechnological products [39-40].

Natural dyes are mostly eco-friendly, biodegradable, less toxic, and less allergenic as compared to synthetic dyes. In spite of many advantages of natural dyes, their short range of shades, non-availability of standard shade cards and low fastness results have been improved by using metallic mordants. Natural dyes are mostly non-substantive and must be applied on textiles by the help of mordants, usually a metallic salt, having an affinity for both the coloring matter and the fiber. After combining with dye in the fiber, these metallic mordants turn into an insoluble precipitate or lake; hence, both the dye and mordant get fixed to become wash fast to a reasonable level [41,42].

Recently, eco–friendly natural dyes have attracted the attention of many researchers and the use of these dyes is increasing day by day in many products such as textiles, cosmetics and food [43–49]. However, uses of fungal

species for dyeing textiles have not been investigated enough until today. In the present study, natural dyes obtained from *L. deliciosus* and *L. sanguifluus* were studied on dyeing of wool yarns.

## 2. EXPERIMENTAL

### 2.1. Material

#### 2.1.1. Plant material (Mushroom samples)

*L. deliciosus* and *L. sanguifluus* (voucher no: FBozok222 and FBozok223, respectively) were collected from Osmaniye province (37°01'15" N, 36°13'53" E, 571 m) of Turkey (Figure 2).



**Figure 2.** *L. deliciosus* (left) and *L. sanguifluus* (right)

#### 2.1.2. Studies on wool

Straygarn woolen yarns, which is %100 pure (Yarn count: Nm 4/2, Twist per meter: 256 t/m), were supplied from Karatepe Kilim Cooperative in Osmaniye, Turkey. Wool used to dye was obtained from sheep which are native to the Eastern Mediterranean region. The hank samples (each 3 g) were produced using hank winder for dyeing.

#### 2.1.3. Chemicals

The metallic salts employed were alum ($KAl(SO_4)_2.12H_2O$) and ferrous sulphate heptahydrate ($Fe_2SO_4, 7H_2O$) for pre-mordanting. Acetic acid ($C_2H_4O_2$, glacial) was used to adjust the pH. Mushroom samples were extracted in ethanol. Nonionic detergent (Setalan HE, Setas–Chem.) was utilized to wash after dyeing. All chemicals were of laboratory grade.

### 2.2. Methods

#### 2.2.1. Natural dye extraction

Fresh mushroom samples were dried in dehydrator for 48 h at 50 °C and pulverized by using a blender (Waring Blender, HGB2WTS3). 50 g powder from both mushroom samples were extracted in 500 ml of ethanol during 24 h at 50 °C and filtered by Whatman filter paper. Ethanol was then removed by using a rotary evaporator at 78 °C. Natural colorants obtained from both mushroom samples were preserved in a refrigerator (+4 °C) until used.

## 2.2.2. Spectrophotometric analysis

To examine absorbance properties of *L. deliciosus* and *L. sanguifluus* crude extracts, the adsorption UV–Vis spectra were measured and the obtained spectra in full UV–Vis range are presented in Figure 3. The absorption spectra of natural dyes from *L. deliciosus* and *L. sanguifluus* in the present study found to be between 250 and 400 nm for azulene and its derivatives as in the study of Matênovâ et al. (2014) [50]. It is thought that major colorants in the edible Lactarius species could be azulene and its derivatives.

### 2.2.3. FTIR analysis

An FTIR (Fouirer Transform Infrared Spectroscopy, PerkinElmer Spectrum 65) that have Universal ATR (attenuated total reflectance) sampling accessory was used and IR spectra were obtained in the 600–4000 cm$^{-1}$ (Figure 4). Measurements from each sample were done 5 times in the room temperature (25 $^{o}$C). It was known that the absorbance of azulene was about 760 cm$^{-1}$ in FTIR [45].

### 2.3. Mordanting and Dyeing

Pre–mordanting method was applied to study and the wetted wool yarns were mordanted by using 3 % owf of ferrous sulfate and potassium aluminum sulfate mordants at 80 °C and liquor ratio 1:50 for 45 minutes. After mordanting, each sample was not rinsed but only squeezed.

The wool yarns used in the production of carpets and rugs were dyed with natural dyes extracted in the laboratory. Different dyeing concentrations (1, 2 and 3 g/l) and mordant materials (Ferrous Sulphate and Potassium

Aluminum Sulfate) were used for dyeing wool yarns. 150 ml of original dye solution was used for each a hank sample at liquor ratio 1:50. Acetic acid was used to adjust the pH of the dyebath to 5. Dyeing was done at 80 °C for 60 min. The dyed wool yarns were then washed with 2 g/l nonionic (Setalan HE, Setas–Chem.) detergent for 30 min at 80 °C, rinsed with tap water and dried at room temperature in shade. Laboratory type dyeing machine was used in all dyeing processes.

### 2.4. Color Measurement

Swatch cards were made by using yarn sample winding machine for color measurement (spectrophotometer). A spectrophotometer (Minolta CM 3600D) coupled to a PC was used to measure the color coordinates of dyed yarn between 400–700 nm under D65/10° illuminant. K/S (Color Strength) values were obtained from Kubelka Munk Equation (1);

$$K/S = (1–R)^2/2R \qquad (1)$$

where K is a constant associated with the light absorption of the fabric, predominantly determined by dyestuff, S is the constant of light scattering of the fabric, determined only by the textile material, and R is the reflection of the dyed fabric measured at the wavelength of maximum light absorption. The CIE L*a*b* formula is used to assess small color differences and recommended for use by DIN 6174. The color difference is determined using a color difference formula from the colorimetric measures L*, a*, b* which result from the CIE tristimulus values X, Y, Z. In the CIE L*a*b* uniform color space, the coordinates are:



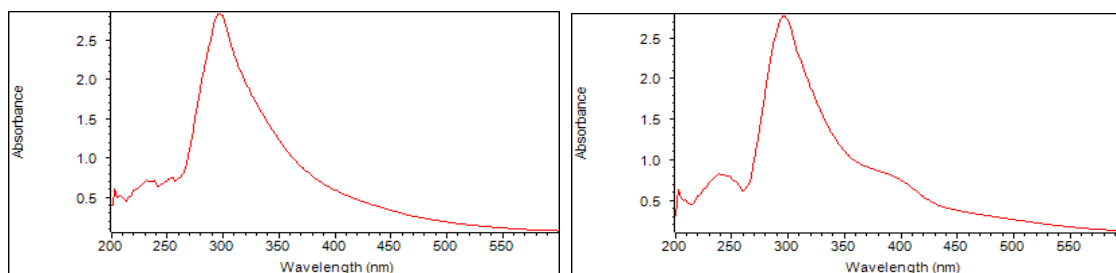**Figure 3.** The absorption UV–Vis spectra of *L. deliciosus* (left) and *L. sanguifluus* (right)
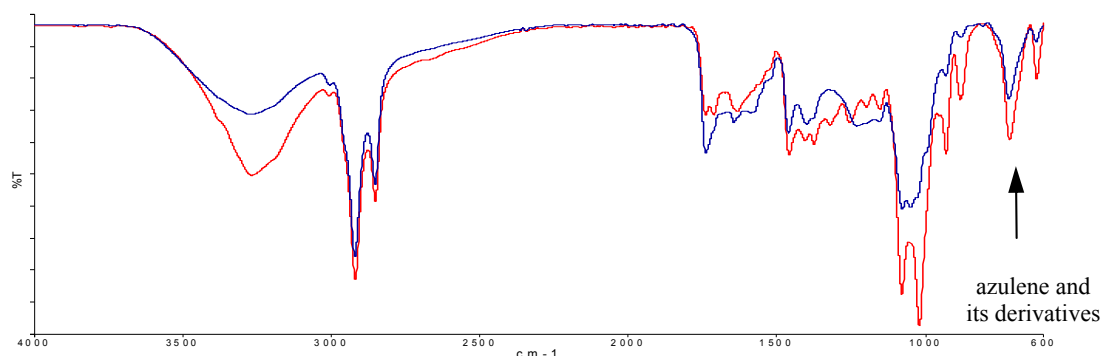


azulene and its derivatives

**Figure 4.** FTIR analysis of natural dyes obtained from *L. deliciosus* (blue) and *L. sanguifluus* (red) extracts

L* - the lightness coordinate.

a* - the red/green coordinate, with +a* indicating red, and -a* indicating green.

b* - the yellow/blue coordinate, with +b* indicating yellow, and -b* indicating blue

According to DIN 6174, the ΔE*ab color difference is calculated as Equation (2) [51,52]:

$$\Delta E*_{ab} = [(\Delta L*)^2 + (\Delta a*)^2 + (\Delta b*)^2]^{1/2} \quad (2)$$

$\Delta L* = L_i* - L_o*$ (light difference)

$\Delta a* = a_i* - a_o*$ (red-green difference)

$\Delta b* = b_i* - b_o*$ (yellow-blue difference)

$\Delta E^*_{ab}$ : total color difference

i: Sample o:Reference

## 2.5. Fastness Properties

The washing and rubbing (crock) fastnesses of the naturally dyed yarn samples were determined according to TS EN ISO 105-C06 A1S (steel balls are not used) and TS EN ISO 105–X12 standards after conditioning in standard atmospheric conditions (20ºC±2 temperature and 65 ± 4 % RH) for 24 hours. The wash fastness of the dyed samples was assessed both in terms of alteration of shades and degree of staining on white cotton adjacent fabric. Dry and wet rub fastness of dyed wool yarn samples was tested using the Crockmeter. Washing and dry cleaning fastness machine was used to measured wash fastness values of dyed wool yarn samples. The results were evaluated with the gray scale values (rating 1-5, 1= poor, 5=excellent) for washing fastness and rubbing fastness.

## 3. RESULTS AND DISCUSSION

As a result of color measurements, brown shades of color were obtained by using two various mordants at different concentrations (1, 2 and 3 g/l) for dyeing with *Lactarius deliciosus* and *Lactarius sanguifluus*. Color measurements on spectrophotometer are given in Table 1–4. Cream–its shades and brown–its shades in wools dyed with extracts of *L. deliciosus* and *L. sanguifluus* were obtained for dyeing without mordant (Table 1 and 2). In the use of ferrous sulphate mordant (FeSO₄), darker colors (dark brown) in *L. deliciosus* and brown in *L. sanguifluus* were obtained with high K/S values (Figure 5), while light brown and its shades with *L. deliciosus* extract and cream and its shades with *L. sanguifluus* extract were obtained with aluminum potassium sulphate (KAl (SO4)₂.12H₂O) respectively. Lightness (L*) values decreased while red/green (a*) values in wool dyed with *L. deliciosus* extract increased with the increase in concentration and the use of mordant.

Color characteristics are highly affected by the type of mordant used [42]. In Figure 5, it is observed that while the K/S values of dyed samples with Alum and unmordanted increased depending on concentration, the K/S values of dyed samples with ferrous sulfate did not change much for both mushrooms extracts. In another result, *L. sanguifluus* K / S values are lower than other *L. deliciosus* for dyeing with mordant. While it was found that K/S values increased in the order of ferrous sulfate > alum >unmordanted for *L. deliciosus* extract, and they increased in the order of ferrous sulfate > unmordanted > alum for *L. sanguifluus* extract. It is remarkable that the woolen yarns dyeing with *L. deliciosus* extract using mordant have higher K/S values. This situation is thought to be related to the chemical structure of two different fungi belonging to the genus Lactarius. In addition, the high K / S values obtained from pre-mordanting with ferrous sulphate can be explained by the fact that azulene acts as a ligand for low-value metals such as ferrous and can especially form stronger chemical bonds in organometallic chemistry.

**Table 1.** Colour measurements of wool dyed with extracts of *L. deliciosus* without and with mordanting

| Dyeing | | Color measurements | | | | | | | Color |
|---|---|---|---|---|---|---|---|---|---|
| Mordant | Con. (g/l) | L* | a* | b* | C* | h | K/S | | |
| Without | 1 | 60.83 | 05.81 | 22.86 | 23.59 | 75.74 | 03.87 | Cream | |
| | 2 | 55.50 | 07.33 | 23.07 | 24.20 | 72.37 | 05.32 | Ivory | |
| | 3 | 53.28 | 07.96 | 22.94 | 24.28 | 70.85 | 06.06 | Grayish Brown | |
| Potash alum | 1 | 58.24 | 08.12 | 25.51 | 26.77 | 72.35 | 05.18 | Fawn (Fulvous) | |
| | 2 | 52.50 | 08.76 | 25.24 | 26.71 | 70.86 | 07.48 | Light Brown | |
| | 3 | 46.70 | 09.21 | 23.72 | 25.44 | 68.78 | 09.92 | Brown | |
| Ferrous Sulphate | 1 | 46.83 | 15.19 | 31.44 | 34.91 | 64.21 | 16.68 | Bombay Brown | |
| | 2 | 41.80 | 09.97 | 23.29 | 25.34 | 66.82 | 16.62 | Dark Brown | |
| | 3 | 41.36 | 09.56 | 22.18 | 24.15 | 66.69 | 16.14 | Dark Brown | |

Con.: Concentrations

| Dyeing | | Color measurements | | | | | | | Color | |
|---|---|---|---|---|---|---|---|---|---|---|
| Mordant | Con. (g/l) | L* | a* | b* | C* | h | K/S | | | |
| Without | 1 | 62.58 | 6.59 | 18.73 | 19.85 | 70.60 | 04.19 | Grayish Brown | | |
| | 2 | 54.88 | 8.88 | 21.66 | 23.41 | 67.70 | 07.36 | Brown | | |
| | 3 | 47.13 | 9.13 | 18.43 | 20.57 | 63.65 | 10.44 | Dark Brown | | |
| Potash alum | 1 | 63.96 | 5.36 | 19.74 | 20.45 | 74.80 | 03.64 | Cream | | |
| | 2 | 59.82 | 7.07 | 20.60 | 21.78 | 71.04 | 05.27 | Cream | | |
| | 3 | 56.48 | 7.45 | 20.59 | 21.90 | 70.12 | 06.54 | Fawn (Fulvous) | | |
| Ferrous Sulphate | 1 | 49.04 | 8.68 | 23.37 | 24.93 | 69.62 | 09.82 | Fawn (Fulvous) | | |
| | 2 | 48.92 | 9.64 | 24.17 | 26.03 | 68.25 | 10.98 | Brown | | |
| | 3 | 48.83 | 9.70 | 24.47 | 26.32 | 68.37 | 11.07 | Brown | | |

Con.: Concentrations
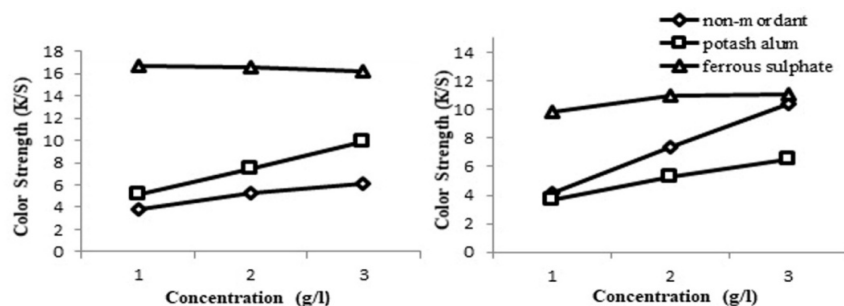


**Figure 5.** The effect of different mordants on color strength of *L. deliciosus* (left) and *L. sanguifluus* (right) extracts

$\Delta L^*$, $\Delta a^*$, $\Delta b^*$ values and the total color difference ($\Delta E$) can help to explain how the mordant changes color. The samples of dyeing without mordanting were taken as a reference for comparison. Total color difference ($\Delta E$) values are given for three different concentrations in Table 3 and 4. Table 3 and 4 indicate that there are significant color differences between the results of dyeing without and with mordanting. As shown in Table 3, dyeing samples with extract of *L. deliciosus* are dyed darker, redder and more yellow for most concentrations. While dyeing samples with extract of *L. sanguifluus* are dyed darker, redder and more yellow for ferrous sulphate mordant, samples of *L. sanguifluus* are dyed lighter, greener and more yellow for potash alum mordant for all concentrations in Table 4. The red/green (a*), yellow/blue (b*) and croma (C*) values increased depending on dyeing concentration for wool dyed with *L. sanguifluus* extract, while lightness (L*) values decreased.

In a previous study, anthraquinone dyestuff (60g anthraquinone powder from 10 kg fresh mushroom) was obtained in fruiting bodies of *Cortinarius sanguineus* and *C. semisanguineus* collected from Kuopio and Tuusula region of Finland, respectively [53] and natural and synthetic fibres were dyed with pure emodin and dermocybin found as major compounds in both *Cortinarius* species, as well as tap water extract. It was found that natural anthraquinones which produced light and dark colors such as yellow, orange and brown, could be suitable in dyeing and printing different textile materials. Maldonado and Ibarra [23] stated that *L. deliciosus,* which contained lactarazulene, lactaroviolin, has blue, reddish crystal, violet pigments and that extract of this mushroom painted the yarns in beige color by using different mordants (iron sulfate, tin chloride, potassium dichromate, alum and copper sulfate mordants).

K/S values increase, and L values decrease with the use of ferrous sulfate mordant. In case of ferrous sulphate mordant, brownish black shades are observed due to reacted with oxygen in air and light. The ferrous and ferric forms are found together on the fiber and their spectra overlap that alter $\lambda_{max}$ and the dyed fibers appear darker [54]. In other words, iron sulfate can form stable complex structures with both wool fibers and natural dyestuff such as "dihydroazulen–1–ol (R=H).

The wool fibre morphology, chemical constituents and its complex histological structure play a major role in dyeing. Wool mainly consists of amino acid units, which is composed of free amino and carboxyl groups. During the dyeing process, auxochrome groups of dyestuff bind with amino groups of the fibers via hydrogen bonding. Azulene is an organic compound. The organic compounds of the mushrooms (Figure 1) show dyeing properties for wool fibers due to their chromogen group such as benzene ring. Therefore, it is expected that chemical interactions between the dyestuffs in the mushrooms and the yarns occurred between $-R=CH_3$ or $-R=H$ groups of the dye molecule and functional groups of the fabrics via H-bonding. When the different dyes are combined with the mordant to form dyed-mordant complexes, different shades are than attained under different concentrations, and fastness such as washing and rubbing of many natural dyes could be improved by treatment with definite metal ions [55].

Rubbing and washing fastness values of dyed wool yarns with and without mordant are given in Table 5. Rubbing fastness is found to be in range of 2-4/5. All mordanted wool yarns and dry rub fastness are found to have better fastness values than non–mordanted and wet rub fastness, respectively. When comparing rubbing fastness, similar values were observed for *L. deliciosus* and *L. sangiufluus*. Washing fastness is also found to be in range of 2-4/5. The obtained staining washing fastness is good and the same as each other. But the changing washing fastness is bad/moderate. In addition, it can be said that the use of mordant changes slightly the washing fastness values for *L. sangiufluus* and *L. deliciosus*.

In fact, the metal complexes were easily formed with the fibers, and this could create affinity between natural dye and wool fiber [56]. Low washing and wet rubbing fastness values might to be due to the increased size of dye molecules when mordant molecules bind to the fiber and because water molecules removed some water–soluble dyes by the action of rubbing and washing conditions [57, 58].

## 4. CONCLUSION

Due to decreasing fossil resources in the world, increasing sensitivity to ecological and human health, natural dyes have become increasingly popular. Natural pigments and dyes which extracted from different natural resources such as plant, animal and fungal species since ancient times are used in pharmaceutical, food, cosmetic and textile dyeing industries. In this study, natural dyes from *L. deliciosus* and *L. sanguifluus* collected from Osmaniye province of Turkey were extracted and wool dyeing properties of these natural dyes were investigated. It has been indicated that cream and brown colors can obtained from natural dyestuff extracted from two different fungal species (*L. deliciosus* and *L.*

*sanguifluus*). According to the results of fastness tests, dry rubbing fastness values were high, but wet rubbing and washing (changing) fastness values were low. As a result, these colors can be used easily in textile field and especially in natural dyeing for traditional textile products such as carpets and rugs which are not washed often. It is a fact that commercially natural dyes cannot meet the needs of textile industry in the world and the natural dyes obtained from plants have still some drawbacks. Thus, the papers published associated with the use of bio-colorants show that the poor reproducibility, time-consuming extraction methods, insufficient degree of fixation and low color fastness properties are the main problems ahead the natural dyers to use this products in textile finishing industry. However, considering factors such as health and environment, it has been revealed that natural dyes can be an alternative to synthetic dyes. The study on the mushroom may be beneficial in terms of raising awareness. In particular, babies and elderly people should prefer textile apparel dyed with natural dyes for the sake of health. In addition, this study revealed that some mushrooms that are usually consumed as food and grow in many areas of Turkey can be used for natural dyeing. Fungi that are not used in nature are important for sustainability, because they can be easily used as a dyestuff in homes and cooperatives. In further studies, it is necessary to identify each natural dyestuff in different fungal species and to investigate their staining properties on wool yarns.

**Table 3.** Comparison of difference color measurement values for natural dyeing with *L. deliciosus* extracts

| Reference | Con. (g/l) | Samples Pre-mordanting | ΔL* | Δa* | Δb* | ΔE | Color comparison |
|---|---|---|---|---|---|---|---|
| Dyeing without mordanting | 1 | Potash alum | −2.59 | 2.31 | 2.65 | 04.36 | Sample is darker, redder, more yellow |
| | | Ferrous sulp. | −13.99 | 9.38 | 8.58 | 18.90 | Sample is darker, redder, more yellow |
| | 2 | Potash alum | −3.00 | 1.43 | 2.17 | 03.97 | Sample is darker, redder, more yellow |
| | | Ferrous sulp. | −13.70 | 2.64 | 0.23 | 13.96 | Sample is darker, redder, more yellow |
| | 3 | Potash alum | −6.58 | 1.24 | 0.78 | 06.74 | Sample is darker, redder, more yellow |
| | | Ferrous sulp. | −11.92 | 1.59 | -0.76 | 12.05 | Sample is darker, redder, more blue |

Con.: Concentrations

**Table 4**. Comparing of color difference measurement values for natural dyeing with *L. sanguifluus* extracts

| Reference | Con. (g/l) | Samples Pre-mordanting | ΔL* | Δa* | Δb* | ΔE | Color comparison |
|---|---|---|---|---|---|---|---|
| Dyeing without mordanting | 1 | Potash alum | 1.38 | −1.23 | 1.01 | 02.11 | Sample is lighter, greener, more yellow |
| | | Ferrous sulp. | −13.54 | 2.09 | 4.64 | 14.47 | Sample is darker, redder, more yellow |
| | 2 | Potash alum | 4.94 | −1.81 | −1.07 | 5.37 | Sample is lighter, greener, more blue |
| | | Ferrous sulp. | −5.96 | 0.76 | 2.51 | 6.51 | Sample is darker redder, more yellow |
| | 3 | Potash alum | 9.35 | −1.68 | 2.16 | 9.75 | Sample is lighter, greener, more yellow |
| | | Ferrous sulp. | 1.70 | 0.57 | 6.04 | 6.30 | Sample is darker, redder, more yellow |

Con.: Concentrations

**Table 5.** Rub and wash fastness properties of dyed samples

| Mordant | Con. (g/l) | *Lactarius deliciosus* | | | | *Lactarius sanguifluus* | | | |
|---|---|---|---|---|---|---|---|---|---|
| | | Rub Fastness | | Washing Fastness | | Rub Fastness | | Washing Fastness | |
| | | (dry) | (wet) | Changing | Staining | (dry) | (wet) | Changing | Staining |
| Without Mordant | 1 | 4 | 2/3 | 3 | 4/5 | 4 | 3 | 3 | 4/5 |
| | 2 | 4 | 2/3 | 3 | 4/5 | 3 | 2/3 | 3 | 4/5 |
| | 3 | 3/4 | 2 | 3 | 4/5 | 3 | 2/3 | 3 | 4/5 |
| Potash alum | 1 | 4/5 | 4 | 2 | 4/5 | 4/5 | 4/5 | 3 | 4/5 |
| | 2 | 4/5 | 3/4 | 2 | 4/5 | 4/5 | 4/5 | 3 | 4/5 |
| | 3 | 4/5 | 3/4 | 1/2 | 4/5 | 4 | 4 | 3/4 | 4/5 |
| Ferrous sulphate | 1 | 4/5 | 4/5 | 2/3 | 4/5 | 4/5 | 4/5 | 3 | 4/5 |
| | 2 | 4/5 | 4 | 2/3 | 4/5 | 4/5 | 4 | 3 | 4/5 |
| | 3 | 4/5 | 4 | 3 | 4/5 | 4/5 | 3/4 | 3/4 | 4/5 |

Con.: Concentrations

# REFERENCES

1. Hamano, P., Kilikian, B. (2006). Production of red pigments by *Monascus ruber* in culture media containing corn steep liquor. *Braz J Chem Eng*. 23, 443–449.

2. Goktas, O., Duru, ME., Yeniocak, M., Ozen, E. (2008). Determination of the color stability of an environmentally friendly wood stain derived from laurel (*Laurus nobilis L.*) leaf extracts under UV exposure. *For Prod J*. 8, 77–80.

3. Neeraj, N., Neera, M., Sayan, C. (2011). Microbial pigments with health benefits—A mini review. *Trends Biosci*. 4, 157–160.

4. Cardon, D., Higgitt, C. (2007). *Natural dyes: sources, tradition, technology and science*. London: Archetype Publications.

5. Hernández, VA., Galleguillos, FA., Sagredo, N., Machuca, Á. (2018). A Note on the dyeing of wool fabrics using natural dyes extracted from rotten wood–inhabiting fungi. *Coatings* 8(77), 1–6.

6. Becker, ZE. (1988). *Physiology and biochemistry of fungi*. Moscow University (Moscow): Publishing House, 1–229.

7. Velíšek, J., Cejpek, K. (2011). Pigments of higher fungi: A review. *Czech J. Food Sci*. 29(2), 87–102.

8. Lacheva, M. (2014). Morphological and biochemical study of Bulgarian species *Agaricus bohusii*. *Journal of Biodiversity and Environmental Sciences* 4(3), 32–39.

9. Hernández, VA., Galleguillos, F., Thibaut, R., Muller, A. (2019). Fungal dyes for textile applications: Testing of industrial conditions for wool fabrics dyeing. *The Journal of the Textile Institute* 10(1), 61–66.

10. Schweppe, H. (1993). *Handbuch der Naturfarbstoffe*. Landsberg/Lech.: Ecomed.

11. Hoiland, K. (1985). Garnfargning med sopp. Historikk. *Ottar* 152, 3–4.

12. Sundström, E., Ilona, S. (2003). *Värjäämme yrteillä, sienillä ja jäkälillä*, Kustannus-Mäkelä, Karkkila.

13. Sundström, C., Sundström, E. (1983). *Sienivarjays*. Otava, Helsinki.

14. Rice, M. (1980). *Mushrooms for Color*. Eureka, California: Mad River Press.

15. Edwards, RL., Lewis, G., Wilson, DV. (1961). *Constituents of the higher fungi. Part I. Hispidin, a new 4–hydroxy–6–styryl–Z–pyrone from Polyporus hispidus (Bull.) Fr.*, Department of Chemical Technology, Bradford Institute of Technology Bradford 7.

16. Gill, M., Steglich, W. (1987). Pigments in fungi (*Macromycetes*), in W. Herz, H. Grisebach, G.W. Kirby and Ch. Tamm (ed), *Progress in the Chemistry of Organic Natural Products* 51, 125–174.

17. Gill, M., Gimenez, A. (1990). Pigments of fungi. Part 17. (S)–(+)–Dermochrysone, (+)–Dermolactone, Dermoquinone, and Related Pigments; New Nonaketides from the Fungus *Dermocybe sanguinea* (sensu Cleland). *J Chem Soc Perkin Trans*. 1, 2585–2591.

18. Gill, M. (1994). Pigments of fungi (Macromycetes). *Natural Product Reports* 11, 67–90.

19. Hynninen, PH., Raisanen, R., Elovaara, P., Nokelainen, E. (2000). Preparative isolation of anthraquinones from the fungus *Cortinarius sanguineus* using enzymatic hydrolysis by the endogenous β–glucosidase. *Z. Naturforsch* 55,600–610.

20. Gruber, G. (2002). Isolierung und strukturaufklarung von chemotaxonomisch relevanten sekundarmetaboliten aus hoheren pilzen, insbesondere aus der ordnung der boletales, PhD Thesis, Faculty of Chemistry and Pharmacy, Ludwig–Maximilians University Munich.

21. Davoli, P., Mucci, A., Schenetti, L., Weber, RWS. (2005). Laetiporic acids, a family of non–carotenoid polyene pigments from fruit–bodies and liquid cultures of *Laetiporus sulphureus* (Polyporales, Fungi). *Phytochemistry* 66, 817–823.

22. Yang, XL., Luo, DQ., Dong, ZJ., Liu, JK. (2006). Two new pigments from the fruiting bodies of the Basidiomycete *Lactarius deliciosus*. *Helvetica Chimica Acta*. 89, 988–990.

23. Maldonado, MC., Ibarra, LV. (2006). Colorantes orgánicos de hongos y líquenes. *Revista Científica* 8(2), 141–162.

24. Zhou, ZY., Liu, JK. (2010). Pigments of fungi (Macromycetes). *Natural Products Reports* 27, 1531–1570.

25. Harmon, AD., Weisgraber, KH., Weiss, U. (1980). Preformed azulene pigments of *Lactarius indigo* (Schw.) Fries (Russulaceae, Basidiomycetes). *Experientia* 36, 54–56.

26. Ayer, WA., Browne, LM. (1981). Terpenoid metabolites of mushrooms and related basidiomycetes. *Tetrahedron* 37, 2197–2248.

27. Koul, SK., Taneja, SC., Ibraham, SP., Dhar, KL., Atal, CK. (1985). A C–formylated allene from *Lactarius deterrimus*. *Phytochemistry* 24, 181–182.

28. De Rosa, S., De Stefano, S. (1987). Guaiane sesquiterpenes from *Lactarius sanguifluus*. *Phytochemistry* 26, 2007–2009.

29. Spiteller, P., Steglich, W. (2002). Blennione, a green aminobenzoquinone derivative from *Lactarius blennius*. *Journal of Natural Products* 6, 725–727.

30. Mueller GM, Schmit JP (2006). Fungal biodiversity: what do we know? what can we predict?. *Biodiversity and Conservation* 16, 1–5.

31. Chen, L., Shi, Z., Wu, C., Zhao, C. (2020*). Gloeodontia yunnanensis* sp. nov. (Russulales, Basidiomycota) from China, evidenced by morphological characters and phylogenetic analyses. *Phytotaxa* 432(2), 111–118.

32. Dogan, HH., Bozok, F., Taşkın, H. (2018). A new species of Barssia (Ascomycota, Helvellaceae) from Turkey. *Turkish Journal of Botany* 42, 636-643.

33. Han, Li-Hong; Guo, Ting; Yang, Rui-Heng; Liu, Chao; Tang, Li-Zhou. (2019). *Strobilomyces sculptus* sp. nov. (Boletaceae) from eastern China with morphological and molecular evidence. *Nova Hedwigia* 109(1-2), 111-120.

34. Rossi, W. Vávra, J.C., Barták, M. (2019). New species and new records of Laboulbeniales (Ascomycota) from the Czech Republic and Slovakia. *Nova Hedwigia* 109(1-2), 149-159.

35. Ševčíková, H., Moreau, P., Borovička, J. (2020). *Pluteus keselakii* (Pluteaceae, Agaricales), a new species in section Celluloderma. *Phytotaxa* 432(2), 181–189.

36. Elliott, TF., Trappe, JM. (2019). Australasian sequestrate Fungi 20: *Russula scarlatina* (Agaricomycetes: Russulales: Russulaceae), a new species from dry grassy woodlands of southeastern Australia. *Journal of Threatened Taxa* 11(12), 14619-14623.

37. Hawksworth DL, Lücking R. (2017). Fungal diversity revisited: 2.2 to 3.8 million Species. *Microbiology Spectrum* 5, 79–95.

38. Bechtold, T. and Mussak, R. (2009). *Handbook of natural colorants*. Wiley Series in Renewable Resources. 183-200.

39. Durân, N., Teixeira, MFS., De Conti, R., Esposito, E. (2002). Ecological-friendly pigments from fungi. *Critical Rev. Food Sci. Nutrition* 42, 53-66.

40. Perumal, K., Sumathi, E., Chandrasekarenthiran, S. (2006). Microbial pigments for textile dyeing, Presentation at the International Symposium/Workshop on Natural Dyes, 5-12 November 2006.

41. Saxena, S., and A. S. M. Raja. (2014). *Natural dyes: Sources, chemistry, application and sustainability issues*. In Roadmap to sustainable textiles and clothing, ed. S. S. Muthu, 37–80. Singapore: Springer Science + Business Media.

42. Özdemir, H., 2017. Dyeing Properties of Natural Dyes Extracted from the Junipers Leaves (*J. excelsa Bieb. and J.oxycedrus L.*). *Journal of Natural Fibres*, 14(1), 134-142.

43. Wissgott, U, Bortlink, K. (1996). Prospects for new natural food colorants. *Trends Food Sci Technol.* 7:298–302.

44. Duran, N., Teixeira, MFS., De Conti, R., Esposito, E. (2002). Ecological–friendly pigments from fungi. *Critical Rev Food Sci, Nutrition* 42, 53–66.

45. Velíšek, J, Davidek, J., Cejpek, K. (2007). Biosynthesis of food constituents: Natural pigments, Part 1 – A review. *Czech J Food Sci.* 25(6), 291–315.

46. Hanson, JR. (2008). *The Chemistry of fungi*, The Royal Society of Chemistry, Thomas Graham House, Science Park, Milton Road, Cambridge CB4 0WF, UK, Chapter 7: Pigments and odours of fungi. 127–146.

47. Riikka, R. (2009). Dyes from lichens and mushrooms, Bechtold, T., Mussak., R. (ed.) *Handbook of natural colorants*, John Wiley & Sons, Ltd. ISBN: 978–0–470–51199–2. 183–200.

48. Jaklitsch, WM., Stadler, M., Voglmayr, H. (2012). Blue pigment in *Hypocrea caerulescens* sp. nov. and two additional new species in sect. Trichoderma. *Mycologia* 104(4), 925–941.

49. Saxena, S., Raja, ASM. (2014). *Natural dyes: Sources, chemistry, application and sustainability issues*. Textile Science and Clothing Technology. Singapore. 37–80.

50. Matênovâ, M., Horhoiu, VL., Dang, FX., Pospîsil, P., Alster, J., et al. (2014). Energy transfer in aggregates of bacteriochlorophyll c self–assembled with azulene derivatives. *Phys Chem Chem Phys.* 16, 16755–16764.

51. Needles, HL. (1986). *Textile fibers, dyes, finishes, and processes a concise guide*, New Jersey. Noyes publications.

52. Vigo, TL. (2005). *Textile processing and properties preparation, dyeing, finishing and performance*, United Kingdom: Elsevier science.

53. Reaisanen, R. (2018). Fungal colorants in applications–focus on *Cortinarius* species. *Coloration Technology* 135, 22–31.

54. Bhattacharya, SD., Shah, AK. (2000). Metal ion effect on dyeing of wool fabric with catechu. *Coloration Technology* 116(1), 10–12.

55. Eser, F., Tutak, M., Önel, A., Meral, B. (2016). Dyeing of wool and cotton fabrics with leaves of apple (*Malus domestica*) Tree. *Journal of Natural Fibers* 13(3), 289–298.

56. Baaka, N., Mahfoudhi, A., Mhenni, M.F. (2019). Tannin-rich natural dye extracted from kermes oak (*Quercus coccifera L.*): Process optimization using response surface methodology (RSM). *Journal of Natural Fibers* 16(8), 1209–1220.

57. Haji, A. (2010). Functional dyeing of wool with natural dye extracted from *Berberis vulgaris* wood and *Rumex hymenosepolus* root as biomordant. *Iran Journal Chemical Engineering* 29(3), 55–60.

58. Haji, A. (2012). Antibacterial dyeing of wool with natural cationic dye using metal mordants. *Materials Science* 18(3), 267–270.

59. 2019, 07 15. Index Fungorum, http://www.indexfungorum.org

60. 2019, 08 02. Azulene, https://spectrabase.com/spectrum/8gb9I2Uf4SM

# New Technology for Production of Leather for Gloves and Fancy Goods

Aigul Kudabayeva[1], Bekzhan Abzalbekuly[1], Urana Dandar[2], Ersin Onem[2], Behzat Oral Bitlisli[2]

[1]M. Kh. Dulaty Taraz State University, Tolei bi str. 60, 080000 Taraz, Kazakhstan
[2]Department of Leather Engineering, Faculty of Engineering, Ege University, 35100 Bornova-Izmir, Turkey

**Corresponding Author:** Ersin Onem, ersin.onem@ege.edu.tr

## ABSTRACT

The results of the development of chromium saving method for obtaining of glove-haberdashery leather, allowing to improve the quality of leather and to provide the ecological safety of production, were presented in the paper. Leather tanning with ecologically harmless tannages under proper parameters and consumption of chemical materials was carried out in semi-production conditions. The improvement of glove-haberdashery leather quality was achieved by partial replacement of chromium by complex compounds, containing titanium and aluminum. Physical and mechanical properties of glove-haberdashery ecologically harmless leathers corresponded the standard norms and can be recommended for production of men's and women's gloves.

## 1. INTRODUCTION

The most rational technological decision, allowing improvement of ready leather quality and providing ecological safety of leather industry, is the use of ecologically harmless chemical materials. Application of such chemical materials allows to intensify technological processes and to apply leather raw material rationally.

Tanning is one of the main leather processing including sufficient changes of dermis structure and determining the leather quality and economic component of production to a great extent. In this process, ecologically harmless complex compounds including metals like titanium and aluminum are wide spread. Their application is based on their ability to interact with various active groups of collagen in order to obtain tanned and filled skin tissue. In tanning process ecologically harmless complex mineral hardeners react with collagen mainly due to the same functional groups and form the links, which are inherent to their components [1-6]. It is especially valuable in the production of glove-haberdashery leather as soon as more strict requirements are made to thin glove leather. Their appearance and color must satisfy

consumer. Glove-haberdashery leather must be soft, plastic, dimensionally stable and strong tensile.

At present time great number of tanning methods with application of two, three or more tanning components have been worked out. Perspective kinds of mineral tanning methods are: chromium-titanium tanning, which complexes are strong and stable, and give dimensional stability and high occupancy to the leather [7-9]; chromium-aluminum tanning, allowing obtaining of soft leather with delicate front layer, which is easily colored and possesses some properties of chromium leather [10-12]. The use of chromium-aluminum complex is reducing the content of chromium in wastewaters and simplifies the further processing of leather [13].

Titanium and aluminum agents are used in leather production for the replacement of chromium in different ecological researches; on the other hand this study focuses the production of leather for gloves and fancy goods, and related the suitable implementation and results with the use of these complexes.

## 2. EXPERIMENTAL DETAILS

### 2.1. Material and production experiments

In order to obtain glove-haberdashery leather from Kazakh domestic rabbit pelts searching experiments on domestic rabbit pelt sample compiled by halves method have been carried out.

Moistening and soaking-liming processes have been conducted according to previously defined optimal parameters – according to the standard method of production of glove-haberdashery leather. It was stated that aluminum-chromium ratio in tanning is to be $Cr_2O_3 : Al_2O_3 = 1:1$, and for titanium-chromium ratio is to be $Cr_2O_3 : TiO_2 = 3:1$. Such conditions provide obtaining of soft, filled glove-haberdashery leather with improved appearance.

In order to work out optimal parameters of chromium-titanium and chromium-aluminum tanning on the base of the experiment planning theory these processes have been optimized.

The temperature of collagen welding is used as indicator of tanning degree of skin [14-17]. Therefore, the temperature of welding of semi finished products has been estimated during tanning process. Experimental results allowed determining optimal parameters of tanning, at which necessary temperature of welding at minimal expense of tanning reagents was reached. Data on welding temperature, pH and concentration of tanning reagents in semi finished products show that maximal effect is reached at the following consumption of reagents in terms of metal oxides in chromium-titanium tanning: $Cr_2O_3 - 1.0\%$ from the total mass of raw hide, $TiO_2 - 0.6\%$; in chromium-aluminum tanning: $Cr_2O_3 - 1.0\%$, $Al_2O_3 - 0.8\%$ at tanning duration – 3 hours [18].

### 2.2. Calculations and coefficient of the process

Ecologically harmless chromium-aluminum and chromium-titanium complex hardeners are characterized by good tanning activity, and respectively by high filling and plasticizing effects which determine the feasibility of joint use of these hardeners aimed to the development of three component complex chromium-aluminum-titanium hardener. The scheme of chromium-aluminum-titanium tanning for obtaining of glove-haberdashery leather is analogous to chromium-titanium and chromium-aluminum tanning.

The chromium consumption $(X_1)$, aluminum consumption $(X_2)$ and titanium consumption $(X_3)$ have been chosen as the factors influencing the efficiency of tanning. As optimization criteria welding temperature of semi products samples has been adopted as $Y_1$, $Y_2$ content of aluminum, $Y_3$ – content of titanium and $Y_4$ – content of chromium.

The intervals and level of factor variation have been selected taking into account the results of searching experiment. Symbols and variation levels of factors are represented in Table 1.

**Table 1.** Main characteristics of experiment

| Factor name | Parameters | $X_1$ | $X_2$ | $X_3$ |
|---|---|---|---|---|
| $X_1$-consumption of chromium hardener ($Cr_2O_3$) % from total mass of raw hide | Top level of factor (-1) | 1.2 | 1.2 | 0.9 |
| | Lower level of factor | 0.6 | 0.9 | 0.3 |
| $X_2$ - consumption of potassium alum ($Al_2O_3$) % from total mass of raw hide | Basic level of factor (+1) | 0.9 | 1.05 | 0.6 |
| | Variation levels of factor (0) | 0.3 | 0.15 | 0.3 |
| $X_3$ - sulfate titanilate of ammonia $TiO_2$ % from total mass of raw hide | Ratio | 3 | 7 | 2 |

Coefficients of regression equations have been calculated and evaluation of their significance has been carried out with a help of Fisher's criterion. The equations obtained adequately characterize the dependence between welding temperature and content of $Al_2O_3$, $TiO_2$ and $Cr_2O_3$ in the samples of produced leather.

### 2.3. Modelling of the process

The hypothesis of adequate model has been verified by Fisher's criterion (F-criterion) [19]. Conditionality is sustained, therefore the second order mathematical model obtained can be regarded adequate with a probability of 95%, the calculated Fisher coefficient is 2,63 for $Y_1$, 2,08 for $Y_2$, 0,88 for $Y_3$, 1,04 for $Y_4$.

As a result of mathematical processing the following regression equations have been obtained:

$$Y_1(T_{cs}) = 107,25 + 8,23 * X_1 +$$
$$+ 2,17 * X_2 + 4,85 * X_3 +$$
$$+ 0,63 * X_1 * X_2 + 1,38 * X_1 X_3 -$$
$$- 0,63 * X_2 X_3 - 3,27 * X_1^2 +$$
$$+ 0,43 * X_2^2 - 2,21 * X_3^2; \tag{1}$$

$$Y_2(Al_2O_3) = 2,03 - 0,02 * X_1 +$$
$$+ 0,23 * X_2 + 0,14 * X_3 +$$
$$+ 5,55 * X_1 * X_2 - 0,05 * X_1 X_3 +$$
$$+ 5,55 * X_2 X_3 + 0,31 X_1^2 +$$
$$+ 0,281 * X_2^2 + 0,24 * X_3^2; \tag{2}$$

$$Y_3(TiO_2) = 1,30 - 0,03 * X_1 +$$
$$+ 0,05 * X_2 + 0,23 * X_3 +$$
$$+ 0,03 * X_1 X_2 + 0,03 * X_1 X_3 +$$
$$+ 0,03 * X_2 X_3 + 0,02 * X_1^2 -$$
$$- 0,01 * X_2^2 - 0,02 * X_3^2; \tag{3}$$

$$Y_4(Cr_2O_3) = 3{,}17 + 0{,}43 * X_1 +$$
$$+ 0{,}06 * X_2 - 0{,}24 * X_3 -$$
$$- 0{,}1 * X_1 * X_2 - 5{,}6 * X_1 * X_3 +$$
$$+ 5{,}55 * X_2 * X_3 - 0{,}15 * X_1^2 -$$
$$- 0{,}08 * X_2^2 - 0{,}18 * X_3^2;$$
(4)

Based on the analysis of regression equations we can make the following conclusions: the positive signs "+" at $X_1X_2$ and $X_1X_3$ indicate that in joint tanning by aluminum ($X_2$) titanium ($X_3$) and chromium ($X_1$) compounds (the last acts as stabilizer) these metals are complementary, but do not displace each other. Pair interactions in equation (1) chromium-aluminum and chromium-titanium show that they promote raising of welding temperature of experimental samples of semi-finished products, and aluminum-titanium on the contrary lowers the temperature (sign "-" at $X_1X_2$).

The analysis of equation (2) proves that joining of chromium and aluminum (positive sign "+" at $X_1X_2$) promotes the formation of stable complexes and fastens the links of aluminum with collagen.

Adsorption of aluminum and titanium from the solution depends largely on the chromium consumption. Sign "-" at $X_1$ in equations 2, 3 denote that decrease of chromium content leads to the increase of waste aluminum and titanium content in the solution. This is proved by pair contribution (sign "+" at $X_1X_2$).

In equation (3) pair interaction of factors (sign "+" at $X_1X_2$, $X_1X_3$, and $X_2X_3$) indicate the formation of stable complexes increasing the links with collagen. Negative signs at $X_2^2$ and $X_3^2$ indicate that decrease of aluminum and titanium consumption slow down penetration into the dermis structure.

Equation (4) confirms that decrease of expense of aluminum compounds in combination with chromium compounds (sign "-" at $X_1X_2$ and $X_1X_3$) will influence the decrease of linking of these compounds with collagen. Sign "-" at $X_3$ indicates that decrease of titanium expense worsens its absorption may be because of strong hydrolysis, therefore it is necessary to increase the quantity of chromium and aluminum (sign "+" at $X_1$ and $X_2$), rendering stabilization effect on titanium.

## 2.4. Characterization techniques applied on leather

Chemical and physical analyses were carried out as defined in GOST 15092-80 [20]. Analyses of thickness according to TS EN ISO 2589 [21], tensile strength and percentage extension tests to TS EN ISO 3376 [22], pH to TS EN ISO 4045 [23], moisture content to TS EN ISO 4684 [24], chrome oxide TS EN ISO 5398-1 [25] and matter soluble content to TS EN ISO 4048 [26] were performed.

## 3. RESULTS AND DISCUSSION

As a result of the experiment optimal values of parameters of chromium-titanium tanning have been estimated and maximal tanning effect have been stated at following parameters and consumption of chemical materials: consumption of potassium alum, counting on ($Al_2O_3$; basicity 40%) is 0.8% from the mass of raw hide; consumption of sulfate titanilate of ammonia, counting on $TiO_2$ (basicity 60%) is 0.6% from the raw hide mass; consumption of chromium tanner, counting on ($Cr_2O_3$; basicity 38%) is 0.9% from the raw hide mass; sodium carbonate – 1.0% from the raw hide mass; liquid ratio 0.4; tanning duration – 3 hours; initial temperature of tanning – 21°C.

Application of chromium-aluminum-titanium complex leads to lowing of chromium compounds expense to 44%, that is only 0.9% of chromium salts instead of 1.6% of chromium oxide used according to standard method of tanning of glove- haberdashery leather that provide improvement of wastewater conditions. At the same time high thermal stability of glove- haberdashery leather is reached.

Water-soaking, liming, pre tanning and tannin processes according to elaborated technologies of glove-haberdashery leather production of chromium-titanium, chromium-aluminum and chromium-aluminum-titanium tanning at proper parameters of chemical reagent consumption, and dying-fat liquoring processes according standard methods of glove-haberdashery leather production.

As a result of experiment light colored samples have been obtained which had following organoleptic properties: good density, fullness and softness. At the same time the distinctive grain pattern, which uniformly located over the entire surface single points, have been retained.

Physical and mechanical properties are the main characteristics of leather quality (strength, longevity, etc.). They are due to the ability of leather to resist to various types of loading, and its deformation capacity as well.

Samples of semi finished products obtained by chromium-titanium, chromium-aluminum and chromium-aluminum-titanium tanning have been exposed to physical-mechanical tests. The results of physical-mechanical parameters are represented in Table 2.

Chromium-titanium tanned leather is characterized by good density, fullness, dimensional stability and high strength index.

Chromium-aluminum tanned leather is characterized by softness, plasticity and soft front surface.

Chromium-aluminum-titanium tanned leather is characterized by softness, dimensional stability, good density and fullness, and high strength index and elastic-plastic properties as well.

**Table 2.** Results of physical-mechanical tests of glove-haberdashery leather obtained by chromium-titanium (CT), chromium-aluminum (CA) and chromium-aluminum-titanium (CAT) tanning

| The name of leather | | Glove- haberdashery leather | | |
|---|---|---|---|---|
| Tanning method | | CT | CA | CAT |
| Thickness, mm | | 2 | | |
| Cross-sectional area | | 2 | | |
| Loading, N | Cracking of front layer | 17.2 | 14.8 | 17.6 |
| | Breaking of the sample | 18.8 | 16.2 | 19.2 |
| Conditional elastic modulus, N/m$^2$ | | 4.9 | 3.8 | 4.1 |
| Rigidity, N | | 9.8 | 7.6 | 8.2 |
| Breaking point, MPa | Cracking of front layer | 8.6 | 7.4 | 8.8 |
| | Under tension | 9.4 | 8.1 | 9.6 |
| Coefficient of uniformity | | 8 | | |
| Elongation, mm | Under tension of 9.8 Mpa | 10 | 13 | 12 |
| | Cracking of front layer | 22 | 26 | 25 |
| | Breaking of the sample | 25 | 30 | 29 |
| | Elastic | 10 | 12 | 12 |
| | Residual | 15 | 19 | 17 |
| Relative elongation, % | Under tension of 9.8 Mpa | 20 | 26 | 24 |
| | Cracking of front layer | 44 | 52 | 50 |
| | Breaking of the sample | 50 | 60 | 58 |
| | Elastic | 20 | 24 | 24 |
| | Residual | 30 | 36 | 34 |
| Data represented are arithmetic mean of three measurements | | | | |

Experiments allowed to adjust that physical-mechanical properties of glove- haberdashery leather correspond standard characteristics for glove-haberdashery leather and have following differences: leather of chromium-titanium tanning exceeds leather of chromium tanning in strength parameter; leather of chromium-aluminum tanning – in elongation parameter; leather of chromium-aluminum-titanium tanning exceeds on strength and elastic-plastic parameters.

So, optimal mass ratio $Cr_2O_3 : Al_2O_3 : TiO_2 = 0.9 : 0.8 : 0.6$ was determined, at which the highest welding temperature, even leather filling and high elastic-plastic parameters had been reached [27].

Chemical composition and mechanical properties of glove-haberdashery leather of chromium-titanium, chromium- aluminum and chromium-aluminum-titanium tanning are compiled in Table 3.

**Table 3.** Chemical composition and mechanical parameters of glove-haberdashery leather of chromium-titanium, chromium-aluminum and chromium-aluminum-titanium tanning

| Parameter | State Standard 15092-80 | Experimental | | |
|---|---|---|---|---|
| | | CT | CA | CAT |
| Moisture, % | 10-16 | 14.6 | 14.6 | 14.6 |
| Compounds, extracted by organic solvents, % | 12-20 | 12.4 | 12.4 | 12.4 |
| Chromium oxide, % | 3 | 3,2 | 3,2 | 3 |
| Titanium oxide, % | 0 | 1.6 | 0 | 1.4 |
| Aluminum oxide, % | 0 | 0 | 2,4 | 2 |
| Grease (for all kinds of skin, except pigskin) | 4-12 | 6 | 6 | 5,8 |
| pH of water extract | 4-6 | 4.6 | 4.6 | 4.6 |
| Ultimate strength of elongation, MPa (for all kinds of skin, except pigskin) | 8-10 | 9.4 | 8.1 | 9.6 |
| Ultimate strength of elongation of front layer, MPa, no less than | 8-10 | 8.6 | 7.4 | 8.8 |
| Elongation at breaking point, %, no less than | 40-45 | 50 | 60 | 58 |

The most common method of estimation of strength properties of leather is the test on mono axial tension [28-31].

The semi-products samples of chromium, chromium-titanium, chromium-aluminum and chromium-aluminum-titanium tanning have been exposed to the mono axial tension test. As it can be seen from Figure 4, elongation curves for semi-products obtained from rabbit pelts by various tanning methods are just like the curves for soft leather, namely these curves are convex to the elongation axis that is quite important for glove-haberdashery leather.

For glove-haberdashery leather the elongation index is of great importance, because during exploitation gloves meet permanent elongation causing deformation of their initial form, and regeneration is possible only in the presence of elastic properties.

At the beginning of exploitation of gloves leather must have certain level of permanent deformation for easy and convenient removal and donning of gloves.

If the curves are conditionally divided into three intervals: I- permanent elongation, II-elastic elongation, III-plastic elongation and destruction phase, then, as it can be seen from Figure 1 elongation curves of semi-products of chromium, chromium-aluminum and chromium-aluminum-

titanium tanning have a large percent of permanent elongation – 1- area of smooth beginning of the curves.

The existing dependence between increase of loading and elastic elongation show that increase of elastic elongation – II- area of the curves, convex to the elongation axis – is behind the loading increase, it testifies high elastic properties of given samples of semi-products of chromium and chromium-aluminum-titanium tanning (Figure 1).
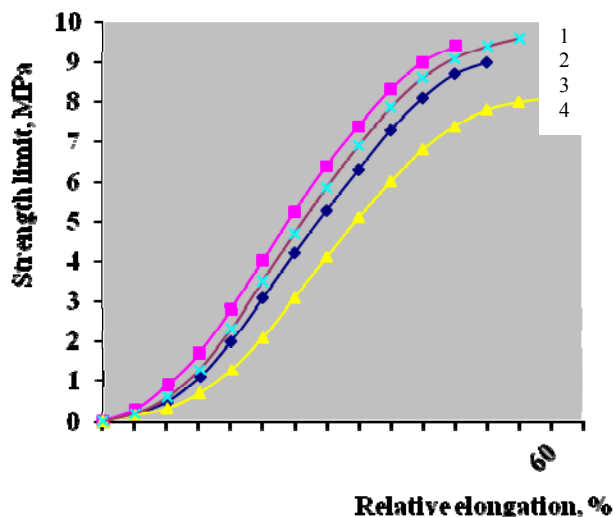


**Figure 1.** Curves of elongation of semi-product samples obtained by various tanning methods (1- chromium-titanium, 2- chromium-aluminum-titanium, 3- chromium, 4- chromium-aluminum)

Maximum curvature of the curve of semi-product sample obtained by chromium-aluminum tanning is probably due to the particles of aluminum and chromium compounds absorbed on the surface of structural elements, which facilitate their orientation (irreversible movements), that decreases leather facility for elastic elongation; and thus enhances its plastic properties [32]. However, excessively high plastic properties are not reliable for glove-haberdashery leather because they contribute weak dimensional stability. The curvature of the curve of semi-product sample obtained by chromium-aluminum tanning indicates that leather processed by this tanning method will have low strength.

The curve of semi-product sample obtained by chromium-titanium tanning, the growth of loading in sector I is quicker than the growth of relative elongation, apparently due to the particles of titanium tanner absorbed on the surface of structural elements, lowing their orientation ability and creating rigid frame, enforcing fibrous structure of dermis that leads to the growth of strength limit and to the decrease of elongation of semi-products. More rectified course of the curve of semi-product obtained by chromium-titanium tanning indicates insufficient softness which is quite necessary for glove-haberdashery leather. It has also been confirmed by relatively high elastic module.

The comparison of courses of deformation curves show that semi-finished products obtained by chromium-aluminum-titanium tanning are preferable, because in terms of elongation they are not interior to chromium-aluminum tanned semi-finished products, and at the same time have better strength parameters than semi-finished chromium-titanium tanned semi-finished products. The best elastic-plastic properties of these samples are due to better flexibility of structural elements of dermis, which have the most adequate response to the load, causing the deformation. To great extent in is caused by joint application of separate types of mineral tanners – Cr, Al and Ti as three component complex mineral tanner.

Glove-haberdashery leather samples have been produced by applying the results of experiments based on the developed technology. Organoleptic qualitative evaluation of glove-haberdashery leather which confirmed following properties; complete tanning, good appearance, softness, even surface and color, smooth and well processed reverse side, have been carried out (Figure 2).
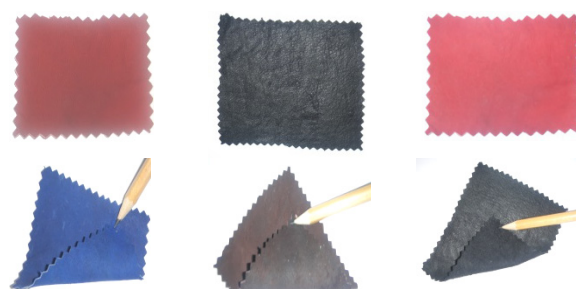


**Figure 2.** Experimental samples of glove-haberdashery leather produced from domestic rabbit pelts (face and reverse sides)

Men's gloves have been made from glove-haberdashery leather obtained (Figure 3). Further works are related to improvement of constructive-technological solution of this model and design of men's and woman's gloves.



**Figure 3.** Appearance of men's gloves

## 4. CONCLUSION

During production of the glove-haberdashery leathers with proper correction of process parameters, necessary ecologically harmless materials have been chosen and their expense has been taken into account, properties of the material have been clarified. Investigation of physical-mechanical properties of glove-haberdashery leather has shown that they provided the standard requirements. According to our study, men's gloves have been successfully manufactured with satisfactory results from ecologically harmless recipe designed for glove-haberdashery leathers by chromium saving methods.

# REFERENCES

1. Zengin ACA, Crudu M, Maier SS, Deselnicu D, Albu L, Gulumser G, Bitlisli BO, Basaran B, Mutlu MM. 2012. Eco-leather: Chromium-free leather production using titanium, oligomeric melamine-formaldehyde resin, and resorcinol tanning agents and the properties of the resulting leathers. *Ekoloji*, 21, 17-25.

2. Madiev UK. 1987. Mineral'noe dublenie v proizvodstve kozh. *Moskva: Legprombytizdat*, 120p.

3. Peng BY, Shi B, Ding KY, Fan HJ, Shelly DC. 2007. Novel titanium (IV) tanning for leathers with superior hydrothermal stability - III. Study of factors affecting titanium tanning and an eco-friendly titanium tanning method. *Journal of the American Leather Chemists Association*, 102, 297-305.

4. Gerasimova LG, Shchukina ES, Ohrimenko RF, Maslova MV. 2013. On the behavior of titanium(IV) sulfate in aqueous media used in leather tanning. *Russian Journal of Applied Chemistry*, 86, 453-457.

5. Mutlu MM, Crudu M, Maier SS, Deselnicu D, Albu L, Gulumser G, Bitlisli BO, Basaran B, Tosun CC, Zengin ACA. 2014. Eco-leather: Properties of chromium-free leathers produced with titanium tanning materials obtained from the wastes of the metal industry. *Ekoloji*, 23, 83-90.

6. Rosu L, Varganici CD, Crudu AM, Rosu D. 2018. Influence of different tanning agents on bovine leather thermal degradation. *Journal of Thermal Analysis and Calorimetry*, 134, 583-594.

7. 7. Kozyreva NV, Bajandin VV, Klenovskaja NV. 1990. Fiziko-mehanicheskie svojstva kozh dlja verha obuvi titanhromovogo metoda dublenija. *Kozhevenno-Obuvnaja Promyshlennost*, 4, 58-60.

8. Crudu M, Deselnicu V, Deselnicu DC, Albu L. 2014. Valorization of titanium metal wastes as tanning agent used in leather industry. *Waste Management*, 34, 1806-1814.

9. Wang KJ, Chen YN, Dan NH, Li F, Dan WH. 2018. Chrome-less tanning - a non-pickling process based on Zr-Al-Ti complex tanning agent. *Journal of the Society of Leather Technologists and Chemists*, 102, 1-6.

10. Zissel A, Schmidt G, Magerkurth B. 1980. Der Erstz des Chroms durch aluminium und andere Gerbstoffe im Hinbiick uf Leder character Gerbsoffbindund. *Leder*, 2, 17-24.

11. Han W, Zhou CF, Zhang WH, Shi B. 2017. Molecular level understanding of the stability difference in collagen induced by chromium sulfate and aluminum sulfate. *Journal of the Society of Leather Technologists and Chemists*, 101, 273-279.

12. Wang L, Han WM, Yu Y, Zhou JF, Zhang WH, Shi B. 2017. Thermodynamic investigations on chrome and aluminum tanning. *Journal of the American Leather Chemists Association*, 112, 360-366.

13. Krawecki CZ. 1980. Methode non convetionnelle de tannage chrome/aluminium. *Technicuir*, 4, 73-76.

14. Dilek Y, Basaran B, Sancakli A, Bitlisli BO, Yorgancioglu A. Evaluation of collagen hydrolysate on the performance properties of different wet-white tanned leathers. *Journal of the Society of Leather Technologists and Chemists*, 103, 129-134.

15. Tang HR, Covington AD, Hancock RA. 2003. Use of DSC to detect the heterogeneity of hydrothermal stability in the polyphenol-treated collagen matrix. *Journal of Agricultural and Food Chemistry*, 51, 6652-6656.

16. Hui C, Zhi-Hua S. 2008. Changes in hydrothermal stability of collagen with several catechin-metal compounds: A DSC study. *Journal of the Society of Leather Technologists and Chemists*, 92, 93-95.

17. Wang YJ, Guo J, Chen H, Shan ZH. 2010. Influence of containing moisture on hydrothermal stability of modified collagen thermal characteristics analysis by DSC. *Journal of Thermal Analysis and Calorimetry*, 99, 295-300.

18. Urudzhev RS, Demirova AM, Gadzhieva AM. 2005. O mehanizme vlijanija dublenija na termostojkost' kollagena. *Kozhevenno-Obuvnaja Promyshlennost'*, 2, 47-48.

19. Li Y, Zhao WG, Pan JH. Deformable patterned fabric defect detection with fisher criterion-based deep learning. *IEEE Transactıons on Automation Science and Engineering*, 14, 1256-1264.

20. GOST 15092-80. 1982. Interstate Standards, Leather for gloves and mittens. *Specifications*, Moscow, 12p.

21. TS EN ISO 2589. 2016. Leather - Physical and mechanical tests - Determination of thickness. *Turkish Standards Institution*, Ankara, 11p.

22. TS EN ISO 3376. 2012. Leather - Physical and mechanical tests - Determination of tensile strength and percentage extension. *Turkish Standards Institution*, Ankara, 13p.

23. TS EN ISO 4045. 2018. Leather - Chemical tests - Determination of pH. *Turkish Standards Institution*, Ankara, 14p.

24. TS EN ISO 4684. 2006. Leather - Chemical tests - Determination of volatile matter. *Turkish Standards Institution*, Ankara, 14p.

25. TS EN ISO 5398-1. 2018. Leather - Chemical determination of chromic oxide content - Part 1: Quantification by titration. *Turkish Standards Institution*, Ankara, 18p.

26. TS EN ISO 4048. 2018. Leather - Chemical tests - Determination of matter soluble in dichloromethane and free fatty acid content. *Turkish Standards Institution*, Ankara, 22p.

27. 27. Danilkovich AG, Chursin VI. 2002. Praktikum po himii i tehnologii kozhi meha. *Uchebn. Posobie Dlja Vuzov, Moskva: CNIIKP*, 413p.

28. Venkatachalam PS. 1962. Lecture Notes on Leather. *Central Research Institute*, Madras, India.

29. Kontou E, Farasoglou P. 1998. Determination of the true stress–strain behaviour of polypropylene. *Journal of Materials Science*, 33, 147-153.

30. Case J, Chilver A, Ross CTF. 1999. Strength of materials and structures. *Butterworth-Heinemann*, 720p.

31. Roylance D. 2001. Stress-strain curves. *Massachusetts Institute of Technology*, Cambridge University Press.

32. Nalbat S, Onem E, Basaran B, Yorgancioglu A, Yilmaz O. Effect of finishing density on the physico-mechanical properties of leather. *Journal of the Society of Leather Technologists and Chemists*, 100, 84-89.

# Sound-Absorption Properties of Composite Materials Containing Waste-Wool / Polyamide Fibers and Their Relationship with Fractal Dimensions

Lihua Lyu[*], Jing Lu, Yongfang Qian, Hong Li, Changwei Li, Jing Guo

School of Textile and Material Engineering, Dalian Polytechnic University, Dalian 116034, P.R. China

**Corresponding Author:** Corresponding Author: Lihua Lyu, lvlh@dlpu.edu.cn

## ABSTRACT

To solve the problems related to the recycling of waste fibers, composite materials were prepared by the hot-pressing method using waste-wool fibers and waste low-melting-point polyamide fibers combined into a net as the raw materials. The effects of the volume density, mass fraction of waste-wool fibers, and thickness on the sound-absorption properties of the resulting composite materials were studied by the controlling-variable method. The sound-absorption properties of the composite materials were studied by the transfer-function method, and under optimized technological conditions, the sound-absorption coefficients were above 0.8 and the sound-absorption bands were wide. According to the box-counting-dimension method, which is based on the fractal theory, the fractal dimensions of the composite materials were calculated using the Matlab program. The relationships between the fractal dimensions and the volume densities, mass fractions of waste-wool fibers, and thicknesses of the composite materials were also analyzed. Then, quantitative relationships between the fractal dimension and the maximum sound-absorption coefficient, and between the fractal dimension and the resonant sound-absorption frequency, which play a major role in the sound-absorption design of composite materials, were deduced.

## 1. INTRODUCTION

China is currently the world's largest wool producer and sheep breeder, and it is also one of the countries with the largest wool consumption and import volume [1]. According to statistics, China's annual wool production is stable at about 400,000 tons, while the annual waste accounts for 40% of the world's annual waste [2]. However, these waste-wool resources have not yet been rationally utilized, which not only causes a terrible waste but also requires landfill disposal, causing serious environmental pollution, threatening human health, and posing a hidden risk of fire. Therefore, finding a way to recycle the waste-wool fibers has become an attractive research topic.

As early as the 1990s, Japanese scholars studied the use of waste-wool fibers. Then they made composite materials based on waste-wool and feathers by hot pressing and tested the bending strength of the materials to open up a new direction for the reuse of waste-wool fibers [3]. Alzeer et al. [4] used an aluminosilicate inorganic polymer and wool fibers to prepare a new fiber-reinforced composite material and measured its mechanical properties. Patnaik et al. [5] used wool fibers and regenerated polyester fibers (RPET) as raw materials to prepare nonwoven products. To meet the requirements of materials in the construction industry in terms of fire and moisture resistance, a flame-retardant and moisture-resistant finishing was carried out on the fibers, and the recyclability and biodegradability of the samples were ensured, which provided a new idea for the

reuse of waste-wool fibers in the future. Li et al. [6] prepared an ultra-short waste-wool-fiber nonwoven fabric by a wet nonwoven process. To improve the recovery rate of waste-wool fibers, He et al. [7] developed a quality-control method and a technology suitable for mass production. This method was mainly a physical method and did not damage the wool microstructure. At present, the conventional treatment is based on chemical methods, such as that by Yao et al. [8-10] who devoted themselves to the study of wool keratin, continuously optimizing and perfecting the process of wool-keratin solution, and summarizing the progress of wool-keratin dissolution and recycling. Li et al. [11] used a self-made ionic liquid to dissolve wool and cellulose to produce a blend film with excellent flame-retardant properties and compatibility. The keratin-based industrial production of waste-wool fibers by hydrolysis is very difficult and costly. In addition, LV et al. [12, 13] prepared flame retardant waste fiber/polyurethane insulation and flame retardant waste corn husk fiber/polylactic acid composites by blending-hot pressing method. At present, the development of waste-wool fibers is mostly concentrated in the above fields. With the aggravation of noise pollution, the fabrication of sound-absorbing materials containing waste fibers is also beginning to rise. From the acoustic point of view, wool fiber has a smaller density, compared to other natural fibers, has a certain curliness, and is easy to be clustered together to form a large number of interconnected pores, which provides favorable conditions for the preparation of porous sound-absorbing materials. Zhejiang University scholars studied the acoustic and thermal properties of this series of wool products. Recently, Cheng et al. [14] studied a kind of thermally insulating and sound-absorbing material that combines a net formed by mixing natural fibers with hot-melt fibers and a flame-retardant adhesive layer. There are some articles [15-17] on wool-based sound-absorbing materials, and the noise-reduction coefficients of the prepared wool-based sound-absorbing materials were all above 0.6, but the sound-absorbing mechanism of wool has not been thoroughly studied.

The word "fractal" is derived from the Latin "fractious" and means fragmented. A fractal is defined as a mathematical object with a fractional (non-integer) dimension. It seems that wherever there is structural disorder and chaos, fractal geometry can be an efficient way of describing and analyzing the system. The fractal dimension is a very good mathematical method for studying unequal geometric substances and can reflect characteristics appearing in nature. The application of a fractal system allows us to explain numerous states of fragmenting and branching occurring in ecological, biological, and other systems [18-21]. The inside of a nonwoven fabric [22], a fiber-reinforced composite material [23, 24], a fiber aggregate [25], or a similar substance is characterized by a porous body composed of fibers and pores. The pore shapes are not regular or smooth, the pore sizes are also different, and there is no characteristic dimension that can indicate the internal pore structure [22]. Fractal geometry is a new tool to simulate irregular pore structures of materials. The relationship between the fractal dimension and the structural parameters of porous materials can be obtained through fractal image processing and mathematical calculations. The larger the fractal dimension, the rougher the pore surface or the more complex the pore structure [26]. Fractal theory is applied to quantitatively analyze the structure and characteristics of materials, making the structural analysis of materials more intuitive.

Herein, a composite material was prepared using waste-wool fibers and waste low-melting-point polyamide fibers as raw materials by combing them into a net and applying the hot-pressing method. The effects of the volume density of the composite material, the mass fraction of the waste-wool fibers, and the thickness of the composite material on the sound-absorption coefficient curve were carefully analyzed by single-factor experiments. The sound absorption curves of composites were given. But, at low thickness values, the composites show very low sound absorption behavior especially at low and medium frequency ranges. Noise in application areas such automotive, panels lies in the in the acoustic range between 100 and 2000 Hz. The sound absorption characteristics obtained over the frequency of 2000 Hz are not significant for these end-uses. According to the self-similarity, the quantitative relationships between fractal dimension and maximum sound-absorption coefficient, and between fractal dimension and resonant sound-absorption frequency were deduced by the box-counting method.

## 2. MATERIALS AND METHODS

### 2.1 Materials and Equipment

The type of waste wool was sweeping wool. Waste-wool fibers with an average length of 30–70 mm, diameter of 15-30μm and a density of 1.384 g·cm$^{-3}$ (Fudi Wool Textile Factory, Shandong, China) and waste low-melting-point polyamide fibers with a density of 1.14 g·cm$^{-3}$, an average length of 60–70 mm, and a melting point 100°C (Kaitai Special Fiber Technology Co., Ltd., Zhejiang, China) were used as the raw materials. A DSCa-01 digital sample carding machine (provided by Jiacheng Mechanical and Electrical Equipment Co., Ltd., Tianjin), an MP2000D Shanghai Jingke Analytical Balance (Tianma Instrument Factory, Tianjin), a QLB-50D/Q hot-pressing machine (provided by Zhongkai Rubber Machinery Co., Ltd., Jiangsu), an SW422/SW477 impedance-tube sound-absorption test system (provided by Shengwang company, Beijing), and a JEOL JSM-6460LV scanning electron microscope (provided by JEOL Ltd. Japan) were used for testing.

### 2.2 Preparation of the Composite Materials

The composite materials were prepared by combing the raw materials, that is, the waste-wool fibers and the waste low-

melting-point polyamide fibers, into a net and applying the hot-pressing method. The waste-wool fibers and waste low-melting-point polyamide fibers were mixed in a certain proportion using a digital sample carding machine and heated to 110°C at 10 MPa for 30 min using a QLB-50D/Q hot-pressing machine. Cmposite materials with mass fractions of waste-wool fibers of 0%, 30%, 40%, 50%, 60%, 70%, and 100% were prepared. Then, the composite materials were formed and test samples were prepared as disc-shaped composites with sizes of Φ100 × 5 mm, Φ100 × 10 mm, Φ100 × 15 mm, Φ100 × 20 mm, Φ100 × 25 mm, Φ100 × 30 mm, and Φ100 × 35 mm.

## 2.3 Testing of the Composite Materials

### 2.3.1 Testing of the Sound-Absorption Coefficient

Testing of the sound-absorption coefficient was done according to the standard GB/T 18696.2-2 002 and GB/T 186 96.1-2004. Under the conditions of atmospheric temperature (24°C), velocity of sound wave (345.6 m/s), a characteristic impedance of air of 409.78 Pa·s/m, and a relative humidity of 65%, the sound-absorption coefficient curves of the samples were tested using an SW422/SW477 impedance-tube sound-absorption test system [27]. The measured sound-absorption coefficient curve was the average of six measurements. Figure 1 shows a schematic diagram of the sound-absorption test.

### 2.3.2 Calculation of the Porosity

The sound-absorption performance of the composite material was closely related to the porosity, which can be indirectly calculated according to the thickness and areal density of the sample [28]. The porosity of the sample was calculated using equation 1:

$$\eta \% = ( 1 - \frac{G}{\rho \times \sigma} ) \times 100 \qquad (1)$$

where $\eta$ is the porosity of the sample (%), G is the surface density of the sample (g·cm$^{-2}$), $\rho$ is the mixed specific gravity of the fibers (g·cm$^{-3}$), and $\sigma$ is the thickness of the sample (m).

### 2.3.3 Fractal Characterization

The surface morphology of the samples was studied using a JEOL JSM-6460LV scanning electron microscope, and the pixel size of the intercepted images was 1024 × 1024. The software Photoshop was used to process the gray levels of the obtained scanning electron microscope images, and an image threshold was set. Then, the image with gray levels was converted into a binary image that could be recognized by the computer, and the box-counting method [29] was applied to calculate the fractal dimension of the sample using the Matlab program (the procedure is described in annex A).

The calculation principle of the box-counting dimension method is based on taking a small cube box with an edge length of $\varepsilon$ and covering the curve graph with fractal characteristics. Some boxes are empty, some boxes contain a part of the curve, and the number of boxes containing the curve is recorded as N ($\varepsilon$). Then, the size of the box is shortened and N ($\varepsilon$) increases correspondingly. If $\varepsilon$ is close to 0, the fractal dimension of the curve can be obtained using equation 2:

$$D = -\lim_{\varepsilon \to 0} \frac{\log N(\varepsilon)}{\log \varepsilon} \qquad (2)$$

However, in the actual calculation process, the value of $\varepsilon$ is not infinite; it is finite. By fitting and mapping with the least-square method, a straight line is obtained, and the fractal dimension is given by the slope of that straight line. For the box-counting dimension analysis of two-dimensional digital images, Matlab offers a rich visual graphic representation function and a convenient programming ability [30], so Matlab was used for image processing, numerical analysis, and other operations.
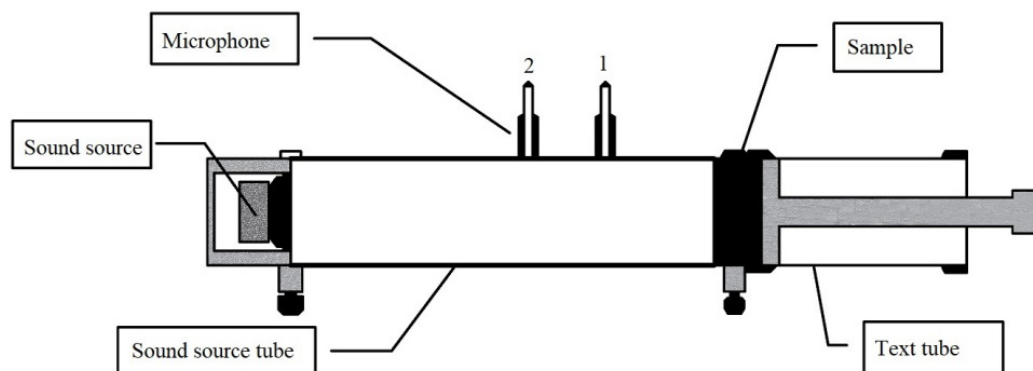


**Figure 1**. Schematic diagram of the sound-absorption test

## 3. RESULTS AND DISCUSSION

### 3.1 Effect of the Technological Parameters on the Sound-Absorption Coefficient

#### 3.1.1 Effect of the Volume Density on the Sound-Absorption Coefficient

Under technological conditions consisting of a mass fraction of waste-wool fibers of 50% and a material thickness of 10 mm, composite materials with densities of 0.153, 0.191, 0.229, 0.267, and 0.306 g·cm$^{-3}$ were prepared. Figure 2 shows the calculated porosity of the composite materials for different volume densities. Figure 2 shows that with an increase in the volume density of the composite materials, the porosity decreased from 88.06% to 76.13%. The reason might be that as the volume density increases, the number of fibers per unit volume increases, and the porosity between the fibers decreases; thus, the porosity of the composite materials decreases too.
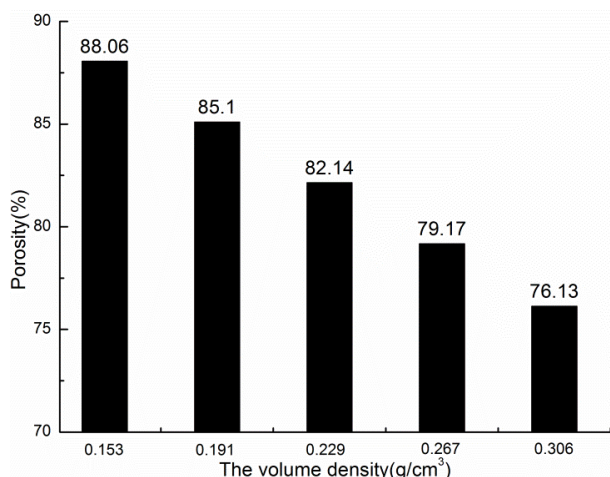


**Figure 2.** Porosity of composite materials with different volume densities

Figure 3 shows the measured sound-absorption coefficient curves of composite materials with different densities. It can be seen from Figure 3 that as the density increases, the peak of the sound-absorption coefficient gradually moves in the low-frequency direction. When the volume density was 0.229 g·cm$^{-3}$, the peak appeared in the test range, and the maximum sound-absorption coefficient was obtained [31]. To sum up, when the volume density of the composite materials was 0.229 g·cm$^{-3}$, the sound-absorption performance at high frequencies was the best, the maximum sound-absorption coefficient could reach 0.96, and the sound-absorption frequency band was wide, so the volume density of the composite materials was 0.229 g·cm$^{-3}$.

This is because as the density increased, the porosity of the material decreased, which reduced the pore size and the number of micro-pores in the material, increasing both the friction and the vibration between air and the fibers in the material, thus increasing the consumption of acoustic energy and the sound-absorption performance. However, if the internal structure of the material is too tight, the internal

flow resistance increases, leading to an increase in the reflected acoustic energy and a decrease in the transmitted acoustic energy, which results in a decrease in the sound-absorption coefficient.
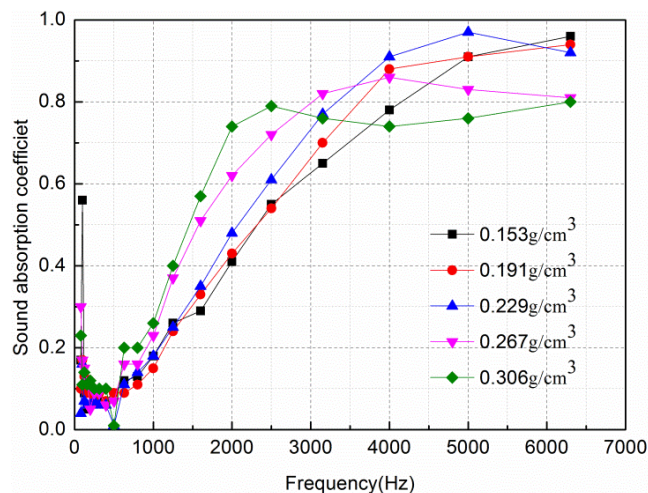


**Figure 3.** Sound-absorption-coefficient curves for composite materials with different densities.

#### 3.1.2 Effect of the Mass Fraction of Waste-Wool Fibers on the Sound-Absorption Coefficient

Under technological conditions consisting of a volume density of 0.229 g·cm$^{-3}$ and a material thickness of 10 mm, composite materials with mass fractions of waste-wool fibers of 0%, 30%, 40%, 50%, 60%, 70%, and 100% were prepared. Figure 4 shows the calculated porosity of composite materials with different mass fractions of waste-wool fibers. An increase in the mass fraction has a certain influence on the porosity of the composite materials. When the mass fraction of waste-wool fibers increased from 0% to 100%, the porosity increased from 80.59% to 83.45%. This is because the voids in a unit volume of materials containing pure waste-wool fibers (mass fraction = 100%) are larger than those in the materials containing pure waste low-melting-point polyamide fibers, so the porosity of the composite materials increases with an increase in the mass fraction of waste-wool fibers.



**Figure 4.** Porosity of composite materials with different mass fractions.

Figure 5 shows the sound-absorption-coefficient curves of composite materials with different mass fractions. It can be seen from Figure 5 that the sound-absorption coefficient gradually moves in the low-frequency direction. This is because the surface of the waste-wool fibers is relatively rough for the scale. When a sound wave passes through the waste-wool fiber, it increases both the friction and the heat loss, and therefore, the sound-absorption performance is good. However, the polyamide fibers have a smooth surface and show less resistance when sound waves pass through, so their sound-absorption performance is lower. Therefore, with an increase in the mass fraction of waste-wool fibers, the sound-absorption curve of the composite materials approaches the curve of pure waste-wool fibers and gradually tends to be flat. To sum up, when the mass fraction of waste-wool fibers is 30% and 50%, the sound-absorption performance of the composite materials is better. If the mass fraction of the waste-wool fibers is too high, it is not possible to ensure sufficient contact between the fibers. Therefore, the selected mass fraction of the waste-wool fibers was 50%.
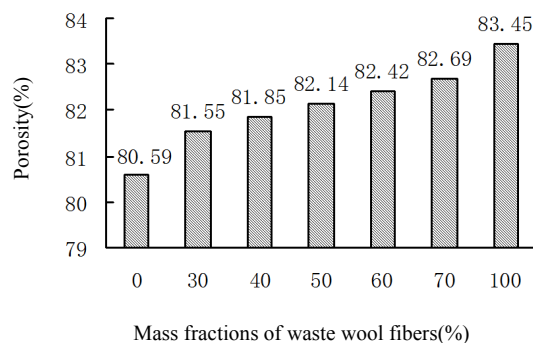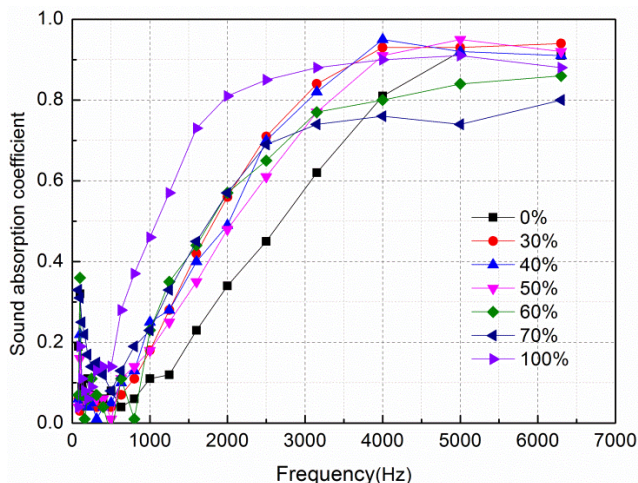


**Figure 5.** Sound-absorption-coefficient curves for composite materials with different mass fractions.

### 3.1.3 Effect of the Thickness on the Sound-Absorption Coefficient

Under technological conditions consisting of a volume density of 0.229 g·cm$^{-3}$ and a mass fraction of waste-wool fibers of 50%, composite materials with thicknesses of 5, 10, 15, 20, 25, 30, and 35 mm were prepared. Figure 6 shows the sound-absorption-coefficient curves for composite materials with different thicknesses. It can be seen from Figure 6 that with an increase in the thickness, the peak of the sound-absorption coefficient rapidly moves in the low-frequency direction, and the effective sound-absorption frequency range is expanded [32]. However, when the thickness reached 20 mm, the sound-absorption-coefficient curve in the middle-frequency and high-frequency bands basically tended to be stable. At frequencies below 1500 Hz, the sound-absorption coefficients increased with an increase in the thickness of

the composite materials, and the amount of increase was remarkable. At frequencies above 1500Hz, the sound-absorption-coefficient curves gradually tended to be stable with an increase in the thickness.
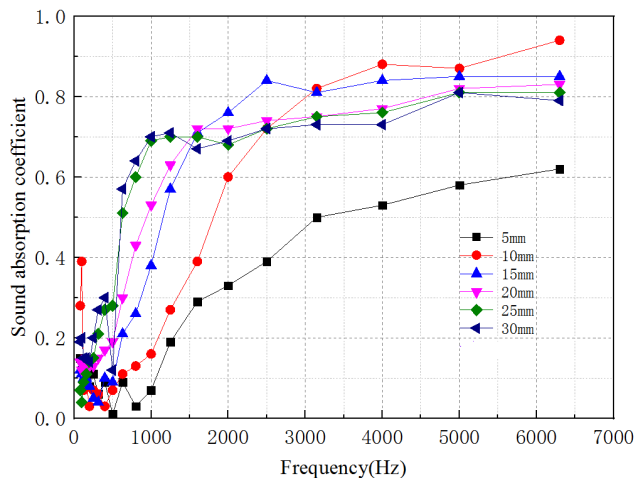


**Figure 6.** Sound-absorption-coefficient curves for composite materials with different thicknesses.

The reason for this observation is that low-frequency sound waves have a longer wavelength, the distance between the sound wave and the material increased, and the blockage caused by pore bending increased. Therefore, low-frequency sound waves are mainly absorbed by the interior of the composite material. High-frequency sound waves have a short wavelength and are mainly absorbed by the surface of the composite materials [33]. Therefore, an increase in the material thickness can effectively improve the low-frequency sound-absorption performance but has less influence on the high-frequency sound-absorption performance. To sum up, considering the cost of the raw materials and other factors, the thickness of the composite materials was set to 15 mm.

### 3.2 Fractal Characterization Results



**Figure 7.** Schematic diagram showing the fractal distortion of α-keratin inside waste-wool fibers

The waste-wool fibers were distorted macroscopically, and this change had self-similarity. Its inherent natural distortion was a unique fractal structure, which was fractal dimension change in accordance with fractal theory [34].

Figure 7 shows a schematic diagram of the fractal distortion of α-keratin inside waste-wool fibers. There are four layers between the wool's cortical cells and the basic fibrils, and the difference of each layer was about 10 times. The first distortion was α-keratin with a diameter of 1 nm, which was not an integer dimension. Each fibril consisted of three mutually twisted α-keratin units, and the low-density matrix (about 36%) was filled in between keratins, basic fibrils, fibrils, and microfibers. Three α-keratins in the basic fibrils occupied the remaining space (about 64%), which might be due to stress transmission caused by the natural twisting of α-keratins. About 10 basic fibrils in the microfibers were arranged in parallel, accounting for about 64% of the cross-sectional area. Similarly, the cross-sectional area occupied by microfibers and large fibrils was about 64% of that of large fibrils and cortical cells, so that a wool self-similar fractal dimension could be calculated [35]. The fractal structures of waste-wool fibers and synthetic fibers are essentially different. Synthetic fibers (including waste low-melting-point polyamide fibers) show one-dimensional, two-dimensional, or even three-dimensional integer dimensional changes. The inherent natural distortion of waste-wool fibers had non-strict self-similarity. In statistical sense, its whole and shape had self-similarity. Although it also had complex details in nanometer scale, it was difficult to describe such details with traditional geometry, that was, irregularities [36]. Therefore, from the microscopic to the macroscopic physical structure, the composite materials prepared using waste-wool fibers and waste low-melting-point polyamide fibers exhibited obvious fractal characteristics, and the sound-absorption performance of the composite materials could be forecasted by the fractal method.

### 3.2.1 Image Acquisition of the Composite Materials

The composite materials were thick and exhibited a large unit area. Natural light could not penetrate, so it was difficult to explore the internal structure. Therefore, a JEOL JSM-6460LV scanning electron microscope was used to obtain images of the composite materials at a magnification of 50 times. After image processing, the basal plane fiber layer was taken for pore-structure analysis. This treatment was based on the fact that the composite materials consisted of many layers of fibers with arbitrary orientation. It was assumed that most of the fiber layer aggregates were perpendicular to the propagation direction of the sound waves. Some properties (such as the sound-absorption properties) of the single layer (base plane fiber layer) could reflect the properties of the entire composite materials.

Figure 8 shows scanning electron microscopy (SEM) images of composite materials with volume densities of 0.153, 0.191, 0.229, 0.267, and 0.306 g·cm$^{-3}$ (a–e).

Figure 9 shows SEM images of composite materials with different mass fractions of 0%, 30%, 40%, 50%, 60%, 70%, and 100% (a–g).

Figure 10 shows scanning electron microscopy images of composite materials with different thicknesses of 5, 10, 15, 20, and 25 mm (a–e).



(a) 1#    (b) 2#    (c) 3#



(d) 4#    (e) 5#
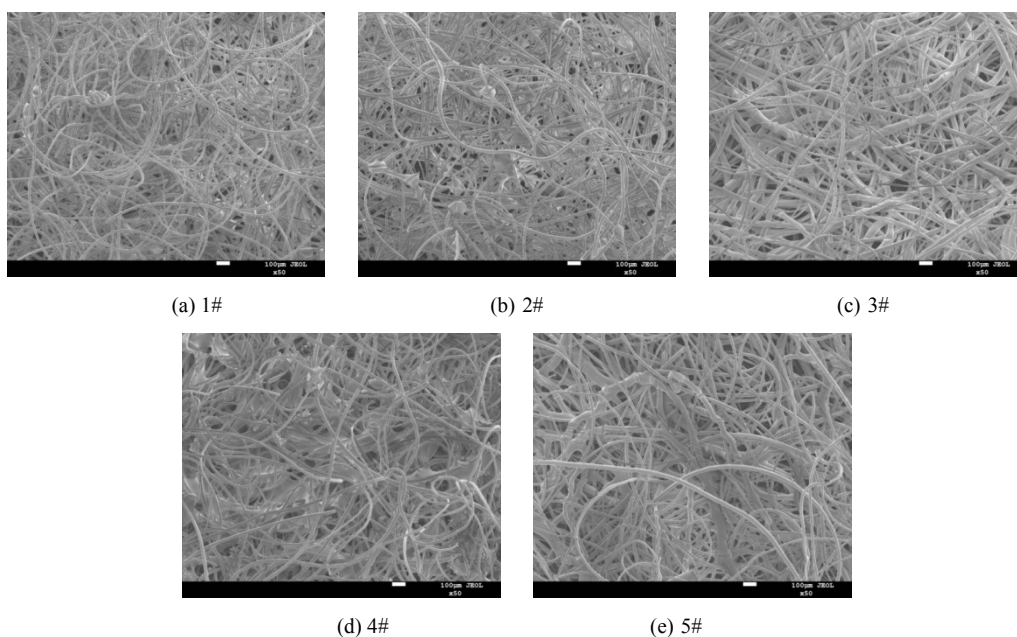
**Figure 8.** Scanning electron microscopy images of composite materials with different volume densities.

(a) 6#

(b) 7#

(c) 8#

(d) 9#

(e) 10#

(f) 11#

(g) 12#
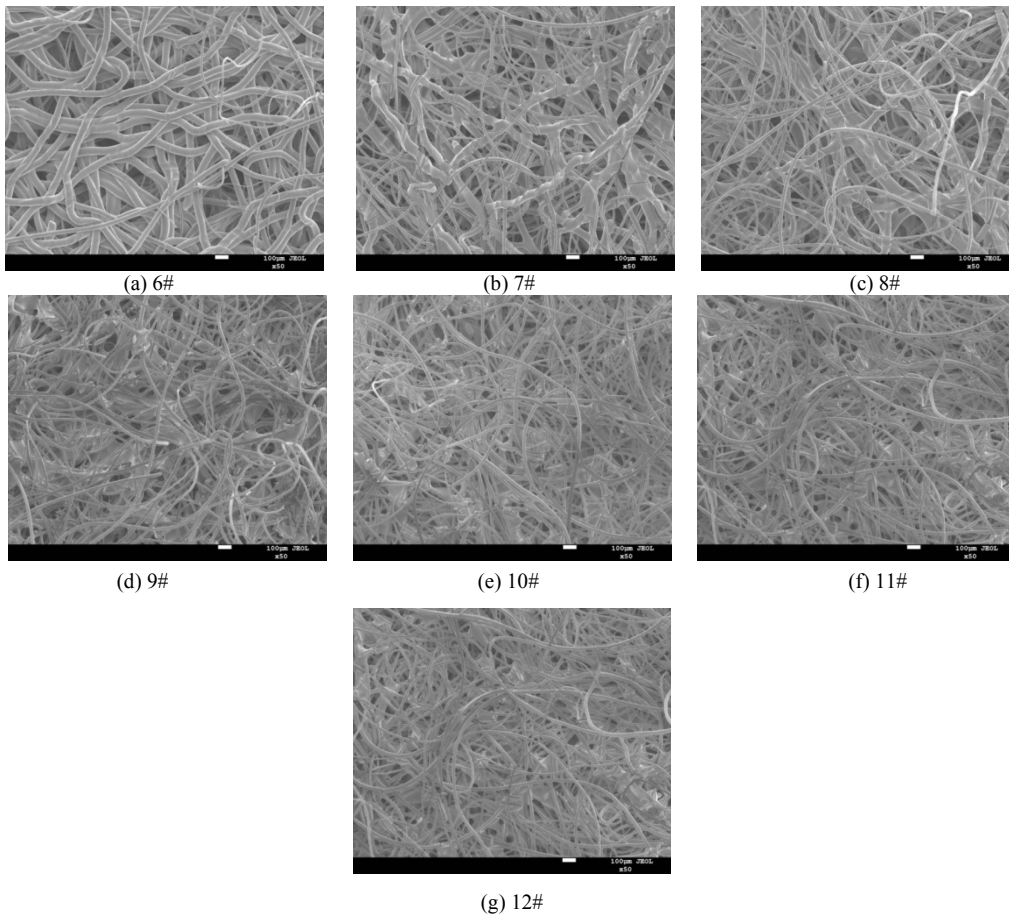
**Figure 9.** Scanning electron microscopy images of composite materials with different mass fractions.



(a) 13#

(b) 14#

(c) 15#

(d) 16#

(e) 17#
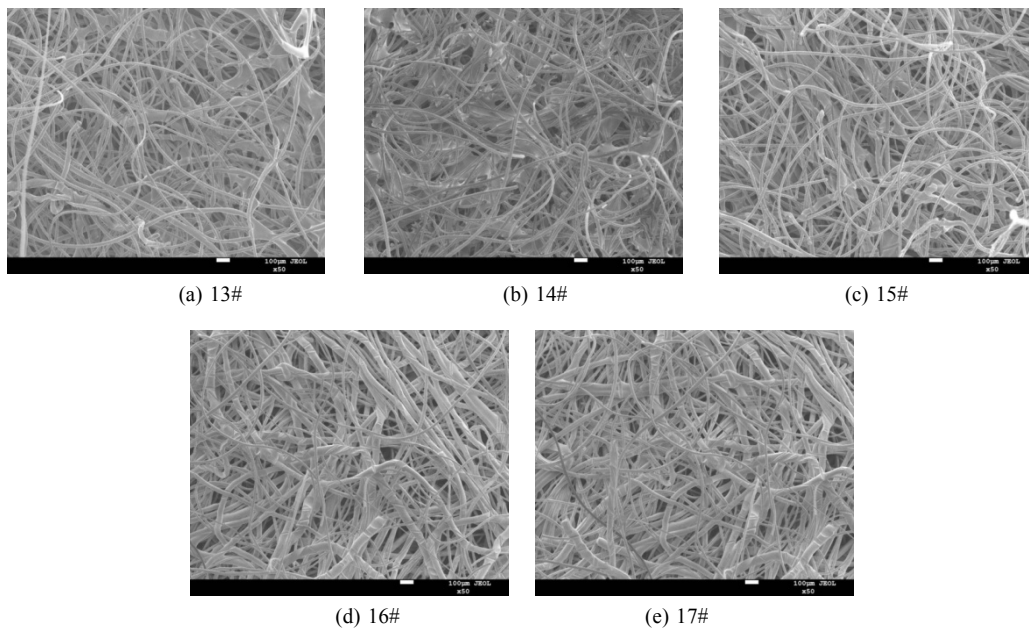
**Figure 10.** Scanning electron microscopy images of composite materials with different thicknesses.

### 3.2.2 Pretreatment of the Images of the Composite Materials

Pretreatment of the images of the composite materials was mainly performed to enhance the contrast between fibers and pores. Firstly, the SEM images of the composite materials taken under various conditions were converted into gray-scale images, and the images were enhanced by expanding the gray-scale range to the whole gray-scale area, so that the contrast of pixels in the range was obvious, the bright areas were brighter, and the dark areas were darker. Next, the histogram distribution of the images was equalized by histogram equalization to increase the gray-

value range of the composite-material images to further enhance the overall contrast of the images. Finally, median filtering was carried out on the previously processed images to eliminate isolated noise and reduce image blur [37].

### 3.2.2.1 Eliminating the Background



(a)                                    (b)
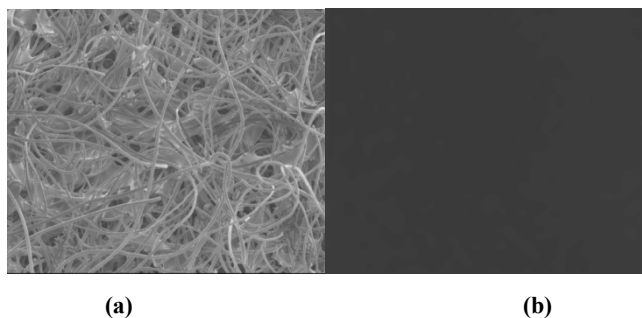
**Figure 11.** Eliminating the background.

An uneven surface or an uneven illumination distribution of the composite materials can easily cause brightness differences throughout the whole image, which has a great influence on the further processing and analysis of the image. Therefore, it was necessary to eliminate the background before enhancing the image. In other words, when collecting images of the composite materials, images of the composite-materials sample were taken under the same shooting conditions. Figure 11(a) shows an original image, and Figure 11(b) shows an image of the background without sample. The effect of an uneven background can be eliminated by subtracting the two images.

### 3.2.2.2 Enhancement of the Images

Figure 12 shows an original image and its gray-scale histogram. As can be seen in Figure 12, the contrast ratio of the SEM image is too low, which confuses fibers and pores, but the gray-scale stretching technology can be adopted to maximize the contrast ratio of the image



(a)



(b)
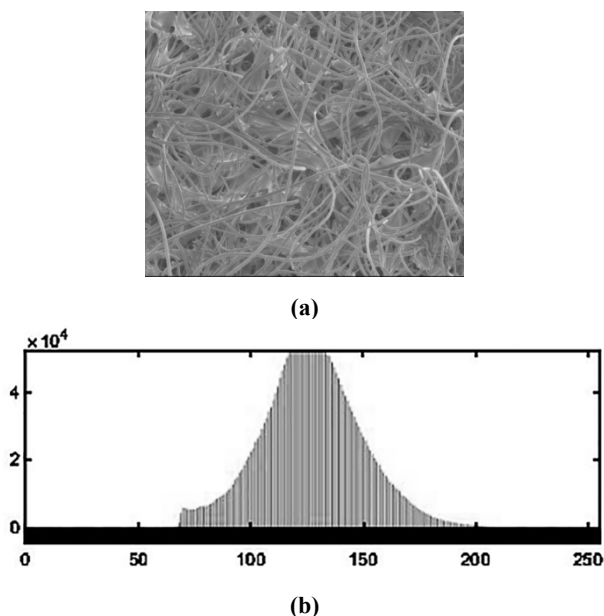
**Figure 12.** Original image and its gray-scale histogram.

After gray-scale stretching, the gray-scale histogram with the original concentrated distribution was stretched between 0 and 255, the distribution became more uniform, and the contrast of the image was significantly improved. Figure 13 shows the image after gray-scale stretching and its gray-scale histogram. As can be seen in Figure 13, the differences between the fibers and the pores became very clear, which was conducive to the binarization of the image in the next step



(a)



(b)
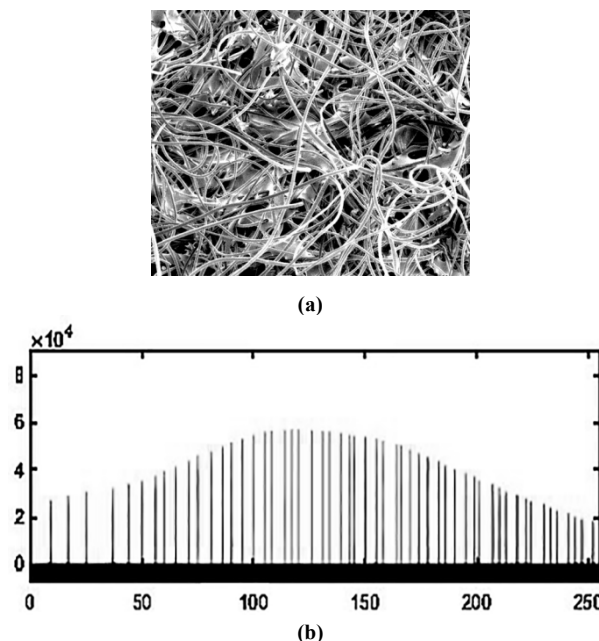
**Figure 13.** SEM image after gray-scale stretching and its gray-scale histogram.

### 3.2.2.3 Binarization of the Images

The images were divided into 256 gray levels, black was represented by 0, white was represented by 255, and the other colors were represented between 0 and 255. Image binarization refers to the setting of a threshold value. At the same time, the threshold value is used as a threshold to convert the image (multi-gray level) into a black-and-white image (two-gray level). The color of each pixel was set to black or white, and the pixel values were 0 and 1, respectively. Differences in the threshold setting methods would lead to differences in the binarization process, so the threshold should be selected reasonably. The way to divide the pores and fibers was to binarize the composite-material images by converting the points with gray value greater than or equal to the threshold value into white points (gray level 255) and the points with gray value less than the threshold value into black points (gray level 0). This topic was based on the threshold set artificially by the gray distribution map, that is, the designated threshold was 0.43, as shown in Figure 14(a). Of course, the maximum variance between classes method could also be used to calculate the threshold value of gray images, as shown in Figure 14 (b). This method was set to 255 when the gray value of a certain point was greater than the threshold value, and set to 0

when it was less than or equal to the threshold value. This was mainly done to automatically set and easily weaken the contrast of images under the same factor. Therefore, this paper adopted the method of specifying the threshold value [38].

### 3.2.3 Calculation of the Fractal Dimension

Figure 15 shows the calculation process for obtaining the fractal dimension.

### 3.2.4 Relationship between Fractal Dimension and Various Factors

### 3.2.4.1 Relationship between Fractal Dimension and Volume Density

Table 1 shows relevant parameters of the samples obtained with different volume densities. Figure 19 shows the relationship between the fractal dimension of the samples and the maximum sound-absorption coefficient for different volume densities.

As can be seen in Figure16, with an increase in the volume density, the fractal dimension and the maximum sound-absorption coefficient of the samples all showed a decreasing trend. The fractal dimension of the sample pores was linearly related to the average pore size (i.e. porosity). If the volume density of the sample was larger, the porosity

was smaller, the pore structure was denser, and the pore fractal dimension was smaller. When exploring the influence of the volume density on the sound-absorption performance of the composite materials, the peak of the sound-absorption coefficient moved to the low-frequency direction with an increase of the volume density. When the volume density of the sample was $0.229 \cdot cm^{-3}$, the combination of the hole shape and the aperture size of the composite materials improved the sound-absorption performance throughout the whole sound-absorption frequency band. The peak of the maximum sound-absorption coefficient appeared in the test frequency range, which made the maximum sound-absorption coefficient higher but did not affect the overall trend.



**(a)**      **(b)**
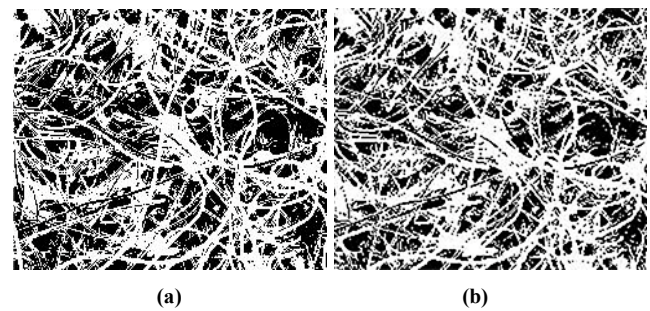
**Figure 14.** Images after binarization.
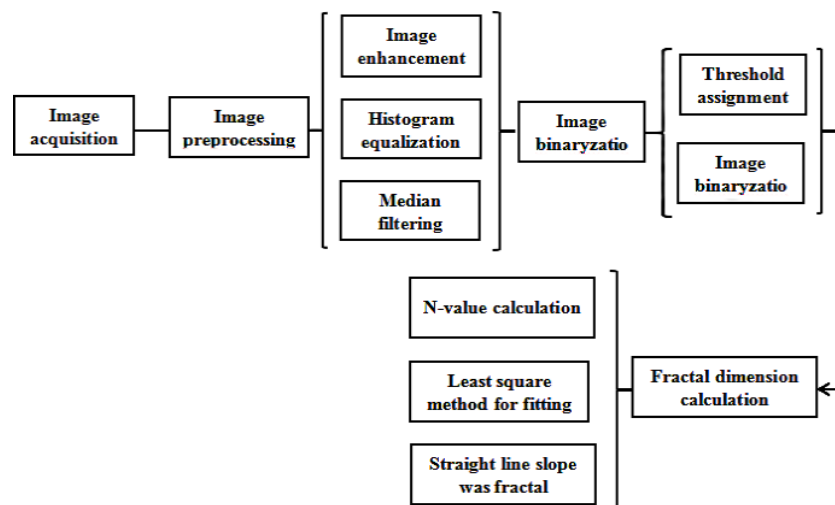


**Figure 15.** Calculation process for obtaining the fractal dimension.

**Table 1.** Relevant parameters of samples with different volume densities

| Sample number | Volume density [g·cm⁻³] | Maximum sound-absorption-coefficient | Porosity[%] | Fractal dimension | $R^2$ |
|---|---|---|---|---|---|
| 1# | 0.153 | 0.96 | 88.06 | 1.913 | 0.9983 |
| 2# | 0.191 | 0.94 | 85.10 | 1.901 | 0.9980 |
| 3# | 0.229 | 0.95 | 82.14 | 1.923 | 0.9987 |
| 4# | 0.267 | 0.86 | 79.17 | 1.889 | 0.9971 |
| 5# | 0.306 | 0.80 | 76.13 | 1.875 | 0.9972 |
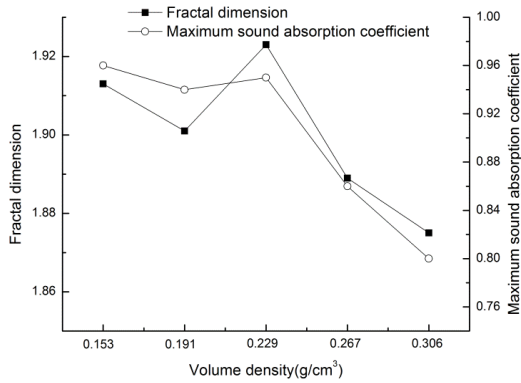
**Figure 16.** Relationship between fractal dimension and maximum sound-absorption coefficient for samples with different volume densities.
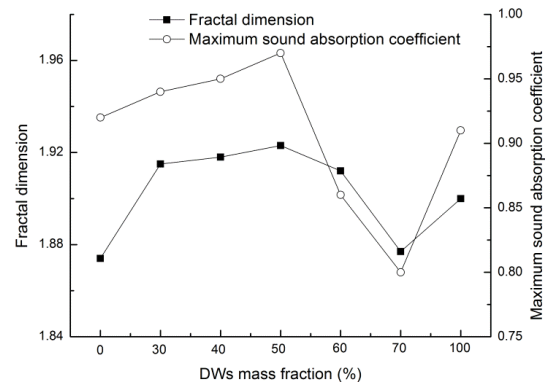
**Figure 17.** Relationship between fractal dimension and maximum sound-absorption coefficient for samples with different mass fractions of waste-wool fibers.

### 3.2.4.2 Relationship between the Fractal Dimension and the Mass Fraction of Waste-Wool Fibers

Table 2 shows relevant parameters for samples with different mass fractions of waste-wool fibers. Figure 17 shows the relationship between the fractal dimension and the maximum sound-absorption coefficient of samples with different mass fractions of waste-wool fibers. It can be seen from Figure 17 that samples 6# and 12# were samples with mass fractions of waste-wool fibers of 0% and 100%, respectively, being different from the other samples. They did not participate in the relationship between the maximum sound-absorption coefficient and the fractal dimension and were only analyzed as comparison samples. The fractal dimension was consistent with the variation trend of the maximum sound-absorption coefficient and had a linear correlation. The maximum sound-absorption coefficient was obtained at the best mass fraction of waste-wool fibers. When the mass fraction of waste-wool fibers was 0%, the fractal dimension was low, which is due to the fact that when pure polyamide fibers are prepared, the fibers melt and shrink when heated, the pore diameter of the material decreases, and the pore fractal dimension is small. Similarly, it can be explained that with an increase in the mass fraction of waste-wool fibers, the influence of the composite materials decreases, the internal complexity of the material decreases, and the pore fractal dimension slightly increases. If the mass fraction of waste-wool fibers is above 50%, the composite materials are less affected by heat, the number of pores between fibers increases, and the fractal dimension decreases accordingly.

### 3.2.4.3 Relationship between Fractal Dimension and Thickness of the Composite Materials

Table 3 shows relevant parameters for samples with different thicknesses. Since the thickness of the composite materials has a great influence on their sound-absorption performance, the sound-absorption-coefficient curve shifted in the low-frequency direction with an increase in the thickness. The maximum sound-absorption coefficient of the composite materials did not change significantly with the thickness, so the relationship between the fractal dimension and the resonant sound-absorption frequency corresponding to the turning point of the sound-absorption coefficient was explored.

Figure 18 shows the relationship between the fractal dimension and the resonant sound-absorption frequency for samples with different thicknesses. From Figure 18, it can be concluded that the fractal dimension has a good correlation with the sound-absorption resonance frequency, indicating that the turning point of the sound-absorption performance of the composite materials can be explored through the fractal dimension. As the thickness of the composite materials increased, the corresponding fractal dimension decreased, and the resonance frequency corresponding to the turning point moved to lower frequencies. The reason for this might be that the thickness of the composite materials was increased, the length of the channel of the acoustic wave entering the inside of the material was prolonged, and the depth of the hole was increased, thereby reducing the fractal dimension.

**Table 2.** Relevant parameters of samples with different mass fractions of waste-wool fibers.

| Sample number | Mass fraction of waste-wool fibers [%] | Maximum sound-absorption-coefficient | Porosity[%] | Fractal dimension | $R^2$ |
|---|---|---|---|---|---|
| 6# | 0 | 0.92 | 80.59 | 1.874 | 0.9972 |
| 7# | 30 | 0.94 | 81.55 | 1.915 | 0.9987 |
| 8# | 40 | 0.95 | 81.85 | 1.918 | 0.9986 |
| 9# | 50 | 0.95 | 82.14 | 1.923 | 0.9987 |
| 10# | 60 | 0.86 | 82.42 | 1.912 | 0.9981 |
| 11# | 70 | 0.80 | 82.69 | 1.877 | 0.9967 |
| 12# | 100 | 0.91 | 83.45 | 1.900 | 0.9978 |

**Table 3.** Relevant parameters for samples with different thicknesses of the composite materials.

| Sample number | Thickness of composite material [mm] | Resonance sound-absorption frequency | Fractal dimension | $R^2$ |
|---|---|---|---|---|
| 13# | 5 | 6300 | 1.949 | 0.9994 |
| 14# | 10 | 4000 | 1.923 | 0.9987 |
| 15# | 15 | 2000 | 1.915 | 0.9987 |
| 16# | 20 | 1500 | 1.914 | 0.9985 |
| 17# | 25 | 1250 | 1.907 | 0.9982 |
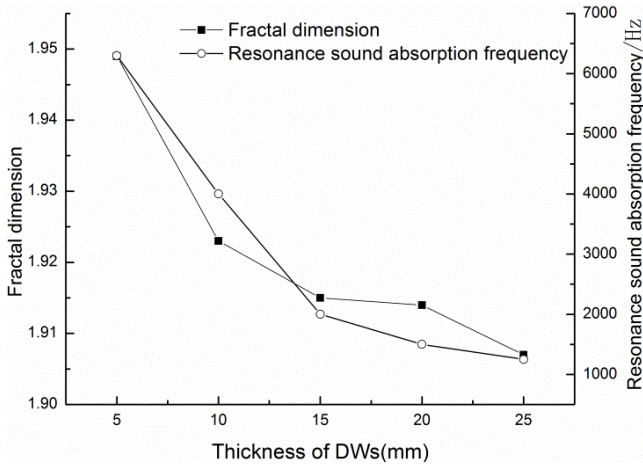


**Figure 18.** Relationship between the fractal dimension and resonant frequency for samples with different thicknesses.
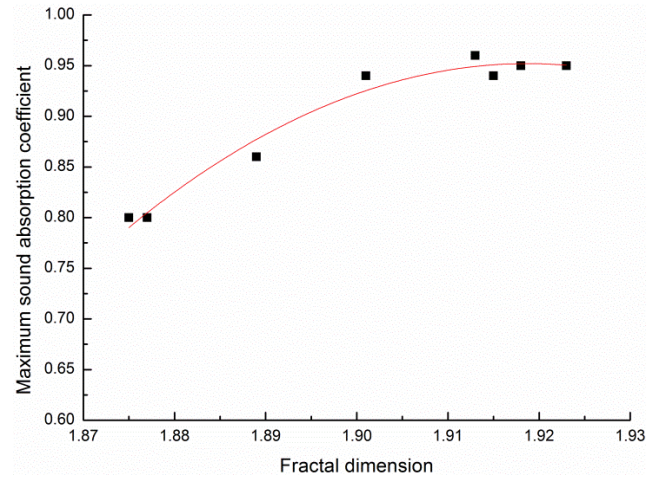


**Figure 19.** Fitting curve between fractal dimension and maximum sound-absorption coefficient

### 3.2.5 Relationship between Fractal Dimension and Maximum Absorption Coefficient

Due to the influence of deviations when acquiring images, the images with larger deviations were selected, and a relationship curve between the fractal dimensions of samples $1^\#$, $2^\#$, $3^\#$, $4^\#$, $5^\#$, $7^\#$, $8^\#$, and $11^\#$ and the maximum sound-absorption coefficient was established. The fractal dimension was fitted to the maximum sound-absorption coefficient, and the fitting curve is shown in Figure 19.

The fitting relation was as follows:

$$Y = -84.375X^2 + 323.796X - 309.695 \qquad (3)$$

where Y is the maximum sound-absorption coefficient and X is the fractal dimension.

The correlation coefficient between the fractal dimension and the maximum sound-absorption coefficient was 0.9741, which shows that there is a strong positive correlation between the fractal dimension and the maximum sound-absorption coefficient. In the actual design of composite materials, the fitting relation obtained above could be used to predict the maximum sound-absorption coefficient of the composite material.

A relationship curve between the fractal dimensions and the resonance absorption frequencies of samples $13^\#$, $14^\#$, $15^\#$, $16^\#$, and $17^\#$ was established. The fractal dimension was fitted to the resonance sound-absorption frequency, and the fitting curve is shown in Figure 20.
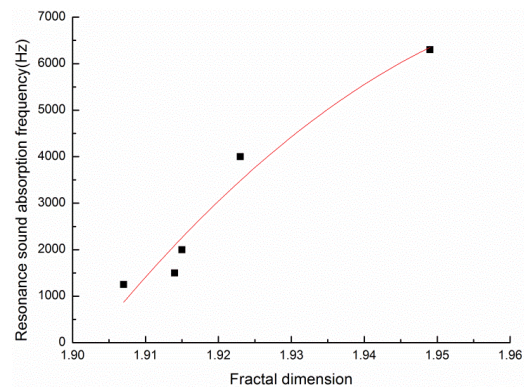


**Figure 20.** Fitting curve between fractal dimension and resonance sound-absorption frequency.

The fitting relation was as follows：

$$Y = -1266600X^2 + 5014500X - 4955600 \qquad (4)$$

where Y is the resonance sound-absorption frequency and X is the fractal dimension.

The correlation coefficient between the fractal dimension and the maximum resonance sound-absorption frequency was 0.9086, which shows that there is a strong positive correlation between the fractal dimension and the resonance sound-absorption frequency. In the design of the actual thickness of a composite material, the fitting relation

obtained above could be used to predict its resonance sound-absorption frequency, that is, the turning point of the sound-absorption coefficient.

## 4. CONCLUSION

In this paper, the sound-absorption properties of the composite materials were studied by the transfer-function method. The results of single-factor experiments showed that the optimized technological conditions were: a volume density of the composite materials of 0.229 g·cm$^{-3}$, a mass fraction of waste-wool fibers of 50%, and a thickness of the composite materials of 15 mm. Under the optimized technological conditions, the sound-absorption coefficients of the composite materials were above 0.8 and the sound-absorption bands of the composite materials were wide,which could be applied in the construction field, decoration field , automobile industry and so on.

 The microscopic physical structure and macroscopic physical structure of the composite were analyzed, and the fractal dimensions of the composite under different factors were calculated by using the box-counting dimension method (fractal theory), the correlation coefficients were high, which showed that the structure of the composite materials containing waste-wool/polyamide fibers had strong fractal characteristics. Fractal theory was used to quantitatively characterize the complex structure of

composite materials, and the relationship between fractal dimension and material density, mass fraction of waste wool fibers and material thickness were mainly analyzed. A theoretical model of structural identification index (i.e. Fractal dimension) and sound-absorption properties parameters of composite materials was established. The linear relationship between the fractal dimension and its maximum sound absorption coefficient was established as follows: $Y = -84.375X^2 + 323.796X - 309.695$, the correlation coefficient was 0.9741. The linear relationship between the fractal dimension and the resonant frequency was: $Y = -1266600X^2 + 5014500X - 4955600$, the correlation coefficient was 0.9086.Through experimental characterization and theoretical prediction analysis, the sound absorption mechanism of composite materials containing waste-wool/polyamide fibers sound absorption composites was shown. The research results provided experimental and theoretical basis for the design of sound-absorption composite materials with wide sound-absorption frequency bandwidth and high sound-absorption coefficient.

**Conflicts of Interest:** The authors declare no conflict of interest.

## REFERENCES

1. Tian CY, Wang F, Rong VH. 2005. Discussion on Sustainable Development Countermeasures of Fine Wool Sheep Industry in Inner Mongolia. *Animal Husbandry and Feed Science*, 26(4), 48.

2. Zhangye Comprehensive Test Station of National Wool Sheep Industry Technology System. 2017. Development Trend and Policy Suggestions of National Wool Sheep Industry in 2017. *Gansu Animal and Veterinary Sciences*, 47(4), 27-28.

3. .Jiang ZH. 2002. Japan Developed a Technology to Use Scrap Wool & Feather *China Resources Comprehensive Utilization*, (2), 8.

4. Alzeer M, MacKenzie KJ. 2012. Synthesis and mechanical properties of new fibre-reinforced composites of inorganic polymers with natural wool fibres. *Journal of Materials Science*, 47(19), 6958-6965.

5. Patnaik A, Mvubu M, Muniyasamy S, Botha A, Anandjiwala RD. 2015. Thermal and sound insulation materials from waste wool and recycled polyester fibers and their biodegradation studies. *Energy and Buildings*, 92, 161-169.

6. Li Y, Zhang DK. 2018. Preparation of wet-laid nonwoven fabric using super-short waste wool fiber. *Journal of Xi'an Polytechnic University*, 32(6), 623-627.

7. He YZ, Wang HF. 2012. Research for recycle process of waste wool fiber. *Wool Textile Journal*, 40(9), 14-17.

8. Yao JB, He TH. 2003. Preparation of wool's keratin solution. *Wool Textile Journal*, (4), 16-19.

9. Jia JR, Yao JB. 2015. The latest progress in research of recycling scrap of wool keratin. *Wool Textile Journal*, 43(1), 45-49.

10. Sun YL, Yao JB, Li B, Jia SG. 2015. Application of wool keratin solution in wool fabric shaping. *Journal of Textile Research*, 36(4), 97-101.

11. Li K, Wang M. 2018. Preparation and properties of blended membrane based on abandoned wool protein. *Dyeing and Finishing*, 44(5), 8-23.

12. Lv LH, Liu YJ, Li CT, Guo J, Ye F. 2019. Properties of Waste Fiber/Polyurethane Flame Retardant Insulation Board. *Tekstil ve Konfeksiyon*, 29(2), 152-161.

13. Lv LH, Bi JH, Ye F, Qian YF, Zhao YP, Chen R, Su XG. 2017. EXTRACTION OF DISCARDED CORN HUSK FIBERS AND ITS FLAME RETARDED COMPOSITES. *Tekstil ve Konfeksiyon*, 27(4), 408-413.

14. Cheng G. 2009. Performance and application of wool sound absorption and thermal insulation product. *New Building Materials*, 36(5), 63-66.

15. Luan QL, Qiu H, Cheng G, Ge MQ. 2016. Preparation and sound absorption properties of waste wool nonwoven material. *Journal of Textile Research*, 37(7), 77-81.

16. Luan QL, Qiu H, Cheng G, Ge MQ. 2016. Preparation of porous sound absorbing material based on discarded wool fiber. *Chinese Journal of Environmental Engineering*, 10(10), 6081-6086.

17. Luan QL, Qiu H, Cheng G, Liu XY. 2017. Sound absorption properties of nonwoven material based on wool and its hybrid fibers. *Journal of Textile Research*, 38(3):67-71.

18. Burrough PA. 1981. Fractal dimensions of landscapes and other environmental data. *Nature*, 294(5838), 240-242.

19. Milne BT. 1988. Measuring the fractal geometry of landscapes. *Applied Mathematics and Computation*, 27(1), 67-79.

20. West BJ, Goldberger AL. 1987. Physiology in fractal dimensions. *American Scientist*, 75(4), 354-365.

21. Du CJ, Sun DW. 2004. Recent developments in the applications of image processing techniques for food quality evaluation. *Trends in food science & technology*, 15(5), 230-249.

22. Yang XH. 2003. Expression and Fractal Simulation of Morphologic Structures of Nonwovens (Doctoral dissertation). Available from CNKI and Wangfang database. (DOI:10.7666/d.y645366).

23. Wang YH. 2018. T700/BMI Porosity Detection and Fractal Research of Pore Morphology Feature (Master's thesis). Available from CNKI and Wangfang database. (DOI:10.7666/d.y01662570).

24. Lyu L, Liu Y, Bi J, Guo J. 2019. Sound Absorption Properties of DFs/EVA Composites. *Polymers*, 11(5), 811.

25. Yang S, Li MS. 2017. Relationship between fractal structure and warmth retention properties of wool fiber assembly. *Journal of Textile Research*, 38(08), 11-15.

26. Chen L, Jiang Z, Jiang S, Liu K, Yang W, Tan J, Gao F. 2019. Nanopore Structure and Fractal Characteristics of Lacustrine Shale: Implications for Shale Gas Storage and Production Potential. *Nanomaterials*, 9(3), 390.

27. Lyu LH, Li CW, Wu CX. 2018. Preparation of Discarded Peanut Shell/EVA Composite and Its Sound Absorption Properties. *Advanced Textile Technology*, 26(4), 12-16.

28. Ma YX. 2010. STUDY ON SOUND ABSORPTION PROPERTIES OF COMPOSITE NEEDLE-PUNCHED NONWOVENS (Master's thesis). Available from CNKI and Wangfang database. (DOI:10.7666/d.y1864290).

29. Sun X, Wu ZQ, Huang Y. 2003. Fractal and cone. In 2 Editor (Ed.), *Fractal Principle and Its Application*. Anhui, China: China University of Science and Technology Press, 23–41.

30. Li HT, Deng Y. 2002. Fundamentals of M-File Programming. In 8 Editor (Ed.), *Matlab program Tutorial*. Beijing, China: Higher Education Press, 187-213.

31. Li CW, Lyu LH. 2018. Preparation and properties of sound absorption composites based on waste wool. *Journal of Textile Research*, 39(10), 74-80.

32. Zhao M. 2004. Mechanical Noise Control Technology. In 9.2 Editor (Ed.), *Mechanical Vibration and Noise*. Beijing, China: Science Press, 221–223.

33. Peng LM, Wang JF, Fu F, Wang D, Zhu GY. 2015. Experimental Study on Sound Absorption of Wood Fiber/Polyester Fiber Composite Materials. *Journal of Building Materials*, 18(1), 172-176

34. Mandelbrot BB. 1983. The fractal geometry of nature/Revised and enlarged edition. New York, *WH Freeman and Co.*, 1983, 495.

35. Gao XS, Tong Y, Zhuang Y, Hong JQ. 2000. THE FRACTAL STRUCTURE OF NATURAL FIBERS AND THE DEVELOPMENT OF FIBER WITH FRACTAL STRUCTURE. *CHINA SYNTHETIC FIBER INDUSTRY*, 23(4), 35-38.

36. Zhang JZ. 2011. *Fractal*. Beijing, China: Tsinghua University Press.

37. Yang S, Yu WD, Pan N. 2010. Effect of nonwovens pore fractal dimensions on their acoustic absorption behaviors. *Journal of Textile Research*, 31(12), 28-32, 38.

38. .Gao G, Zhong HJ, Song XJ, Liu XR, Mi XQ. 2005. Fractal characteristic analysis of non-woven fabrics. *Journal of Tianjin Polytechnic University*. 24(2):86-88.

# Workwear Fabric Suitability to Molten Metal Industry

Tuğçem Bitgen[1], Bengi Kutlu[2]

[1]Dokuz Eylul University, The Graduate School of Natural and Applied Sciences, Textile Engineering Department, Izmir-Turkey
[2]Dokuz Eylul University, Faculty of Engineering, Textile Engineering Department, Izmir-Turkey

Corresponding Author: Bengi Kutlu, bengi.kutlu@deu.edu.tr

## ABSTRACT

In the scope of the foundry processes, there are vital risks when melting of metals at high temperatures, carrying this molten metal to molds and pouring it to molds. In this study, wide range of workwear materials which are used in foundries in Turkey were collected and their protection properties were investigated to observe their performances. Determining suitable material to molten metal processing was aimed. These workwear materials were produced from FR-cotton, cotton denim, modacrylic-viscose-FR cotton, meta-aramid, aluminized aramid, FR viscose-wool-polyamide and leather. Their performances were very different. Except from meta-aramid and both of the FR cotton fabrics, other fabrics failed flame spread. Contrary to flame spread, leather, aluminized aramid, FR viscose-wool-polyamide and cotton denim materials showed the highest values in molten metal splash test. Besides, leather had no air permeability but has some water vapor permeability and aluminized aramid has poor air and water permeabilities.

## 1. INTRODUCTION

Metal foundry industry in Turkey is one of the most important sectors taking 3rd place in Europe and 11th place in the world having nearly 34,000 employees of this industry. Aluminium die casting is rising in area Turkey, total production 20% increased from 2017 to 2018. This is the reason of our decision to investigate aluminium protection properties of varios fabrics. Foundry process involves three main steps, heating metal until it becomes molten; pouring molten metal into a mold; and allowing the metal to cool and solidify in the shape of the mold. Correct casting temperatures are important for quality of cast product. Melting temperatures of metals are very high, i.e. 660ºC for Aluminium, 1536ºC for iron, etc. These processes endanger the life of workers; however, proper workwear can protect them. Wide range of fabrics are used in foundry workwear from cotton to special fibers like modacrylic, aramid, even leather and each of them has different performances and prices. In general, there are three types of molten metal exposures in industry: poured molten metal, welding droplets and molten metal splashes due to an electric arc. In foundry sector, poured molten metal is the main exposure for employees. In addition,

foundries are very hot environments and this causes uncomfortable feelings causing loosing attention in shortterm exposure and heat stress hazards in longterm exposure. In protective product selection, temperature, density, size of droplets and the reactivity (sticking) of droplets are determining factors [1,2].

There are few works about molten metal protective textile materials, most of them rather old. Barker and Yener, worked on molten iron protection. They found iron resistance was correlated with fabric thickness, weight, air permeability and flammability properties [3]. Benisek, Edmondson and Philips aimed at measurement of protection properties of especially zirpro FR (flame retardant) wool and other protective clothing against convective and radiant heat and aluminum splashes. They developed the molten aluminum protection test method similar to recent one. They concluded that increased fabric weight and density, low thermal conductivity and smooth fabric surface were important for molten aluminium protection [4]. Benisek and Edmondson in 1981, evaluated the effects of different conductive heat sources as molten metals (cast iron, steel, copper, aluminium, zinc, lead and tin) on various FR fabrics. They indicated inherent flame

retardant property (i.e. glass, asbestos and aramid fibers) is not sufficient for molten metal protection. Zirpro wool was find to be a good example of molten metal protection, untreated cotton showed slightly lower protection while FR treated cotton fibers worser than the others against aluminium and zinc [5]. Proctor and Thompson in 1992 focused on finished wool fibers and effects of the finish chemicals to molten metal adhesion. They found that chrome dyeing and zipro finish on wool increase adhesion of molten aluminium and zinc. This result of chrome dyeing is similar to the results from Benisek and Edmondson in 1984 [6, 7]. Coughlan worked with different fabrics against molten aluminium. It is found that damage to skin simulant was not dependent on flame retardancy but dependent on surface properties of fabrics at high temperatures and duration of molten metal-fabric contact (sticking). FR treatments on cotton causes sticking and softening of synthetic inherently flame retardant fibers occurs and causes trapping of metals are the other conclusions [8]. Magnússon et al., investigated molten aluminium protection properties of FR cotton, FRviscose/wool/cotton, viscoseFR/PVA/modacrylic, viscose FR/wool fabrics. They concluded that to obtain D3 level protection of ISO11612, underwear usage was essential. Additionally, they examined the behavior of molten aluminium when small and big folds occur in the fabric. If there was big fold, molten aluminiun may stop and cause damage in skin simulant [9]. Mäkinen et al. studied fabric layer combinations instead of single fabrics. They found that use of FR underwear is useful to increase the level of molten iron protection [10]. Lee highlighted the number of PPE advancements in Australia. Paper explained the preferred not only clothing but all components of personal protective equipment (PPE) [11].

Surveying literature, it is seen that molten metal protection properties of various fabrics were investigated in detail [3-11]. Although performances of certain types of fabrics are known, a workwear's overall performance cannot be concluded without mechanical performances and comfort properties convenient to work conditions. In addition, there are very wide range of workwear fabrics available and in use for foundry workers in Turkey. However, due to very high temperatures, carefully selected specific materials should be used regarding protection and the other performances. That was our motivation and in this research, we investigated primarily molten aluminium and flame protection properties of various fabrics and one leather sample, together with physical-mechanical and permeability features. Leather cannot be found in literature but it is in common use for molten metal processing especially as gloves and aprons. The aim of the research was to determine properties of fabrics and leather used in workwear clothing in Turkey and to assess the better material showing suitable performance.

## 2. MATERIAL AND METHOD

### 2.1 Material

Seven types of fabrics that are mostly used in workwear of Turkey's foundry industry and one type of leather were provided. Firstly, fabric structures, area weight (TS 251), thickness (TS 7128 EN ISO 5084 - 5 g/cm$^2$ pressure), warp and weft yarn numbers, fabric settings and tensile strength (TS EN ISO 13934-1 for fabrics and TS EN ISO 3376 for leather) properties were determined. The results are given in Table 1.

**Table 1.** Physical properties of fabrics and leather

| Code | Samples | Weave Type | Area weight (g/m$^2$) | Fabric Thickness (mm) | Weft count (thread/cm) | Warp count (thread/cm) | Weft yarn number | Warp yarn number | Tensile Strength (N) |
|------|---------|-----------|------------|-----------|-----------|-----------|-----------|-----------|-----------|
| **101** | Meta-aramid | Plain weave | 248.61 | **0.642** | 30 | 19 | Nm 17 | Nm 12 | 1565.8 |
| **102** | Modacrylic-Viscose-FR cotton | twill (2/2) | 249.23 | **0.474** | 33 | 30 | Nm 22 | Nm 30 | 603.7 |
| **103** | Cotton 1- FR1 (Apyrol CEP-CHT) | twill (1/3) | 565.21 | **1.110** | 17 | 30 | Nm 14 | Nm 12 | 1026.5 |
| **104** | Leather | - | 735.35 | **1.042** | - | - | - | - | 308.5 |
| **105** | Cotton 2- FR2 (Proban-Solvay) | twill (1/5) | 331.06 | **0.708** | 30 | 41 | Nm 14 | Nm 22 | 1194.5 |
| **106** | Aluminized aramid | - | 273.52 | **0.736** | - | - | - | - | 884.0 |
| **107** | Cotton 3- Denim | twill (2/2) | 431.42 | **0.780** | 24 | 32 | Nm 17 | Nm 12 | 1387.4 |
| **108** | FRViscose-Wool-Polyamide | Plain weave | 420.68 | **0.770** | 30 | 30 | Nm 17 | Nm 17 | 592.4 |

## 2.2 Method

Flame retardancy, molten metal protection, pH values, fat content of the leather, abrasion strength, resistance to water penetration, air and water vapor permeability features of the materials were examined.

ISO 15025 standard - procedure A was used for limited flame spread test. pH values that are important when materials contacts to skin were measured according to TS 477 EN 1413 for fabrics and TS EN ISO 4045 for leather. Fat content of the leather was found according to TS EN ISO 4048. In foundries, wearing out of clothing by mechanical effects are occurred, therefore, TS EN ISO 12947-1 was used to obtain abrasion resistance. 30000 cycles were applied to samples and after every 5000 cycles weight losses were calculated. Additionally, resistance to water penetration (TS 257 EN 20811), air (TS 391 EN ISO 9237) and water vapor permeability (BS 3424-24) tests were applied to observe permeability properties.

Molten metal protection was measured according to TS EN ISO 9185 standard with home-made device (Figure 1(a)). Aluminium (99.5%) was used as metal. In this test method, certain amount of molten metal starting from 50grams is poured at a certain speed onto fabrics that are placed on 60° inclined apparatus. Under fabric sample, a specific PVC film as skin simulant is used. At the end, 30s after completion of pouring, damage to skin simulant (not to fabric) is examined. The damage means 5mm in width or bigger stain on skin simulator as seen in Figure 1(b). If there is no damage, test is repeated with new specimen using a quantity 50g greater molten metal than the amount of previous test. If there is damage, test is repeated with new specimen using a quantity 10g less than the amount of previous test. The result is the highest mass of metal poured that does not caused damage. So fabrics are ranked by the quantity of molten aluminium that they can protect skin in heat and flame protective workwear standard, ISO 11612. Molten alumnium protective fabrics or assemblies should meet the criteria at least level D1 (100g-199g) as protection from minimum 100g of molten aluminium. (D2: 200g-349g; D3: equal or higher than 350g) Aluminium pouring temperature is 780°C [2].

## 3. RESULTS AND DISCUSSION

### 3.1 Tensile and Abrasion Strength of Samples

Workwear fabrics must show protective properties against hazards in the workplaces, however, without durability of fabrics, protective excellence loose importance. In order to determine better material, breaking strength and elongation values of fabric samples were measured and shown in Table 2.



**(a)**                                                     **(b)**
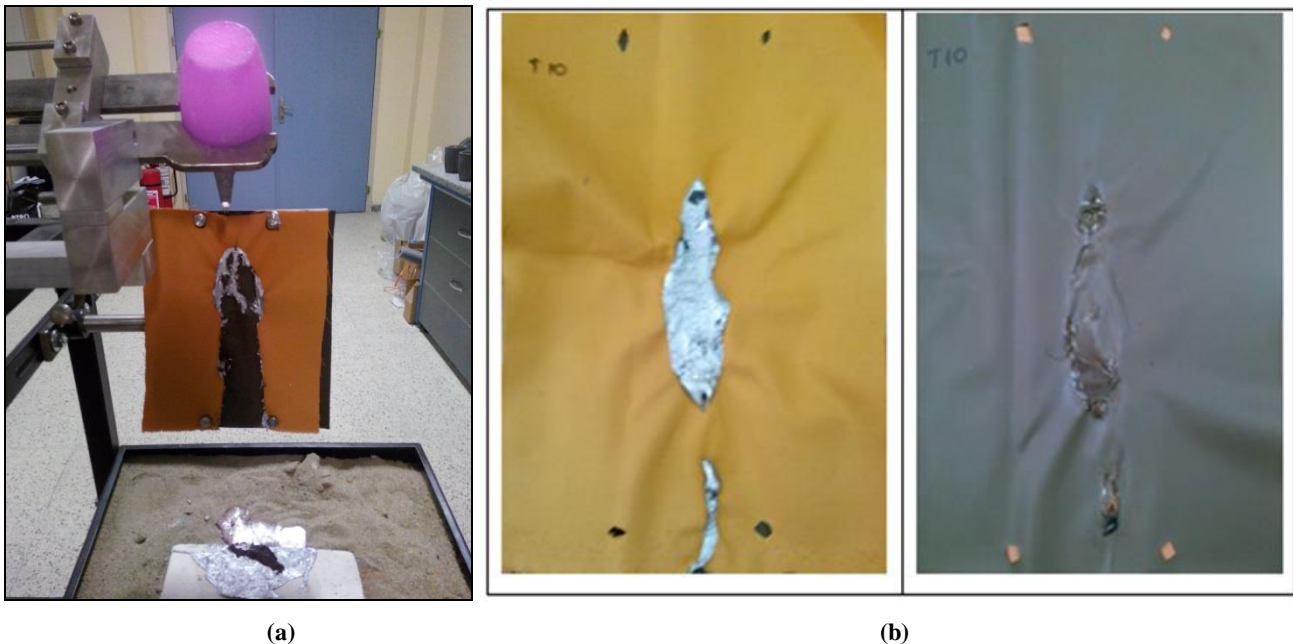
**Figure 1. (a)** Molten metal protection measurement device, **(b)** Damaged fabric and skin simulator with damage bigger than 5mm in width (101-aramid fabric with 10g of molten aluminium)

**Table 2.** Tensile strength and elongation at break values of the samples

| Fabric Code | Tensile Strength-Weft direction (N) | Tensile Strength-Warp direction (N) | Average Tensile Strength (N) | Weft-elongation | Warp-elongation | Average Elongation |
|---|---|---|---|---|---|---|
| **101** | 1602,5 | 1529,0 | 1565,8 | %45,7 | % 24,3 | % 35,0 |
| **102** | 619,5 | 587,8 | 603,7 | %19,4 | %26,9 | % 23,2 |
| **103** | 889,2 | 1163,8 | 1026,5 | % 8,1 | % 19,7 | % 13,9 |
| **104** | - | - | 308,5 | - | - | % 49,1 |
| **105** | 1713,0 | 676,0 | 1194,5 | %12,3 | %13,9 | % 13,1 |
| **107** | 909,7 | 1865,1 | 1387,4 | %13,0 | %27,2 | % 17,2 |
| **108** | 658,2 | 526,6 | 592,4 | %21,4 | %30,5 | % 28,9 |
| | **Course direction** | **Wale direction** | | **Course direction** | **Wale direction** | |
| **106** | 844.8 | 923.9 | 884,0 | %78,2 | %19,0 | % 48,6 |

When look through the table, there are remarkable differences in the values. The reasons seem to be the types of weave and the fibers. Because meta-aramid fiber strength is inherently high. Cotton fabrics whose weave types were twill showed high strength values. Additionally, fiber strengths of cotton, wool, modacrylic and polyamide fibers are 0.45 N/tex, 0.11 N/tex, 0.27 N/tex and 0.29 N/tex, respectively. Course direction elongation of aluminized aramid was extremely high. This coated product was in warp knitted structure and the elongation extend can be seen in Figure 2. Three twill cotton fabrics have the lowest degrees of elongation because cotton fibers have lower elongation at break values than the other fibers [12-15].



**Figure 2.** Elongation of aluminized aramid fabric

The same protective workwear piece may show different properties in different factories depending on product of the foundry, processing units, production conditions, etc. Abrasion resistance of fabrics is affected by fiber type, yarn properties, fabric structures and finishing treatmens [13]. The results are seen in Figure 3.
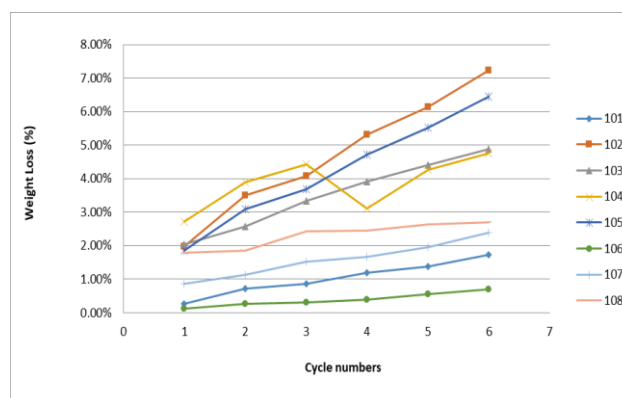


**Figure 3.** Abrasion strength of materials (cycle numbers x 5000)

The best result was obtained from aluminized aramid sample. It may be due to metalic coating on the fabric gave it protection layer against abrasion. Meta-aramid fabric and cotton denim fabric samples are following aluminized aramid. Modacrylic-viscose-FR cotton blended fabric was the worst sample in abrasion test. Thickness may be the reason hence this fabric is the thinnest fabric sample [13,16].

### 3.3 pH Value and Fat Content of the Leather

The results of pH value measurements and fat content of leather is seen in Table 3.

**Table 3.** pH values of the samples and fat content of the leather

| Fabrics | pH values |
|---|---|
| **101 - meta-aramid** | 6.66 |
| **102 - Modacrylic-Viscose-FR cotton** | 6.65 |
| **103 - Cotton 1- FR1** | 7.26 |
| **104 - Leather**  Mean Fat Content: 0.862 % | 3.75 |
| **105 - Cotton 2- FR 2** | 8.72 |
| **106 - Aluminized aramid** | 6.45 |
| **107 - Cotton 3 – Denim** | 7.65 |
| **108 - FRViscose-Wool-Polyamide** | 7.86 |

Because these workwear fabrics are in direct contact with skin, their pH value must be harmless to skin of the wearer. For innocouousness, pH should be close to neutral pH (pH 7). Except leather, all test samples seem to have compatible

pH degree with human skin. Fat content of leather materials should be below 15% according to TS EN ISO 11612. Therefore, the leather sample of this study is suitable for this criteria.

### 3.3 Limited Flame Spread

The criteria when applying this test are not quantitative. Requirements of TS EN ISO 11612 are no specimen shall permit any part of the lowest boundary of any flame to reach the upper or either vertical edge; no specimen shall give flaming or molten debris; no specimen shall give hole formation of 5 mm or greater in any direction, except for an interlining that is used for specific protection other than heat and flame protection; afterglow time shall be ≤2 s and afterflame time shall be ≤2 s. If all criteria are fulfilled, this means that the sample passes the test. The results of this test is given in Table 4.

**Table 4.** Results of limited flame spread test

| Fabric type | Fabric Thickness (mm) | Vertical Flame Spread Test- (Pass / Fail) |
|---|---|---|
| Meta-aramid | 0,642 | Pass |
| Modacrylic-Viscose-FR cotton | 0,474 | Fail |
| Cotton 1- FR1 | 1,110 | Pass |
| Leather | 1,042 | Pass |
| Cotton 2- FR 2 | 0,708 | Pass |
| Aluminized aramid | 0,736 | Fail |
| Cotton Denim 3 | 0,780 | Fail |
| FRViscose-Wool-Polyamide | 0,770 | Fail |

In this test, inherently flame retardant meta-aramid fabric, flame retardant treated cotton fabrics and leather passed the criteria as expected. The other fabrics showed worse results because their 'afterflame time' exceeded limits, even aluminized fabric. Aluminized fabrics are produced mainly for heat reflectance. Besides, because its high thermal conductivity causes other types of heat transfer easily to fabrics lowering protection properties. Additionally, aluminium can melt under the flame condition, due to flame temperature of propane is higher than its melting burning point as approximately 660ºC (in our device we measured flame temperature approximately 720ºC) [17-19].

### 3.4 Molten Aluminium Protection Test

Starting amount of molten aluminium was 50g. Evaluation criteria for the test is any damage in the size of 5mm in width on PVC skin simulator. The results are given in Table 5.

As seen from the table, protection degrees of the samples are in two extreme group. One half of the fabrics are maximum protective against molten aluminium but the other half is absolutely inadequate to use in this field even they have flame retardant properties. We can conclude that flame retardant property does not refer to molten aluminium protective property, similar to literature [5]. In Figure 4, pictures of results of protective fabrics are shown. Aluminized fabric is also protective and image of samples tested with different molten aluminium weights are given in Figure 5. Result from fabric sample 101-meta-aramid was given in Figure 1.(b).

**Table 5.** Molten aluminium protection test results

| Fabrics | Amount of poured molten aluminium that does not damage PVC skin (g) | Weighed amount of aluminium (g) |
|---|---|---|
| 101 - Meta-aramid | <7.04 g | 10 |
| 102 - Modacrylic-Viscose-FR cotton | <6.33 g | 10 |
| 103 - Cotton 1- FR1 | 26.69 g | 30 |
| 104 - Leather | >334.00 g | 350 |
| 105 - Cotton 2- FR 2 | <8.99 g | 10 |
| 106 - Aluminized aramid | >343.83 g | 350 |
| 107 – Cotton 3 - Denim | >345.54 g | 350 |
| 108 - FRViscose-Wool-Polyamide | >346.66 g | 350 |



**Figure 4.** 350g - molten aluminium tested samples and related PVC skin simulant (from left to right: LenzingFR-Wool-Polyamide, Cotton 3-Denim, leather)
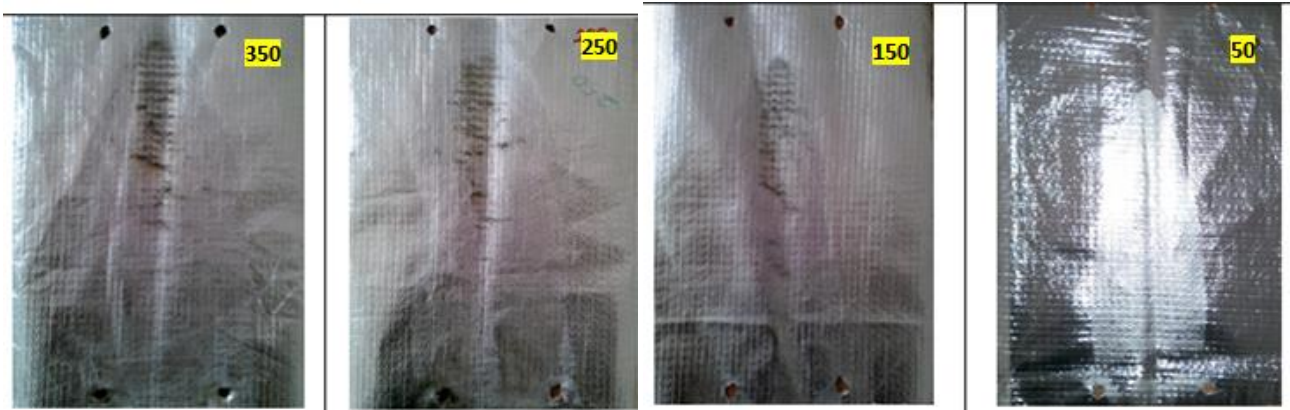
**Figure 5.** Aluminized aramid fabric tested with different amounts of molten aluminium

As seen from the Figure 1(a), meta-aramid fabrics showed a sticky surface for aluminium metal, therefore, damage to PVC skin was severe. The reason is softening of meta-aramid fibers when a molten metal poured on. Figure 4 shows the views of 350g weigthed aluminium poured materials (leather, denim and LenzingFR-wool-polyamide) and PVC skins. As seen in the picture, none of the fabrics shrinked and was damaged, PVC film was not damaged, too. Figure 5 shows the change on the surface of aluminized aramid fabric. Altough surface was changed by increasing amount of molten aluminium, PVC skin was not damaged.

### 3.5 Water, Watervapor and Air Permeability Tests

In addition to protection, permeability properties must be taken into account because using the protective clothing at work require comfort and ability to work with these clothes (Table 6).

Air and water vapor permeability properties are related to comfort feeling of a textile structure. Feeling comfortable is important to be able to do work properly in any work field. From the table, air permeability values of leather and aluminized fabric seem to feel workers uncomfortable because they are not breathable. Aluminized fabric has a water vapor permeability value lowest among others, however, leather has some watervapor permeability to permit watervapor to pass through. Except from aluminized aramid, none of the fabrics have water resistance. In fact foundry work does not need water resistance, if the work is realized in outdoor condition.

### 4. CONCLUSION

All these fabric samples were available for molten metal industry in Turkey, even from expert suppliers or from conventional workwear fabric sellers. Wide range of physical and performance properties were obtained from the tested eight different materials. Besides having good protective performances, some samples showed poor comfort related properties. Except from leather, meta-aramid and two FR cotton fabrics, other fabrics were failed from flame spread test because same specimens continued burning. Contrary to results of the flame spread test, leather, aluminized aramid, FR viscose-wool-polyamide and cotton denim materials show the highest values in molten metal protection test. Regarding flame spread test and molten metal protection, only leather sample showed good results for both tests. However, leather has some water vapor permeability but has no air permeability. This means protection good but comfort of the wearer cannot be obtained. For this reason, as a result, novel protective fabrics may be investigated to be used in our country for molten metal protection. Besides, as an alternative, in the production of protective clothing for foundry workers, a clothing design approach combining different materials in one clothing in order to obtain protection, comfort, and affordability at the same time should be regarded for engineered manufacturing.

**Table 6.** Air and water vapor permeability and water resistance results

| Fabrics | Air permeability (l/m²s) | Water vapor permeability index (%) | Water resistance (cm-water column) |
|---|---|---|---|
| **101 - Meta-aramid** | 80.56 | 103.29 | 20.7 |
| **102 - Modacrylic-Viscose-FR cotton** | 81.80 | 95.07 | 23.4 |
| **103 - Cotton 1- FR1** | 89.96 | 94.37 | 23.7 |
| **104 - Leather** | 0.00 | 79.41 | 53.1 |
| **105 - Cotton 2- FR 2** | 160.20 | 129.52 | N/A |
| **106 - Aluminized aramid** | 4.29 | 7.62 | 310.0 |
| **107 - Cotton 3 - Denim** | 52.92 | 110.80 | 13.8 |
| **108 - FRViscose-Wool-Polyamide** | 77.34 | 94.76 | N/A |

## REFERENCES

1. Tudoksad (Turkish Foundry Association), 2020, April 20, We add value to metals, retrieved from https://www.tudoksad.org.tr/upload/files/Dokum_Sanayi_Bilgi_Foyu.pdf

2. Mäkinen, H. 2013. Flame Resistant Textiles for Molten Metal Hazards, In F.S. Kilinc (Ed.), *Handbook of Fire Resistant Textiles*, Cambridge: Woodhead Publishing Limited, pp.581-602.

3. Barker, R., Yener, M. 1981. Evaluating the Resistance of Some Protective Fabrics to Molten Iron, *Textile Research Journal* 1981; 51; 533

4. Benisek, L., Edmondson, G.K., Philips, W.A. 1979. Protective Clothing—Evaluation of Wool and Other Fabrics, *Textile Research Journal* 1979; 49; 212

5. Benisek, L., Edmondson, G.K., 1981. Protective Clothing Fabrics: Part I. Against Molten Metal Hazards1 *Textile Research Journal* 1981; 51; 182

6. Proctor, T.D. and Thompson, H. 1992. Effect of Fabric Finish On the Adhesion of Molten Metal to Wool, Performance of Protective Clothing: Fourth Volume, ASTM STP 1133, James P. McBriarty and Norman W.Henry, Eds., American Society for Testing and Materials, Philadelphia

7. Benisek, L., Edmondson, G.K., 1984. Effect of Chrome Dyeing on Protection of Wool Against Molten Aluminium, *Textile Research Journal* 1984; 54; 214

8. Coughlan, J.E. 1992. Protective Clothing Development at New Zealand Aluminum Smelters Ltd., Performance of Frotective Clothing; Fourth Volume, ASTM STP 1135, J. P. McBriarty and N. W. Henry, Eds., American Society for Testing and Materials, Philadelphaia, p.252

9. Magnússon, V., Gunnarsson, G. & Jónsson, H. 2001. Safety Clothing for the Aluminium Industry, 1st International Conference and Workshop on Anode Rodding Plants for Primary Aluminium, Reykjavik, Iceland

10. Mäkinen, H., Laiho, H., Pajunen, P., 1997. 'Evaluation of the Protective Performance of Fabrics and Fabric Combinations against Molten Iron,' Performance of Protective Clothing: Sixth Volume, ASTM STP 1273, Jeffrey O. Stull and Arthur D. Schwope, Eds., American Society for Testing and Materials.

11. Lee, M, 2009. Recent Developments In Australian Aluminium Casthouse Personal Protective Clothing, *Materials Science Forum*, Vol.630, pp.19-25.

12. Gabara, V. 1994. High performance fibers 1: Aramid fibers, H. Brody, (Ed.), Synthetic fiber metarialism, New York: Longman publishing group. pp.239-260

13. Hearle, J. W. S. ve Morton, W E. (2008), Physical properties of textile fibres (4th Ed.). Cambridge: Woodhead Publishing Limited.

14. Fan, J. (2009). Durability of fabric and garment. J. Fan. ve L. Hunter, (Ed.), Engineering Apparel Fabrics and Garments. Boca Raton: Woodhead Publishing Limited. pp.161-195.

15. Bunsell, A.R. (Ed.) 2009. Handbook of tensile properties of textile and technical fibres. United Kingdom: Woodhead Publishing Limited.

16. Horrocks, A. R. 2014. High performance textile for heat and fire protection. C. Lawrence, (Ed.), High Performance Textile For Heat and Fire Protection. Cambridge: Woodhead Publishing Limited. pp.144-190.

17. Udayraj, Talukdar, P., Das, A., Alagirusamy, R. 2016. Heat and mass transfer through thermal protective clothing – A Review, International Journal of Thermal Sciences, 2016, 106, 32.

18. Hao, L., Yu, W. 2011. Comparison of thermal protective performance of aluminized fabrics of basalt fiber and glass fiber, *Fire and Materials*, 2011, 35, 553.

19. Jin, L., Park, P. K., Hong, K.A., Yoon, K.J. 2015. Effect of Aluminized Fabrics on Radiant Protective Performance of Fire Proximity Suit Materials, Annals of Occupational Hygiene, 2015, 59, 243.

# An Investigation on Suit Choices of Men with Muscular Body Structure

Zümrüt Bahadır Ünal

Ege University, Department of Textile Engineering, İzmir, Turkey

**Corresponding Author:** Zümrüt Bahadır Ünal, zumrut.bahadir.unal@ege.edu.tr

## ABSTRACT

It is necessary desired that men's suit frequently worn at working conditions and special days should be cozy and comfortable. Consequently suits are produced according to generated size charts for various body structures. However there is not any production intended for men practicing sports for body built and having muscular bodies. In order to generate size chart to meet such people, a survey has been applied to persons doing bodybuilding sports and their ideas and detecting the problems. For finding solution to these questions a special size chart was developed necessary for production of suit by measurements taken from such people. The results were compared with normal body sizes.

## 1. INTRODUCTION

The suit is one of the most important clothing groups of the classic men's clothing style. Suits mainly consist of jackets and trousers. The clothes worn by men in official places, ceremonies, feasts and invitations have become very comfortable in daily wear today. More comfortable clothes can be produced by improving the performance properties of natural and synthetic fabrics. Single row buttons, double row buttons and vests can be produced. The suit should match your body size. Otherwise, one feels uncomfortable in the garment. For this reason, a wide variety of size tables are used in the production of suits. The dimensions in these tables are drop size tables prepared by considering the circumference of the navel. The most important reason for this is the increase in the belly circumference in overweight men. Similar size problem is experienced in people with muscular body structure. Changes in body structures of people doing sports with body build intention basically manifest differences according to exercises done, nutritional status and genetic structure of body. When the muscular body is said, body shape with an inverted triangle image comes to mind, People having such body shape generally are doing sport with body built intention.

At the end of the exercise, muscle tissues develop and grow in volume. Shoulder expands, especially with the development of chest muscles and upper arm muscles. With the melting of belly fat, abdominal muscles develop and waist circumference decreases. Accordingly, man who does not do any physical activity owns a very different body structure than the man who builds body on a regular basis.

The volume of growth and shrinkage in certain parts of the bodies of people, especially with high muscle density, doing sports for bodybuilding brought also the problem of fitting the use of suits to the body. For this reason, it is not correct to produce clothes with normal patterns for people with high muscular bodies.

With this study, the expectations of the people who do sports for muscle building were determined by a questionnaire study and their body measurements were taken. The measurements obtained for the production of their suits were compared and evaluated with those of the normal body sizes.

## 2. LITERATURE REVIEW

Dongshengve Qing, studied the evaluation of the degree of pressure of the suit on the bodies of various mannequins.

Therefore, they obtained some data for the comfort analysis of the garment (1).

Muratoğlu and Kılınç in a study conducted in 2004, analyzed men body types, standard sizes used in men clothes, body sizes, classification of men clothes and materials needed in men's jacket and trousers (2).

In line with Turkish Standard Institute body sizes for Turkish men, Sezer in his study in 2006, has tried classic men shirt patterns 46, 48, 50 and 52 sized classical men shirts prepared by Muller pattern system on 46, 48, 50 and 52 sized sportsmen typed male students and parallel to his data, he has developed classic men shirt patterns (3).

Mori and Matsudaria examined the warp yarn density was changed for men's suit fabrics and the effect of weave density on fabric handle, heat-water transfer property, appearance of clothes, wrinkle resistance, and color brightnessare examined. The total hand value (THV) showed the highest at similar density of warp and weft yarn. The total appearance value (TAV) decreased when warp and weft yarn density was smaller. Wrinkle resistance was high in the condition of the maximum warp and weft yarn density. This paper contributes to the development of a fundamental database of designing ideal fabrics (4).

Kinetic performance evaluation of suit jacket was examined by Kanai via measuring the clothing pressure. Subjects wearing three suitjacket of different size performed three different exercises in volving therotation of the upper limbs. The clothing pressure was measured by theair pack sensor and the partial compression feeling and the constrained feeling were evaluated by subjects(5).

Öndoğan, conducted a study in 2007 about the use of simulation systems on the most important stages of production as garment design, body sizing and marketing (6).

Young-Hee and Seung-Hee diagnosed the differences of preference about demand performance with design of men's suit according to demographic characteristic and figured out the needs of adult men consumers. This study is a survey research in order to collect data, a questionnaire was used. To analyze the collected data, fact analysis, $\chi^2$, ANOVA, Duncan's multiple comparisons and the rest were carried out with using SPSS 14.0. Result of this study could get as following. According to silhouette and color, there was a difference to age, attainments in scholarship and preference according to job. Also young people preferred fitted-silhouette and in occasion of color, all of them preferred best black. It was no difference according to demographic characteristic in preferring pattern but preferred best solid on the whole. Demand performance of men's suit appeared by five main causes of design, practicality, comfort, appearance appropriateness, another person awareness and functional materials. (7).

Günay, conducted a study in 2012 about searching the historical process of men sports jackets, examining the men body types and in line of his research he formed new men sport jacket patterns(8).

In his article written in 2015, Öngen presented the men's costumes in the Istanbul Textile Costume and Fashion Research Association collection and the European fashion effects seen in the clothes with visual data, in order to reflect the change in the men's fashion concept in the first years of the Republic and the change in the men's fashion concept in this period (9).

In his study conducted in 2015, Erkılıç examined the relationship between morphological variables and the anaerobic performance values obtained from the upper extremity in young male athletes studying in School of Physical Education and Sports (10).

Ünal and Şamlı examined the size numbering system of suits in their work in 2018. Various brands of suits were researched and the drop sizes applied by these brands and the body types that are the target audience of these body sizes were evaluated [11].

## 3. SIZE NUMBERS IN SUITS

Ready-to-wear production requires mass production. However, people's body sizes and proportions differ unlimitedly, not only in the same country but also from country to country. For this reason, standardization of body sizes is extremely important in the production of ready-made clothing. It is not possible to go to standardization in all body sizes. For this, some basic measures were selected and standardization was made on these measures. In men's clothing, these dimensions may be based on the type of clothing; chest circumference, waist circumference or collar circumference. Chest size is taken into account for size numbering in men's suits and jackets. Size number in men's suits and jackets is calculated as half of the chest circumference at 4 cm intervals (2).

The size numbering system of suits, which have an important place in men's clothing, is different from other clothing. The drop system that specifies the width of the core zone has been developed. Suits are commonly available are presented in 4, 6 and 8 drops. Intermediate drop sizes, such as 7, can also be seen in Italian cut suits. Applications and naming vary according to the companies. Drop numbers, defined as 4, 6 and 8, are obtained by finding the difference of the values of the chest and waist measurements in inches (1inch = 2.54 cm) (11).

## 4. MATERIAL AND METHOD

### 4.1 Material

The material of the research consisted of 188 male sportsmen living in Izmir and who regularly exercise in order to improve their body muscles, between the ages of 19-39. In order to reach these people, various sports complexes were determined and a survey was conducted with the permission of these places.

The survey study was composed of 3 groups as personal information, physical information and purchasing behavior. Personal information section includes the person's marital status, profession, monthly earnings, age, and how many years he has been doing sports for bodybuilding purposes. Physical information section contains the person's upper body number and lower body number measurements. Finally, in the purchasing behavior section, it was asked the preferred clothing style, in which order of priority when purchasing the clothing, whether it was able to find clothes according to the appro(1 Euro=6.666 TL) spent on the suit.

In the continuation of the survey, body measurements used in the production of suits were taken from the sportspersons and a size table was prepared for these people.

### 4.2. Method

First of all, a survey was conducted to determine the characteristics and expectations of people interested in bodybuilding sports. The questionnaire was created from closed and open-ended questions. Questionnaire questions were first asked to individuals, and then the necessary body measurements were taken for the production of suits.

After evaluating the questionnaire questions, the measurement table used by a company that produces a high quality suit and markets it to a large audience, and the data of the measurement table obtained as a result of the survey were evaluated statistically.

### 5. RESULTS AND DISCUSSION

It is required to spend time and effort in a serious sense to this sport. For this reason, considering the survey data consisting of multiple choice and one open-ended 11 questions replied by young and bachelor students who are interested in this sport, certain issues were determined on the measures taken and studied people at the evaluation of this questionnaire. 162 students, 4 represents, 3 sales consultants, 3 academicians, 1 lawyer, 1 doctor, 1 instructor, 1 chemist and 12 coaches participated in the survey. Data obtained from questionnaire was evaluated with graphics.
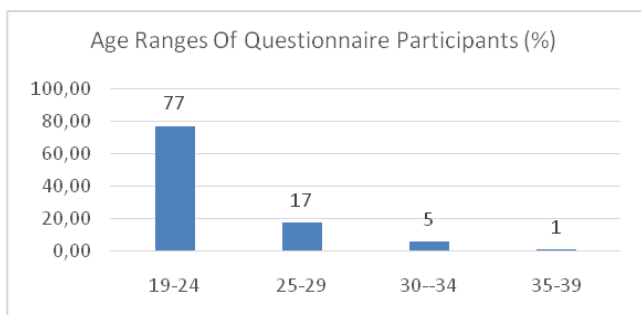


**Figure 1.** Age ranges of questionnaire participants

77 % of questionnaire participants were young men between 19-24 age ranges. As the age increases number of people doing sports in this field was decreased.
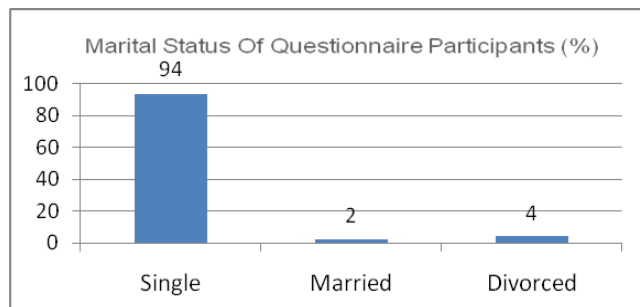


**Figure 2.** Marital status of questionnaire participants

94 % of people interested in bodybuilding sports were single men. This acquired results shows the proof of single young men wanted to look muscular.
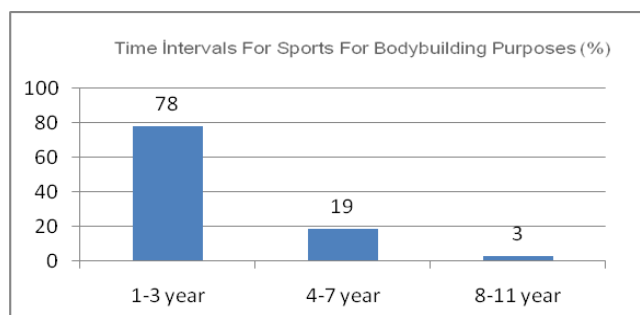


**Figure 3.** Time intervals for sports for bodybuilding purposes

78% of those interested in bodybuilding have been interested in this sport for 1-3 years. This ratio has decreased over the years.
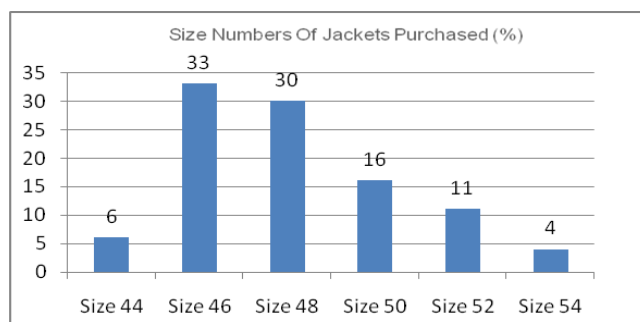


**Figure 4.** Size numbers of jackets purchased

It was determined that in the ratio of 33% to 30%, the sportsmen wore 46 and 48 size jackets. As the body number increases, this ratio was decreased.
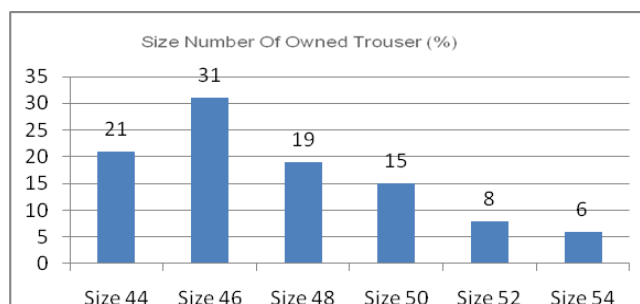


**Figure 5.** Size number of owned trouser

31% of the sportsmen wear 46 size pants. The ratio decreased with the size of the trousers increased as with the size of the jacket.



**Figure 6.** Preferred clothing style

When the clothing styles of the people who do regular sports are evaluated, 83% of them prefer sports and 17% prefer stylish clothing.
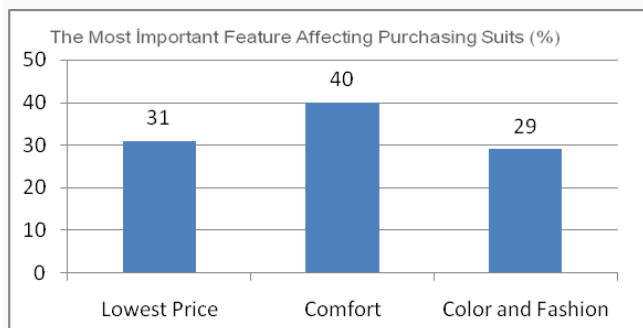


**Figure 7.** The most important feature affecting purchasing suits

In purchasing suits, 40% of the participants stated that they attached importance to the comfort of the garment first. While it is important for 31% to be affordable, 29% prioritize its color and fashion appeal.Comfort comes first as it is seen from the figures
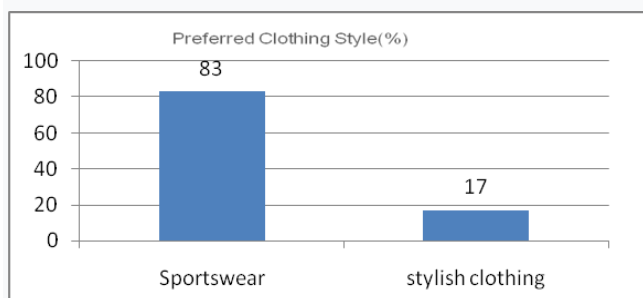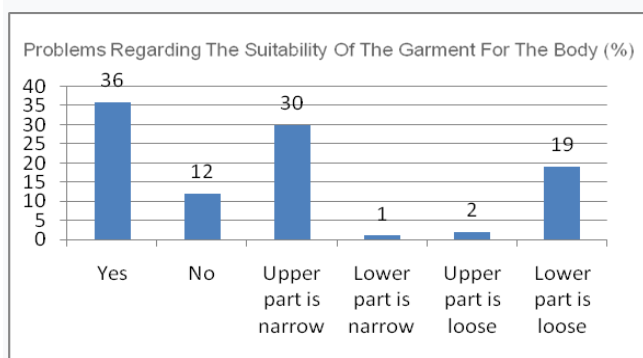


**Figure 8.** Problems regarding the suitability of the garment for the body

While 36% of the sportsmen can find clothes suitable for their size, 12% stated that they could not find it. An important rate such as 30% stated that they are disturbed by the narrowness of the upper body and 19% of them are disturbed by the width of the lower body.
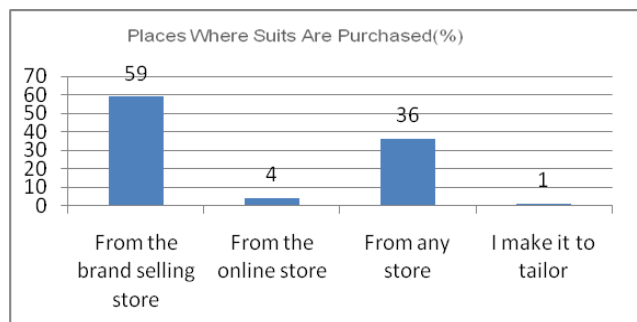


**Figure 9.** Places where suits are purchased

59% of respondents prefer stores selling brands to buy suits; 36% stated that they purchased from any store.
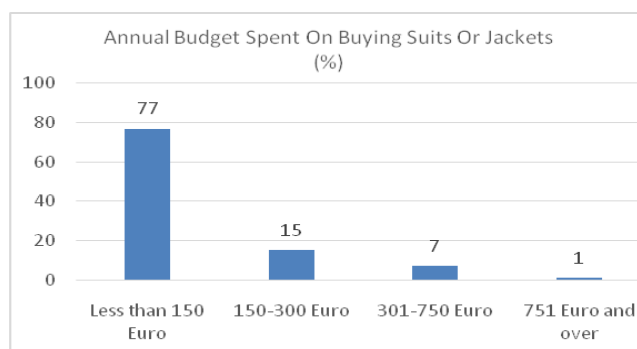


**Figure 10.** Annual budget spent on buying suits or jackets

77% of the respondents stated that they spend less than 1000 TL per year for suits, 15% spend 1000-2000 TL and 7% spend 2000-5000 TL.
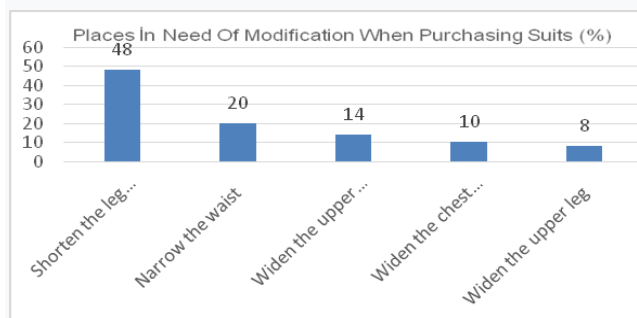


**Figure 11.** Places in need of modification when purchasing suits

Whether the survey respondents need modification at the end of the purchase consists of different rates. 48% of the participants stated that they needed to shorten the leg length, 20% to narrow the waist, 14% to widen the upper arm, 10% to widen the chest circumference and 8% to widen the upper leg.

## 6. CONCLUSION AND SUGGESTIONS

The main purpose in muscle building is to look fitter and more attractive. However, doing and maintaining this sport requires a great deal of effort. The most important reason of this situation is due to serious time and heavy nutrition criteria required to spend for this sport. Nutrition taken

before and after this sport has great importance for body building formation. Men who have difficulty in making this sport a lifestyle leave this sport in time.

As seen in Figures 4 and 5, it has been observed that men with very high body mass index are not interested in this sport. The ratio of the participant has decreased with the size of the pants has increased as with the size of the jacket.

As seen in Figure 6 most of the participants prefer sports wear in daily life since they do sports intensely. For them, suit is the garment to be preferred on special days.

However high ratio of young people at survey participants become effective in that affordability and fashion appeal of the suit was also high so that cannot be ignored.

As seen in Figure 8 the young people, intensely uses arm, chest, abdomen and leg muscles. As a result upper arm becomes thicker and chest muscles expand. Abdomen fat melts and flat abdomen with muscle is formed. Fat ratio in leg also decreases and muscular structure is also formed.

As seen in Figure 9 the suit even not preferred in daily life is preferred in case of need. For such cases the ratio of brand choice was found higher which shows that young people want to look better.

As seen inFigure 10 is the majority of the participants were students, it was found that they did not spend a lot of money on the suit. However, most of the respondents stated that they rarely need suits because they prefer sportswear. When necessary, the people who wore the existing suit dresses stated that they were not very comfortable in their old suits, and even needed renovation. However, the renovation of the suit is often impossible and the athletes said that they had to buy new suits.

In the individuals who focus on lower bodybuilding, the upper body comes in harmony with the body size they choose, while it is observed that there is an incompatibility between the waist of the pants and the leg part due to the muscle volume on the legs.

The measurements obtained from the people who participated in the survey with the measurements used by a brand producing a classic suit and used as normal body measurements are shown in Table 1 below.
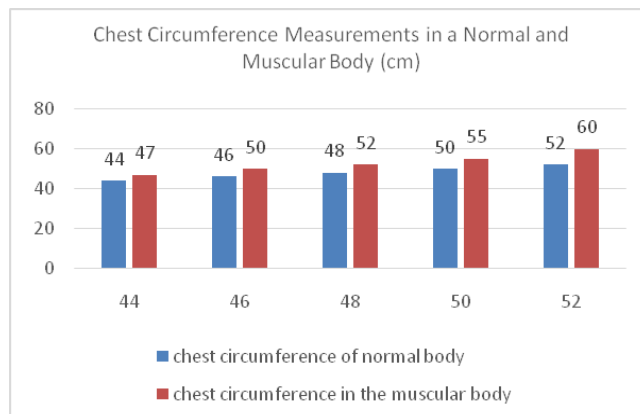


**Figure 12.** Chest circumference measurements in normal and muscular body
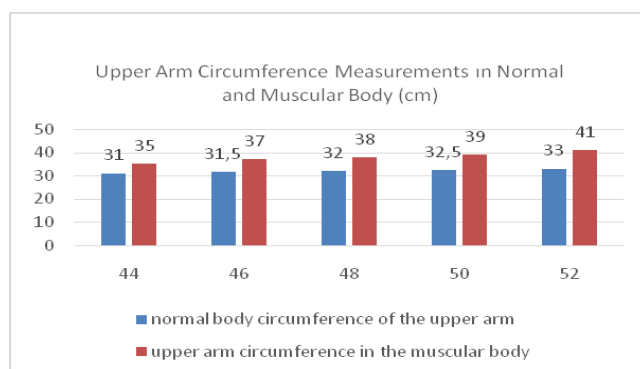


**Figure 13.** Upper arm circumference measurements in normal and muscular body

One of the first goals of muscular athletes is to develop their arm muscles. As seen in Figures 12 and 13, there was a regular increase in chest and upper arm circumference. Subsequently, the aim is to turn all fat tissues into muscle. It is possible with a tight body, muscular arms, muscular chest, belly and legs.

**Table 1.** Measurement table obtained from normal body and survey participants (12)

| | Normal Body Measurements | | | | | Measurements Obtained From The People Who Participated In The Survey | | | | |
|---|---|---|---|---|---|---|---|---|---|---|
| Sizes | 44 | 46 | 48 | 50 | 52 | 44 | 46 | 48 | 50 | 52 |
| Chest Width | 44 | 46 | 48 | 50 | 52 | 47 | 50 | 52 | 55 | 60 |
| Waist Width | 40 | 42 | 44 | 46 | 48 | 40 | 42 | 43 | 45 | 47 |
| Hip Width | 46 | 48 | 50 | 52 | 54 | 46 | 47 | 48 | 50 | 53 |
| Arm Length | 62 | 63 | 64 | 65 | 66 | 61 | 62 | 64 | 66 | 68 |
| Upper Arm Circumference | 31 | 31,5 | 32 | 32,5 | 33 | 35 | 37 | 38 | 39 | 41 |
| Side Length for Trousers | 100 | 102 | 104 | 106 | 108 | 100 | 104 | 107 | 110 | 112 |
| Inner Leg Length | 78 | 80 | 81 | 82 | 83 | 78 | 80 | 82 | 84 | 86 |
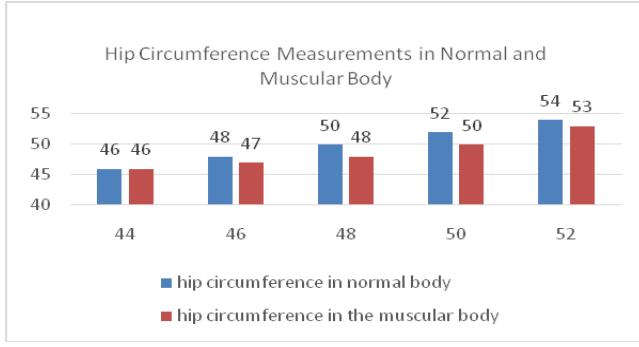
**Figure 14.** Hip circumference measurements in normal and muscular body

With muscle work, a regular tightening occurs around the hip and the size becomes smaller.Due to the muscle activity, a regular tightening occurs around the hip and the body size becomes smaller.Considering the result of the study; it has been determined that the basis of the problems experienced by men doing bodybuilding was caused by body parts with high muscle density. Incompatibility occurs when one of the same size jackets and trousers fits the body, while the other is slack or appear as deviation at incompatible areas such as in waist, chest and height at the person's normal size trousers or jacket. As a result, bodybuilding men experience a fit problem when they buy suits made with standard patterns. As a solution to this, it was concluded that a suit pattern with new measures should be developed in line with the data obtained as a result of the study.

Muscular people find it difficult to find a suit that fits nicely on their body among the sizes available on the market. Such people approve the situation which knitted garments are flexible and make the details of the body clearer. For this reason, the biggest problem is experienced in the clothes produced from woven fabrics. Therefore, taking into account the muscular people, a different size table and patterns worked with these sizes are needed for shirt and suit production. This research is important in terms of determining the suit problems of people who do sports for muscle building purposes and speeding up the clothing pattern studies in this field to raise awareness about this issue before anything else.

## REFERENCES

1. Dongsheng, C.,Qing, Z., 2003, "A Study On Clothing Pressure Formen's Suitcomfort Evaluation", International Journal of ClothingScienceandTechnology, Vol. 15, Issue 5.

2. Muratoğlu, Y., Kılınç, N., 2004, "Erkek Giysi Üretimi", Bizim Büro Yayınevi, Ankara.

3. Sezer, B., 2006, "Müller Kalıp Sistemi 46-52 Beden (38-41 Yaka )Klasik Erkek Gömleği Kalıplarının Antropometrik ve Ergonomik Uyumunun İncelenmesi", Selçuk Üniversitesi Sosyal Bilimler Enstitüsü, Yüksek Lisans Tezi, sayfa:39,40

4. Mori, M., Matsudaira, M., 2007, "TheEffect of WeaveDensity on FabricHandleandAppearance of Men'sSuitFabrics", ResearchJournal of TextileandApparel, Vol.11, No.3, pp. 71-78.

5. Kanai, H.,Tsuji, H., Kamijo, M., Matsumoto, Y., Nishimatsu, T., Shibata, K., "Evaluation of KineticPerformanceforMen'sSuitJacket in Exercise of ShoulderJoint", Sen'i Gakkaishi, Vol. 63, No.6.

6. Öndoğan Z., Pamuk, O., Topal, E., Çelikkaş, M., Ünver, o., Işıkoğlu, P., 2007, "Giysi Tasarımı, Vücut Ölçülendirme ve Giysi Pazarlaması Konularında Simülasyon Sistemlerinin İncelenmesi", Tekstil Ve Konfeksiyon, sayfa: 15

7. Young-Hee, P., Seung-Hee, H., 2010, "A Study on thePreference Design andtheDemandPerformanceforAdultMen'sSuit", TheResearchJournal of theCostumeCulture, Volume 18 Issue 1, Pages.1-12.

8. Günay S., 2012, "Erkek Spor Ceket Tasarımında Kullanımı Kolaylaştırıcı Kalıp Çözümlemeleri", Dokuz Eylül Üniversitesi,Yüksek Lisans Tezi.

9. Öngen A. G., 2015, "Cumhuriyet Dönemi Modernleşme Politikasının Erkek Giyim Tarzına Etkisi", Akdeniz Sanat Dergisi, sayfa: 3,5

10. Erkılıç A.O.,2015, "Beden Eğitimi Ve Spor Yüksekokulu'nda Eğitim Gören Genç Erkek Sporcularda Morfolojik Değişkenler İle Üst Ekstremiteden Elde Edilen Anaerobik Değerler Arasındaki İlişkinin İncelenmesi", Bartın Üniversitesi Eğitim Bilimleri Enstitüsü, Yüksek Lisans Tezi.

11. Bahadır Ünal Z., Şamlı, B.E., 2018, "Takım Elbiselerde Drop Sistemi Uygulamaları", Mesleki Bilimler Dergisi, sayfa: 2, 4.

12. Firma Ölçüleri, 2019.

# A Study on Coating with Nanoclay on the Production of Flame Retardant Cotton Fabrics

Nuriye Kertmen[1], Eylen Sema Dalbaşı[1], Ayşegül Körlü[1], Arif Taner Özgüney[1], Saadet Yapar[2]

[1] Ege University / Engineering Faculty, Textile Engineering Department / 35100 Bornova, İzmir, Turkey
[2] Ege University / Engineering Faculty, Chemical Engineering Department / 35100 Bornova, İzmir, Turkey

**Corresponding Author:** Eylen Sema Dalbaşı, E-mail: sema.namligoz@ege.edu.tr

## ABSTRACT

In this study, 100% cotton fabrics' flame retardant properties were improved using commercial nanoclay (Cloisite 20A), clay-based montmorillonite. Flame retardancy and thermal decomposition behavior of the samples were characterized by the vertical burning test, limiting oxygen index (LOI), and thermogravimetric analysis (TGA). The surface morphology of untreated and treated fabric was examined using a scanning electron microscope (SEM). Fourier-transform infrared spectroscopy (FTIR) analysis was carried out for Cloisite 20A, untreated, and coated fabrics. The test results showed that the coating treatment, even at low nanoclay concentration, is enough to have a considerable flame retardant effect. This result was attributed to the barrier effect of the nanoclay.

## 1. INTRODUCTION

Fires are dangerous events that cause material damages and loss of life if they cannot be stopped. The increasing population in the world increases the risk of fire. Moreover, fire has become one of the most critical issues, especially in public places [Liu et al., 2011; Cordner et al., 2013; Gao et al., 2015]. The demand for the production of protective materials with high fire resistance increases because most of the products in our environment are highly flammable [Holder et al. 2017]. Due to its soft, comfortable, and breathable properties, cotton fiber is a prevalent and widely used natural fiber in the textile industry. Cotton fibers are always preferred because of their natural structure, no risk to health, and easy processibility [Du et al. 2011; Yuan et al. 2010]. Therefore, it is mostly used to produce garments, upholstery fabrics, tents, pillowcases, towels, and linens. However, cotton is a flammable fiber [Zhang et al., 2017; Başyiğit and Kut, 2018]. The cotton fibers have an LOI of 18.4% [Ghoranneviss and Shahidi 2014] so that even a tiny spark is sufficient for the fibers to burn, and the flame spreads rapidly. For this reason, numerous studies have been carried out to improve the combustion behavior of such highly preferred cotton fibers [Gao et al., 2015; Carosio et al., 2012]. The flame-retardant agents are applied to cotton fabrics by using different methods [Zhang et al. 2017; Shahidi and Ghoranneviss 2014]. Although there are many commercial flame-retardant products, the numbers of

environmentally friendly ones have limited [Holder et al., 2017]. At this point, clay minerals come to popular with their environmentally friendly properties, and they are used in the production of flame-retardant textiles [Ghosh 2011; Uddin 2008]. There are many studies on flame retardant textiles [Gao et al. 2015; Başyiğit 2018; Shah et al. 2017; Guo et al. 2017; Majka et al. 2017; Makhlouf et al. 2017; Rehan et al. 2018; Chowdary and Kumar 2015] by various methods such as melt-spinning [Bhat et al. 2008], layer by layer [Holder et al. 2017; Qiu et al. 2017], sol-gel [Zhang et al. 2017] and plasma [Shahidi and Ghoranneviss 2014].

Clay minerals are generally considered nanomaterials, as they possess layers with thickness and inter-layer spaces both within the nanoscale range, so the term 'clay minerals' is often used interchangeably with 'nanoclay'. There is increasing evidence to suggest that nanomaterials are different from their bulk counterparts in terms of their physicochemical and toxicological properties. The increase in clay materials, particularly in food, agriculture, animal feed, environmental remediation, and medicine, will inevitably increase the environmental and human exposure to different clay materials. Clay minerals are layered substances consisting of sheets of silicate tetrahedra ($SiO_4$) and octahedra (containing Al, Mg, and Fe). Natural clay minerals are built of layered structural units with a layer thickness of approximately one to a few nanometres and lateral dimensions varying from 30 nm to several microns,

which gives a ratio of length to a thickness greater than 1000 [Zhu and Njuguna 2014].

Clays and clay minerals have been evaluated for diverse potential applications, as pollutant adsorbents for sustaining the environment and their use in human and veterinary medicine. They have large adsorption capacities, excellent mechanical and chemical properties [Yapar et al., 2015]. Through the replacement of interlayer metal cations of montmorillonite with quaternary alkylammonium salts, the hydrophobicity is increased [Erkan et al. 2010], the interlayer space is expanded [Schumann et al. 2014], and thus the organo-montmorillonite obtained, allowing it to be used in a wide range of technological applications [Ruiz-Hitzky et al. 2010].

The clay minerals are composed of silicate and alumina layers containing metal oxides and cations [Zeng et al. 2005]. These layers parallel to each other and located at a distance of about 1 nm, and their structures have varying ions and OH groups and the clays in the crystalline structure generally have Van der Waals bonds between the layers [Zeng et al. 2005; Mittal et al. 2018]. Clay minerals can be found in 3 different types as 1:1 and 2:1 [Zhang et al. 2017] depending on the ratio of silica and alumina layers [Mittal et al. 2018; Azeez et al. 2013]. Montmorillonites, a clay mineral of type 2:1 is highly advantageous clays due to its wide surface area, morphological structure, abundant presence, ecological nature and low cost [Uddin 2008; Yelkovan et al. 2014].

In order to be used in some industrial applications, clays must have an organophilic structure which is dispersed in organic phases. The conversion of clays to organoclay occurs by a simple displacement reaction. After the reaction, the surface of the clay gains organophilic properties by using alkyl ammonium and alkyl phosphonium cations [Visakh 2015].

Montmorillonites are widely used in the textile industry. They have (Na, Ca) (Al, Mg)6(SiO10)3(OH)6-nH$_2$O formula [Ghosh 2011]. Because they have average surface energy, they can be modified more easily than other clay types [Visakh 2015; Cao et al. 2014]. Montmorillonites have recently come to the forefront with their environment-friendly flame retardant properties in the textile industry. There are many studies about using montmorillonite clays to improve textiles' thermal properties [Gao et al. 2015; Shahidi and Ghoranneviss 2014; Bourbigot et al. 2002; Li et al. 2010]. Montmorillonite clays form a protective layer during the combustion process, slow the evaporation of the flammable gas released during the combustion and block the oxygen transfer to prevent heat transfer and thus disrupt the combustion cycle [Gao et al. 2015].

Nanoclays are nanoparticles of layered mineral silicates organized into several classes such as montmorillonite (MMT), bentonite, kaolinite, hectorite, and halloysite on chemical composition and morphology. The most commonly used layered silicate in polymer nanocomposites is MMT, which has encouraged much improvement in the mechanical, thermal, flammability, and barrier properties of polymers due to its high aspect ratio and large surface area, extraordinary modulus, and nanoscale dispersion [Norouzi et al. 2015]. The layered silicates enhance the flame retardancy properties of polypropylene textile articles. The use of nanoclay and polyhedral oligomeric silsesquioxanes in polyurethane coating applied to polyester and cotton reduces peak heat release [Rault et al. 2015]. The additives such as a nano additive made of synthetic clay montmorillonite and two polyhedral oligomeric silsequioxanes are incorporated into the polyurethane resin [Devaux et al. 2015].

In this study, flame retardant properties of 100% cotton woven fabrics were tried to be improved by using commercial nanoclay (Cloisite 20A) which is a montmorillonite based organoclay. Cloisite was also used in the other studies targeting the flame retardancy. For instance, it has been applied to polyethylene terephthalate (PET) polymer [Fabia et al. 2020], polyethylene terephthalate fiber and nanocomposites in studies conducted to date. Yelkovan and et al. (2014) applied Cloisite to PET polymer. In that study, Cloisite and PET polymer were combined with melt blending method in terms of twin screw extruder [Yelkovan et al. 2014]. Devaux and et al. (2002) applied Cloisite to polyurethane resins (PU) nanocomposites [Devaux et al. 2015]. Unlike the studies reported in the literature, in this study, cloisite was applied directly to the cotton fabric. In particular, it is intended to provide a flame retardant effect in technical textile fabrics that are not washed. Flame retardancy and thermal decomposition behavior of the samples were characterized by the vertical burning test, limiting oxygen index (LOI), and thermogravimetric analysis (TGA). The surface morphology of untreated and treated fabrics was examined using a scanning electron microscope (SEM). Fourier-transform infrared spectroscopy (FTIR) analysis was carried out for Cloisite 20A, untreated and coated fabrics. The obtained results were evaluated and discussed.

## 2. MATERIAL AND METHOD

### 2.1 Material

The physical properties of 100% cotton woven fabrics (desized, scoured and bleached) used for experiments are given in Table 1.

**Table 1.** The physical properties of fabrics used in coating experiments

| Specifications | | |
|---|---|---|
| Fiber type | | 100% Cotton |
| Fabric construction | | Plain |
| Fabric weight (g/m$^2$) | | 154.7 |
| Yarn density | Warp density | 42 |
| (threads/cm) | Weft density | 28 |

In this study, nanoclay called Cloisite 20A (Figure 1) was used as a flame retardant material supplied by Feza Kimya Company. It is montmorillonite modified with a quaternary ammonium salt. The thickener (Alginate SMT T, high viscosity sodium alginate) and wetting agent (Biomegapal D40) were supplied from CHT Company and Bozzetto Company respectively.
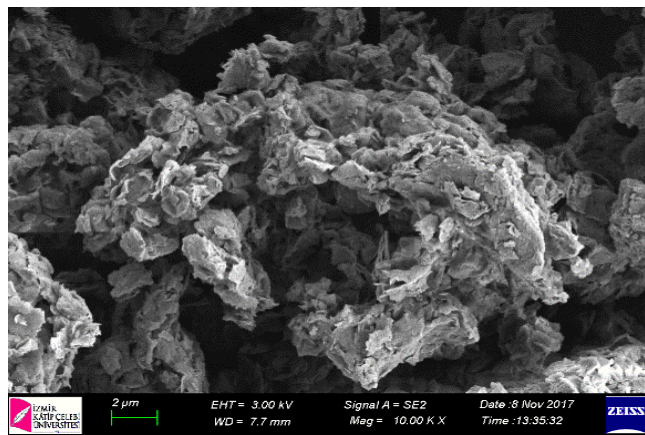


**Figure 1.** SEM image of the Cloisite 20A nanoclay (magnified 10000 times)

## 2.2 Method

The fabrics were coated by paste containing Cloisite 20A (Table 2), alginate and wetting agent (at 2 g/kg concentration). Alginate SMT T was used to prepare thickener paste by using at a 4% (w/v) concentration and the paste was mixed for 5 minutes after the adding Cloisite 20A and wetting agent. The coating treatment was carried out by a laboratory type coating machine (Mathis AG). After coating, the fabric samples were dried at 100°C for 6 minutes in a laboratory-type stenter (Ataç 40 GK). In the coating method, only one surface of fabric was coated and the used knife was over an endless rubber band. The thickness coating (the gap between fabric and knife), was 2 mm.

**Table 2.** Applied recipes in coating treatments

| Code | Chemical concentration(g/kg) |
|------|------------------------------|
|      | Cloisite 20A |
| UT* | - |
| A | 2.5 |
| B | 5 |
| C | 10 |
| D | 15 |

*Untreated fabric

## 2.3. Characterization and the flame retardant effect determination

Cloisite 20A and the untreated and coated cotton fabric samples were subjected to Scanning Electron Microscopy (SEM), thermogravimetric (TGA) and FTIR analyses for characterization. Vertical burning and Limiting Oxygen Index (LOI) tests were conducted to determine of the flame-retardant effect coating.

The surface morphology of nanoclay and uncoated and coated cotton fabrics was observed by a scanning electron microscope (SEM, Carl Zeiss 300VP) with an accelerating voltage of 15 kV. The samples were pre-coated with gold, using a sputter coater (Quorum Q150 RES).

Thermogravimetric analyses were conducted to determine the thermal properties of the nanoclay and uncoated and coated cotton fabrics. The samples were tested by using a TA TGA-STD Q600 thermal gravimetric analyzer operating under nitrogen atmosphere. The samples of 5-6 mg was heated from room temperature to 600°C at a heating rate of 10 °C/min under nitrogen atmosphere at a flow rate of 60 ml/min.

FTIR measurements of the nanoclay, uncoated and coated cotton fabrics of were carried out by a Thermo Scientific Nicolet IS50 infrared spectrometer using KBr pellet technique in the range of 4000-450 cm$^{-1}$ with a resolution of 4 cm$^{-1}$.

The burning tests of the coated fabrics were performed by SDL Atlas-M233B vertical burning test device according to BS 5438:1989 standard. After the test, the fabrics' char width and length were measured [BS 5438 standard, 1989].

LOI values of the coated cotton fabrics were measured according to method using a limiting oxygen index chamber [ASTM D 2863 standard, 1997].

## 3. RESULTS AND DISCUSSION

### 3.1 SEM analysis

Figure 2 and Figure 3 SEM photographs of the untreated and coated cotton fabrics; Sample A and Sample D were given for 100x and 1000x magnifications.

A close examination of the Figure 2 revealed that the yarns at the surface of Sample A were partially covered whereas the surface of the other sample coated using a higher amount of Cloisite 20A is relatively homogenous. In the case of higher magnification, the coverage of the yarns with a film made of alginate and Cloisite 20A was distinguished. While the yarns under the film layer were observed in Sample A, Sample D's surface was covered with a continuous and relatively homogeneous coating without leaving any trace of the fabric's yarns nanoclay particles were also more visible.

### 3.2 Thermogravimetric analysis

Figure 4 illustrated TGA and DTA graphs of Cloisite 20A. Table 3 showed the thermal decomposition temperatures and residues of Cloisite 20A.

As shown in Figure 4, Cloisite 20A has a broad peak in a temperature range changing from 199.39°C to 482.60°C and maxima at 309.12°C. The corresponding weight losses were 1.84%, 32.15% and 13.34%, respectively. The end of the test, the total weight loss of nanoclay was 39.85%.

Figure 5 illustrated TGA graphs of untreated and coated fabrics (sample A and sample D).
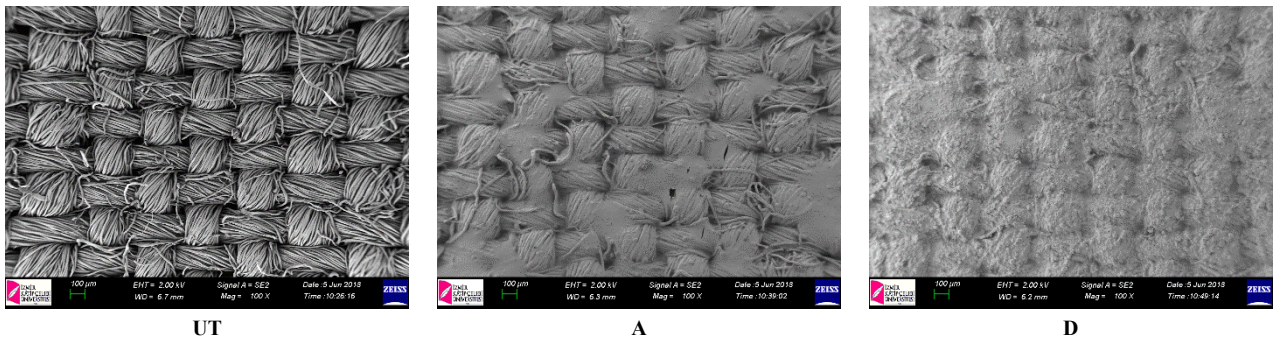
**Figure 2.** SEM photographs of the untreated and coated cotton fabrics (100x magnifications)
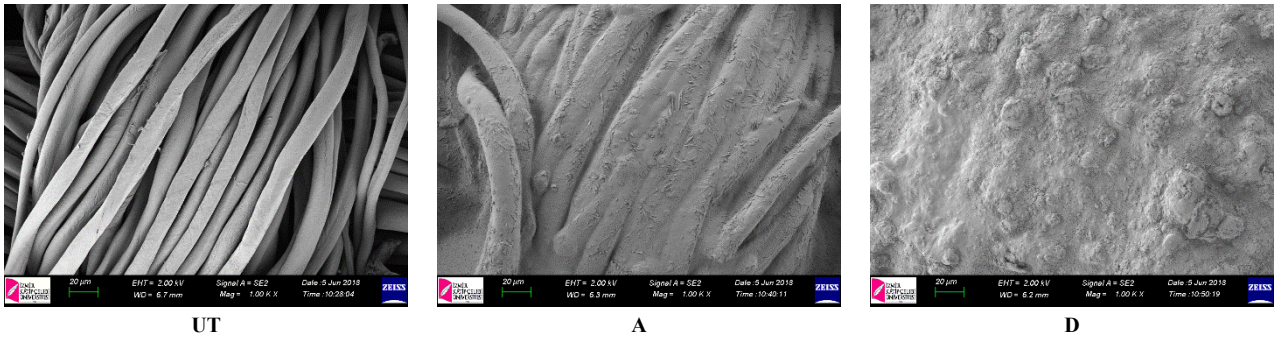


**Figure 3.** SEM photographs of the untreated and treated cotton fabrics with Cloisite 20A (1000x magnifications)
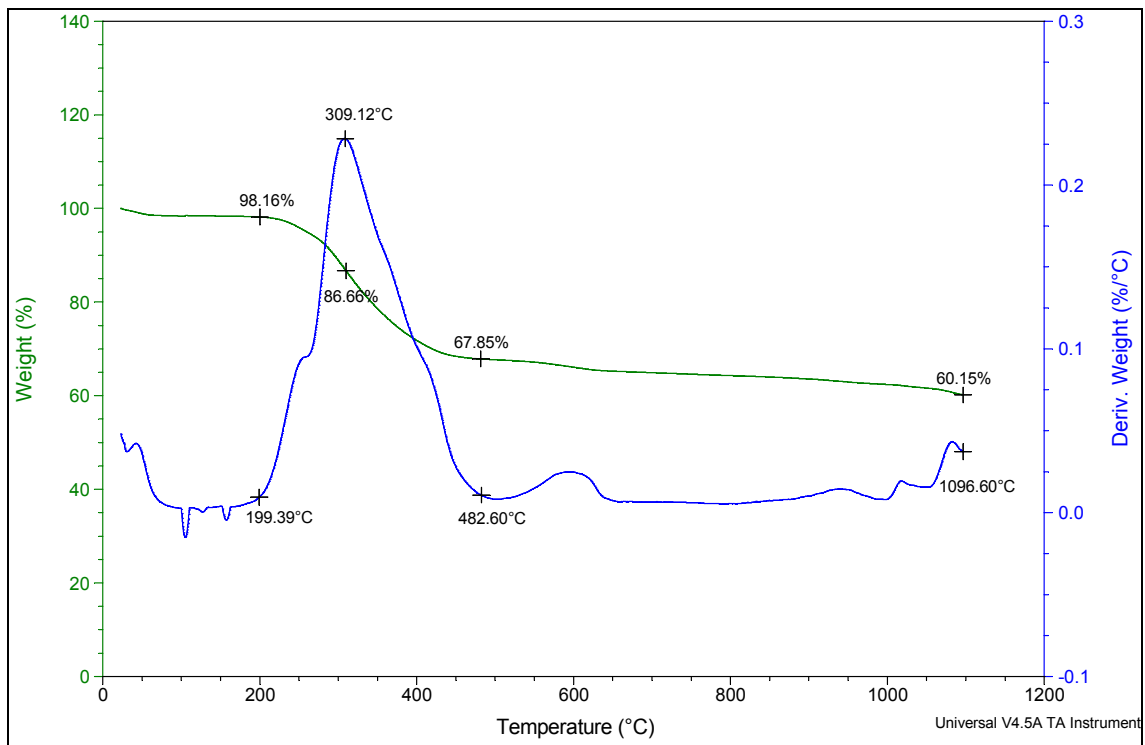


**Figure 4.** TGA and DTA graphs of Cloisite 20A

**Table 3.** Thermal decomposition temperatures and residues of Cloisite 20A

| Material | Initial decomposing temperature (°C) | Decomposition end temperature (°C) | The residue (%) | | | | Maximum peak point (°C) |
|---|---|---|---|---|---|---|---|
| Cloisite 20A | 199.39 | 482.60 | 199.39°C | 309.12°C | 482.60°C | 1096.6°C | 309.12 |
| | | | 98.16 | 86.66 | 67.85 | 60.15 | |
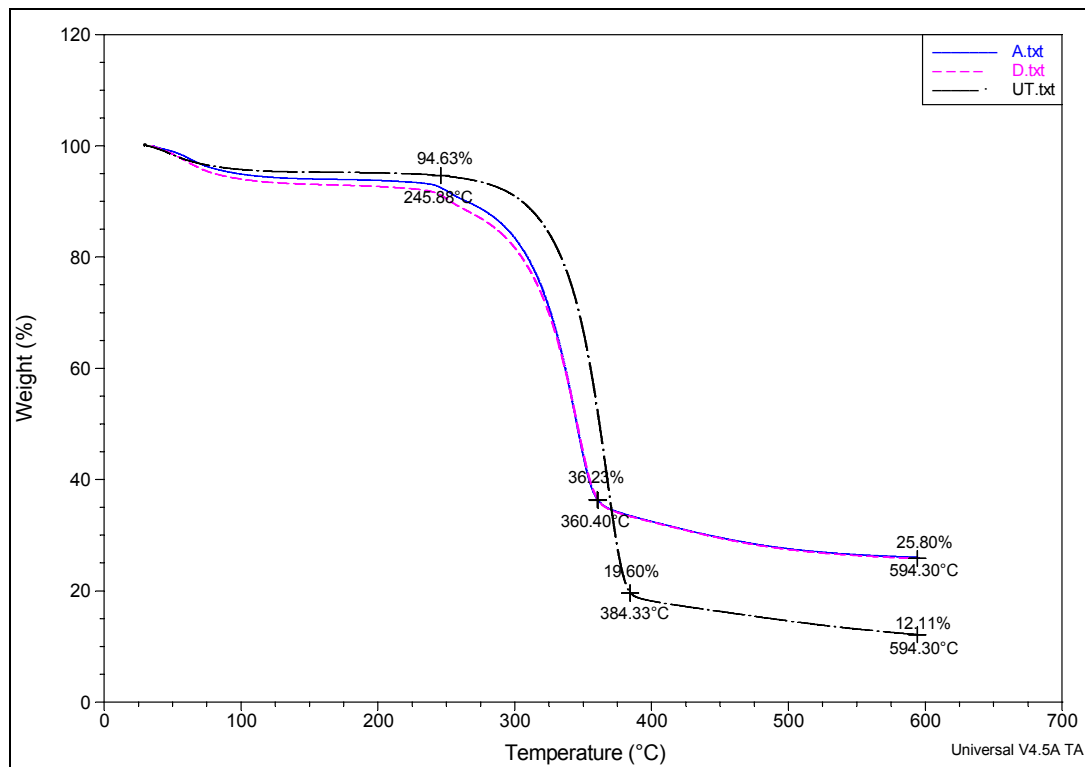
**Figure 5.** TGA graphs of untreated and coated fabrics (sample A and D)

The weight losses of untreated and coated fabrics were observed in a temperature range between 200°C and 600°C. As shown in Figure 5, two regions were observed in the temperature range studied. The first region covers 200°C-400°C temperature range. A considerable weight loss was observed in this range, and the weight loss in the second region is gradual. This range involves pyrolysis temperature of cotton fabric (250-270°C), the critical temperature (350°C) at which a spark causes a sudden burning due to the high ratio of flammable gases and then the spontaneous ignition temperature (400°C) when energized [Zhu et al. 2004; Zhu and Li 2011].

Table 4 showed the thermal decomposition temperatures and residues of untreated and coated fabrics.

The total weight losses were 87.89%, 74.20% and 74.20% for untreated fabric, Sample A and Sample D, respectively. The weight losses of coated samples were the same, when they were compared. Therefore, it was concluded that low

clay concentration (sample A, 2.5 g/kg concentration) was even enough. It was found that as the temperature increased, the weight losses also increased rapidly. Consequently, the coated cotton fabrics' degradation reaction rates with nanoclay were slower than those of untreated fabric. Due to the clay mineral barrier effect, the enhancement of coated cotton fabrics' thermal stability was provided.

## 3.3 FTIR analysis

FTIR spectrum of Cloisite 20A is given in Figure 6. In the spectrum, the bands observed at 2923 $cm^{-1}$, 2851 $cm^{-1}$ and 1471 $cm^{-1}$ were assigned to antisymmetric and symmetric $CH_2$ stretchings and methylene scissoring vibration [Yapar 2009]. The other bands observed at 1653 $cm^{-1}$, 1117 $cm^{-1}$ and 1013 $cm^{-1}$ are typical for clay minerals and they represent OH deformation of water and Si-O stretchings, respectively [Madejová and Komadel 2001].

**Table 4.** Thermal decomposition temperatures and residues of untreated and coated fabrics

| Material | Decomposition Temperature range | | The residue (%) | | | Weight loss (%) |
|---|---|---|---|---|---|---|
| | Beginning (°C) | End(°C) | | | | |
| UT | 245.88 | 384.33 | 245.88°C 94.63 | 384.33°C 19.60 | 594.30°C 12.11 | 87.89 |
| Sample A | 245.88 | 360.40 | 245.88°C 94.63 | 360.40°C 36.23 | 594.30°C 25.80 | 74.20 |
| Sample D | 245.88 | 360.40 | 245.88°C 94.63 | 360.40°C 36.23 | 594.30°C 25.80 | 74.20 |

**Figure 6.** FTIR spectrum of Cloisite 20A

FTIR spectra of untreated and coated fabrics (sample A and sample D) are given in Figure 7 and the peak wavenumbers and bonds are given in Table 5. Due to the existence of the common structural groups such as -CH$_2$, the spectra has similar features; however, the typical bands given in Table 5 are distinguished. A close examination of the figure and the table reveals that the peak observed at 1653 cm$^{-1}$ in Cloisite is shifted to a lower wavelength and the peaks at 1423 cm$^{-1}$ and 1416 cm$^{-1}$ observed in untreated fabric and in alginate spectra are disappeared and a new peak appears at 1402 cm$^{-1}$ as a result of the interaction among the functional groups. The peaks at 1423 cm$^{-1}$ and 1416 cm$^{-1}$ were showed in Figure 7.

Table 5 showed FTIR analysis results of untreated, coated fabrics, Cloisite 20A and alginate.
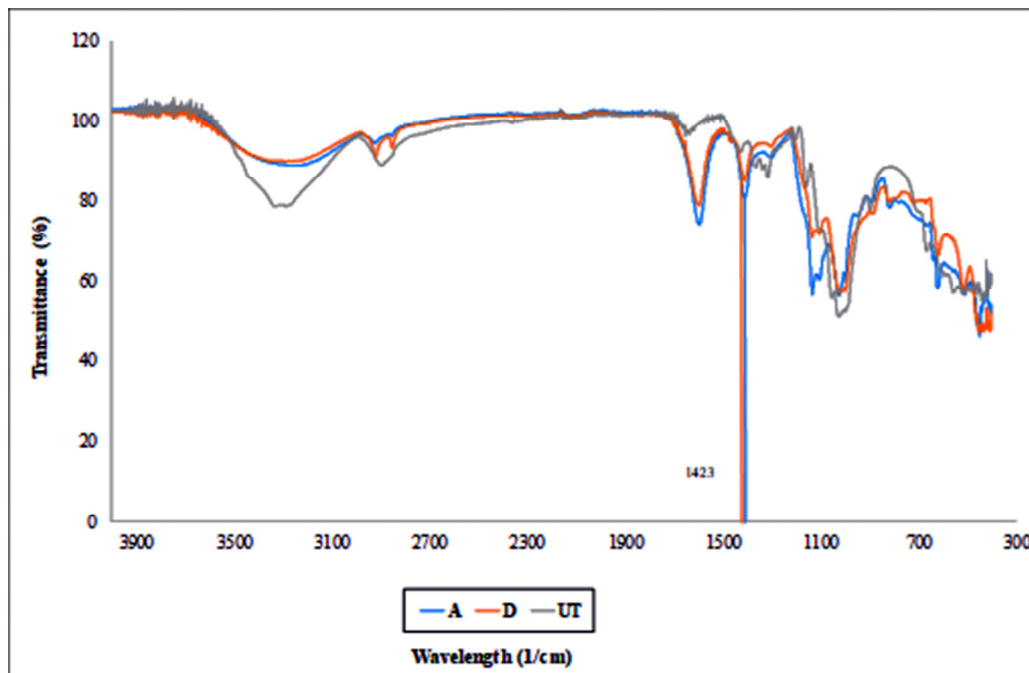


**Figure 7.** FTIR graphs of untreated and coated fabrics (sample A and sample D)

**Table 5.** FTIR results of Cloisite 20A, alginate, untreated and coated fabrics [Yapar 2009; Madejová and Komadel 2001; Sartori 1997]

| Sample | Peak wavenumber (cm$^{-1}$) | Bonds |
|---|---|---|
| UT | 3326-3256 | OH stretching |
| | 2896 | C-H symmetrical stretching |
| | 1647 | OH deformation |
| | 1423 | HCH and OCH in-plane bending vibration |
| | 1314 | CH$_2$ rocking vibration at C6 |
| | 1158 | C-O-C symmetrical stretching |
| | 1018 | C-C, C-OH, C-H ring and side group vibrations |
| Sample A | 2981-3503 | OH stretching |
| | 2934 | antisymmetric CH$_2$ stretching |
| | 2836 | symmetric CH$_2$ stretching |
| | 1595 | OH deformation |
| | 1402 | HCH and OCH in-plane bending vibration and/or methylene scissoring vibration and/or symmetric stretching vibration |
| | 1129 | C-C and C-O stretching |
| | 1098 | Si-O stretching |
| | 1037 | Si-O stretching |
| Sample D | 2981-3503 | OH stretching |
| | 2917 | antisymmetric CH$_2$ stretching |
| | 2838 | symmetric CH$_2$ stretching |
| | 1589 | OH deformation |
| | 1402 | HCH and OCH in-plane bending vibration and/or methylene scissoring vibration and/or symmetric stretching vibration |
| | 1126 | C-C and C-O stretching |
| | 1098 | Si-O stretching |
| | 1037 | Si-O stretching |
| Cloisite 20A | 3651 | C-H symmetrical stretching |
| | 2923 | antisymmetric CH$_2$ stretching |
| | 2851 | symmetric CH$_2$ stretching |
| | 1653 | OH deformation of water |
| | 1471 | methylene scissoring vibration |
| | 1117 | Si-O stretching |
| | 1013 | Si-O stretching |
| | 922 | AlAlOH deformation |
| | 893 | AlFeOH deformation |
| Alginate | 1610 | O-C=O asymmetric stretching |
| | 1416 | O-C=O asymmetric stretching |
| | 1125 | C-C and C-O stretching |
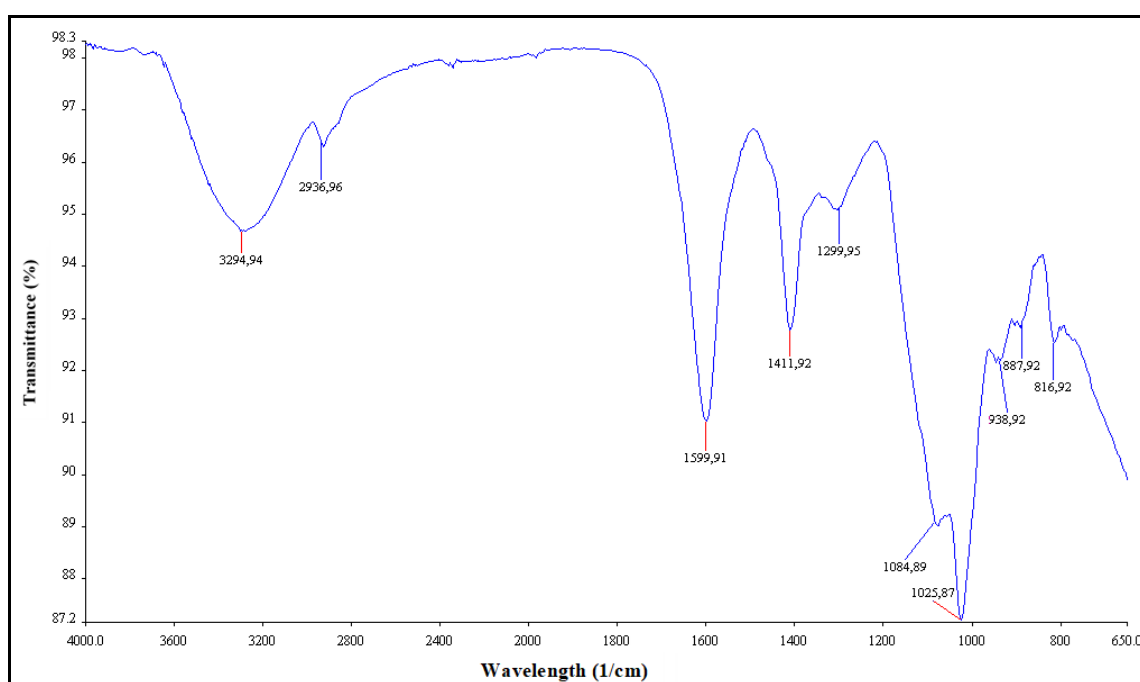


**Figure 8.** FTIR spectrum of alginate

FTIR spectrum of coated fabric with alginate is given in Figure 8. The bands observed at 1599 cm⁻¹ and 1411 cm⁻¹ were assigned to O-C=O antisymmetric stretchings in the spectrum. These bands are typical for Alginate.

## 3.4 Vertical burning test

The vertical burning tests showing the cotton samples' upward burning behavior were given in Figure 9 and Table 6.



**Figure 9.** The images of coated cotton samples after vertical burning tests

**Table 6.** Flame retardant performance of the cotton samples

| Code | Char Width (cm) | Char Length (cm) |
|------|-----------------|------------------|
| UT   | -               | -                |
| A    | 4.4             | 6.1              |
| B    | 4.5             | 12               |
| C    | 5.3             | 10.3             |
| D    | 3.6             | 7.4              |

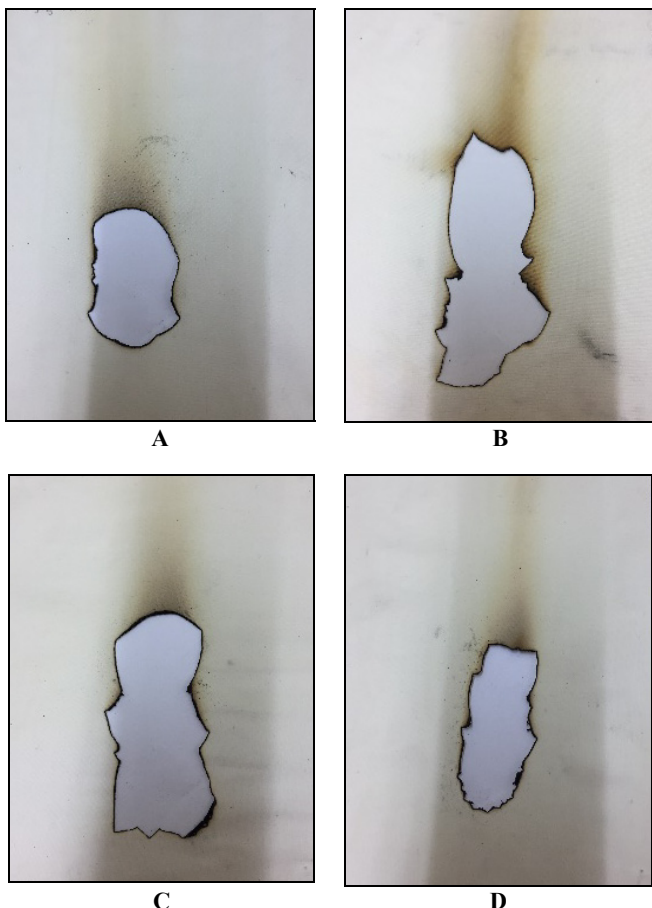During the tests, the untreated fabric burned up, while the coated samples were burned locally, at which the flame contacted. As shown in Table 6, the differences between the samples' char lengths were more obvious than those of char widths. Compared to sample B and C, sample A and D had shorter char widths and shorter char lengths. As a result, all nanoclay concentration provided satisfactory flame

retardant effect. In other words, ignition and burning did not continue after the flame contact. There is no linear relation between the increase in concentration and the flame retardant effect.

## 3.5 LOI test

According to the results of burning tests, the samples' flame-retardant performances exhibited no considerable differences; therefore, only two samples coated by using 2.5 g/kg and 15 g/kg nanoclay concentration were subjected to LOI tests. Table 7 showed LOI values of untreated and coated cotton fabrics.

**Table 7.** LOI values of untreated and coated cotton fabrics

| Code | LOI value (%) |
|------|---------------|
| UT   | 18.2          |
| A    | 25.1          |
| D    | 24.4          |

It can be seen that LOI values of the coated samples were much higher than that of untreated sample. LOI values of sample A and untreated fabrics were 25.1% and 18.2%, respectively. With the increase of Cloisite 20A in the coating paste, the LOI value was not changed so much. Consequently, the coating treatment, even at low nanoclay concentration imparted a satisfactory flame-retardant effect to the cotton fabrics.

## 4. CONCLUSION

In this study, the flame-retardant properties of 100% cotton fabrics were improved using commercial nanoclay (Cloisite 20A) coatings. The coated samples were subjected to the burning test, SEM, FTIR, TGA analyses, and LOI tests. SEM analysis showed that the cotton yarns were partially or completely covered depending on the amount of nanoclay used. FTIR analyses indicated that the peaks observed on Cloisite and alginate spectra were shifted, and also a new peak has appeared on spectra as a result of the interaction among the functional groups. The test results showed that the coating treatment, even at low nanoclay concentration, is enough to have a considerable flame-retardant effect. This result was attributed to the barrier effect of the nanoclay.

Clays and clay minerals have been evaluated for diverse potential applications, as pollutant adsorbents for sustaining the environment and their use in human and veterinary medicine. They have large adsorption capacities, excellent mechanical and chemical properties. These clay minerals are essential for improving textile materials. In this study, the flame-retardant properties of cotton fabrics were improved using commercial nanoclay. Cloisite has been applied to polyethylene terephthalate polyethylene terephthalate fiber, and nanocomposites in studies conducted to date [Fabia et al. 2020; Devaux et al. 2015; Yelkovan et al. 2014]. In this study, Cloisite was applied directly to the cotton fabric with the coating method,

speedy. After applications, the tests showed that the coating treatment with nanoclay on cotton fabrics had a considerable and satisfactory flame retardant effect. In other words, ignition and burning did not continue after the flame contact.

## REFERENCES

1. Liu HS, Zhang XL, Song LX. 2011. Comprehensive evaluation and prediction of fire accidents in China based on statistics. *Chinese Saf Science.* 21(6), p.54-59.

2. Cordner A, Mulcahy M, Brown P. 2013. Chemical regulation on fire: rapid policy advances on flame retardants. Environmental Science & Technology. https://doi.org/10.1021/es3036237.

3. Gao D, Li R, Lv B, Ma J, Tian F, Zhang J. 2015. Flammability, thermal and physical-mechanical properties of cationic polymer/montmorillonite composite on cotton fabric. *Composites Part B.* https://doi.org/10.1016/j.compositesb.2015.03.061.

4. Holder KM, Smith RJ, Grunlan JC. 2017. A review of flame retardant nanocoatings prepared using layer-by-layer assembly of polyelectrolytes. *J Materials Science and Engineering.* https://doi.org/10.1007/s10853-017-1390-1.

5. Du L, Xu G, Zhang Y, Qian J, Chen J. 2011. Synthesis and properties of a novel intumescent flame retardant (IFR) and its application in halogen-free flame retardant ethylene propylene diene terpolymer (EPDM). *Polymer Plastics Technology and Engineering.* https://doi.org/10.1080/03602559.2010.543224.

6. Yuan H, Xing W, Zhang P, Song L, Hu Y. 2012. Functionalization of cotton with UV cured flame retardant coatings. *Industrial & Engineering Chemistry Research.* https://doi.org/10.1021/ie202468u.

7. Zhang DQ, Williams BL, Shrestha SB, Nasir Z, Becher EM, Lofink BJ, Santos VH, Patel H, Peng XH, Sun LY. 2017. Flame retardant and hydrophobic coatings on cotton fabrics via sol-gel and self-assembly techniques. *Journal of Colloid And Interface Science.* https://doi.org/10.1016/j.jcis.2017.06.087.

8. Başyiğit ZO, Kut D. 2018. Formaldehyde-free and halogen-free flame retardant finishing on cotton fabric. *Tekstil ve Konfeksiyon.* https://doi.org/10.32710/tekstilvekonfeksiyon.482884.

9. Ghoranneviss M, Shahidi S. 2014. Flame retardant properties of plasma pretreated/metallic salt loaded cotton fabric before and after direct dyeing. *Journal Of Fusion Energy.* https://doi.org/10.1007/s10894-013-9642-9.

10. Carosio F, Alongi J, Malucelli G. 2012. Layer by layer ammonium polyphosphate based coatings for flame retardancy of polyester-cotton blends. *Carbohydrate Polymers.* https://doi.org/10.1016/j.carbpol.2012.02.049.

11. Shahidi S, Ghoranneviss M. 2014. Effect of plasma pretreatment followed by nanoclay loading on flame retardant properties of cotton fabric. *J Journal Of Fusion Energy.* https://doi.org/10.1007/s10894-013-9645-6.

12. Ghosh A. 2011. Nano-clay particle as textile coating. *International Journal Of Engineering Science Technologies IJET-IJENS* 11(5), p.34-36.

13. Uddin F. 2008. Clays, nanoclays and montmorillonite minerals. *Metallurgical and Materials Transactions.* https://doi.org/10.1007/s11661-008-9603-5.

14. Başyiğit ZÖ. 2018. Improvement of flame retardant characteristic of raw silk fabric. *Tekstil ve Konfeksiyon* 28(3), p.199-206.

15. Shah AR, Prabhakar MN, Song J. 2017. Current advances in the fire retardancy of natural fiber and bio-based composites: A Review. *International Journal of Precision Engineering and Manufacturing-Green Technology.* https://doi.org/10.1007/s40684-017-0030-1.

16. Guo Y, Chang CC, Halada G, Cuiffo MA, Xue Y, Zuo X, Pack S, Zhang L, He S, Weil E Rafailovich MH. (2017). Engineering flame retardant biodegradable polymer nanocomposites and their application in 3D printing. *Polymer Degradation and Stability.* https://doi.org/10.1016/j.polymdegradstab.2017.01.019.

17. Majka TM, Leszczyńska A, Kandola BK, Pornwannachai W, Pielichowski K. 2017. Modification of organo-montmorillonite with disodium H-phosphonate to develop flame retarded polyamide 6 nanocomposites. Applied Clay Science. https://doi.org/10.1016/j.clay.2017.01.012.

18. Makhlouf G, Hassan M, Nour M, Abdel-monem YK, Abdelkhalik A. 2017. A novel intumescent flame retardant: synthesis and its application for linear low-density polyethylene. *Arabian Journal For Science And Engineering.* https://doi.org/10.1007/s13369-017-2443-0.

19. Rehan M, El-Naggar ME, Mashaly HM, Wilken R. 2018. Nanocomposites based on chitosan/silver/clay for durable multi-functional properties of cotton fabrics. *Carbohydrate Polymers.* https://doi.org/10.1016/j.carbpol.2017.11.007.

20. Chowdary MS, Kumar M. 2015. Effect of nanoclay on the mechanical properties of polyester and s-glass fiber (Al). *International Journal of Animal Science and Technology.* http://dx.doi.org/10.14257/ijast.2015.74.04.

21. Bhat G, Hegde RR, Kamath MG, Deshpande B. 2008. Nanoclay reinforced fibers and nonwovens. *Journal of Engineered Fibers and Fabrics.* https://doi.org/10.1177/155892500800300303.

22. Qiu X, Li Z, Li X, Zhang Z. 2017. Flame retardant coatings prepared using layer by layer assembly: A review. *Chemical Engineering Science.* https://doi.org/10.1016/j.cej.2017.09.194.

23. Zhu H., J. Njuguna. 2014. Nanolayered silicates/clay minerals: uses and effects on health. In Njuguna J., Pielichowski K., Zhu H. (Eds.), *Health and Environmental Safety of Nanomaterials.* The Netherlands, Woodhead Publishing, p.133-146.

24. Yapar S., Özdemir G., Fernández Solarte A.M., Torres Sánchez R.M. 2015. Surface and Interface Properties of Lauroyl Sarcosinate-Adsorbed CP$^+$-Montmorillonite. *Clays and Clay Minerals.* Vol. 63, No. 2, p.110-118 https://doi.org/10.1346/CCMN.2015.0630203).

25. Erkan I., Alp I., Çelik M.S. 2010. Characterization of organo-bentonites obtained from different linear-chain quaternary alkylammonium salts. *Clays and Clay Minerals.* Vol.58, p.792-802.

26. Schumann D., Hesse R., Sears S.K., Vali H. 2014. Expansion behavior of octadecylammonium-exchanged low to high-charge reference smectite-group minerals as revealed by high-resolution transmission electron microscopy on ultrathin sections. *Clays and Clay Minerals.* Vol.62, p.336-353.

27. Ruiz-Hitzky E., Aranda P., Darder M., Rytwo G. 2010. Hybrid materials based on clays for environmental and biomedical applications. *Journal of Materials Chemistry.* Vol.20, p.9306-9321

28. Zeng QH, Yu AB, Lu GQ, Paul DR. 2005. Clay-based polymer nanocomposites: research and commercial development. *Journal Of Nanoscience And Nanotechnology.* https://doi.org/10.1166/jnn.2005.411.

29. Mittal G, Rhee KY, Mišković-Stanković V, Hui D. 2018. Reinforcements in multi-scale polymer composites: Processing, properties, and applications. *Composites Part B-Engineering.* https://doi.org/10.1016/j.compositesb.2017.11.028.

30. Azeez AA, Rhee KY, Park SJ, Hui D. 2013. Epoxy clay nanocomposites - processing, properties and applications: A review. *Composites Part B-Engineering.* https://doi.org/10.1016/j.compositesb.2012.04.012.

31. Yelkovan S, Yılmaz D, Aksoy K. 2014. A study of organo-modified clay type on pet-clay based nanocomposite properties. *Materials Science.* Vol.3, No.1, p.33-46.

32. Visakh PM. 2015. *Advances in flame retardant of different types of nanocomposites.* In: PM. Visakh, Y. Arao (Eds.), In Flame Retardants: Polymer Blends, Composites and Nanocomposites, Springer Press, New York, p.1-14.

33. Cao GF, Sun Y, Chen JG, Song LP, Jiang JQ, Liu ZT, Liu ZW. 2014. Sutures modified by silver-loaded montmorillonite with antibacterial properties. *Applied Clay Science.* https://doi.org/10.1016/j.clay.2014.03.007.

34. Bourbigot S, Devaux E, Flambard X. 2002. Flammability of polyamide-6/clay hybrid nanocomposite textiles. *Polymer Degradation and Stability.* https://doi.org/10.1016/S0141-3910(01)00245-2.

35. Li YC, Schulz J, Mannen S, Delhom C, Condon B, Chang S, Zammarano M, Grunlan JC. 2010. Flame retardant behavior of polyelectrolyte-clay thin film assemblies on cotton fabric. *ACS Nano.* https://doi.org/10.1021/nn100467e.

36. Norouzi M., Zare Y., Kiany P. 2015. Nanoparticles as Effective Flame Retardants for Natural and Synthetic Textile Polymers: Application, Mechanism, and Optimization. *Polymer Review.* Vol.55, No.3, pp.531-560, doi: 10.1080/15583724.2014.980427

37. Rault F., Giraud S., Salaün F. 2015. Flame retardant/resistant based nanocomposites in textile. In Visakh M.P., Arao Y. (Eds.), *Flame Retardants: Polymer Blends, Composites and Nanocomposites.* Switzerland, Springer International Publishing: Cham, p.131-165.

38. Devaux E, Rochery M, Bourbigot S. 2002. Polyurethane/clay andpolyurethane/POSS nanocomposites as flame retarded coating for polyester and cotton fabrics. *Fire and Materials.* Vol.26, p.149-154.

39. Fabia J., Gawłowski A., Rom M., Ślusarczyk C., Brzozowska-Stanuch A., Sieradzka M. 2020. PET fibers modified with cloisite nanoclay. *Polymers.* Vol.12, No.4, p.1-19.

40. BS 5438:1989 Methods of test for flammability of textile fabrics when subjected to a small igniting flame applied to the face or bottom edge of vertically oriented specimens - ISBN:0 580 17341 0 https://shop.bsigroup.com.

41. ASTM D 2863:1997 Standard test method for measuring the minimum oxygen concentration to support candle-like combustion of plastics (Oxygen Index) https://www.astm.org.

42. Zhu P, Sui S, Wang B, Sun K, Sun G. 2004. A study of pyrolysis and pyrolysis products of flame-retardant cotton fabrics by DSC, TGA, and PY-GC-MS. *Journal of Analytical and Applied Pyrolysis.* https://doi.org/10.1016/j.jaap.2003.09.005.

43. Zhu FL, Li KJ. 2011. Numerical modeling of heat and moisture through wet cotton fabric using the method of chemical thermodynamic law under simulated fire. *Fire Technology.* https://doi.org/10.1007/s10694-010-0201-x.

44. Yapar S. 2009. Physicochemical study of microwave-synthesized organoclays. *Colloids and Surfaces A: Physicochemical and Engineering Aspects.* https://doi.org/10.1016/j.colsurfa.2009.04.032.

45. Madejová J, Komadel P. 2001. Baseline studies of the clay minerals source society: infrared methods. *Clays and Clay Minerals.* Vol.49, No.5, p.410-432.

46. Sartori C. 1997. The characterisation of alginate systems for biomedical applications (Doctoral dissertation). Brunel University, Department of Materials Engineering, London.

# Investigation of Elasticity and Growth Properties of Denim Fabrics Woven with Core and Siro Spun Yarn

Serin Mezarcıöz, R. Tuğrul Oğulata, Ahmet Nergis [*]

Cukurova University / Textile Engineering Department / Adana, Turkey

**Corresponding Author:** Serin Mezarcıöz, smavruz@cu.edu.tr

## ABSTRACT

In this study, elasticity and growth parameters which are important for denim fabrics were investigated. Elasticity and growth performances were determined after three home laundering and compared in fabrics produced with different weft yarn counts, elastane draft ratio, elastane lineer density, spinning method and weft density parameters. The elasticity and growth values obtained from the produced fabrics were evaluated by SPSS statistical analysis program and significant conclusions were obtained. As a result of the study, it is observed that all of these variables have a significant effect on elasticity and growth values.

## 1. INTRODUCTION

People want to feel comfortable in their clothes and they want their clothes to look good. Designers use flexible yarns in woven and knitted fabrics to increase the comfort of the garments and enhance their aesthetic appearances [1].

Elastic fabrics can stretch under the natural forces that are exposed in the areas where they are used in our daily lives, can be restored to their original size in great dimensions and can provide comfort and ease of movement. These kinds of fabrics do not deform during clothing and can maintain their shape, which are not overly wrinkled during washing and dry cleaning, which can maintain its original size and shape [2, 3]. While elastic fabrics that stretches with the effect of the elastane yarns are subjected to a force, the non-elastic yarn tries to pull the fabric in a narrower area. In this case, an orange peel effect can be observed in the fabric, since the fabric swells and there is not enough space to move. Therefore, when an elongation of 20% is desired in the fabric, the weft density should be 20% lower than the weft density in the non-elastic fabric [3].

Therefore, streching is an important requirement for the comfort and convenience of the user. It is usually necessary to stretch comfortably in accordance with body movements,

and also to maintain its original shape without any deformation after stretching. If the clothes do not have a lot of flexibility, deformation occurs, which called fabric is bagging. It causes some problems in aesthetic appearance [4].

Elastane was first used in classical underwear, corset and added new applications in the field of sportswear. The rate of use of elastic fabrics in ladies' and men's top wear continued to rise. Elastic fabrics are required to have elastic properties of 18-25% for classic top garment products, 35-60% for sportswear, and 80-120% for corset type functional garments [3].

Elastane fibers have an important share in the production of elastomeric denim production. Those fibers can be used with many staple fibers thanks to the core yarn production method. In elastic denim production, it is possible to reach elasticity levels (10-100%) which will provide consumer expectations with yarns containing elastane in weft or warp. For this reason, almost all of the world's elastane-containing denim productions are realized with the use of elastane [5].

Elastane fibers are used in combination with various yarns and fiber types in order to ensure that fiber structure does not deteriorate, to meet different requirements and to

provide ease in post-spinning processes. Combined yarns with elastane content produced for these purposes have characteristics which vary according to the type of yarn forming components and systems used in production. The most widely accepted method is the production of core spun elastane yarn [3].

Core spun yarns have a structure in which one of the constituents, in most cases a synthetic filament either mono or multi is concealed by a different component, a staple fibre sheath. Therefore a core yarn consists of a core part and a sheath. Meanwhile, the spandex remains in the center of the yarn and is covered with the fiber used. Thus, it is ensured that the spandex remains in the center and is covered with the used blend and covered perfectly [6].

The main aim of using core spun yarn is to take advantage of the different properties of its both components. The filament increases the yarn strength and also permits the use of lower twist level, while the sheath provides the staple fibre yarn appearance and surface physical properties. Core-spun yarn is preferred in knitted and woven fabrics [7]. Core yarns are used in awning fabrics for high tenacity property, special industrial fabrics, medical textiles, underwear clothes, swimsuits, socks, sport clothes and sewing threads. There are different methods for production of core yarns. The most common of them are ring and friction spinning systems [8].

Sirospun is a spinning process that allows a two-fold (two strand) worsted yarn to be produced on a conventional ring spinning machine, dispensing with no need for spinning to be followed by separate two-folding and its attendant processes. In this process, two rovings are drawn separately from each other, then combined and twisted on the same spindle. Sirospun yarns are widely used in the worsted industry because of their better wearability. Sirospun method is to produce two plyyarns in a single spinning process [9].

Many studies were managed to optimize and evaluate the physical and mechanical properties of core spun yarns and fabrics. Qadir et al. (2014) investigated the effects of elastane linear density and draft ratio on the physical and mechanical properties of single core-spun yarns According to the statistical evaluations they found that elastane linear density and the draft have statistically significant effect on yarn tenacity, elongation and hairiness but the yarn IPI and CVm are not significantly affected by these parameters [10].

The influence of spinning parameters on sheath slippage of core-spun yarn was studied by Miao et al. (1996). It was observed that the yarn strength increased by increasing filament ratio and increasing filament feeding tension. It has been stated that the pre-twist applied to the filament has an important effect on the abrasion resistance of the yarn [11].

Celik and Kaynak (2017) examined the effects of elastane draw ratio on air permeability of denim woven fabrics [12].

Celik et al. (2009) researched on the effects of core-sheath ratio and twist coefficient on the yarn properties of the ring PET core-spun yarns. According to the experiments and statistical evaluations; it has been determined that the change of core / sheath ratio and twist count affects the tenacity, elongation at break and yarn vitality. When the core ratio is increased, the strength value increases [13].

Cataloglu (2007) investigated the elasticity and growth properties of elastane composed denim fabrics and stated that alternative to elastane, using bi-component polyester fibres and polybutylene terephthalate (PBT) has inspired interest with regarding to higher strength due to better chemical resistance, better recovery, dimensional stability and elasticity properties [5]. Romdhane et al. (2016) has investigated the effect drafting tension of Multifilament "T400" on the dual core spun yarns to enhance the quality of denim stretch fabric [14]. Many researchers attempted to produce short staple yarn with siro spun system. Cheng and Sun (1998) found that spinning performance of sirospun yarns can be improved by decreasing the strand spacing and increasing the twist coefficient. [15]. Su et al. (2003) investigated the optimum drafting conditions for siro spinning by changing the roving spacing using lyocell roving. They concluded that there is a limited break draft beyond which the drafting force decreases, and consequently an increase in the variation of the drafting force causes deterioration in yarn evenness, leading to an increase in yarn faults [16].

Also some studies conducted in denim fabric stretch properties are available in the literature. Bedez Üte, (2019) revealed the effect of the composition of double-core (dual-core) and core-spun weft yarns and weft density on the some mechanical properties of denim fabrics and concluded that weft density is found to be more effective than weft yarn composition for mechanical and dimensional properties of denim yarns [17]. Çeven et al. (2018) investigated the denim fabrics produced at three different weft and warp density with different yarn numbers and elastane ratios in terms of tenacity and stretching properties (elongation, permanent elongation, elastic recovery) considering the different washing cycles of 0, 5 and 15. According to the results, higher values for stretching ratios (%) and permanent stretching ratios (%) of denim samples were obtained as the washing cycle increased whereas there was a fluctuation observed for the elastic recovery ratios (%) regarding to washing cycles [18]. The effects of different aesthetic finishes applied while manufacturing, different elastane content and fabric weight on denim fabric's mechanical and stretch properties were researched by Choudhary and Sheena (2018). It was observed that the tensile strength of denim fabric decreases with increasing elastane percentage, while breaking extension increases.

Elastane content percentage shows significant influence on air permeability of denim [19]. The interactive effect of twist multiplier of weft yarn, denier elastane fibre and fabric areal density on performance of denim fabric was investigated by Choudhary, Sheena and Nikhil (2018) and they show that the tensile strength and breaking elongation properties of denim fabric, for both before and after cyclic loading show the same trend. Higher twist multiplier results in higher fabric tensile strength, but decrease in breaking elongation [20].

Although there are a few studies to compare the properties of fabrics manufactured from two-strand, single and plied yarns, there is still a lack of information in the literature which investigates the properties of elasticity and growth parameters of denim fabrics manufactured with core spun and sirospun yarns. This experimental study investigates and focus on this subject. Weft yarn counts, elastane draft ratio, elastane lineer density, weft density and spinning methods are the variables used in the study. Elasticity and growth values obtained from the produced different fabrics and evaluated with SPSS statistical analysis program and significant inferences were obtained [21].

## 2. MATERIAL AND METHOD

### 2.1 Material

Elasticity is the percent of elongation under tension on the yarn or fabric. Growth is the return to its original length, shape and size when the tension is removed [3]. In the experiments 3/1 Z twill denim fabrics were produced. Ne 13.5 conventional ring spun %100 cotton yarns were used as warp direction and warp density is the same for all fabrics (43 ends/cm). Ne 13, 16, 20 yarns were used in the weft direction. 3, 3,5 and 3,8 draft ratios, 18,5 and 20 weft density, 78 and 135 dtex elastane, cotton-elastane (CO) core-spun, cotton-polyester (CO + PES) sirospun blend yarn experiments were performed. In fact, since there were 5 variables, mentioned above, with different levels, 72 different fabrics, having different specifications, should be produced to cover all of the variations. However, due to the factory restrictions, only 14 fabrics could be produced. Table 1 presents the specifications of the denim fabrics.

### 2.2 Method

All tests were carried out after the specimens were conditioned in standard atmospheric conditions (temperature 20 ± 2 °C, 65 ±2 % relative humidity). Elasticity and growth properties were determined after three home laundering according to ASTM 3107 [22]. A stretch testing instrument, consisting of a frame with separate clamps fixed at the top and at the bottom, was implemented to determine the stretch properties of the fabrics. 3 strips for each sample from weft direction were hung on the apparatus after marking a 250 mm index in the central part

of each specimen. A 1360 gram load, which was hung according to the fabric weight in the bottom hanger, was applied to the sample three times and after the fourth application; the marked distance was measured. The samples were hung for 30 minutes, and the distance was measured again for elasticity. The distance between the marked points after 1 hour of relaxation was measured once again for growth. Elasticity and growth values were calculated from these measured outcomes.

For elasticity in percent values, the formulas were used.

$$Elasticity~(\%) = \frac{B-A}{A}~x100 \qquad (1)$$

A: The distance marked between the upper and bottom parts of the fabric (250 mm)

B: The distance between the marked points after hanging the sample for 30 minutes with the load (mm).

Elastic recovery was calculated by inducluding a proportion between the difference in the distance of the marked points of the fabric after hanging it for 30 minutes, and the distance to maximum stretching after 1 hour relaxation time.

Growth was calculated as follows:

$$Growth~(\%) = \frac{C-A}{A}~x100 \qquad (2)$$

C: The distance between the marked points after 1 hour of relaxation.

A: The distance marked between the upper and bottom parts of the fabric (250 mm).

## 3. RESULTS AND DISCUSSION

Since the elastane is used in the weft yarn, elasticity and growth tests are performed only in the weft direction. Performance characteristics of fabrics weaved using elastic core-spun yarns and siro-spun yarns in different properties were examined. Three tests were carried out for each sample. The mean values and standard deviations (SD) obtained after the tests are given in Table 2.

According to the findings, the effect of yarn and fabric technical parameters on elasticity and growth were statistically analyzed. Statistical analysis program SPSS was applied according to ANOVA method and the parameters formed by the parameters based on the model of the significant relationship was obtained. In order to determine whether the effects of parameters affecting elasticity and growth were significant, statistical analysis revealed that the value of p was less than 0.05 (α = 0.05) [21].

### 3.1. Assesment of Dependent Factors

#### 3.1.1. Elasticity

As can be seen in Table 3, p-value was less than 0.05 in all variables of weft yarn count, weft density, elastane draft ratio, elastane lineer density and spinning method. Test results showed that all of the parameters have a significant effect on elasticity property.

#### 3.1.2. Growth

The expectation from all of the fabrics is that the growth value is as close to zero as possible. Clothing manufacturers want the growth value to be maximum 2% in trousers and clothes, and maximum 3% in daily and sportswear depending on the finishing processes. Bagging behavior is observed when the growth values of the clothes are 3% and above [4, 5]. The elasticity and growth value of the fabric change according to the comfort properties expected by the end user and the usage area of the product. In the denim market, although stretching fabrics are desired, yarn structures and fabric constructions having lower growth value as much as possible during the stretching process are preferred.

According to the results of the analysis in Table 4 below, it has been determined that these parameters have a meaningful effect on growth because all the factors' p-value values are less than 0.05.

**Table 1**. Samples specifications of denim fabrics and their codes

| Sample code | Weft yarn count (Ne) | Weight per unit area | Weft density (picks/cm) | Elastane draft ratio | Elastane lineer density (dtex) | Weft spinning method |
|---|---|---|---|---|---|---|
| CS1 | 13 | 340 | 18,5 | 3 | 78 | CORE SPUN |
| CS2 | 13 | 343 | 18,5 | 3 | 135 | CORE SPUN |
| CS3 | 13 | 340 | 18,5 | 3,5 | 78 | CORE SPUN |
| CS4 | 13 | 339 | 18,5 | 3,8 | 78 | CORE SPUN |
| CS5 | 13 | 347 | 20 | 3,8 | 78 | CORE SPUN |
| CS6 | 16 | 330 | 20 | 3 | 78 | CORE SPUN |
| CS7 | 16 | 329 | 20 | 3,5 | 78 | CORE SPUN |
| CS8 | 16 | 326 | 20 | 3,8 | 78 | CORE SPUN |
| CS9 | 16 | 333 | 20 | 3,8 | 135 | CORE SPUN |
| SS1 | 13 | 341 | 18,5 | 3,8 | 78 | SIRO SPUN |
| SS2 | 16 | 334 | 20 | 3,8 | 78 | SIRO SPUN |
| SS3 | 16 | 332 | 20 | 3,8 | 135 | SIRO SPUN |
| SS4 | 20 | 314 | 20 | 3,8 | 78 | SIRO SPUN |
| SS5 | 20 | 309 | 18,5 | 3,8 | 78 | SIRO SPUN |

**Table 2.** Test results of denim fabrics

| Sample code | Weft yarn count (Ne) | Weft density (picks/cm) | Elastane draft ratio | Elastane lineer density (dtex) | Weft spinning method | Elasticity (%)/(SD) | Growth (%)/(SD) |
|---|---|---|---|---|---|---|---|
| CS1 | 13 | 18,5 | 3 | 78 | CORE SPUN | **62,0** / (4,8) | **7,9** / (0,4) |
| CS2 | 13 | 18,5 | 3 | 135 | CORE SPUN | **57,9** / (7,4) | **5,9** / (0,5) |
| CS3 | 13 | 18,5 | 3,5 | 78 | CORE SPUN | **64,1** / (3,9) | **8,8** / (1,0) |
| CS4 | 13 | 18,5 | 3,8 | 78 | CORE SPUN | **66,9** / (7,0) | **10,4** / (0,4) |
| CS5 | 13 | 20 | 3,8 | 78 | CORE SPUN | **60,5** / (8,6) | **8,9** / (0,8) |
| CS6 | 16 | 20 | 3 | 78 | CORE SPUN | **63,9** / (6,0) | **6,7** / (0,2) |
| CS7 | 16 | 20 | 3,5 | 78 | CORE SPUN | **68,0** / (4,9) | **6,9** / (0,2) |
| CS8 | 16 | 20 | 3,8 | 78 | CORE SPUN | **70,3** / (3,8) | **7,9** / (0,5) |
| CS9 | 16 | 20 | 3,8 | 135 | CORE SPUN | **67,6** / (5,2) | **5,9** / (0,3) |
| SS1 | 13 | 18,5 | 3,8 | 78 | SIRO SPUN | **68,4** / (1,9) | **6,8** / (0,5) |
| SS2 | 16 | 20 | 3,8 | 78 | SIRO SPUN | **70,1** / (9,9) | **6,4** / (1,1) |
| SS3 | 16 | 20 | 3,8 | 135 | SIRO SPUN | **73,6** / (6,6) | **4,1** / (0,3) |
| SS4 | 20 | 20 | 3,8 | 78 | SIRO SPUN | **78,1** / (4,6) | **5,2** / (0,7) |
| SS5 | 20 | 18,5 | 3,8 | 78 | SIRO SPUN | **84,7** / (7,4) | **6,8** / (0,6) |

**Table 3.** The effect analysis of weft yarn count, draft, elastane lineer density, weft density and spinning method to elasticity

| Tests of Between-Subjects Effects | | | | | |
|---|---|---|---|---|---|
| Dependent Variable: | ELASTICITY | | | | |
| Source | Type III Sum of Squares | df | Mean Square | F | Sig. |
| Weft yarn count | 635,003 | 2 | 317,502 | 370,419 | ,000 |
| Weft density | 125,453 | 1 | 125,453 | 146,362 | ,000 |
| Elastane lineer density | 7,864 | 1 | 7,864 | 9,175 | ,005 |
| Spinning method | 30,091 | 1 | 30,091 | 35,106 | ,000 |
| Draft | 96,693 | 2 | 48,347 | 56,404 | ,000 |

**Table 4.** The effect analysis of weft yarn count, draft, elastane lineer density, weft density and spinning method to growth

| Tests of Between-Subjects Effects | | | | | |
|---|---|---|---|---|---|
| Dependent Variable: | GROWTH | | | | |
| Source | Type III Sum of Squares | df | Mean Square | F | Sig. |
| Weft yarn count | 1,533 | 2 | ,766 | 8,748 | ,001 |
| Weft density | 7,053 | 1 | 7,053 | 80,500 | ,000 |
| Elastane lineer density | 18,818 | 1 | 18,818 | 214,770 | ,000 |
| Spinning method | 25,662 | 1 | 25,662 | 292,881 | ,000 |
| Draft | 10,898 | 2 | 5,449 | 62,188 | ,000 |

According to Anova results (Table 3-Table 4), yarn count and linear density of elastane have a significant effect on fabric elasticity and growth. When 78 dtex elastane and 135 dtex elastane samples for both core spun and siro spun were analyzed comparatively, it was observed that elasticity levels are similar. But the growth value decreased in the samples using 135 dtex. Rising elastane yarn count results increase of yarn elastane percentage. Because of high elastane percentage occurred in 135 dtex elastane the recovery force are higher than 78 dtex elastane result. Cataloglu indicated in his study that in cases where high elasticity and low permanent elongation values are expected, elastane type change can also be made to provide these values. Especially with the increase in the weight of the fabric, higher elastane yarn count can also be used in order to increase the recovery force [5]. It is clear that through the use of more powerful elastane can be reduced growth value in denim fabrics.

According to effect analysis shown in Table 3 and Table 4, since the p values are lower than 0,05, spinning methods have significant effect on elasticity and growth results. It was found that the elasticity results are higher and growth results of siro spun yarns are lower than core spun yarns. This is due to the fact that the polyester fiber, which has a more even surface, exhibits less friction and facilitates the return of the elastane, on the other hand there is high friction of the elastane with cotton.

### 3.2. Assesment of Independent Factors

Figure 1 and 2 show the elasticity and growth values of the core spun and siro spun samples according to the weft yarn count and elastane draft ratio.
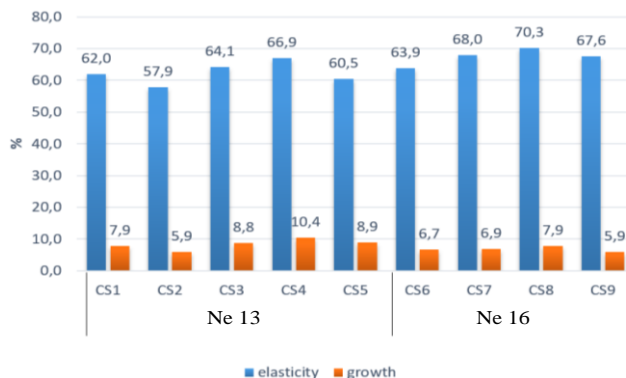


**Figure 1.** Elasticity and growth values for core spun yarns

According to the results shown in Figure 1 and 2, the observed elasticity for the average of CS5, SS1 samples in

Ne 13 is 65,4 %, for CS8, SS2 samples in Ne 16 is 70,2 %, and for SS4, SS5 samples in Ne 20 is 81,4 %. The outcomes revealed that elasticity values increase when the counts of yarn increase. In addition that the growth averages for the same samples are observed as in Ne 13 is 8,4 % , in Ne 16 is 6,6 % and in Ne 20 is 6 %. This is due to the increase of yarn count, resulting an increase of elastane percentage and effect of yarn. High elastane percentage resulted with high fabric stretch and because of high recovery force it resulted with lower growth value.
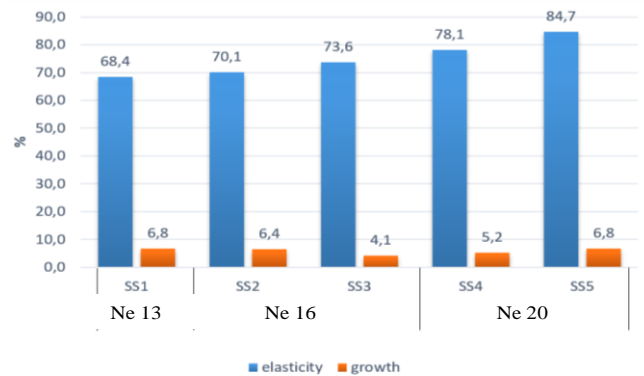


**Figure 2.** Elasticity and growth values for siro spun yarns

In spinning process elastane percentage decreases by increasing the elastane draft. However test results in Figure 1 displays that the increase in elastane draft resulting increase of fabric elasticity. When the test results of CS1, CS3 and CS4 group and CS6, CS7 and CS8 group are compared in the same yarn count, elastane yarn count, weft density and spinning method, the averages of elasticity are observed as for draft (3) 62,9 %, for draft (3,5) 66,0 %, and for draft (3,8) 68,6 %. This can be explained with high retraction force of high draft of elastane yarns. Qadir et al. indicated in their study that when a fabric containing elastane yarns spun with higher draft is taken off the loom then due to higher retraction force, the fabric contracts more in width as compared to a fabric containing elastane yarns spun with lower draft. A fabric that has higher contraction is more stretchable than one which has less contraction [10]. When the growth averages of the same fabric samples are compared, they are observed as for draft (3) 7,3 %, for draft (3,5) 7,8 %, and for draft (3,8) 9,1 %. It is obvious that the fabric growth values are increasing by increasing elastane draft ratio. Since the elastane percentage decrases by increasing elastane draft ratio, it results with high growth values.

It is seen in Figure 1 and 2 that the elasticity values are decreasing with the increase of weft density. This outcome is similar to previous studies (Cataloglu, 2007). Although the amount of elastane in the unit area increases as a result of increasing weft density, elasticity decreases. Cataloglu indicated in his study the reason for this is thought to be the blocking of the weft yarn as a result of the internal tensions [5].

### 3.3. Regression Analysis

The cause-effect relationship between two variables, Y dependent and X independent variables, is determined by regression analysis in stepwise method. The variables elasticity and growth dependent on analysis made to estimate elasticity and growth values of denim fabrics, independent variables weft yarn count, elastane draft ratio, weft density and elastane lineer density were started. Since the spinning method is not numerical, it is not included in the model. In this method the variables with weak effect in t-test were subtracted and regression analysis was repeated. After these processes, it is aimed to explain the relationship between dependent and independent variables by using regression analysis method.

### Elasticity

Analysis was started with all independent variables predicted to affect the elasticity value, and according to the t-test results elastane factor was removed from the model as significance value was more than 0.05 and the output images given in Table 5 were obtained. The adjusted $R^2$ value of the model is 0.925 which is shown in model summary that means 92.5 % of the elasticity value in denim fabric is explained by the weft yarn count, weft density and draft ratio. Adjusted $R^2$ show that the predictive power of the model is high enough.

In "Anova table", significance value obtained as less than 0,01 and that means model is meaningful. "B" values titled in "Coefficients" table shows the coefficients of each indenpedent variables in this model. Since all significance values are less than 0,05 here, this specifies a significant relation between dependent and independent variables.

According to the coefficients, while weft yarn count and draft ratio has a positive effect on elasticity, weft density has negative. Curve fit plots for elasticity are shown in Figure 3. Finally the equation for elasticity in denim fabrics is shown as below;

$$E= 60,650+2,486xWC-3,132xWD+8,442xD \qquad (3)$$

E: elasticity, WC: weft yarn count, WD: weft density, D: draft ratio

### Growth

According to t-test analysis, as the significance values are more than 0,05, draft and weft density variables were removed from the model. Therefore only weft yarn count and elastane lineer density variables remained in the model. The adjusted $R^2$ value is obtained 0,625 as shown "Table 6a model summary". In Anova Table 6b, significance values are obtained less than 0,01 and this means model is meaningful. Since all significance values are less than 0,05 in t analysis, there is a significant relation between draft, weft density independent variables and growth.

Based on "Coefficients Table 6c", both weft yarn count and elastane lineer density have negative effects on growth results. Curve fit plots for growth are shown in Figure 4. As a result, the obtained formula for growth is shown in the following equation;

$$G= 16,524-0,376xWC-0,041xE \qquad (4)$$

G: growth, WC: weft yarn count, E: elastane lineer density

**Table 5.** Regression analysis results for elasticity

**a)** Model Summary[b]

| Model | R | R Square | Adjusted R Square | Std. Error of the Estimate |
|---|---|---|---|---|
| 1 | ,965[a] | ,931 | ,925 | 1,89455 |

**b)** Anova Table

| Model | | Sum of Squares | df | Mean Square | F | Sig. |
|---|---|---|---|---|---|---|
| 1 | Regression | 1832,264 | 3 | 610,755 | 170,158 | ,000[b] |
| | Residual | 136,395 | 38 | 3,589 | | |
| | Total | 1968,659 | 41 | | | |

**c)** Coefficients

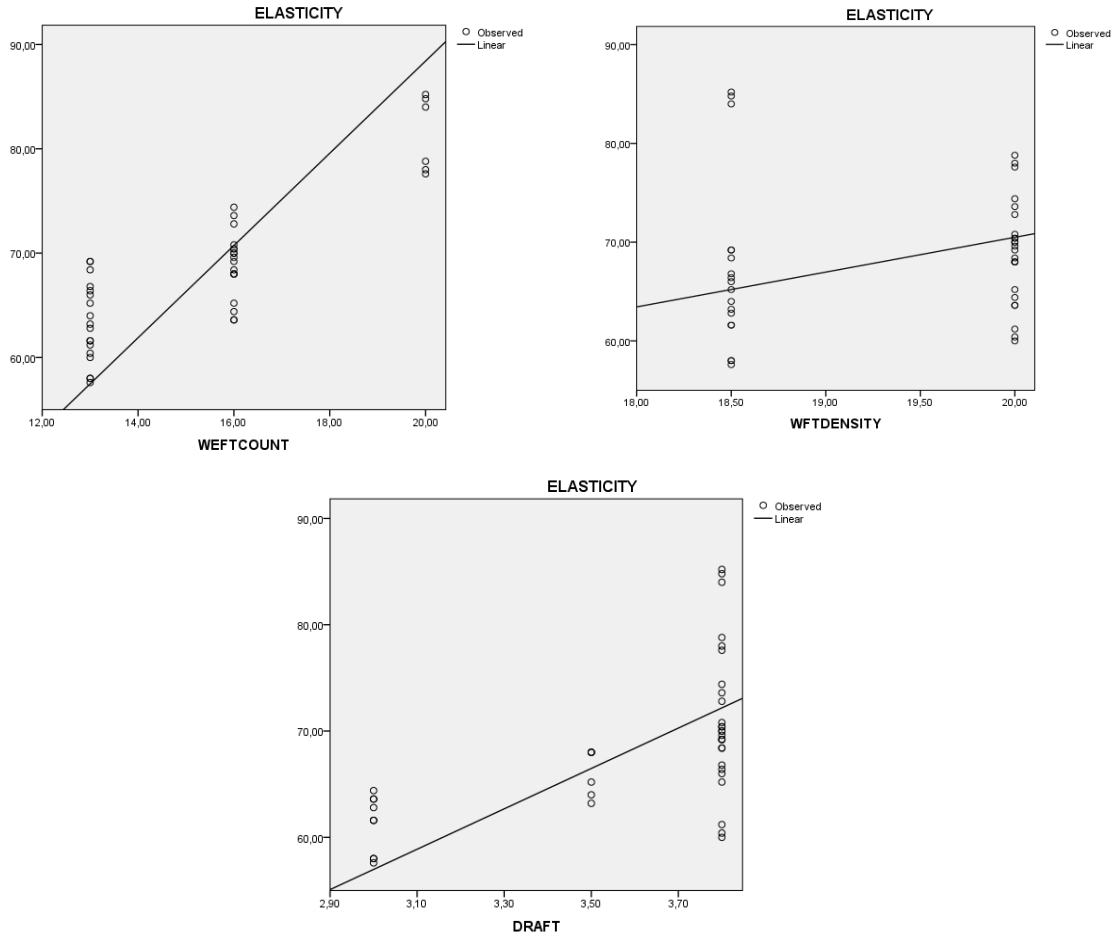| Model | | Unstandardized Coefficients | | Standardized Coefficients | t | Sig. |
|---|---|---|---|---|---|---|
| | | B | Std. Error | Beta | | |
| 1 | (Constant) | 60,650 | 7,908 | | 7,669 | ,000 |
| | Weft yarn count (WC) | 2,486 | ,139 | ,862 | 17,840 | ,000 |
| | Weft density (WD) | -3,132 | ,437 | -,340 | -7,164 | ,000 |
| | Draft (D) | 8,442 | ,973 | ,398 | 8,672 | ,000 |
| a. Dependent Variable: ELASTICITY | | | | | | |

**Figure 3.** Curve fit plots for elasticity

**Table 6.** Regression analysis results for growth

**a)** Model Summary[b]

| Model | R | R Square | Adjusted R Square | Std. Error of the Estimate |
|---|---|---|---|---|
| 1 | ,802[a] | ,643 | ,625 | ,98594 |

**b)** Anova Table

| Model | | Sum of Squares | df | Mean Square | F | Sig. |
|---|---|---|---|---|---|---|
| 1 | Regression | 68,348 | 2 | 34,174 | 35,156 | ,000[b] |
| | Residual | 37,911 | 39 | ,972 | | |
| | Total | 106,259 | 41 | | | |

**c)** Coefficients

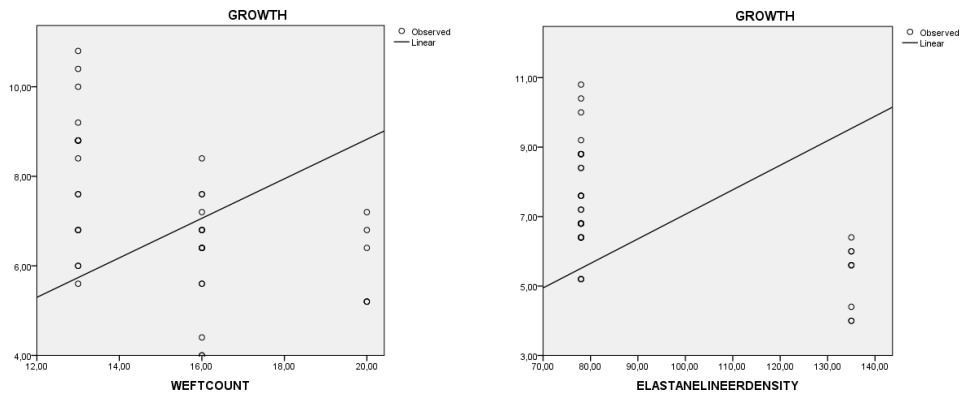| Model | | Unstandardized Coefficients | | Standardized Coefficients | | |
|---|---|---|---|---|---|---|
| | | B | Std. Error | Beta | t | Sig. |
| 1 | (Constant) | 16,524 | 1,185 | | 13,939 | ,000 |
| | Weft yarn count (WC) | -,376 | ,064 | -,561 | -5,853 | ,000 |
| | Elastane lineer density (E) | -,041 | ,007 | -,610 | -6,361 | ,000 |

**Figure 4.** Curve fit plots for growth

## 4. CONCLUSION

As a result of the obtained data and the analyses, the following conclusions were reached;

1. It has been clearly determined that the weft yarn count, elastane draft ratio, elastane lineer density, spinning method and density factors have significant relationship with all denim fabric elasticity and growth properties. For this reason, it is necessary to keep these parameters in the denim production processes and fabric designs.

2. In particular, it is observed that the usage of elastane is one of the most effective factors in decreasing the growth value. Elastane lineer density has a significant effect on fabric growth values. Regression analysis show us growth performance is better with 135 dtex elastane after stretching.

3. It is observed that the increase of the draft ratio is a factor increasing the ability of the extension to increase accordingly. Fabric growth and elasticity results increase by increasing weft draft ratio.

4. According to the results obtained in the study, it is seen that there is a significant relationship between composition

of yarn and elasticity, growth levels of fabric. While the yarns produced by polyester cotton blend with siro spun method have higher elasticity performance, it has been seen that growth values are less than core spun cotton elastane yarns. This is due to the fact that the polyester fiber, which has a more even surface, has less friction and facilitates the return of the elastane, on the other hand there is high friction of the elastane with cotton.

5. The effect of the same count of elastane in the fabrics produced by thin weft yarn is higher than the fabrics woven with thick weft yarn. The increase in elasticity was observed with the increase of the effect of elastane, while it was determined that there was a decrease in growth values. According to these results, it is observed that elasticity and growth performances are better with thin weft than thick weft yarns in denim fabric containing elastane yarns.

6. It has been observed that the effect of elastane on the fabric increases with the proportional increase of elastane depending on the increase in the weft density. It is concluded that even with a small increase in the weft density, a significant reduction can be obtained in elasticity values.

## REFERENCES

1. Şengöz, N. G. 2004. Bagging in Textiles, Textile Progress 36 (1) pp 1-64.

2. DUPONT Technical Bulletin, 1997a. "Core Spun Yarns", L-519.

3. DUPONT Technical Bulletin, 1997 b. "Wovens Certification Program", L-528.

4. Özdil, N. 2008. Stretch and bagging properties of denim fabrics containing different rates of elastane, *Fibres & Textiles in Eastern Europe*, January / March 2008, Vol.16, No.1(66), 63-67.

5. Çataloğlu, A. 2007. A study on elasticity and growth properties of elastane composed denim fabrics. (Doctoral dissertation), Ege University, Institute of Natural and Applied Sciences, Department of Textile Engineering, p.79. İzmir, Turkey.

6. Ruppenicker, G.F., Harper, R.J., Sawhney, A.P., Robert, K.Q. 1989. Comparison of cotton polyester core and staple blend yarns and fabrics, *Textile Research Journal*, 59(1), 12-17.

7. Hyung, J. K., Hee W. Y., Cheng, Y.Z., You, H. 2009. Influence of the core-sheath weight ratio and twist on the tensile strength of the ring core yarns with high tenacity filaments, *Fibers and Polymers*, 10(4), 546-550.

8. Erez, E., Çelik, P. 2014. A research on the parameters of the affecting yarn properties of cotton-polyester rigid core-spun yarns, *Tekstil ve Konfeksiyon*, 24(2), 195-201.

9. Elkhamy, D.A. 2007. Processing Mechanics of Alternate Twist Ply (ATP) Yarn Technology. PhD thesis, Drexel University, Germany, p. 267.

10. Qadir, M.B, Hussain, T., Malik, M., Ahmad, F., Jeong, S. H. 2014. Effect of elastane linear density and draft ratio on the physical and mechanical properties of core-spun cotton yarns, *The Journal of the Textile Institute*, 105 (7) pp. 753-759.

11. Miao, M., How, Y. L., Ho, S. Y. 1996. Influence of spinning parameters on core yarn sheath slippage and other properties, *Textile Research Journal*, 66(11), 676-684.

12. Çelik, H.İ., Kaynak, H. K. 2017. An investigation on the effect of elastane draw ratio on air permeability of bi-stretch denim fabrics, 17th AUTEX World Textile Conference, 29-31 May, Corfu, Greece.

13. Celik, P., Üte, T.B., Özden, D., Çömlekçi, H., Akkale, E.C. 2009. The effect of core/sheath ratio and twist amount on yarn characteristics of filament core yarns, *Tekstil Teknolojileri Elektronik Dergisi*, 3(2):29-37.

14. Romdhane, B., Béchir, A., Faouzi, S. 2016. Optimization of drafting tension of multifilament "t400" on the dual core spun yarns to enhance the quality of denim stretch. International Conference of Applied Research on Textile, CIRAT-7 November 10 – 12, 2016 Hammamet, Tunisia ISSN 2286-5659.

15. Cheng, K.P.S., Sun, M.N. 1998. Effect of strand spacing and twist multiplier on cotton siro spun yarn, *Textile Research Journal.* Vol.68, No.7, 520-527.

16. Su, C., I., Liu, C., H., Jiang, J. Y. 2003. Drafting force of twin spun yarn, *Textile Research Journal*, Vol.73, No.9, 815-818.

17. Bedez Üte, T. 2019. Analysis of mechanical and dimensional properties of the denim fabrics produced with double-core and core-spun weft yarns with different weft densities, *The Journal of The Textile Institute*, Vol.110, No.2,179-185. DOI: 10.1080/00405000.2018.1470451.

18. Çeven, E.K, Eren, H.A, Günaydın G.K, Sevim, Ö, Şan, C. 2018. Effect of washing cycle on tenacity and stretching properties of denim fabrics containing elastane, *J Fashion Technol Textile Eng*., S5:002, doi:10.4172/2329-9568.S5-003.

19. Choudhary, A.K, Sheena, B. 2018. Influences of elastane content, aesthetic finishes and fabric weight on mechanical and comfort properties of denim fabrics. J Textile Eng Fashion Technol, 4(1):36–42. DOI: 10.15406/jteft.2018.04.00119.

20. Choudhary, A.K., Sheena, B., Nikhil, L. 2018. The effect of twist multiplier, elastane percentage and pick density on denim quality, Trends Textile Eng Fashion Technol. 1(4). 103-108, TTEFT.000519.2018. DOI: 10.31031/TTEFT.2018.01.000519

21. SPSS 22.0 Statistical Package Program.

22. ASTM D3107 – 07, 2015. Standard test methods for stretch properties of fabrics woven from stretch yarns, ASTM International.